Multi-isotopic and statistical approaches to trace nitrate pollution sources and assess natural attenuation in groundwater: examples from nitrate vulnerable zones in Catalonia (NE Spain)

Roger Puig Caminal

UNIVERSITAT DE BARCELONA

Facultat de Geologia

Departament de Cristal·lografia, Mineralogia i Dipòsits Minerals

MULTI-ISOTOPIC AND STATISTICAL APPROACHES TO TRACE NITRATE POLLUTION SOURCES AND ASSESS NATURAL ATTENUATION IN GROUNDWATER: EXAMPLES FROM NITRATE VULNERABLE ZONES IN CATALONIA (NE SPAIN)

Tesi doctoral presentada per:

Roger Puig Caminal

Per aspirar a l'obtenció del títol de doctor per la Universitat de Barcelona

Tesi realitzada dins del Programa de Doctorat de Ciències de la Terra, sota la co-direcció del Dr. Albert Soler i Gil i el Dr. Josep Mas-Pla, i tutoritzada pel Dr. Albert Soler i Gil

Dr. Albert Soler i Gil
Dpt. Cristal·lografia, Mineralogia
i Dipòsits Minerals
Universitat de Barcelona

Dr. Josep Mas-Pla
Centre de Geologia i Cartografia Ambiental
Dpt. Ciències Ambientals
Universitat de Girona

Barcelona, Abril de 2014

Agraïments

Ja està. Per tant, després de tot aquest temps, ara, en aquestes primeres pàgines, no em queda més que agrair a tota la gent que ha viscut de la vora o de passada el procés d'elaboració d'aquesta tesi, perquè, sense el seu suport, arribar fins aquí no hagués estat possible. Des d'aquelles persones amb qui he conviscut el dia a dia, fins a les que no sabien ben bé què estava fent tots aquests anys, crec que totes, amb més o menys mesura, han contribuït que aquest treball arribés finalment a bon port. És probable que m'oblidi d'algú, que em disculpi.

En primer lloc, si d'una cosa n'estic completament convençut, és que la persona amb qui he d'estar infinitament agraït és amb el Dr. Albert Soler i Gil; per molts motius, però bàsicament per tot el que m'ha ensenyat i he après d'ell, tant a nivell professional com en l'àmbit personal, i també per haver-me iniciat en el món dels isòtops estables, haver-me obert les portes a treballar en un grup de recerca, irradiar passió per la ciència, dia a dia, sense parar sense parar sense parar, i pel seu suport, confiança, comprensió i paciència que, sincerament, m'han ajudat com no s'imagina. De veritat, moltes gràcies.

Evidentment, també amb el mateix ímpetu agraeixo al meu altre codirector, el Dr. Josep Mas Pla, el seu mestratge i suport científic, la seva disposició per resoldre'm tots els dubtes que m'han anat sorgint, així com introduir-me i guiar-me per la hidrogeologia en general, i per la del Baix Ter i la Selva en particular. Moltes gràcies per tot el que m'has ensenyat, i per fer-ho sempre amb el teu bon humor.

Tot i que no ha estat codirectora del treball, vull agrair especialment a la Dra. Neus Otero (la Neus) que sempre hagi estat allà, des del començament i fins al final, que sempre hagi pogut comptar amb ella, ja sigui per discutir i interpretar resultats com per salvar qualsevol mena d'obstacle, i perquè com a companya de feina i amiga ha significat un punt de recolzament constant, i en tot moment ha confiat en mi i m'ha animat. Gràcies per tot.

Agrair també particularment a l'Albert Folch i al Raimon Tolosana, amb els quals ha estat un plaer treballar colze a colze, i que han contribuït de manera important en bona part de la feina que aquí es presenta. Gràcies per tot el que he après treballant amb

vosaltres, que ha estat molt, i per la paciència. Afegeixo a l'agraïment l'Anna Menció, de la Universitat de Girona (UdG), per la coautoria i la feina feta en dues de les publicacions.

Al Dr. Ramon Aravena, per la seva hospitalitat i col·laboració durant la meva estada a la Universitat de Waterloo. De passada, faig extensiu el meu agraïment a totes les persones amb qui vaig compartir uns mesos força intensos, entre les quals: Andrés Urrutia, Monica Pasini, Jason Venkiteswaran, Richard Elgood, John Spoelstra, i els meus amfitrions Craig Miles Robertson i Barbara-Anne Pender.

Al Dr. David Widory, per la seva ajuda amb l'anàlisi de la composició isotòpica del bor, la posterior interpretació dels resultats, i la correcció de l'article, merci beaucoup. Igualment, a la Dra. Vera Pawlowsky, per tota la feina com a editora del llibre d'anàlisi de dades composicionals en que ha aparegut publicat un dels treballs.

Al personal dels Centres Científics i Tecnològics (CCiT) de la Universitat de Barcelona, per la seva professionalitat i paciència, especialment a les responsables dels diferents equipaments, la Dra. Rosa Mª Marimon i la Dra. Pilar Teixidor, així com a tots els tècnics que han participat en les anàlisis, com l'Eva Aracil, en Jaume Sánchez, la Laia Balart, en Toni Padró i la Pili.

A la Mercè Olamendi, per tota la seva ajuda i coneixements al laboratori i per les converses de passadís. I als tècnics en pràctiques, com la Irene Puigivila.

A l'Agència Catalana de l'Aigua, i especialment al Josep Fraile i a la Mireia Iglesias, per interessar-se per la recerca realitzada a les zones vulnerables per nitrats de Catalunya, així com per facilitar-me l'accés a informació i dades de les mateixes.

A la Dra. Marisol Manzano i a l'Horacio Higueras, de la Universitat Politècnica de Cartagena (UPCT), per haver-me donat l'oportunitat d'anar a mostrejar al Parc de Doñana.

Al Dr. Joan Bach de la Universitat Autònoma de Barcelona (UAB) i al Guillem Herrera, estudiant de treball de fi de carrera, per l'interès mostrat.

A tot el personal del Departament de Cristal·lografia, Mineralogia i Dipòsits Minerals, entre els quals: la Dra. Àngels Canals, el Dr. Miquel Àngel Cuevas i el Xabier Anleo.

A tots als participants de la 38ª edició del *Curso Internacional de Hidrología Subterránea* (CIHS), i molt especialment al Julio Pérez, per ajudar-me als mostreigs, i a la Manuela Barbieri i als professors Dr. Fidel Ribera i Dr. Enric Vázquez, amb qui he tornat a coincidir després.

Als meus companys de despatxos, amb qui he compartit i segueixo compartint bonics moments d'estrès i trepidants estones de distensió: la Mireia Garreta, el Joaquim Perona, l'Àngels Piqué, la Laura Vitòria, l'ínclit Jordi Palau, la diligent Clara Torrentó, l'entranyablement mordaç Raúl Carrey, i el temible trident format per l'Alba Grau, la Mercè Olamendi i la Diana Rodríguez. Amb el Massimo Marchesi, tot i que no hem compartit despatx, és com si ho haguéssim fet, grazie per tutti amico.

Vull agrair amb gran èmfasi a la totalitat dels companys, amics i satèl·lits pertanyents al Grup de Mineralogia Aplicada i Medi Ambient (MAiMA), pels moments viscuts tant a dins com a fora de la universitat, farcits d'anècdotes, sopars i aventures de tota índole. Fins aquí encara no havia mencionat a: la Georgina Vidal, la Carme Audí, la Mònica Rosell, la Paula Rodríguez, el Joan Martínez, la Cristina Domènech, el Pablo Lúquez i el Dr. Esteve Cardellach.

Un dedicat agraïment per la Marta Rejas, per ser com és d'estupendament *loca*, i també per la Carme Audí, el Raúl Carrey, la Georgina Vidal i la Mònica Rosell, per tota l'ajuda prestada i els ànims donats durant l'esprint final.

Als estudiants i investigadors visitants: la Larissa Ramage, la Martina Kralj, el Daniele Pittalis, la Geneviève Bordeleau, l'Adriana Rossi, el Daniel Merchán i el Takahiro Osono.

A tots els amics que he deixat de veure durant aquesta última època i que espero retrobar a partir d'ara.

A tots i cada un dels Eutròfics, pels esquitxos en helicòpter.

Al Riki Blanco, per posar-hi la portada.

I agrair-ho tot als meus pares, Llorenç i Marisun, i com que vinc d'ells, això va per ells. I al meu germà Aleix, la meva cunyada Imma, i als meus nebots Arnau i Adrià, agrair-los l'alegria de ser-hi.

I a la Rubi, per la santa paciència i per tots els *bailes* que hem fet i que farem.

Aquesta tesi s'ha portat a terme amb el suport d'una beca predoctoral de Formació de Personal Investigador (FPI) del Ministeri d'Economia i Competitivitat del Govern d'Espanya, en el marc del projecte CICYT-REN2002-04288-C02-02 (*Aplicación multisotópica ($^{15}N_{NH4}$, $^{15}N_{NO3}$, $^{18}O_{NO3}$, $^{13}C_{DIC}$, $^{13}C_{MO}$, $^{34}S_{SO4}$, $^{87}Sr/^{86}Sr$) en la vigilancia del medio ambiente*). El treball realitzat també ha gaudit del finançament dels projectes CICYT CGL2005-08019-C04-01/HID i CGL2008-06373-C03-01/BTE, així com del projecte PET2008-0034 del Ministeri d'Economia i Competitivitat del Govern d'Espanya, dels ajuts de suport al Grup Consolidat de Recerca "Mineralogia Aplicada i Medi Ambient" 2001SGR00073, 2005SGR00933 i 2009SGR103 del Departament d'Universitats, Recerca i Societat de la Informació de la Generalitat de Catalunya, i del projecte *Avaluació de la contaminació per nitrat de les aigües subterrànies a la comarca del Lluçanès: Estudi de la dinàmica hidrogeològica i possiblitats de remediació* del Consell Comarcal d'Osona.

[...] la recullen a la mina *fican* la mà a la terra, com el que agafa un conill al cau, i per canons i canonades que l'engoleixen i se l'empassen com la nou del coll, la porten presa i lligada fins a la casa per tenir aigua viva i la fan servir per beure, per rentar i per regar, perquè com que és mansa com un anyell s'ho deixa fer tot i en fan el que en volen [...]

Francesc Pujols
L'evolució i els principis immutables
Barcelona, 1921

ABSTRACT

In the last decades, anthropogenic inputs of nitrogen to groundwater have dramatically increased, and they nowadays represent one of the most important water resources concerns as NO_3-N has become the most ubiquitous chemical contaminant in the world's aquifers. Agriculture, farming activities and wastewater seepage are the main anthropogenic sources of water contamination in rural areas. Another factor that is known to contribute to the decline of groundwater quality is excessive groundwater withdrawal in relation to the natural average recharge. Intensive groundwater exploitation regimes largely disturb hydrogeological systems modifying natural flow paths, altering relationships between groundwater recharge/discharge areas and modifying the flux among aquifer formations. All these human activities have affected the rates and quality of groundwater resources.

In order to address these issues, the origin, fate and transport of nitrate in groundwater have been extensively studied over the past decades. Stable isotope ratios of NO_3^- ($\delta^{15}N$ and $\delta^{18}O_{NO3}$), SO_4^{2-} ($\delta^{34}S$ and $\delta^{18}O_{SO4}$), B ($\delta^{11}B$) and C ($\delta^{13}C_{HCO3}$) have come to be successful tracers of pollution sources, and useful for assessing physico-chemical processes that affect pollutant fate. Aiming to fingerprint nitrate and sulfate sources and determine whether natural attenuation of pollution is occurring in groundwater, two nitrate vulnerable zones in Catalonia (NE Spain), the Selva and Baix Ter basins, have been studied applying multi-isotope and statistical approaches, in the frame of their hydrogeological settings. Both basins are characterized by regional and local, heterogeneous groundwater flow systems, disturbed by groundwater withdrawal from the different aquifer formations and at distinct rates and frequencies depending on the final water use (mainly for irrigation and for urban and farm supplies).

In accordance with potentiometric, hydrochemical and isotopic data, the hydrogeology of the Selva hydrogeological system has been described in order to characterize the alteration brought about in the system by intensive current groundwater withdrawal, and to define the resulting groundwater hydrodynamics. Hydraulic head data indicate the relationships between geological formations in the range areas and the sedimentary infill of the basin. Tectonic elements, such as fault zones and the basement fracture network, play a significant role in the flow behavior, since they have a direct effect on the recharge and allow upward vertical flow to the aquifers constituted by the sedimentary infilling. The use of fluoride and nitrate as tracers for the contribution of deep and shallow flow systems, respectively, provides a detailed portrait of the effects of pumping on the flow path distribution. Therefore, two distinct flow systems, with specific groundwater qualities, have been identified: a regional, large-scale, longer residence time nitrate-free system, recharged from the surrounding ranges, and a local flow system fed by rainfall infiltration in the lower areas of the basin, and affected by anthropogenic

activities. The interaction between both flow systems produces a dilution effect that modifies nitrate concentration. Indeed, hydrochemical data, along with $\delta^{15}N$, $\delta^{18}O_{NO3}$, $\delta^{34}S$, $\delta^{18}O_{SO4}$ and $\delta^{13}C_{HCO3}$ information, confirmed mixing between regional and local flow systems. The $\delta^{15}N$, $\delta^{18}O_{NO3}$ and $\delta^{34}S$ indicated that the predominant sources of contamination in the basin are pig manure and synthetic fertilizers. Apart from dilution processes that can contribute to the decrease of nitrate concentrations, the positive correlation between $\delta^{15}N$ and $\delta^{18}O_{NO3}$ agreed with the occurrence of denitrification processes. The $\delta^{34}S$ and $\delta^{18}O_{SO4}$ indicated that oxidation of pyrites is not linked to denitrification, suggesting organic matter to be an electron donor. However, $\delta^{13}C_{HCO3}$ did not point to the occurrence of organic matter oxidation. Thus, it is proposed that the mixing processes between deeper regional and local surface groundwater allow denitrification to occur due to the reducing conditions of the regional groundwater.

Results in the Baix Ter basin show a large range of groundwater nitrate concentrations, from no nitrate to up to 480 mg NO_3 L^{-1}. In the studied fluvio-deltaic formations $\delta^{15}N$ and $\delta^{18}O_{NO3}$ prove that natural denitrification is occurring, and in combination with $\delta^{11}B$, confirm that pig manure application is the main vector of nitrate pollution, although sewage and mineral fertilizers are also isotopically fingerprinted. The natural reduction of nitrate happens in near-river environments and in areas hydrologically related to fault zones. $\delta^{34}S$ and $\delta^{18}O_{SO4}$ indicate that denitrification is not linked to the pyrite oxidation, but rather to the oxidation of organic matter.

A statistical treatment attending to the compositional nature of available data has been applied using samples from five nitrate vulnerable zones in Catalonia: Baix Ter, Selva, Lluçanès, Maresme and Osona. Three different sets of variables have been used: only geochemical data, only isotope data, or both together. The aims were twofold. First, to establish a graphical comparative tool to discriminate between the different zones affected by nitrate pollution, looking for combinations of logratios of variables that have significantly different average values between the sampled regions. Second: to put forward a statistical methodology that integrates isotope data together with geochemical data. According to these aims, a linear discriminant analysis entering compositional data has been performed and the corresponding discriminant biplot has been depicted. It is remarkable the notable discriminating power when using only the isotope data set, although the optimal separation of regions is achieved when using both geochemical and isotope data subsets, as predicted by the theory of discriminant analysis.

Obtaining all this information can help to understand the mechanisms that control groundwater nitrate contamination, and to evaluate the influence of anthropogenic activities and pressures over the aquifer system at a local as well as regional scale, as a basis for adopting an appropriate water management strategy.

CONTENTS

1.INTRODUCTION

1.1 GROUNDWATER PROBLEMS

1.1.1 Groundwater contamination

Human activity changes groundwater quality of flow systems by introducing pollutants from different sources. The main groundwater quality problems are 1) salinisation processes, 2) mobilization of naturally occurring contamination (As, Fe, Al, etc.), and 3) anthropogenic pollution. Human distortion of groundwater systems accelerated markedly during the 20th century, as a result of massive groundwater exploitation for urban water-supply and irrigated agriculture, and radical land-use changes in many aquifer recharge zones. Anthropogenic groundwater pollution is the consequence of inadequate protection of vulnerable aquifers against intensification of agricultural cultivation and livestock farming, and discharges and leachates from urban, industrial and mining activities (Foster et al., 2013).

Modern agriculture is a major cause of environmental pollution (Rockström, 2009), and has had deep effects on groundwater geochemistry and water-rock interactions. In many areas of the world, the transfer of major-element chemical loads to shallow aquifers has been dominated by constituents derived directly or indirectly from agricultural practices. Close correlation between high nitrate (NO_3^-) concentrations in shallow groundwater and intensive agricultural cultivation has been widely reported (Böhlke, 2002).

While aquifers are much less vulnerable to anthropogenic pollution than surface water bodies, contamination becomes very persistent when they are damaged, (Wassenar et al., 2006; Sebilo et al., 2013) and it is difficult to remediate, as a result of their physical inaccessibility and porous structure (Foster et al., 2013). However, an important characteristic of soils is their potential for natural contaminant attenuation, which refers to any biotic or abiotic process that leads to a transformation and/or content decrease of a compound.

The development of effective management practices to preserve water quality, and remediation plans for sites that are already polluted, requires the identification of actual contaminant *sources* and an understanding of the *processes* affecting pollution in the aquifers. In particular, a better comprehension of hydrological flow paths and solute sources is necessary to determine the potential impact of contaminants on water supplies (Kendall et al., 2007). But, despite notable efforts intended to control and reduce groundwater contamination levels, the inertia of economic development and

human activities hampers the translation of increasing concerns about resource sustainability into effective government measures.

1.1.2 Hydrogeological system alterations

Expansion in groundwater exploitation has generated major socio-economic benefits, but in many cases current abstraction rates are not sustainable in the long-term, and some are associated with aquifer deterioration and decline of resource availability. The continuous growth in groundwater human demand has modified the natural water balance that defines the amount of available resources (Devlin and Sophocleos, 2005). An excessive groundwater withdrawal in relation to average natural recharge leads to the lowering of the water table over extensive areas, and more localized depletion around some major urban areas. Natural flow patterns and conditions of the hydrogeological system are modified through drawdown (Mahlknecht et al., 2006; Palmer et al., 2007; Li et al., 2008; Folch et al., 2011; Carucci et al., 2012; among others). The intrusion of low quality surface water or groundwater into a freshwater aquifer, because of this change in the hydraulic gradient due to groundwater abstraction, is a frequent cause of quality degradation. Groundwater pumped from wells located in altered aquifers can be a mixture of groundwater from different origins and of different qualities.

In the worst case scenario, an aquifer becomes stressed or overexploited (Custodio, 2002) when there is 1) decline in water levels, 2) deterioration of water quality, 3) land subsidence, 4) hydrological interference with streams and lakes, and 5) ecological impact on groundwater-dependent ecosystems. However, in some cases the existing problems are due to uncontrolled and unplanned groundwater development and not to excessive pumping (Llamas and Martínez-Santos, 2004).

1.2 NITRATE IN GROUNDWATER

1.2.1 Nitrogen cycle

Nitrogen (N) is a biologically active element that participates in a multitude of reactions important to life, and that affect water quality. N exhibits distinct oxidation states and, because of a wide variety of potential sources, it can be found in different chemical forms: nitrate (NO_3^-), nitrite (NO_2^-), ammonium (NH_4^+), organic N compounds (N_{org}), etc. The biogeochemical N cycle presents these various forms of N and the processes by

which they enter, are transformed and lost in the environment: fixation, volatilization, assimilation (uptake by plants, immobilization in soil), mineralization, nitrification, heterotrophic and autotrophic denitrification, dissimilatory nitrate reduction to ammonium (DNRA) and anammox (Fig. 1; Stevenson and Cole, 1999).

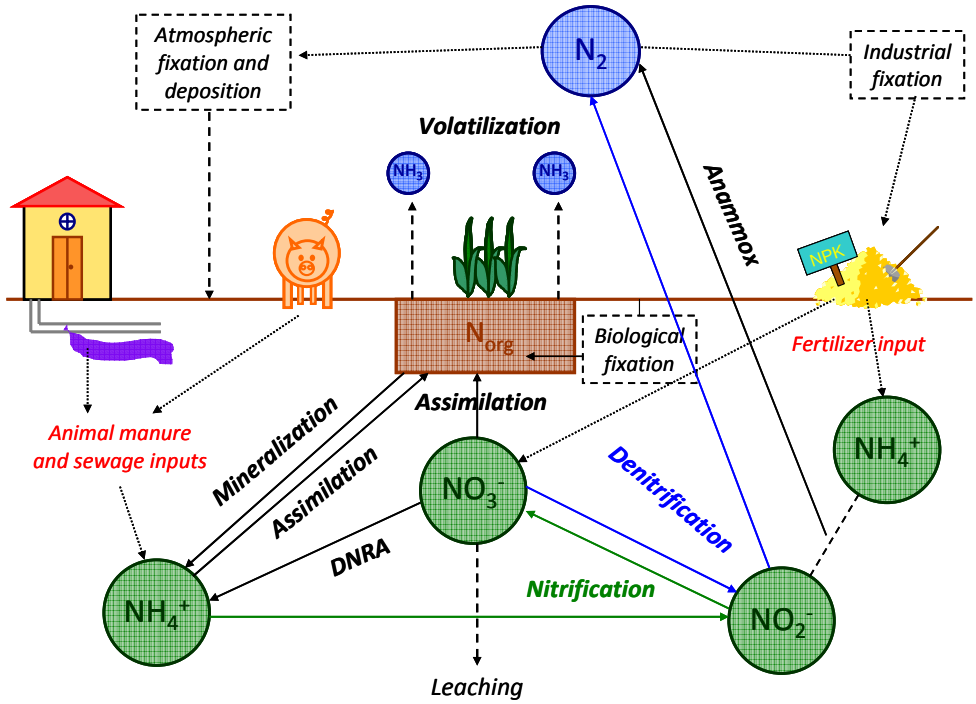

Figure 1. Processes involved in the biogeochemical N cycle.

Many of these processes are carried out by microbes, and affect directly N availability and the organic matter pool. The behavior of N in the environment is closely linked to the redox cycle of C, S, P, and trace elements such as Fe and Mn.

Atmospheric N (N_2) must be processed to become reactive, be used by plants and enter the water-soil system. The ways of transforming unreactive N_2 into other forms of N are:

- the *biological N fixation*, performed by some bacteria that are able to fix N as N_{org}
- the *industrial (human) N fixation*, that includes the Haber-Bosch process, used to make fertilizers and explosives, and the combustion of fossil fuels, which releases N oxides (NO_x)
- the *N fixation by lightning*, where NO is formed from N_2 and O_2 thanks to an enormous input of lightning energy.

1.2.2 Groundwater nitrate pollution

NO_3^- is one of the world's most common pollutants in terrestrial and aquatic ecosystems. Over the past century, humans have significantly impacted the global N cycle in terrestrial and aquatic ecosystems (Galloway et al., 2004), converting atmospheric N_2 into many reactive nitrogen forms (N_r), doubling the total fixation of N_r globally, and more than tripling it in Europe. Inputs of N_r to soils from both fertilizers and manure increased between 1970 and 2010 by ~20% for the EU (Sutton et al., 2011). The increased use of N_r as fertilizer allows a growing world population, but has considerable adverse effects on the environment and human health. Five key environmental and social threats of N_r can be identified: to groundwater and surface water quality, air quality, greenhouse balance, ecosystems and biodiversity, and soil quality (Sutton et al., 2011). Elevated NO_3^- concentrations present a water quality problem of growing concern because they lead to the quality declining of aquifer resources and the eutrophication of surface waters. NO_3^- concentrations in groundwater and rivers in developed areas of the world have risen substantially as a result of the use of synthetic and organic fertilizers and cultivation of N-fixing crops.

Agriculture is the largest contributor of N pollution in Europe (EEA, 2012), with NO_3^- concentrations in groundwater exceeding the international recommendations (WHO, 1993) for drinking water (50 mg NO_3 L^{-1}; Directive 98/83/EC; EC (1998)) under 22% of cultivated land. In 54% of the European groundwater bodies with poor chemical status, NO_3^- concentrations are excessive (EEA, 2012). In Catalonia (NE Spain), the threshold value for drinking water has also been exceeded in many aquifer systems. A total of 17 out of 53 groundwater bodies are classified "at risk" to not fulfill the good quality status in 2015 required by the Water Framework Directive, due to NO_3^- pollution (ACA, 2007).

The protection of drinking water quality often leads to conflicts: on the one hand, farmers have to produce foods to keep up with demand, and on the other hand, municipalities and government agencies have to preserve drinking water resources and public health (Bonton et al., 2010). Thus, it is important to better understand the NO_3^- contamination pattern in a vulnerable zone in order to support the decision-making process underlying the management of groundwater aquifers. The creation of strategies to tackle the problem of recovering groundwater quality and even removing N depends on the particular environmental, hydrogeological and socioeconomic characteristics of every territory.

1.2.3 Health concern

Although NO_3^- is of minor toxicity for human health, concerns arise from the potential bacterial reduction of NO_3^- to NO_2^- in the stomach, small intestine, and colon of individuals, which can be harmful to newborns and young children (methemoglobinemia, referred to as the "blue baby" syndrome) (Bryan et al., 2012; Ward et al., 2005; WHO, 2008). NO_3^- may also be implicated in the formation in human metabolism of nitrosamine compounds, which might promote the risk of cancer (Nolan and Hitt, 2006; U.S.EPA, 2006). As NH_4^+, it is toxic to aquatic life and contributes to oxygen demand.

1.2.4 Legal framework

Increasing NO_3^- pollution and a growing public health concern have caused European countries to enact legislation to address the problem (Laegreid et al., 1999). The *Nitrate Directive* (ND) (91/676/EC; EC, 1991) was a significant measure taken to tackle the water pollution situation in Europe, and it stated that the main non-point source of contamination is NO_3^- from agricultural activities. The ND aims to preserve waters against pollution caused by NO_3^- from agricultural sources, by establishing the designation of protection areas ("Nitrate Vulnerable Zones"), and regulating the amount of manure applications. Spain transposed this EU Directive into a law (Real Decreto 261/1996), whereas in Catalonia, by Decret 283/1998, Decret 476/2004 and Acord Gov/128/2009, 12 areas (Fig. 2) have been declared up to now as vulnerable to NO_3^- pollution, covering more than one third of the Catalan territory. The control and monitoring of these vulnerable zones is carried out by the "Agència Catalana de l'Aigua" (ACA) (Water Catalan Agency), which manages the protection of aquifers and water bodies in Catalonia.

The *Water Framework Directive* (WFD) (2000/60/EC; EC, 2000) proposed the objective of achieving a good status for European water bodies by 2015, including the reduction of NO_3^- levels, and therefore it posed the delimitation and characterization of groundwater bodies of each Member State. However, new terms will have to be set, because several aquifers will not fulfill by 2015 the conditions required by the WFD.

The *Groundwater Directive* (GD) (2006/118/EC; EC, 2006) was designed to complement the measures for preventing or limiting inputs of pollutants into groundwater already contained in the *Water Framework Directive*. The GD aims to go

against the deterioration of the status of all groundwater bodies by applying the following measures:

- establishing criteria for assessing the chemical status of groundwater
- establishing criteria for identifying significant and sustained upward trends in groundwater pollution levels, and for defining starting points for reversing these trends
- preventing and limiting indirect discharges (after percolation through soil or subsoil) of pollutants into groundwater.

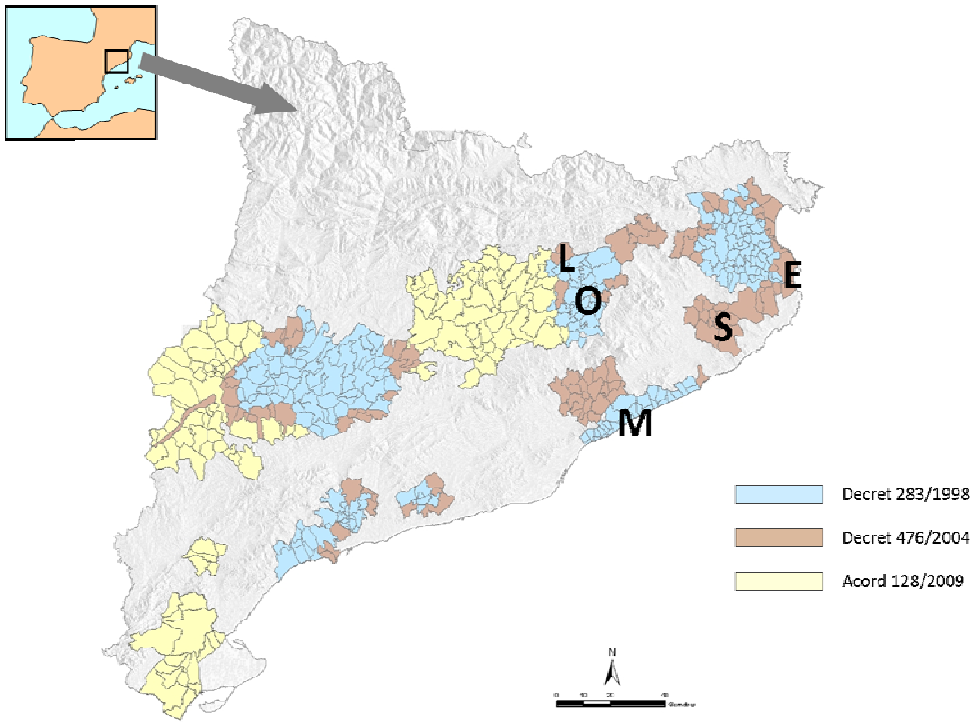

Figure 2. Vulnerable zones to NO_3^- pollution from agricultural sources in Catalonia (E, S, L, O and M indicate the five vulnerable zones compared in this thesis: "E" = Baix Ter (Empordà), "S" = Selva, "L" = Lluçanès, "O" = Osona and "M" = Maresme) (from ACA data).

Regarding a better management of N fertilizer in agricultural and livestock activities, many efforts have been made from the Catalan Government by the "Departament de Medi Ambient i Habitatge" (Environment and Housing Department) and the "Departament d'Agricultura, Alimentació i Acció Rural" (Agriculture, Food and Rural Action Department) approving the following strategies and legislation:

- the code of agricultural beneficial management practices (1998)
- the implementation of the program of agricultural measures in vulnerable zones to nitrate pollution from agricultural sources

- the application of a livestock manure management program (Decret 220/2001)
- strategic plan of agricultural fertilization and livestock manure management in Catalonia (2013-2016)

1.3 ISOTOPES, PROCESSES AND SOURCES

1.3.1 Stable nitrogen and oxygen isotopes

There are two naturally occurring stable isotopes of N: ^{14}N and ^{15}N. The majority of N in the atmosphere is composed of ^{14}N (99.64%) and the remainder of ^{15}N (0.36%). Oxygen is composed of three stable isotopes: ^{16}O (99.763%), ^{17}O (0.0375%) and ^{18}O (0.1995%). Stable isotope ratios are usually expressed by the notation of isotopic deviation (δ) per mil (‰) units relative to the respective international standards or reference materials:

$$\delta_{sample}(‰) = \left[\frac{(R_{sample} - R_{standard})}{R_{standard}} \right] \times 1000$$

where R is the ($^{15}N/^{14}N$) or ($^{18}O/^{16}O$) of the sample and standard for $\delta^{15}N$ and $\delta^{18}O$, respectively (Clark and Fritz, 1997). $\delta^{15}N$ values are reported relative to atmospheric air and $\delta^{18}O$ values relative to Vienna Standard Mean Ocean Water (VSMOW). When δ_{sample} is positive, it indicates enrichment in the heavy isotope, while when δ_{sample} is negative, it indicates depletion.

Stable isotopes undergo kinetic isotopic fractionation, which results in depleted products, while the remaining element becomes gradually more enriched with the heavy isotope. This enhancement is characterized by the *isotopic fractionation* (ε) in ‰ which, in a closed system, can be expressed by the following Rayleigh equation:

$$\delta_t = \delta_0 + \varepsilon \ln\left(\frac{c_t}{c_0}\right)$$

where δ_0 and δ_t represent the initial and residual isotopic compositions, and c_0 and c_t are the initial and residual concentrations of the element, respectively. This equation can be used to calculate ε by plotting measured values of δ_t against $\ln(c_t/c_0)$.

1.3.2 Analysis methods

For the determination of $\delta^{15}N$ and $\delta^{18}O$ of NO_3^-, three analytical techniques have been developed in the last decade:

- *the anion-exchange or $AgNO_3$ method* (Silva et al., 2000):

  All oxygen-bearing anions except NO_3^- are firstly removed from the sample by adding $BaCl_2$ and then filtering the precipitate out. Next, NO_3^- is extracted by passing samples through anion exchange resin columns. NO_3^- is eluted using HCl, neutralized with Ag_2O and then filtered to remove the AgCl. The resulting solution is freeze-dried to produce the $AgNO_3$ salt. $\delta^{15}N$ analysis of the obtained $AgNO_3$ is conducted by conversion to N_2 gas for Isotope-Ratio Mass Spectrometry (IRMS) analysis. $\delta^{18}O$ analysis can be performed using pyrolisis systems that can generate CO by addition of graphite.

- *the bacterial denitrification method* (Sigman et al., 2001; Casciotti et al., 2002)

  This method allows for the simultaneous determination of $\delta^{15}N$ and $\delta^{18}O$ of N_2O produced from the conversion of NO_3^- by denitrifying bacteria which naturally lack the enzyme that catalyses the reduction of N_2O to N_2.

- *the cadmium reduction method* (McIlvin and Altabet, 2005)

  This method consists of two-step chemical reduction procedure: first, conversion of NO_3^- to NO_2^- using cadmium reduction, and then a subsequent reduction of $NO_2^-$to N_2O using sodium azide.

1.3.3 Multi-isotope approach

When aquifer systems show a hydrogeological complexity and multiple potential N sources, distinguishing to what extent different sources are contributing to the observed NO_3^- level in groundwater, as well as reporting the occurrence of dilution, dispersion or denitrification processes, based on the sole concentration measurements, is a tough task. Even when abundant information about the area (i.e., hydrogeology of the zone, soil characteristics, etc.) is available, discriminating source contributions is highly uncertain. This problem can be overcome analyzing nitrogen ($\delta^{15}N$) and oxygen ($\delta^{18}O$) isotopic compositions of NO_3^- dissolved in groundwater. The use of NO_3^- isotopes to trace N

sources and reactions in hydrology gained further attention when it became possible to routinely measure the ^{18}O-contents of NO_3^- (Amberger and Schmidt, 1987). This dual-isotope approach has been extensively used because it enables to distinguish between NO_3^- of different origin (either natural or anthropogenic sources), to estimate semi-quantitatively contributions from distinct sources, to recognize denitrification processes, and to assess the N-budget in the soil-water system (Aravena and Mayer, 2010; Kendall, 1998; Kendall et al., 2007).

Nevertheless, this isotope tool shows some limitations (Xue et al., 2009). With only hydrochemical data and NO_3^- stable isotopes, determining whether groundwater NO_3^- stems either from manure or sewage NH_4^+ is difficult because the isotopic ranges of both sources overlap. Moreover, processes such as volatilization and natural denitrification significantly shift the original isotope compositions of the NO_3^- sources involved. Then, NO_3^- isotopes can be combined with co-migrating discriminators of NO_3^- sources which are not isotopically affected by the same transformation processes (e.g. ^{11}B).

B has two stable isotopes, ^{10}B and ^{11}B, whose abundances are 19.9 and 80.1%, respectively. $\delta^{11}B$ values of natural waters (seawater, river water, rainwater, groundwater, brines, geothermal fluids, etc.) range from -16‰ to +60‰ (Tirez et al., 2010). This wide range of $\delta^{11}B$ may result in significant contrasts between B sources in groundwater. Natural dissolved B in aqueous solutions is principally derived from weathering of rocks, and is present in two dominant species: boric acid $B(OH)_3$ and the borate anion $[B(OH)_4]^-$. The main human application of B is the use of sodium perborate ($NaBO_3 \cdot nH_2O$) as an oxidation bleaching agent in domestic and industrial cleaning products (detergents, soaps, toothpaste, etc.). B is thus commonly detected in anthropogenic wastewater (Barth, 1998). The first studies of B isotopes were intended to discriminate the influence of wastewater dominated by synthetic B in water resources (Vengosh et al., 1994; Basset et al., 1995). Komor (1997), Seiler (2005) and Widory (2004, 2005 and 2013) used $\delta^{11}B$ data coupled with $\delta^{15}N$ and $\delta^{18}O$ of NO_3 in order to distinguish contributions from animal manure, sewage and mineral fertilizers. Hence, B isotopes are useful tracers for identifying contaminant sources of groundwater and surface waters in semirural zones where agricultural and farming practices cohabitate with industrial and urban activities.

$\delta^{15}N$ and $\delta^{18}O$ of NO_3^- can also be influenced by isotopic fractionation during chemical reactions of N compounds. These fractionation processes may largely constrain the accuracy of NO_3^- identification since they might be masking each other. Thus, isotopic analysis of SO_4^{2-} ($\delta^{34}S$ and $\delta^{18}O$) and dissolved inorganic C ($\delta^{13}C_{DIC}$) is a supplementary tool to better examine the origin of contaminants, and to evaluate the transformations undergone by them (Krouse and Van Everdingen, 1986; Krouse et al., 1991; Clark and Fritz, 1997) and which electron donors are promoting denitrification (Schwientek et al., 2008; Otero et al., 2009).

Apart from identifying contaminant sources, a multi-isotope approach offers a deeper understanding of how the extent of contamination is affected by hydrogeology and groundwater management practices (Moore et al., 2006).

1.3.4 Origin, transport and fate of nitrogen

To evaluate the NO_3^- impact on contaminated aquifers, the main issues that need to be addressed, always considering the hydrogeological context, are: (1) geochemical processes that control the NO_3^- concentration in the aquifer, and (2) main sources of the contamination (Aravena and Mayer, 2010).

1.3.4.1 Processes affecting the isotopic composition of nitrogen compounds

It is necessary to know how processes involved in the N cycle (Fig. 1) influence the isotope composition of the main N pools in the unsaturated and saturated zones.

Volatilization

Volatilization of NH_3 is a process derived from the hydrolysis of urea ($CO(NH_2)_2$) consisting in the loss of $NH_{3(g)}$ to the atmosphere (Eq. 1). It occurs in manure ponds, fertilized fields and in the unsaturated zone.

$$CO(NH_2)_2 + H_2O \rightarrow CO_2 + 2\overset{\nearrow NH_{3(g)}\uparrow}{NH_3} \leftrightarrow NH_4^+ \qquad (1)$$

$NH_{3(g)}$ produced has a lower $\delta^{15}N$ value than the residual NH_4^+, because volatilization of $^{14}NH_3$ is kinetically favored over volatilization of $^{15}NH_3$. Hence it can be a highly fractionating process.

The main biologically mediated reactions that control N dynamics in soil and groundwater are assimilation, nitrification and denitrification (Kendall, 2007; Aravena and Mayer, 2010) (Fig. 3). If these reactions are not complete, they commonly result in the increase of the residual $\delta^{15}N$ and the depletion of the $\delta^{15}N$ of the product.

Assimilation

Assimilation is the transformation of inorganic N-bearing compounds into N_{org} during biosynthesis by living organisms (incorporating N into cellular constituents). Plants take N from the soil by absorption through their roots in the form of either NO_3^- or NH_4^+ ions. This process usually does not significantly change the $\delta^{15}N$ of the N source in soils (Aravena and Mayer, 2010)

When plants die, biomass decays and N_{org} is released. Then bacteria transform this N_{org} into NH_4^+ in a process in the opposite direction of assimilation called mineralization (or ammonification). This process usually causes only a small fractionation (±1‰) between soil N_{org} and soil NH_4^+ (Kendall et al., 2007).

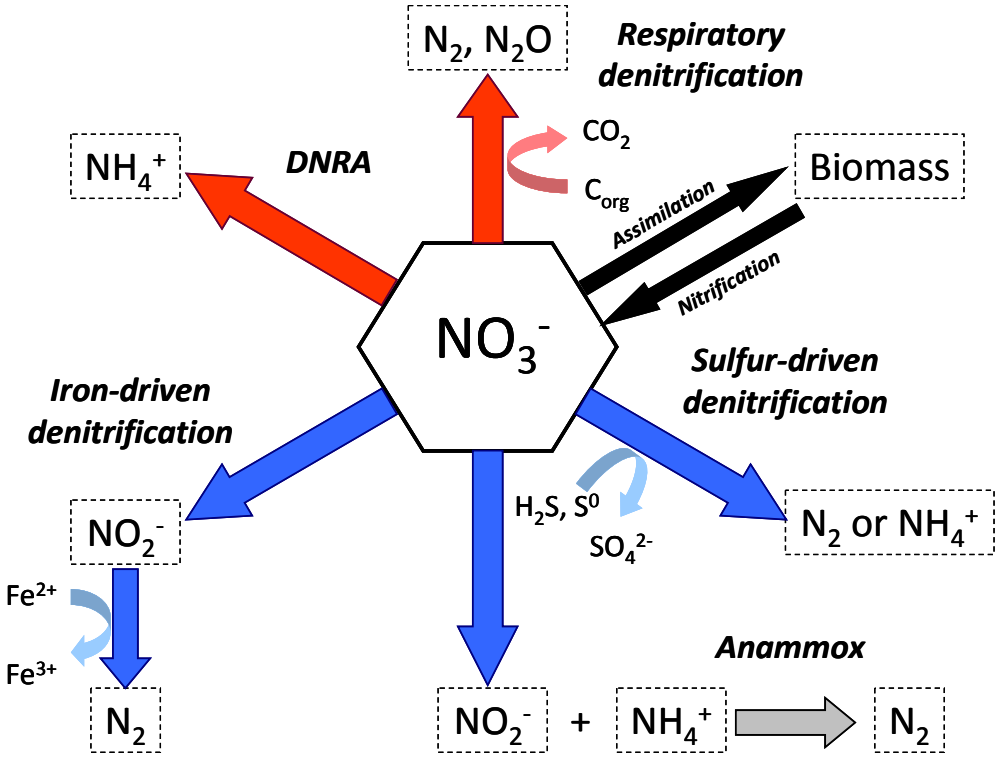

Figure 3. Different pathways and fates of NO_3 removal. Blue and red arrows illustrate autotrophic and heterotrophic pathways, respectively (from Burgin and Hamilton (2007)).

Nitrification

Nitrification is the NH_4^+ oxidation to NO_3^-, and consists of a two-step process where various byproducts can also be produced and released into the environment including aqueous and gaseous compounds (e.g., NO_2^-, NO, N_2O) (Eq. 2). Most of the N that reaches groundwater appears in the oxidized form of NO_3^-, since the availability of oxygen in the unsaturated zone allows nitrification to occur.

$$NH_4^+ \rightarrow NO_2^- \rightarrow NO_3^- \quad (2)$$

NH_4^+ is often rapidly and completely converted to NO_3^-, and in that case the N isotopic composition tends to reflect the isotopic composition of the NH_4^+ source. The $\delta^{18}O$ resulting from nitrification is controlled by the isotopic composition of the O sources (H_2O and O_2). During nitrification reactions, two O atoms from H_2O and one from dissolved atmospheric O_2 are incorporated. Thus, $\delta^{18}O_{NO3}$ is usually calculated as follows:

$$\delta^{18}O_{NO3} = \frac{2}{3}(\delta^{18}O_{H2O}) + \frac{1}{3}\left(\delta^{18}O_{O2}\right) \quad (3)$$

where $\delta^{18}O_{H2O}$ is assumed to be that of groundwater, and $\delta^{18}O_{O2}$ is the $\delta^{18}O$ of atmospheric O_2 (+23.5‰; Kroopnick and Craig, 1972).

Denitrification

Denitrification is a microbially mediated redox process that reduces NO_3^- to gaseous products (N_2, N_2O, or NO) under anaerobic conditions and abundant NO_3^- input, though it has been reported that some organisms can denitrify even in the presence of some O (Rivett et al., 2008). Denitrification is the main natural attenuation process of NO_3^- contamination in groundwater. It has been observed in many fissured and porous confined aquifers, and it is also probable to occur in near-river environments (i.e., riparian and hyporheic zones) (Cey et al., 1999).

Since denitrifying bacteria appear to be almost ubiquitous in the subsurface, denitrification requires the following constraints to be met:

- presence of NO_3^-
- presence of anaerobic conditions

- favorable environmental conditions (e.g. temperature, pH, other nutrients and trace elements)
- the presence of a suitable electron donor (most commonly organic C, but also reduced Fe and/or reduced S)

The microbial availability of electron donors is usually identified as the major critical factor limiting denitrification rates in aquifers.

During denitrification, while NO_3^- concentration decreases, the isotopically light NO_3^- molecules tend to be reduced faster than the isotopically heavy ones. As a consequence, the residual NO_3^- is enriched in the heavy isotopes (^{15}N and ^{18}O), with a relative isotopic fractionation of N and O isotopes ($\varepsilon_N/\varepsilon_O$) ranging between 1.3 (Fukada et al., 2003) and 2.1 (Böttcher et al., 1990), and depending on the aquifer materials and characteristics (Mariotti et al., 1981). Thus, isotope ratio analysis of NO_3^- dissolved in groundwater is an effective tool to show the occurrence of natural denitrification in aquifers, discriminating from other natural attenuation processes that do not shift the NO_3^- isotope composition, like dilution and dispersion, which also result in a decrease in N concentrations, but do not lead to the reduction of the contaminant mass within the aquifer.

The main mechanism for natural denitrification in soils and aquifers is *NO_3^- reduction by heterotrophic bacteria*. Heterotrophic respiration of organic matter can be either aerobic or anaerobic. Both forms of respiration are redox reactions, in which organic C compounds are combined with electron acceptors (O_2, NO_3^-, Fe^{3+}, SO_4^{2-}) to yield oxidized C (CO_2), reduced products (H_2O, N_2, Fe^{2+}, H_2S), and energy (Eq. 4). The respiratory denitrification (Fig. 3) is a form of anaerobic respiration in which organic C is consumed, and NO_3^- serves as an electron acceptor different than O_2:

$$4NO_3^- + 5CH_2O \rightarrow 2N_2 + 4HCO_3^- + CO_2 + 3H_2O \qquad (4)$$

Former research emphasized plant or microbial uptake (assimilation) or respiratory (heterotrophic) denitrification by bacteria as the main NO_3^- removal processes. However, the increasing application of stable isotopes to the study of NO_3^- removal has yielded evidences for alternative microbially mediated processes of NO_3^- transformation (Burgin and Hamilton, 2007; Borch et al., 2010; Rivett el al., 2008). These include:

Chemo-autotrophic denitrification (via S or Fe oxidation)

NO_3^- reduction by sulfide oxidation is a naturally occurring process mediated by bacteria such as *Thiobacillus denitrificans*. This denitrification reaction coupled to oxidation of reduced-S (e.g., pyrite) can be an important NO_3^- removal pathway in fertilizer-impacted aquifers (Schwientek et al., 2008). The S isotope composition of the groundwater SO_4^{2-} tends toward the usually negative $\delta^{34}S$ values of the sedimentary pyrite in the aquifer, while $\delta^{18}O_{SO4}$ shows lighter values than that of SO_4^{2-} coming from dissolution of SO_4^{2-}, due to the oxygen equilibrium with water. SO_4^{2-} concentrations increase following the reaction:

$$14NO_3^- + 5FeS_2 + 4H^+ \rightarrow 7N_2 + 10SO_4^{2-} + 5Fe^{2+} + 2H_2O \quad (5)$$

Furthermore, NO_3^- reduction can also take place through oxidation of Fe^{2+} (Eq. 6; Postma et al., 1991):

$$NO_3^- + 5Fe^{2+} + 6H^+ \rightarrow 1/2N_2 + 5Fe^{3+} + 3H_2O \quad (6)$$

Dissimilatory NO_3^- reduction to NH_4^+ (DNRA)

The *DNRA* is an anaerobic reduction process mediated by fermentative bacteria that converts NO_3^- into NH_4^+ (Eq. 7), in contrast to assimilatory processes that incorporate N into cellular constituents. It is thought to be favored in environments rich in labile C when NO_3^- is limited, while respiratory denitrification would be favored under carbon-limited conditions (Burgin and Hamilton, 2007).

$$NO_3^- + 2CH_2O + 2H^+ \rightarrow NH_4^+ + 2CO_2 + H_2O \quad (7)$$

NH_4^+ produced from DNRA has a much lower $\delta^{15}N$ than the original NO_3^- (McCready et al., 1983).

Anammox

Anaerobic ammonium oxidation (*anammox*) is an autotrophic process by which NH_4^+ is combined with NO_2^- under anaerobic conditions, yielding N_2 (Eq. 8). The NO_2^- is derived from the reduction of NO_3^-, possibly by denitrifying bacteria. According to

Brunner et al. (2013), for the anammox N isotope effects to be fully expressed in the environment, both NH_4^+ and NO_2^- have to be in excess.

$$NH_4^+ + NO_2^- \rightarrow N_2 + 2H_2O \quad (8)$$

1.3.4.2 Isotope fingerprinting of N sources in water

Cultivation-induced mineralization of soil N, mineral fertilizers, animal and sewage wastes, and industrial emissions or residues are the main sources of NO_3^- pollution in the hydrosphere (Heaton, 1986). They can be divided according to their origin (natural or anthropogenic sources) or their spatial and temporal distribution (point or diffuse sources). From Aravena and Mayer (2010) and Llamas and Martínez-Santos (2004), among other authors, NO_3^- pollution in groundwater is mainly attributed to sources associated with:

1) Agricultural and farming practices

These practices range from extensive dry land grazing to intensive animal feeding units, and from dry land cultivation to large irrigation schemes. The spreading and storage of fertilizers may result in the infiltration/leaching of surplus of N into aquifers. The application of synthetic and organic fertilizers has often been excessive in comparison with the N need of crops, i.e. fertilizers might have been overused when the soil and/or the groundwater used for irrigation were already rich in N. Irrigation return, leaking slurry or manure tanks, and abandoned wells are other husbandry sources of contamination. Hence, improvement of N fertilizer management practices is a key point in dealing with NO_3^- contamination problem.

2) Urban and industrial activities

The N impact of sewage on groundwater can be due to the seepage of sewer or drainage network in urban areas, leaking septic systems and cesspools, spillage of sewage without previous treatment to channels, the discharge into streams from water treatment plants, the use of treated wastewater for irrigation, street washing, urban solid waste landfills, effluents from infrastructures like secondary roads, urban areas out of the nucleus, golf courses, atmospheric emissions from vehicles, etc. Leaching from landfills, mine tailings, and atmospheric emissions from power plants can be considered industrial sources of N.

The specific differentiation between sources of fecal contamination is of particular importance, because the risk to humans is usually considered higher from human fecal waste than from animal fecal residue (Fenech et al., 2012).

Mineral Fertilizers

Synthetic N fertilizers generally have N isotope values that fall within a relatively narrow range close to 0‰, in accordance with the $\delta^{15}N$ of atmospheric N, the N source for fertilizers production (industrial N fixation). Data summarized by Kendall (2007) show the great majority of NH_3-containing fertilizers have $\delta^{15}N$ values of 0‰ or lower. In the literature is considered that $\delta^{15}N$ values of mineral fertilizers range between -4 and +4‰ (Xue et al., 2009; Aravena and Mayer, 2010; Table 1). Synthetic NO_3^- fertilizers present $\delta^{18}O_{NO3}$ values between +17‰ and +25‰ (Vitòria et al., 2004b) because their O is derived from atmospheric O_2, whose $\delta^{18}O$ value is around +20‰ (+23.5‰; Kroopnick and Craig, 1972).

$\delta^{11}B$ values of mineral fertilizers reported in the literature range from +8‰ to +17‰ (Xue et al., 2009), but some other studies reported a range between -9‰ and +15‰ (Widory et al., 2005).

Animal and human waste

N isotopic compositions of manure are quite well established and generally have higher $\delta^{15}N$ values and a much wider range of compositions than synthetic fertilizers, reflecting their more diverse origins. Animal manure tends to become isotopically heavier over time due to volatilization of NH_3.

In Catalonia, Vitòria (2004) determined a $\delta^{15}N$ range from +8‰ to +15‰ for pig manure, and Curt et al. (2004) reported for three different vulnerable zones to NO_3^- contamination in Spain a very wide isotopic range for animal waste that overlapped the range found for sludge and effluents from waste-water treatment plants, indicating that these two NO_3^- sources are isotopically indistinguishable.

Animal manure contains B as a minor or trace element. The $\delta^{11}B$ values reported for different types of manure range from +6.9‰ to +42.1‰, and for pig manure are higher than the $\delta^{11}B$ values reported for fertilizers and sewage (Table 1). $\delta^{11}B$ values of sewage reported in the literature range from -7.7‰ to +12.9‰ (Xue et al., 2009).

Soils

N in soil can occur in several forms: as mineral N, as organic N in plants through fixation of atmospheric N, and in bacteria or in soil fauna. The $\delta^{15}N$ range reported for NO_3^- originated in soil organic matter is between +3 and +8‰ (Heaton, 1986; Kendall, 2007; Aravena and Mayer, 2010; Table 1). N isotopic composition of soil N can also be the consequence of land uses thanks to the assimilation processes of mineral N. Crops grown using synthetic N fertilizers have lower N isotope values than crops grown using manure-based fertilizers (Bateman et al., 2005; Yun et al., 2006). To our knowledge, B isotope compositions of agricultural soils have never been reported.

In order to use the multi-isotope approach to discriminate sources and identify process more easily, we summarized from the literature NO_3^-, SO_4^{2-}, B and DIC isotopic composition ranges of the potential NO_3^- sources in Catalonia (Table 1).

Table 1. NO_3^-, SO_4^{2-}, B and dissolved inorganic carbon (DIC, HCO_3^-) isotopic composition ranges of the potential NO_3^- sources.

NO_3^- source / Isotope ratio (‰)	Pig manure	Mineral fertilizers	Sewage	Soil
$\delta^{15}N$	+8 — +16	-4 — +4	+8 — +20	+3 — +8
	Vitòria (2004)	*Bateman and Kelly (2007), Kendall et al. (2007), Vitòria et al. (2004b)*	*Aravena and Mayer (2010), Curt el al. (2004)*	*Aravena and Mayer (2010), Heaton (1986), Kendall et al. (2007)*
$\delta^{18}O_{NO3}$	$2/3(\delta^{18}O_{H2O}) + 1/3(\delta^{18}O_{O2})$	+17 — +25	$2/3(\delta^{18}O_{H2O}) + 1/3(\delta^{18}O_{O2})$	$2/3(\delta^{18}O_{H2O}) + 1/3(\delta^{18}O_{O2})$
	Kendall et al. (2007)	*Aravena and Mayer (2010), Vitòria et al. (2004b), Xue et al. (2009)*	*Kendall et al. (2007)*	*Kendall et al. (2007)*
$\delta^{34}S$	-0,9 — +5,8	0 — +10	+7,6 — +11,7	0 — +6
	Cravotta (1997)	*Vitòria et al. (2004b)*	*Otero et al. (2008)*	*Krouse and Mayer (2000)*
$\delta^{18}O_{SO4}$	+3,8 — +6	+9 — +15	+9 — +11,1	0 — +6
	Otero et al. (2007), Vitòria (2004)	*Vitòria et al. (2004b)*	*Otero et al. (2008)*	*Krouse and Mayer (2000)*
$\delta^{11}B$	+19,5 — +42,4	-9 — +15	-7,7 — +12,9	-
	Widory et al. (2005)	*Komor (1997), Widory et al. (2005), (2013)*	*Bassett et al. (1995), Vengosh et al. (1994), Widory et al. (2013), Xue et al. (2009)*	-
$\delta^{13}C_{HCO3}$	-23,8 — -16,4	-35 — -24	-25 — -13	-23
	Cravotta (1997), Vitòria (2004)	*Vitòria et al. (2004b)*	*Jurado et al. (2013), Li et al. (2010), Waldron et al. (2001)*	*Clark and Fritz (1997)*

1.4 COMPOSITIONAL DATA ANALYSIS

A *composition* is a set of numbers that carries only information regarding the relative weight or abundance of each component in the whole. Compositions are mathematically defined as vectors whose components are positive and sum up to a given constant (Bacon-Shone, 2011). Thus, each set of hydrochemical data (e.g., major anions and cations) constitutes a composition. When conventional statistics is applied to compositional data, the particular characteristics of compositions make the widely-used

classical techniques to lose their meaning. For instance, correlation coefficients computed from raw compositions may give confusing information.

Aitchison (1982) was the first to set up an alternative approach to classical treatments in order to avoid this problem when dealing with compositional data; he proposed:

- transforming the sample compositions through *log-ratios* (*clr* = centred log-ratio, *ilr* = isometric log-ratio)), then applying the standard statistical procedures to the transformed data, and finally back-transforming the results, which is equivalent to:

- defining a *compositional distance* between compositions more suitable to compare them than the Euclidean distance, and a new set of operations.

Geometrically, given a composition with D positive-valued components whose total sum is a constant (κ), the set of points in the real space (R^D) that fulfill both conditions is the support space of compositions called the *D-part simplex* (S^D):

$$S^D = \left\{ x = x_1, x_2, ...x_D \middle| x_i > 0 \wedge \sum_{i=1}^{D} x_i = \kappa \right\} \qquad (9)$$

Simple ways to summarize and display multivariate data are:

- the *linear discriminant analysis* (LDA), whose goal is to find directions of the real space where the separation between the sample groups is optimal.

- the *singular value decomposition* and its graphical representation, the *biplot* (Gabriel, 1971), which provide the necessary tools for analyzing compositional data when adapted to the simplex (Aitchison and Greenacre, 2002). The linear biplot is a powerful graphical technique intended to reveal linear relationships amongst variables (expressed as rays) and samples or observations (expressed as dots). The ray length is proportional to the variance of the variable it represents, exactly to the variance explained by the 2-dimensional system. The discriminant

biplot is a joint graphical representation of variables and observations devised to display differences between groups.

Hydrochemical and isotope data sets obtained in the last decade from the study of different vulnerable zones to NO_3^- contamination in Catalonia (Maresme, Osona, Baix Ter-Empordà, La Selva and Lluçanès) posed the idea of making a comparative analysis between them in order to achieve a more global view of the pollution state in the aquifers. Since hydrochemical data must be considered as compositional data, the statistic treatment chosen is based on the approach established by Aitchison (1982).

2.HYPOTHESIS

2.1 HYPOTHESIS

Due to the intensive anthropogenic pressures on groundwater resources in many of the Catalan aquifers, investigating sources and processes involved in the evolution and fate of NO_3^- contamination has been one of the main research lines developed by the Consolidated Research Group of *Mineralogia Aplicada i Medi Ambient* (MAiMA) (Departament de Cristal·lografia, Mineralogia i Dipòsits Minerals, Facultat de Geologia, Universitat de Barcelona) in the last decade. The background motivation of studying the alteration state of aquifers and the natural and/or induced attenuation processes is bringing a chance to improve environmental conditions, as well as to restore water quality for the benefit of human supply and ecological preservation.

Results obtained in the previous studies and projects carried out by MAiMA have demonstrated the usefulness of the analysis of NO_3^- ($\delta^{15}N$ and $\delta^{18}O$), SO_4^{2-} ($\delta^{34}S$ and $\delta^{18}O$) and dissolved inorganic carbon ($\delta^{13}C_{DIC}$) isotopes as tracers of the origin of the contamination, and as indicators of the occurrence of natural attenuation processes and of which reactions or electron donors control it (Otero et al., 2007; Otero et al., 2009; Vitòria, 2004; Vitòria et al., 2008). To summarize, this research consisted in the laboratory-scale implementation of all these multi-isotope tools, the subsequent application at the field-scale, and the analysis and interpretation of isotope data as a powerful complement to hydrochemical and hydrogeological data. It was found and confirmed that multi-isotope approaches work successfully in NO_3^- vulnerable zones affected by a specific, prevailing and well-known contamination source: synthetic fertilizers, in the case study of Maresme area (Vitòria, 2004; Vitòria et al., 2005), and pig manure, in the case of Osona area (Otero et al., 2009; Vitòria et al., 2008).

Based on this previous research, the logical following step is using the multi-isotope methodology in other more heterogeneous NO_3^- vulnerable zones of Catalonia, e.g. Baix Ter-Empordà, Selva and Lluçanès. Unlike Maresme and Osona, Baix Ter-Empordà and Selva vulnerable zones are characterized by 1) the presence of multiple NO_3^- sources, without a prevailing one over the others, 2) the presence of various anthropogenic activities and pressures (heavy groundwater withdrawal regimes, abundant stock breeding and crop cultivation), and 3) hydrogeological systems constituted by multilayered aquifers. This hydrogeological complexity appears from the presence of converging regional and local flow systems, and also from different degrees

of connectivity between distinct aquifers, giving rise to mixing processes, which in turn are enhanced by the human abstraction activity in the area (Menció et al., 2011). Thus, when applying a multi-isotope approach in this type of areas, we must also take into account the *mixing processes* of groundwater with different origin and chemical composition, because they will influence the hydrochemistry and isotope ratios of the resulting groundwater.

According to this study framework, the primary hypothesis of our research puts forward that in areas where the main cause of NO_3^- contamination is uncertain a priori, and where complex hydrogeological systems present an added handicap, the combination of hydrochemical and isotope data should help to characterize the state of aquifer pollution, to discriminate between potential sources, and to assess the biogeochemical processes that might occur in the subsoil, reaching a deeper insight into NO_3^- contamination problem.

2.2 OBJECTIVES

Under the basic premise previously described, we state a set of specific aims:

1. To characterize the impact of groundwater development on hydrodynamics, and to determine the influence of local and regional groundwater mixing over NO_3^- pollution evolution, in large-scale flow systems such as the Selva and Baix Ter basins, by means of the use of groundwater isotopes.
2. To validate in a more heterogeneous aquifer system the combined use of $\delta^{15}N$ and $\delta^{18}O$ of dissolved NO_3^- in order to identify the main sources of groundwater NO_3^- pollution.
3. To validate the use of B isotope ratio ($\delta^{11}B$) in order to discriminate nitrate pollution from livestock and urban origins.
4. To determine and evaluate the different natural attenuation processes that occur with the isotope compositions of NO_3^- and the other ions (SO_4^{2-}, HCO_3^-) involved in the chemical reactions that control these processes.
5. To compare the different studied vulnerable zones (Baix Ter-Empordà, Selva, Lluçanès, Maresme and Osona) through the application of a suitable statistical treatment (compositional data analysis) that permits integrating isotope data

together with geochemical data, in order to characterize and distinguish zones in accordance with the NO_3^- origin and the dominant processes controlling denitrification.

2.3 OUTLINE

The "Introduction" describes the previous knowledge and the specific environmental problem that motivates the research work developed in this doctoral thesis. Next, hypothesis and specific goals to be achieved are shown as the starting point. In the "Synthesis" section, results and discussions of each publication are summarized, and in the "Thesis" section the general conclusions are presented. The "Annexes" section consists of the four publications as they have appeared in the final published editions (except "Annex 3").

In the "Annex 1", the paper characterizes the effects of intensive groundwater exploitation on hydrodynamics and water resources quality of the large-scale flow system in the Selva basin, from potentiometric, hydrochemical and water isotope data collected in the area. Results reflect the changes in the pattern of local and regional flows produced by pumping activity, the relationship between geological formations of mountain ranges and the sedimentary infilling of the basin, as well as the influence exerted by fault zones and fracture networks in the recharge of the system.

The paper of "Annex 2" shows how a multi-isotope approach applied in the Selva basin, with distinct potential N contaminant sources, indicates that the main contributions of N in groundwater come from manure and mineral fertilizers. The study also shows that NO_3^- natural attenuation is occurring, and that it is more closely linked to oxidation of organic matter. In addition, the combined analysis of hydrogeological, hydrochemical and isotope data suggests that mixing of local and regional groundwater flows, besides causing dilution processes, also promotes denitrification due to the reducing conditions of some deep regional flows.

In another NO_3^- vulnerable zone, the Baix Ter-Empordà aquifer system, the multi-isotope approach presented in "Annex 3" demonstrates that dissolved NO_3^- in groundwater originates mainly from pig manure, although SO_4^{2-} and B isotopes indicate a non-negligible contribution of sewage and mineral fertilizers. The analysis of $\delta^{11}B$ confirms that pig manure is the main source of NO_3^- pollution. NO_3^- isotopes show that

NO_3^- natural attenuation is occurring, and SO_4^{2-} isotopes, that it is not controlled by the pyrites oxidation but rather by the oxidation of organic matter. Data also suggest that heterotrophic denitrification could be favored by either river-aquifer interactions, the presence of organic matter levels in near-river areas, or, by mixing between contaminated groundwater and deeper flows with reducing conditions, in fault zones, similarly as it happens in La Selva basin.

In the "Annex 4", applying an alternative statistical methodology that integrates isotope data together with geochemical data, and deals with the latter as compositional data, a comparative of five NO_3^- vulnerable zones in Catalonia (Baix Ter-Empordà, Selva, Lluçanès, Maresme and Osona) is established. This methodology has consisted in a linear discriminant analysis and the corresponding discriminant biplot. These procedures show the discrimination power when using only the isotope data set, although the optimal separation of sample groups is achieved using both geochemical and isotope data subsets. Moreover, the combination of $\delta^{13}C_{DIC}$, $\delta^{34}S$ and $\delta^{18}O_{SO4}$ variables suggests a separation of sample groups depending on the reactions controlling denitrification processes.

3.SYNTHESIS

RESULTS AND DISCUSSIONS

3.1. EXAMPLE OF SELVA BASIN (1)

Hydrogeological and isotope approach

3.1.1 Piezometric data

In the potentiometric contour maps of the upper unconfined aquifer and the confined and leaky aquifers underneath (Fig. 4), flow lines define two main hydrogeological units, in agreement with the hydrographic boundaries of the two main watersheds in the study area: Santa Coloma River Basin (SCRB) and Onyar River Basin (ORB).

Groundwater flow systems are south-oriented in the SCRB, and north-oriented in the ORB. Between them, a groundwater divide oriented WNW-ESE appears in the central part of the Selva basin, which coincides with the surface limits of both watersheds. This setting reflects a geological control of the head distribution that results in separated flow systems draining in opposite directions, controlled by the drainage pattern of the basin on the surface, and by structural elements at depth.

The two hydrogeological units show differences in the origin of their recharge. The upper unconfined aquifer unit receives superficial recharge through direct rainfall and river infiltration, while deeper aquifer levels are recharged by lateral flow systems and, more importantly, by upward vertical flows from the basement. In addition, lateral flow from the surrounding range areas, through fault zones and fracture networks that define the geological setting of the system, is also significant. At the same time, hydraulic head data indicate a vertical connection between sedimentary aquifer levels at various depths, and also a lateral hydraulic connection between the range-front areas and the basin aquifers.

The behavior of and the interactions between distinct hydrogeological units are seen to be diverse and dependent on location, geological setting, seasonal variation, and pumping rate. The differences observed between aquifer head levels and well productivity indicate the occurrence of recharge fluxes from the range-front and the basement. Non local flow systems originating in the surrounding ranges, and flowing through the main tectonic elements, have a major influence over the recharge of the basin sedimentary infill and, at the same time, allow intensive exploitation rates within the basement. Such behavior illustrates the significant influence of groundwater

pumping over the natural flow fields and the recharge/discharge relationships between large-scale hydrogeological units. Such a degree of interaction affects groundwater quantity as well as its quality, and ultimately the vulnerability of the Selva basin water resources.

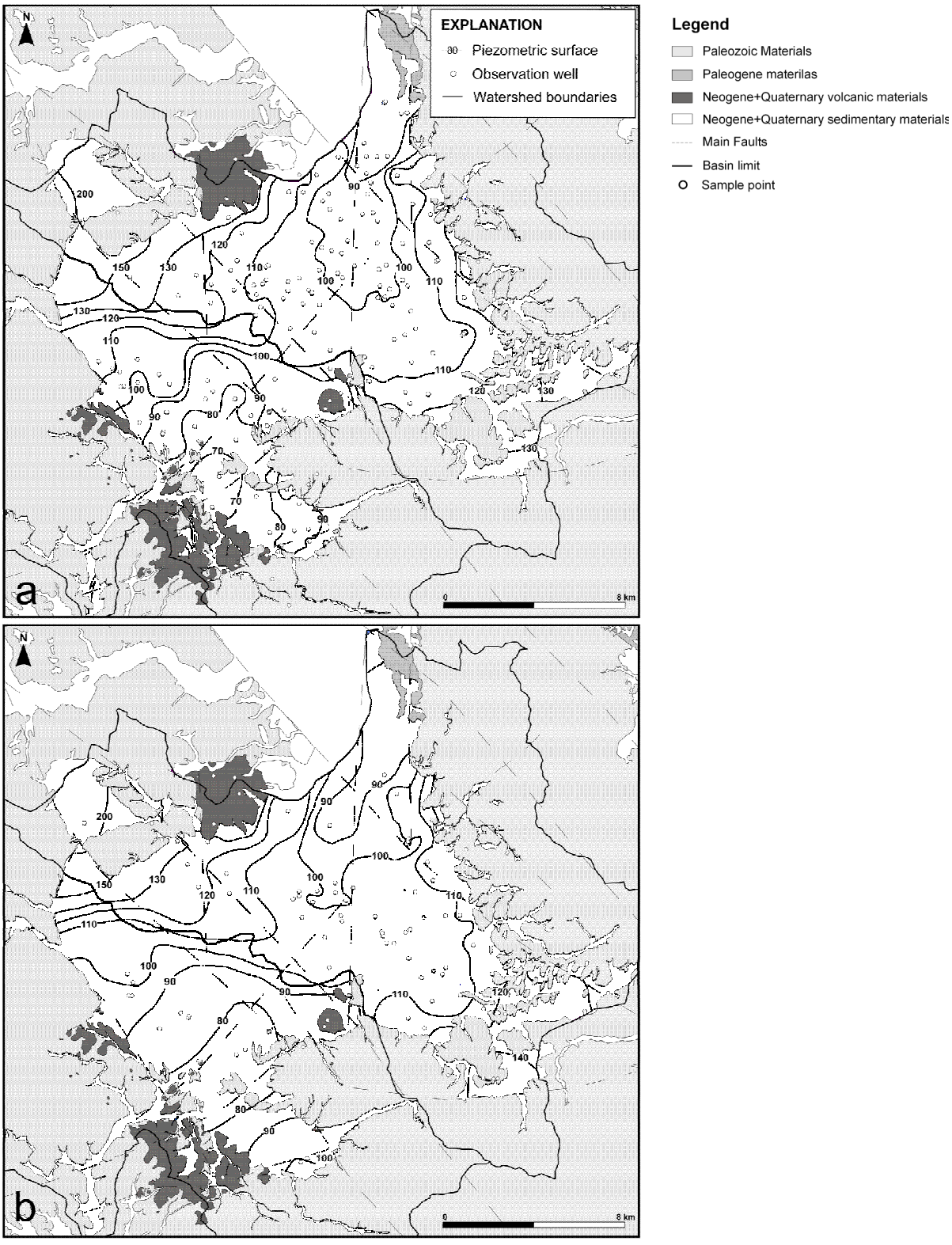

Figure 4. Potentiometric contour map (May 2004) a) Upper unconfined aquifers (around 190 wells less than 30 m deep). b) Deep confined or semi-confined aquifer (around 70 wells over 30 m deep).

3.1.2 Hydrochemistry

Hydrochemical facies allow distinct groundwater sources to be differentiated in the main aquifers of the Selva basin (Fig. 5). Based on their chemical composition, Na-HCO_3 and chloride-rich facies can be attributed to regional flow systems with longer residence times at the subsurface (Gascoyne et al., 1987; Tóth, 1995, 2000; Beaucaire, 1999; and Carrillo-Rivera et al., 2007). These samples also have low nitrate concentrations and high fluoride content of up to 15 mg/L, indicating high water-rock interaction (Piqué, 2008). Conversely, local flow systems have Ca-HCO_3 facies with high nitrate, sulphate and chloride concentrations related to pollution sources. This type of facies indistinctively shows a low fluoride content (< 2.0 mg/L). Among them, Ca-HCO_3 facies with significant sodium content may be attributed to intermediate flow systems, with sulphate and nitrate concentrations lower than samples from local flow regimes. Some enrichment in chloride may be related to evaporation processes in the unsaturated zone, as revealed by isotopic data shown later.

High nitrate samples seldom coincide with high fluoride content, and thus define distinct end-members in the recharge of the Selva basin: inflow from rainfall infiltration within the basin will present nitrate pollution, while vertical upward inflow from the granitic basement, or lateral inflow from the range-front as in the Santa Coloma fault zone, will present a significant fluoride concentration. It is worth noting that the occurrence of fluoride is limited to wells located along the main fault areas, suggesting an efficient flow path through tectonic structures. Most samples located in these fault areas also show high concentrations of HCO_3^- being saturated or close to saturation with calcite, indicating a potential deep CO_2 input or mixing with thermal waters. In this dataset, some wells present high fluoride concentrations as well as moderated nitrate content. Such hydrochemical composition could also be attributable to mixing processes caused by the cones of depression inside the aquifer, or simply to the existence of several screened intervals in the borehole.

In summary, hydrochemical facies permit a classification of groundwater samples in different groups according to basin, hydrogeological unit and hydrochemistry. Thus, the studied samples were divided into the following groups:

1. Samples related to *regional fault zones and granitic aquifers*, mainly having fluoride content higher than 2 mg L^{-1}.

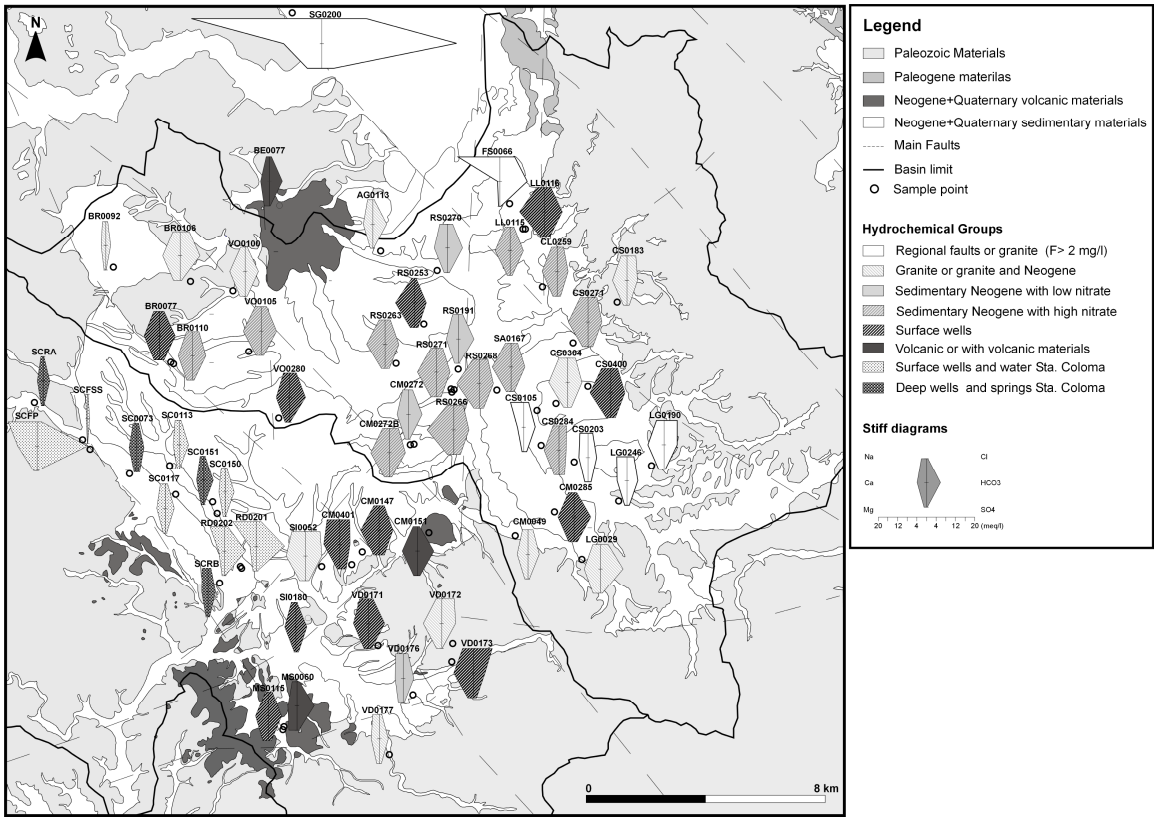

Figure 5. Stiff diagram distribution (May 2006). Refer to text for hydrochemical groups description.

2. Samples from wells in *granitic rocks that may also exploit Neogene sedimentary formations*, usually with Ca–HCO_3 facies and some with high chloride content.

3. Samples from *Neogene sedimentary layers with low nitrate content* (below 38 mg L^{-1} NO_3^-).

4. Samples from *Neogene sedimentary layers with high nitrate content* (usually above 50 mg L^{-1} NO_3^-) showing the influence of groundwater withdrawal at moderate depth from or below shallow aquifer units.

5. Samples from *surface wells*, either in alluvial or in the uppermost Neogene layers, or in weathered granite outcrops, having a characteristic Ca–HCO_3 facies, and likely to have high nitrate concentrations in the eastern SCRB and in the ORB.

6. Samples located totally or partially in *volcanic rocks*, with Ca–HCO_3 and/or Ca–Mg–HCO_3 facies, reaching a possible depth of 80 m and being related to local aquifers and/or deeper system flows.

Finally, two types of wells can be distinguished in the western SCRB with different features from those already described above, for example, lower salinity content. Accordingly, we differentiate between:

1. Samples from *surface wells and stream water in the SCRB* with a lower nitrate content than those of the ORB.
2. Samples from *deep wells and springs in the SCRB*, with a significant fluoride content and low nitrate concentrations.

One of the main outcomes of the dataset is that surface wells are seen to have a wide range of hydrochemical facies. This can be attributed to the effect of aquifer lithology and pollution impacts, mainly from the intensive use of manure as fertilizer.

3.1.3 Environmental Isotopes (δD, $\delta^{18}O$)

The local meteoric water line $\delta D = 7.9 \quad \delta^{18}O + 9.8$ (LMWL-R) from Neal et al. (1992) is considered representative of the range areas surrounding the Selva basin. However, recharge water in the Selva basin is characterized using the precipitation data from the the IAEA/WMO Girona airport station in the central part of the Selva basin.

Groundwater from regional fault zones, granite areas and springs show low isotopic content near to LMWL-R, indicating the basin is recharged from higher altitudes (Fig. 6). Samples from fault zones show the lowest isotopic values and, therefore, confirm a relationship with regional, fluoride-rich, longer-residence time flow systems, and a control of the fault zones upon the flow line distribution. Conversely, most of the samples from wells in the Neogene sedimentary formations show more enriched values of $\delta^{18}O$ and δD than LMWL-R, denoting recharge at the Selva basin.

Seasonal variability is also encountered, as samples tend to lie around the LMWL-R in the September and December surveys, and then shift to heavier values in both May surveys, with some evidence of evaporation processes in the non saturated zone (Clark and Fritz, 1997) in the larger May 2006 dataset (Fig. 6).

Water withdrawn at the end of the summer season, i.e. in September or October, shows higher recharge altitudes and isotopic values aligned according to the LMWL-R. By September, intensive water withdrawal has exhausted local resources, and the isotopic content reveals the dominant influence of groundwater flow from regional systems on the captured water. During the summer season, an evolution to lighter isotopic values coincides with a decrease in nitrate and an increase in fluoride concentrations, when rainfall recharge is almost nil (Menció, 2006). That is to say, the lateral and vertical upward recharge from the surrounding ranges and the basement

provides water to the sedimentary aquifers of the basin, fulfilling major water needs as most of the wells can therefore maintain their exploitation rates.

During May surveys, following the wet season that lasts from October to May, groundwater samples exhibit more enriched isotopic values that have shifted to the local recharge signature in the basin surface. Moreover, specific samples located in the ORB are distinctively aligned along an evaporation line.

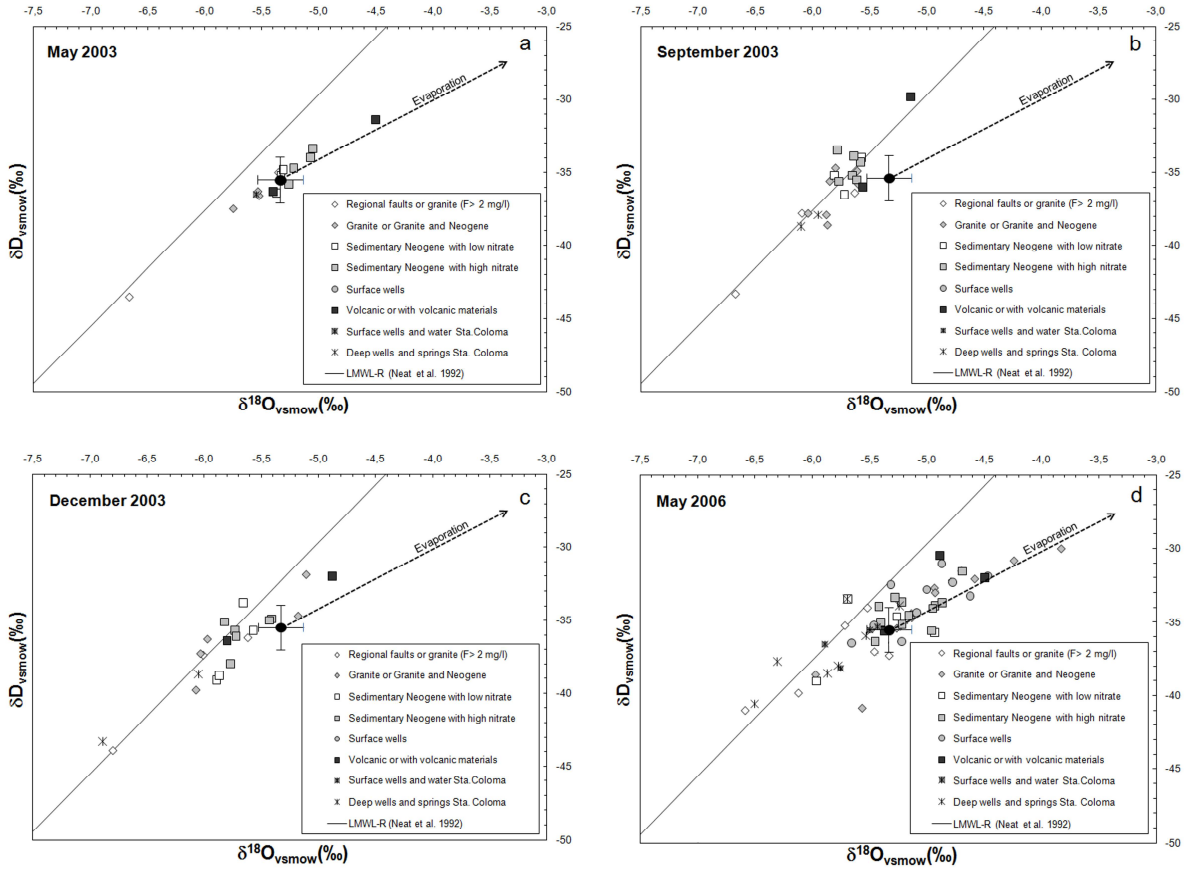

Figure 6. Environmental isotope distribution (δD, $\delta^{18}O$) in the different field surveys. Error bar indicates analytical error and the value weighted with the amount of precipitation calculated with data from the Global Network of Isotopes in Precipitation (GNIP) from station "Gerona Aeropuerto" located in the Selva basin (IAEA/WMO, 2006). "Evaporation" indicates the trend line of evaporated groundwater in the non saturated zone.

Such seasonal conduct emphasizes the effect of the groundwater withdrawal regime on the hydrogeological dynamics of this system, with the origin of captured water being modified from local to regional recharge sources. It also reveals the role of fault zones as preferential flow paths that recharge the overlying sedimentary layers from the basement.

3.2 EXAMPLE OF SELVA BASIN (2)

Multi-isotope approach

Physicochemical parameters related to redox conditions (dissolved O_2 and Eh) indicate that most of the studied samples are oxic groundwater. However, it is worth noting that several samples linked to regional flow or fracture and fault systems presented redox conditions quite favorable to denitrification processes (and in some cases, SO_4^{2-} reduction).

3.2.1 Sulfate isotopes

Dissolved SO_4^{2-} in Selva basin groundwater may have several origins: a) SO_4^{2-} from livestock manure, synthetic fertilizers or sewage leaking (anthropogenic sources related to land use and human pressure) and b) oxidation of reduced S compounds, dissolution of evaporites, soil-derived SO_4^{2-} or CO_2-rich thermal waters (natural sources linked to hydrogeological conditions). $\delta^{34}S$ of groundwater samples ranged between +2.2 and +28.7‰, with a median value of +7.2‰ (n = 33), and $\delta^{18}O_{SO4}$ ranged between +3.2 and +14.4‰, with a median value of +6.7‰ (n = 33). The concentration of dissolved SO_4^{2-} varied from 5 to 238 mg L^{-1} with a median value of 49.3 mg L^{-1} (n = 39). As shown in Figure 7, most of the samples fall in the mixing area defined by the isotopic ranges of fertilizers, pig manure and sewage, indicating that groundwater SO_4^{2-} is mainly controlled by anthropogenic sources. The higher $\delta^{34}S$ values coupled to low SO_4^{2-} concentrations could be linked either to bacteriogenic SO_4^{2-} reduction processes or to the influence of CO_2-rich thermal waters.

Five samples (AG0113, BR0092, RS0191, SC0117 and VO0280) had greater values of $\delta^{34}S$, lower SO_4^{2-} concentrations and were slightly displaced from the clustered samples near the isotopic range of pig manure and fertilizers. They can be interpreted either as an intermediate flow or as mixtures between the local recharge and a ^{34}S-enriched source, like a regional long residence-time flow or CO_2-rich thermal waters.

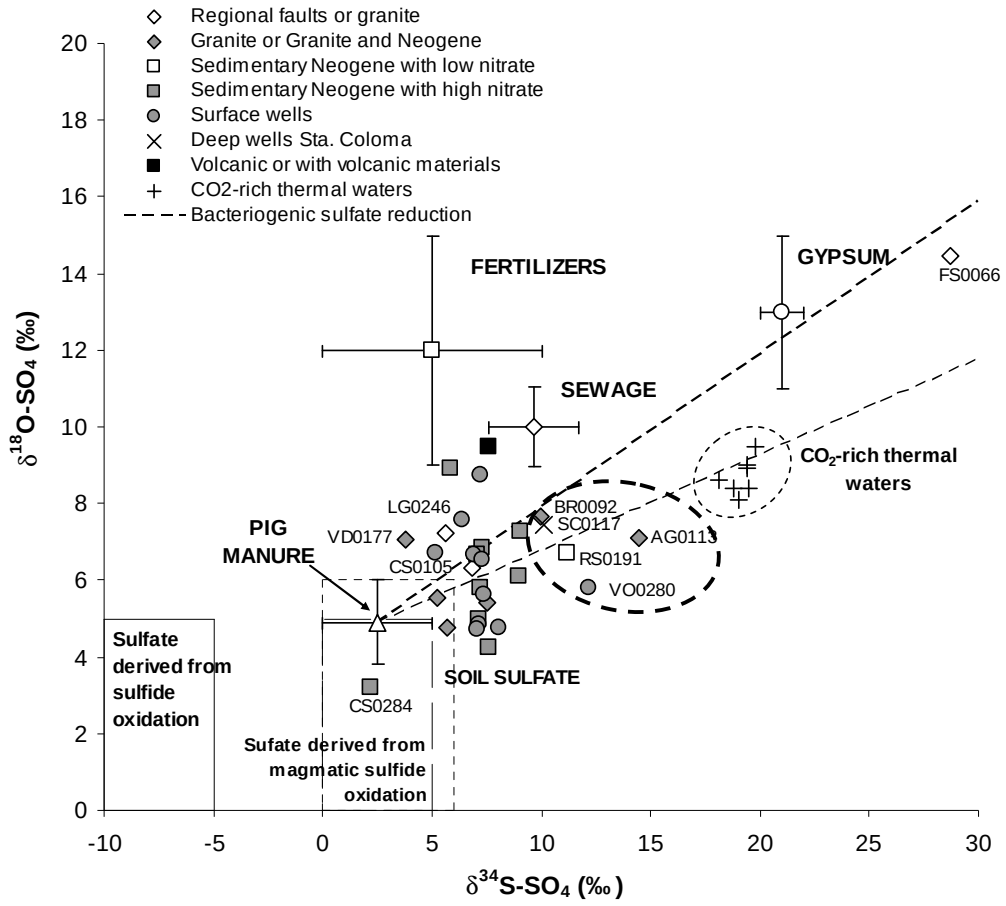

Figure 7. $\delta^{34}S$ vs. $\delta^{18}O_{SO4}$ of dissolved sulfate with the representation of natural and anthropogenic source isotopic ranges. Values for pig manure are taken from Otero et al. (2007) and Cravotta (1997), soil sulfate data from Clark and Fritz (1997), fertilizer data from Vitòria et al. (2004b), and gypsum values from Utrilla et al. (1992). Dashed lines define the isotopic fractionation range ($\varepsilon^{34}S/\varepsilon^{18}O_{SO4}$) in sulfate reduction reactions, which is between 2.5 and 4 (Mizutani and Rafter, 1973). Dashed bold circle indicates samples of intermediate flow system and/or mixing between local and regional flow systems.

3.2.2 Dissolved inorganic carbon isotopes

$\delta^{13}C_{HCO3}$ varied from -19.7‰ to -5.4‰, with a median value of -14.5‰ (n = 38) in the range of $\delta^{13}C_{HCO3}$ in groundwater (from -16‰ to -14‰, Clark and Fritz, 1997). Groundwater had HCO_3^- concentrations ranging between 134 mg L^{-1} and 743 mg L^{-1}, with a median value of 362.3 mg L^{-1}. Hence, the measured inorganic C isotopic composition is mainly controlled by the C signature of groundwater HCO_3^- in equilibrium with soil $CO_{2(g)}$, as well as by the secondary calcite linked to granites (White et al., 2005; Fig. 8).

The highest concentrations of HCO_3^- in the Selva basin groundwater are linked to the interaction with CO_2-rich thermal waters. Results suggest that groundwater samples with $\delta^{13}C$ greater than -14‰, HCO_3^- concentrations greater than 300 mg L^{-1} and calcite SI > 0 may be accounted for by a contribution from CO_2-rich thermal waters and/or a

long residence time along flowpaths. In order to support this explanation, a theoretical mixing model has been calculated assuming two end-members: 1) the CO_2-rich thermal waters, and 2) groundwater. The mixing model trend shown in Figure 8 plots close to the higher $\delta^{13}C$ and HCO_3^- groundwater values and fits well with a few samples (RS0263, LG0029 and FS0066). Therefore, groundwater samples associated with the local flow system can be derived by mixing with CO_2-rich regional flow system groundwater, as pointed out by Folch et al. (2011).

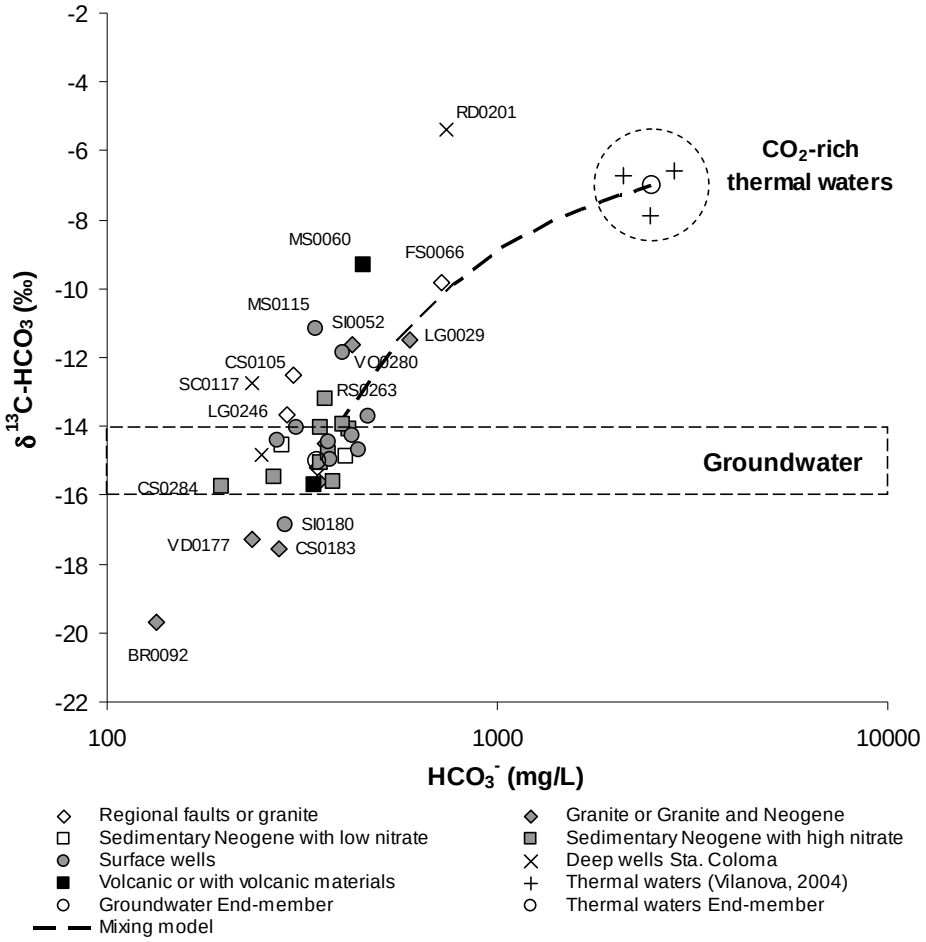

Figure 8. $\delta^{13}C$-HCO_3 plot of the studied samples. The usual range of $\delta^{13}C_{HCO3}$ in groundwater in equilibrium with soil CO_2 (from -14 to -16‰; Clark and Fritz, 1997) and the sparkling spring samples analyzed by Vilanova (2004) are also plotted. Dashed bold curve indicates the two end-member mixing model trend.

3.2.3 Nitrate isotopes

$\delta^{15}N$ of groundwater samples ranged between +6.2 and +18.9‰, with a median value of +10.4‰ (n = 32), and $\delta^{18}O_{NO3}$, between +3.4 and +28.0‰, with a median value of

+5.8‰ (n = 32). The concentration of dissolved NO_3^- varied from 0 to 217 mg L^{-1} with a median value of 47 mg L^{-1} (n = 39).

The lowest $\delta^{15}N$ values were in the range of soil organic N (from +3‰ to +8‰; Kendall et al., 2007) (Fig. 9). NO_3^- concentration values of some of these samples were higher than 200 mg L^{-1}, which makes the mineralization of organic N an unlikely source. Thus, the origin of NO_3^- for some of these samples might also be ammonium fertilizers that, in addition to nitrification, have undergone processes such as volatilization or partial denitrification. This is consistent with the fact that some of these samples (BR0092 and VO0280) were collected in areas with fruit trees and plant nurseries.

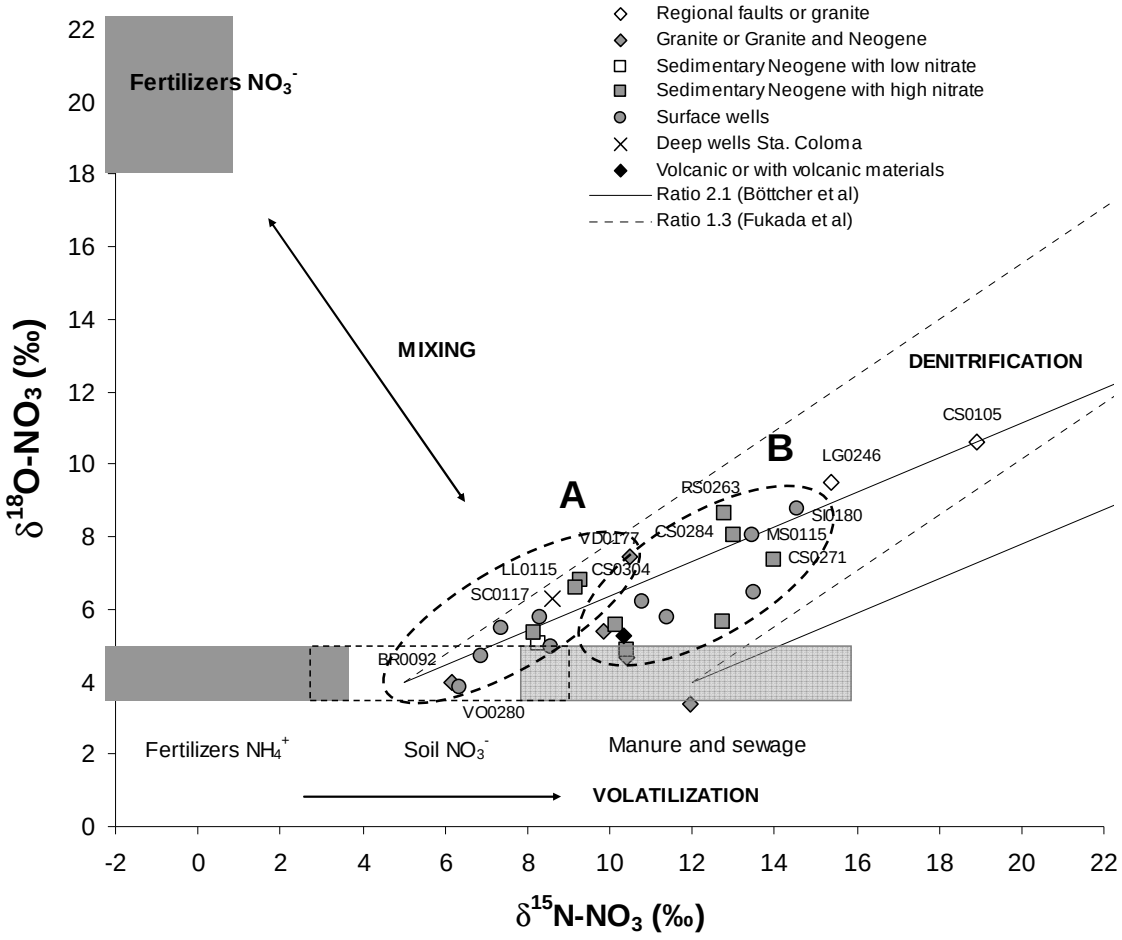

Figure 9. Isotopic values of groundwater dissolved NO_3^- plotted with the ranges of the potential nitrate sources in the study area (Vitòria et al., 2004b, 2008).

For samples with $\delta^{15}N$ in the range of manure (from +8 to +16‰; Vitòria, 2004) and/or sewage, and $\delta^{18}O_{NO3}$ up to +5‰ (the highest estimated $\delta^{18}O_{NO3}$), NO_3^- is the result of volatilization and nitrification processes affecting ammonium of pig manure, in

agreement with the land uses, the extent and pressure of livestock activities. Nevertheless, the impact of NO_3^- derived from sewage can also be significant, since frequent urban dumping attributed to areas not connected to the sewer system is occurring. The influence of NO_3^- coming directly from NO_3^- synthetic fertilizers was not noticed.

In the case of samples with $\delta^{15}N$ in the range of manure and/or sewage, and with $\delta^{18}O_{NO3}$ values greater than +5‰, NO_3^- isotopic values displayed a positive trend in a plot of $\delta^{15}N$ vs $\delta^{18}O_{NO3}$ (Fig. 9) indicating that denitrification processes are taking place. Samples linked to the regional flow system appeared to be clearly affected by natural attenuation processes of NO_3^-.

The samples most affected by the natural attenuation of NO_3^- were VD0177, CS0304, LL0115 and SC0117 (fertilizers-derived nitrate) (group A), and SI0180, RS0263, MS0115, CS0284 and CS0271 (pig manure-derived nitrate) (group B) (Fig. 9). All these wells seem to be influenced by mixing with regional flows with reducing conditions. Therefore, the assessment of processes involved in the transport and fate of NO_3^- by means of the dual NO_3^- isotopes approach seems to indicate that the reducing conditions of long residence time and deep flows favor NO_3^- reduction of polluted local recharge groundwater. Consistent mixing between the regional deeper groundwater and local groundwater plus denitrification superimposes the effects of dilution and consumption on nitrate concentrations. This is coherent with $\delta^{34}S$, $\delta^{18}O_{SO4}$ and $\delta^{13}C_{HCO3}$ data, as they also point out mixing processes between deep and shallow flows.

It does not appear from the SO_4^{2-} isotopes that significant pyrite oxidation was occurring. The sample trend in the $\delta^{13}C_{HCO3}$ vs. HCO_3^- plot (Fig. 8) was the opposite of the expected trend if denitrification linked to organic matter oxidation was occurring. This result, however, does not conclusively mean that NO_3^- was not being reduced by means of heterotrophic denitrification, because the influence of regional CO_2-rich flows and/or other C sources could have been masking it.

3.3 EXAMPLE OF BAIX TER BASIN

Multi-isotope approach

3.3.1 Hydrodynamics

In agreement with the conceptual flow model described in previous studies (Vilanova and Mas-Pla, 2004), the Quaternary piezometry showed groundwater flow lines oriented south to north (from the Gavarres massif to the Ter River) (Fig. 10). The exploitation of the Gualta supply wells produces a depression cone around this municipality. Groundwater withdrawal activity near Gualta village modifies the behavior of the Ter River, inducing surface water to drain into the alluvial aquifer, and making the Ter River a losing stream where the depression cone appears.

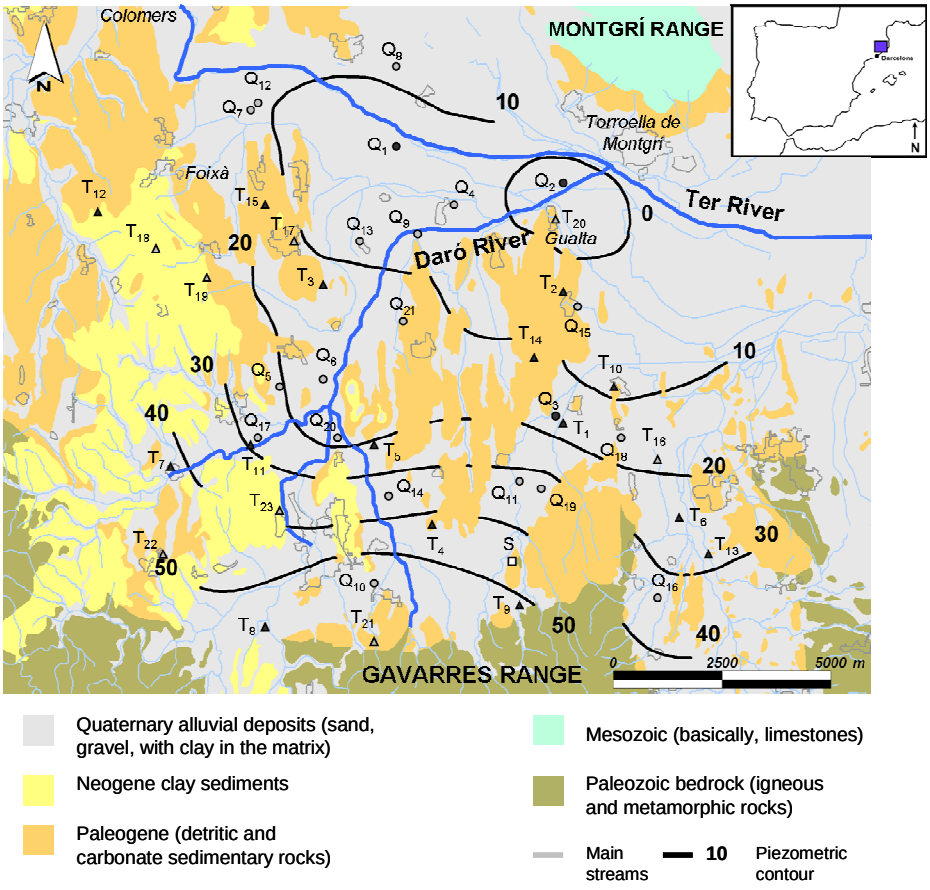

Figure 10. Baix Ter basin map showing the geology and sampling points, labeled according to their hydrogeological formation (round and triangle shapes distinguish between Quaternary and Tertiary aquifers, respectively, and light and bold points, between shallow and deep formations, respectively). Potentiometric contourlines correspond to the water table measurements of the Quaternary unit (August 2004).

3.3.2 Sources of the recharge

The isotope values of samples collected from wells in the Quaternary and Tertiary aquifers were mostly lighter than those of the weighted mean precipitation (δD = -33.5‰, $\delta^{18}O$ = -5.2‰). This indicates that recharge of these aquifers is not only attributable to the infiltration of rainfall within the basin but also to other sources of recharge. The wide range of $\delta^{18}O$ and δD values in the shallow Quaternary aquifer, even within the same sampling campaign, denotes the influence of different recharge flow systems with distinct hydrogeological characteristics, and the mixing among them: 1) the Ter River, 2) local rainfall, and 3) the Gavarres massif.

The overlap between the isotope compositions of some Quaternary and the Tertiary groundwater samples suggests that both aquifers share a common source of recharge or are somehow connected. This is consistent with the conceptual model described by Vilanova and Mas-Pla (2004), who hypothesized an upward groundwater flow from the Tertiary aquifer to the deep Quaternary aquifer in the northern part of the area. On the other hand, the Gavarres massif is a source of recharge for the Tertiary unit, in addition to local rainfall.

3.3.3 Hydrochemistry

60% of the studied samples had NO_3 levels above the legal threshold of 50 mg L^{-1} for drinking water. A spatially complex distribution following a diffuse regional pattern was observed for groundwater NO_3. Moreover, NO_3 is not correlating with well depth. This NO_3 distribution pattern may be explained by the highly complex hydrogeology of the study zone and by the mixing of waters from distinct origins and qualities within the well borehole. Five samples in the Q_D (deep Quaternary) and T_D (deep Tertiary) aquifers contain no NO_3, have an Eh below 200 mV and show the highest ammonium and manganese concentrations. These characteristics are typical of groundwater under reducing conditions, which would agree with the occurrence of denitrification processes.

Samples with high NO_3 concentrations tended to be Cl-SO_4-Ca type waters, in agreement with a contribution of anthropogenic contaminant sources (manure, synthetic fertilizers or sewage). Accordingly, although NO_3 and SO_4 are not strongly correlated, some wells that showed high SO_4 contents coupled with elevated NO_3 concentrations are likely to be affected by human activities. Samples that presented high NO_3 contents coupled with high Cl concentrations are also observed, which can be caused by the input of organic fertilizers since they generally show elevated chloride concentrations

(Karr et al., 2001). Some samples polluted by NO_3 have high B concentrations, which makes sewage another NO_3 and SO_4 potential source. Therefore, our results show that groundwater is affected by more than one source of contamination, but an unambiguous identification of these sources based on the sole hydrochemical data is somewhat difficult, as the signal may be hindered by the mixing of groundwaters from different layers and flow systems.

3.3.4 Isotope identification of the sources of contamination

$\delta^{15}N$ and $\delta^{18}O$ of NO_3

NO_3 isotope composition in groundwater ranged between +5.0 and +32.5‰ for $\delta^{15}N$, with an average value of +13.0‰ (n = 58), and between +1.8 and +18.1‰ for $\delta^{18}O$, with an average value of +7.1‰ (n = 58).

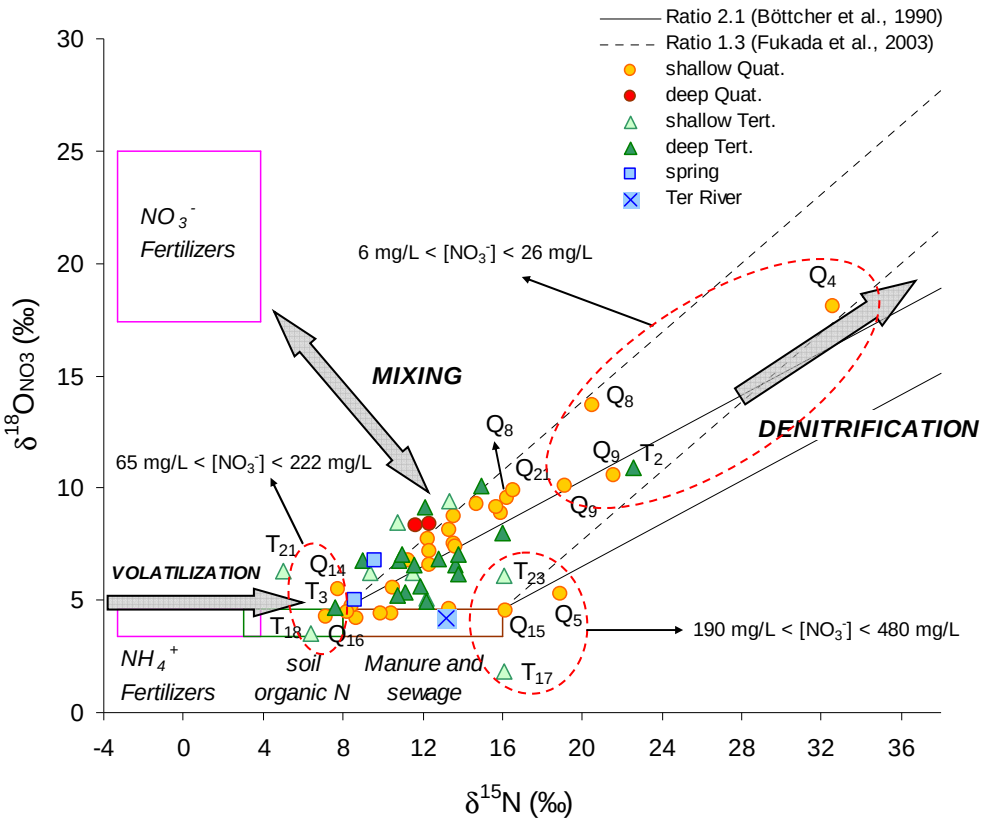

Figure 11. Variations of the $\delta^{15}N$ and $\delta^{18}O$ of dissolved NO_3 in groundwater according to their hydrogeological unit. Isotope ranges of the main NO_3 sources from the literature as well as local sources (Vitòria, 2004; Vitòria et al., 2004b, 2008) are also represented. The extreme isotopic fractionation ratios from the literature are $\varepsilon_N/\varepsilon_O$ = 2.1 (Böttcher et al., 1990) and $\varepsilon_N/\varepsilon_O$ = 1.3 (Fukada et al., 2003). $\delta^{18}O$ of NO_3 deriving from nitrification of fertilizers and manure NH_4 were calculated following the experimental expression: $\delta^{18}O_{NO3} = 2/3(\delta^{18}O_{H2O}) + 1/3(\delta^{18}O_{O2})$ (Kendall et al., 2007), where the $\delta^{18}O_{H2O}$ is assumed to be that of the Baix Ter basin groundwater and the $\delta^{18}O_{O2}$ that of atmospheric O_2 (+23.5‰; Horibe et al., 1973).

Five groundwater samples (Q_{14} and Q_{16} from Q_S, T_3 from T_D, and T_{18} and T_{21} from T_S) presented $\delta^{15}N$ values comparable to soil organic nitrogen (from +3 to +8‰) (Fig. 11). Our results show that NO_3 of T_{21} sample derives from soil nitrogen, and could be assumed to represent the local NO_3 background. However, though a contribution of soil organic nitrogen is possible (Wassenaar, 1995), other sources of NO_3 must be considered to explain the elevated NO_3 contents (from 65 to 222 mg NO_3^- L^{-1}) of Q_{14}, Q_{16}, T_3 and T_{18} samples. For instance, synthetic ammonium fertilizers, whose $\delta^{15}N$ (around 0‰) is enriched in ^{15}N by volatilization processes and can then reach values in the range of soil nitrogen (Vitòria, 2004).

When comparing $\delta^{15}N$ of dissolved NO_3 in our groundwater samples to those of potential sources of contamination (Fig. 11), results show that most of the $\delta^{15}N$ ranged between +8 and +16‰, indicating that NO_3 has probably a pig manure and/or wastewater ammonium origin. $\delta^{15}N$ values higher than +16‰ observed in eleven samples suggest either the occurrence of ammonium volatilization or the reduction of NO_3 in groundwater yielding to N_2 gas (Kendall et al., 2007). Based on $\delta^{18}O$ from NO_3, the following observations can be made: 1) while NO_3-bearing mineral fertilizers are actually applied onto local crops, fertilizer NO_3 did not show their direct influence in groundwater, and 2) most of the samples had $\delta^{18}O$ higher than the maximum expected value.

$\delta^{34}S$ and $\delta^{18}O$ of SO_4

SO_4 isotope compositions ranged between -16.0 and +14.7‰ for $\delta^{34}S$, with an average value of +4.5‰ (n = 64), and between +3.8 and +16.1‰ for $\delta^{18}O_{SO4}$, with an average value of +7.2‰ (n = 64). Most of the groundwater samples from the Q_S (shallow Quaternary) aquifer unit fall within the area defined by the isotope signatures of local anthropogenic sources, showing that SO_4 in the Baix Ter groundwater can be explained by a ternary mixing between 1) mineral fertilizers, 2) sewage and 3) pig manure (Fig. 12). Two sampling sites (T_2 and T_{14}) yielded the lowest negative $\delta^{34}S$ and had $\delta^{18}O_{SO4}$ around +5‰, revealing a SO_4 contribution from a ^{34}S-depleted source of reduced S. Other samples with no NO_3 exhibited the highest $\delta^{34}S$ and $\delta^{18}O_{SO4}$ values. These no-NO_3 samples, along with T_2 and T_{14}, and some other samples with NO_3^- < 25 mg L^{-1} and $\delta^{18}O_{SO4}$ > +8‰, define a linear trend with a slope ($\varepsilon^{34}S/\varepsilon^{18}O_{SO4}$ = 3.3) compatible with bacteriogenic SO_4 reduction (Mizutani and Rafter, 1973) (Fig. 12).

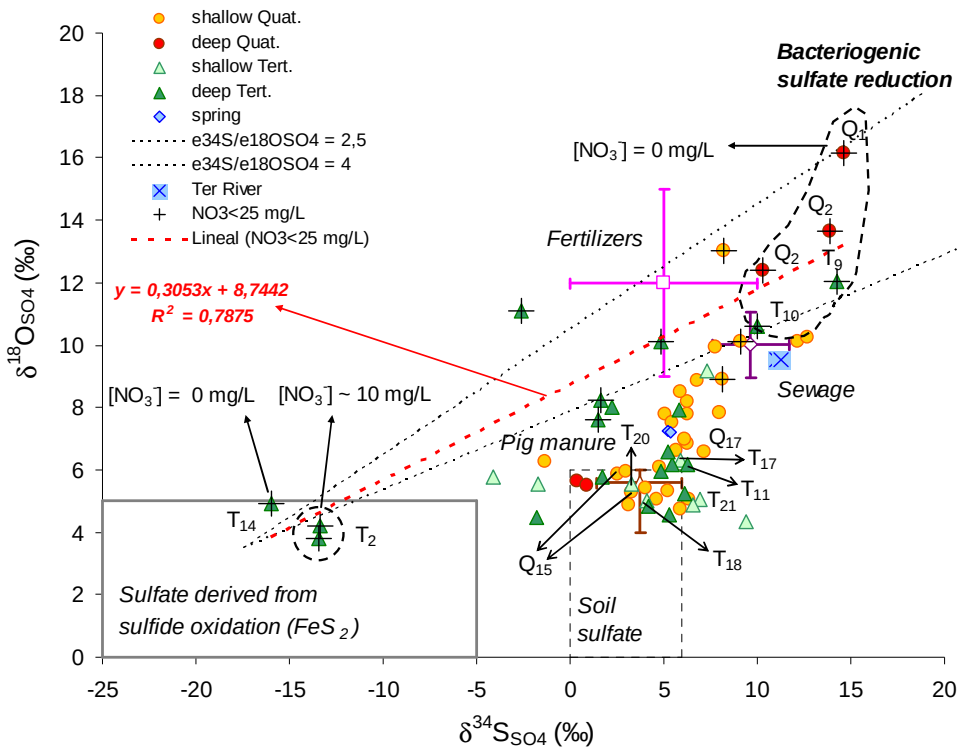

Figure 12. $\delta^{34}S$ and $\delta^{18}O$ of dissolved SO_4 in groundwater according to their hydrogeological unit. Isotope ranges of natural and anthropogenic SO_4 sources and SO_4 reduction are also represented. Values for pig manure are taken from Otero et al. (2007) and Cravotta (1997), soil SO_4 data from Clark and Fritz (1997), and fertilizer data from Vitòria et al. (2004b). Dashed lines define the isotopic fractionation range ($\varepsilon^{34}S/\varepsilon^{18}O_{SO4}$) in SO_4 reduction reactions, which is between 2.5 and 4 (Mizutani and Rafter, 1973).

Boron isotopes

Baix Ter groundwater $\delta^{11}B$ ranged between +1.4‰ and +34.5‰, with an average value of +24.1‰ (n = 12), and B concentrations ranged between 0.051 and 0.232 mg L^{-1}. The $\delta^{11}B$ versus 1/B (Fig. 13a) and $\delta^{11}B$ versus $\delta^{15}N$ (Fig. 13b) diagrams show that most samples fell in the isotope ranges of pig manure, in agreement with the NO_3 and SO_4 isotope data. Only two samples showed $\delta^{11}B$ values consistent with a wastewater origin. They correspond to groundwaters collected in La Bisbal (Q_{20}) and Ullastret (Q_{21}) water supply wells, located downstream the discharge of the La Bisbal water treatment plant into the Daró River. Despite the low number of groundwater samples analyzed, most of them have significantly high $\delta^{11}B$ that can only be explained by a pig manure input, suggesting that the influence of sewage and mineral fertilizers is lesser than the contribution from organic residues.

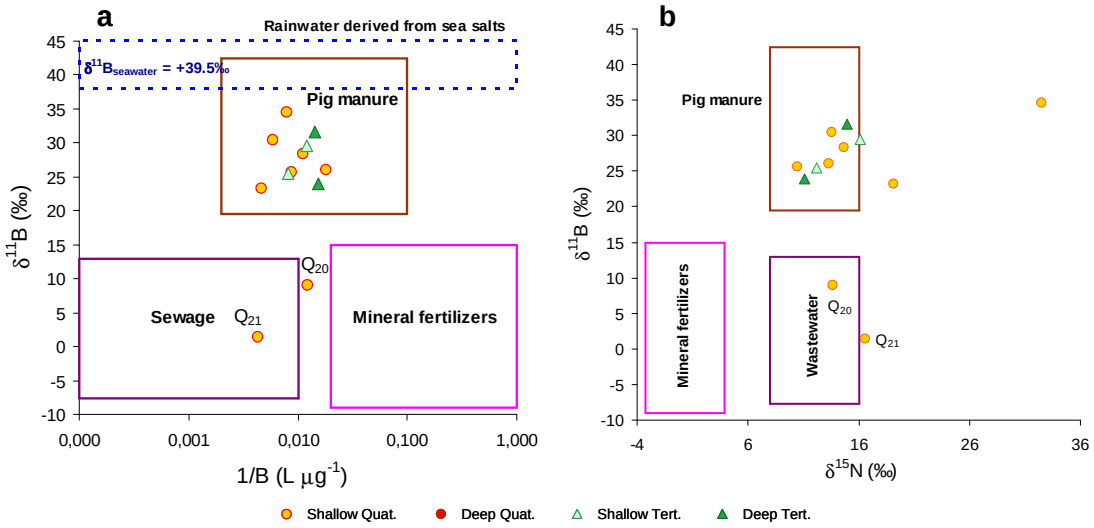

Figure 13. $\delta^{11}B$ values plotted against 1/B (a) and $\delta^{15}N$ values (b).

3.3.5 Evaluation of natural attenuation

In the Baix Ter groundwaters, some of the highest $\delta^{15}N$ were coupled to elevated $\delta^{18}O_{NO3}$: 10 samples had $\delta^{15}N$ and $\delta^{18}O_{NO3}$ higher than +15‰ and +8‰, respectively. Fig. 11 shows that these samples roughly aligned following a 1:2 slope, consistent with natural denitrification (Kendall et al., 2007). The highest denitrified samples were observed either in the shallow Quaternary levels near the Ter River or in deep layers of Quaternary and Tertiary aquifers (e.g. Q_4, Q_8, Q_9 and T_2; Fig. 11). Isotopical and chemical variations between both campaigns suggest that natural denitrification had a moderate activity and/or that it was balanced by the input of new NO_3 into the aquifer.

Biogeochemical processes linked to natural denitrification

Autotrophic denitrification can be eliminated as the main denitrifying process, although a pair of denitrified samples is explained by this mechanism. $\delta^{13}C_{HCO3}$ values ranged between -6.5‰ and -16.2‰, with an average value of -13.1‰ (n = 64), and HCO_3 concentrations between 177 and 619 mg L^{-1}, with an average value of 367 mg L^{-1} (n = 64). Distinct sources of dissolved inorganic carbon may buffer our $\delta^{13}C_{HCO3}$ values: marine marls in the study zone ($\delta^{13}C$ ~ 0‰), CO_2 dissolved in the soil (between -14 and -16‰) (Clark and Fritz, 1997), and pig manure ($\delta^{13}C_{total}$ = -16.4‰; Cravotta, 1997). Heterotrophic denitrification cannot be ruled out as some of the rough trends we observed, e.g. high $\delta^{18}O_{NO3}$ coupled to low ln (NO_3/HCO_3), are in agreement with natural denitrification catalyzed by organic matter oxidation.

Hydrogeological conditions linked to natural denitrification

Two different hydrogeological conditions can be considered as determining factors for our identified denitrified samples:

1) In the shallow Quaternary aquifer, near the Ter River (Q_4, Q_8 and Q_9), NO_3 natural attenuation may have been favored by the aquifer-river interaction, i.e. the infiltration of surface waters in the losing stream areas. Natural denitrification could also happen under the wooded areas at the Ter riverside, which would behave as riparian zones, or thanks to disseminated organic matter layers in the alluvial aquifer.
2) For sites sampled in the deep Quaternary and Tertiary aquifers (Q_1, Q_2, T_2, T_9, T_{10} and T_{14}), the NO_3 reduction can be attributed to their location in fault areas, where local and regional flow paths converge, and the mixing between shallow and deep groundwaters is favored by fractures. The reducing conditions of these deep groundwaters, acquired after crossing reducing environments, can lead to the total removal of NO_3 coming from the shallower groundwaters.

3.4. EXAMPLE OF COMPARATIVE

Statistical approach

The representation of the association between variables and sample groups is intended to (i) discriminate the five sampled zones, (ii) observe which variables or combination of variables condition this discrimination, and (iii) determine whether the associations showed by the plot are related either to the anthropogenic sources of pollution or to the geological background.

In the discriminant plot using only geochemical data (Fig. 14), we can discriminate Osona-Lluçanès, from Empordà-Selva, and from Maresme, but the sample groups are not perfectly split up. The explanatory variables are the couples of NO_3^--Cl^-, Ca^{2+}-Na^+ and Mg^{2+}-HCO_3^- contents. Some of the studied areas are discriminated by NO_3^- contents, but the main nitrate sources that contribute to nitrate contamination, fertilizers and pig manure, represented by the Maresme and the Osona areas, respectively, are not in extreme positions. The separation of Osona-Lluçanès from Empordà-Selva is due to

bedrock signature. Therefore, the discriminant plot entering only geochemical data does not allow an easy distinction of the five vulnerable zones according to the main nitrate source.

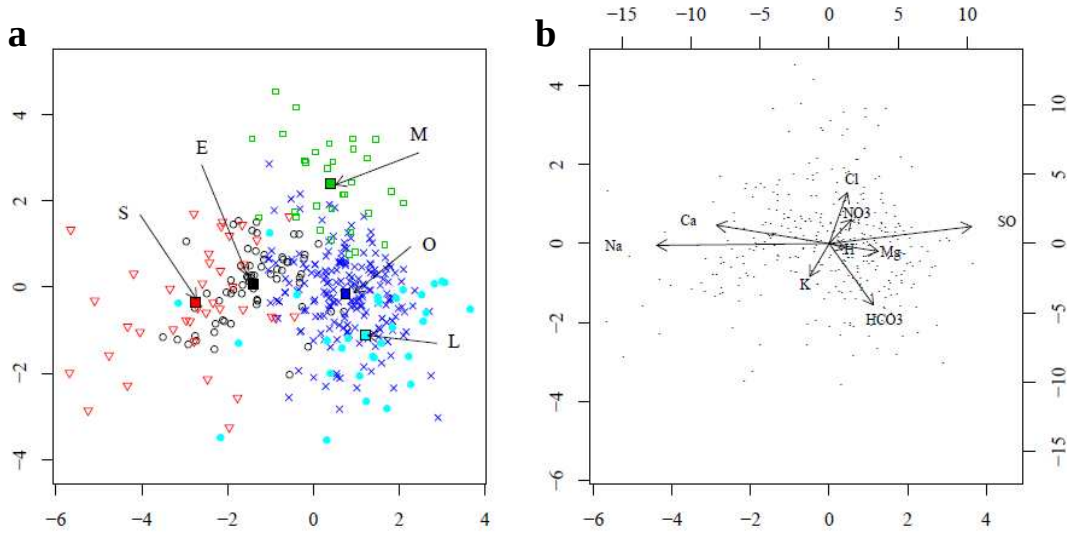

Figure 14. Discriminant plot (a) with indication of group means (plot centred using the global mean), and biplot (b), where arrows represent the explanatory variables using the geochemical data set. A clr transformation was used.

In the discriminant plot using only isotope data (Fig. 15), Osona and Lluçanès samples are well separated from Maresme, Empordà and Selva samples. The explanatory variables are $\delta^{15}N$, $\delta^{18}O_{SO4}$ and $\delta^{34}S$-$\delta^{18}O_{NO3}$, indicating the combined influence of nitrate sources and the processes undergone by nitrate (mainly nitrate reduction favored by sulfide and/or organic matter oxidation). If processes were not involved, from this discriminant plot we could relate pollution origin in the mixed areas mainly to fertilizers, with minor contribution of pig manure. However, we must take into account whether denitrification is occurring, and how it is occurring, because the $\delta^{34}S$ and $\delta^{18}O_{SO4}$ variables can discriminate areas with the same nitrate source, depending on which is the main reaction that is controlling nitrate reduction. The use of only isotope data allows distinguishing the zones in a clearer way by the nitrate source influence, but some difficulties arise interpreting the mixed areas.

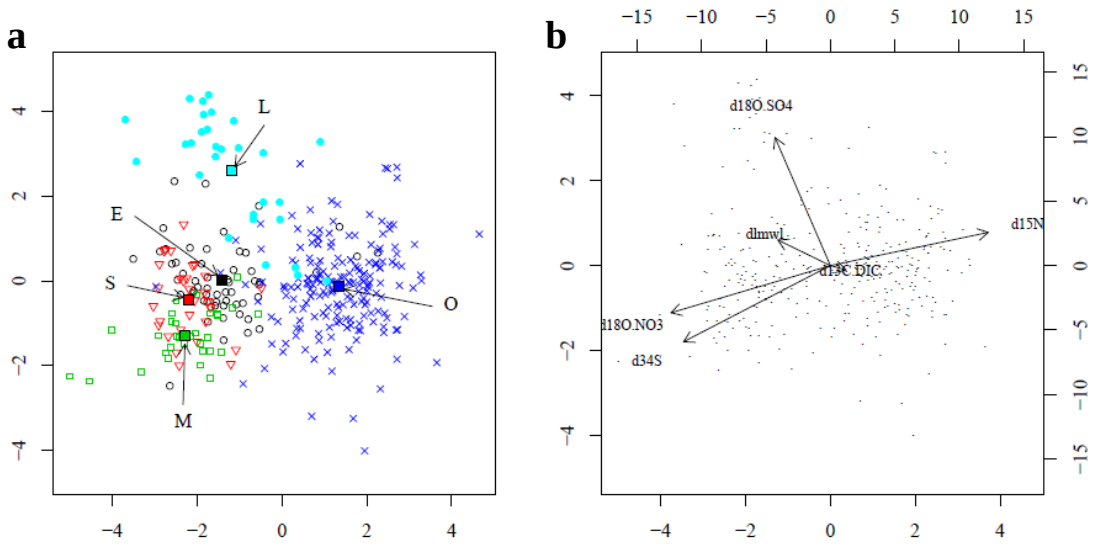

Figure 15. Discriminant plot (a) with indication of group means (plot centred using the global mean), and biplot (b), where arrows represent the explanatory variables using the isotopic data set.

Using both data sets, in the discriminant plot obtained (Fig. 16) the different sample groups are better separated. We have a clear discrimination of samples with the ratio ($\delta^{15}N$-$\delta^{18}O_{NO3}$) + log (HCO_3^-/Cl^-): whereas the Maresme sample group is in one extreme and the Osona sample group in the opposite, which are considered as source end-members, those samples from the mixed areas (Empordà and Selva) are in between. Taking in account the ratio $\delta^{13}C_{DIC}$ - ($\delta^{34}S$-$\delta^{18}O_{SO4}$), the sample group distribution can give us an idea of how denitrification processes are occurring. We must also bear in mind that the length of the arrows is related to the discriminant power of the variables that they represent, so the short length of the $\delta^{13}C_{DIC}$ arrow can be interpreted as if organic matter oxidation is taking place in all the areas where denitrification processes are occurring.

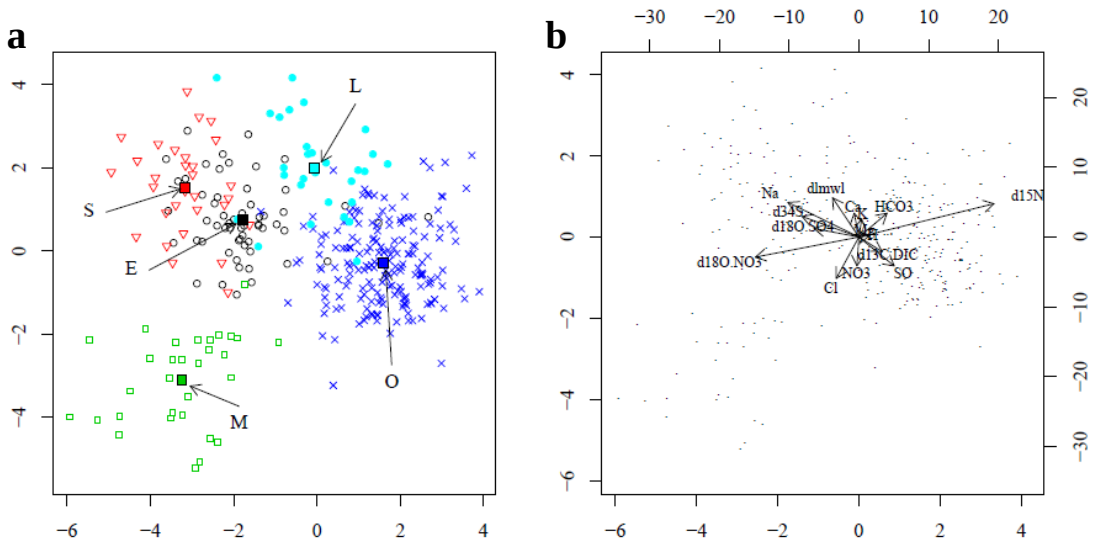

Figure 16. Discriminant plot (a) with indication of group means (plot centred using the global mean), and biplot (b), where arrows represent the explanatory variables, using both the geochemical (clr-transformed) and isotopic data sets.

The discriminant biplots with only geochemical data, only isotope data and both data subsets separate the sample groups according to the following percentages of reclassification: 81, 87 and 93%. As could be expected, the best discrimination is obtained when using both data subsets, but the discriminant biplot with only isotope data is useful enough to separate sample groups affected by different nitrate sources. Thus, the isotope data set is a powerful tool by itself, though some Empordà and Selva samples are misclassified.

4.THESIS

GENERAL CONCLUSIONS

This hydrogeological, geochemical and isotopical research work focuses on the study of regional, heterogeneous and disturbed groundwater flow systems, which *per se* entail complexity. This complexity is characterized by multiple factors and parameters that interrelate, e.g. geological settings with characteristic structural elements and geochemical environments, multilayered aquifers with different hydraulic connectivities and recharge/discharge areas, distinct regional/local and surface-/groundwater flow systems, seasonal groundwater abstraction regimes, multiple natural and anthropogenic solute sources, etc. In this type of groundwater flow systems, water mixing processes may have a major effect on their hydrochemical characteristics and on contaminant evolution. Thus, considering the implicit difficulties this object of study brings about, this research work concludes some features and findings which are explained next.

1) Hydrogeological systems are greatly disturbed by groundwater withdrawal regimes, which modify natural flow paths, either at regional or local scale. For instance, the two studied basins show this type of complexity. Such natural flow modifications, which govern the water balance within the basin and, therefore, the amount of available water resources, can be identified with the aid of potentiometric, hydrochemical and isotopic data; as shown by previous studies (Vilanova, 2004; Menció; 2006; Folch, 2010). This dissertation corroborates their results and adds a further insight based on isotopic data.

In particular, fault zones and fracture networks in the Selva basin represent a significant preferential flow path that plays an important role in the recharge from the ranges towards the sedimentary infilling of the basin. According to δD and $\delta^{18}O$ groundwater values and hydraulic head evolutions, regional flow systems related to fault zones supply current demands that could not be fulfilled by only the local rainfall recharge. Moreover, these systems allow the recovery of stored water resources during low demand seasons. Potentiometric data indicate the presence of vertical connectivity in this leaky multilayered aquifer system, as well as the existence of a lateral inflow from the range-front and a vertical upward flow from the granitic basement; being the last two processes related to the effect of fault zones on the regional flow field. This is consistent with hydrochemical data, since the occurrence of nitrate at depth is indicative of vertical downward recharge induced by intense groundwater withdrawal, and the

spatial distribution of fluoride points to those areas where wells are fed by recharge from the basement. Local flow systems, originated from the recharge within the basin, only feed the shallowest layers of the system, as alluvial aquifers and the uppermost levels of the Neogene formations.

Potentiometric and isotopic data from the fluvio deltaic aquifer system in the Baix Ter basin also reveal distinct groundwater and recharge flow systems: a large-scale regional flow from the Gavarres range to the basin, and a local flow, recharged from rainfall infiltration in the basin surface. Moreover, river-aquifer interactions and a vertical upward contribution from the regional flow, both forced by groundwater withdrawal, complete the hydrological balance for this aquifer. Groundwater mixing of regional and local flows can thus occur between all these groundwater sources. Hydrochemical and isotope data suggest that these mixing processes (which take place in areas hydrogeologically related to fault zones), besides producing a dilution of contamination, could give rise to natural attenuation of NO_3^- thanks to the reducing condition innate to some deep groundwater flows.

All this knowledge is useful and usable to go a step further in the management of heterogeneous hydrogeological basins under human pressures. No doubt that quality issues are better understood when a regional hydrogeological perspective is used, providing helpful explanations for the occurrence of natural or anthropogenic pollutants (e.g. fluoride and nitrate). Being aware of the location of the main hydrogeological features, such as vertical recharge from faults, downward flow due to pumping, the relation between aquifer units, etc., is essential to improve groundwater resource management.

2) The multi-isotope approach has allowed determining the main sources of NO_3^- in the Selva and Baix Ter basins. At the same time, the variety and mixing of contamination sources in these areas has been reflected by isotope data. The isotopic composition of dissolved NO_3^- ($\delta^{15}N$ and $\delta^{18}O$) in groundwater confirmed that the main contribution of N in the Selva and Baix Ter aquifer systems comes from pig manure, though non-negligible contributions from mineral fertilizers and sewage have also been isotopically identified. This result agrees with the isotopic composition of dissolved SO_4^{2-} ($\delta^{34}S$ and $\delta^{18}O$), which revealed that the origin of SO_4^{2-} in groundwater is related to a ternary mixing between pig manure, mineral fertilizers and sewage, in the Baix Ter basin, and

pig manure, mineral fertilizers and CO_2-rich waters, in the Selva basin. Therefore, although hydrochemical and isotope data evidence a mixing of mainly anthropogenic sources, which is consistent with the mixing processes described for the studied areas, both NO_3^- and SO_4^{2-} isotopes coincide with pig manure application as a main vector of pollution. Moreover, the analysis of boron isotope ratios ($\delta^{11}B$) in a few representative groundwater samples clearly supported and confirmed the major role of pig manure with regard to groundwater contamination. Nevertheless, a pair of samples has also revealed the contribution of wastewater to the aquifer resources. Consequently, for both case studies, the multi-isotope approach allows a better characterization of the contaminant origin than with hydrochemical data only.

3) The identification of natural attenuation processes at a field scale involves a complex relationship of environmental and geochemical parameters. Therefore, *a priori*, recognizing NO_3^- reduction processes could be problematic in regional and heterogeneous cases due to variability in the aquifer hydrogeological and geochemical settings. Despite this handicap, the dual NO_3^- isotope approach indicates that natural denitrification is occurring in both the Selva and Baix Ter basins. Thus, a major conclusion of this research work is that, even in regional large-scale systems where multiple factors can influence the NO_3^- evolution, the isotopic composition of N and O of NO_3^- can still give information about whether natural attenuation is occurring. In other words, this dual-isotope tool successfully indicates NO_3^- consumption in hydrogeological systems under different human pressures, despite the spatial heterogeneity observed in groundwater dynamics. Isotope and hydrochemical results from both studied areas suggest that natural denitrification rather had a moderate activity and/or it was balanced by the input of new NO_3^- into the aquifer.

Regarding the electron donors that promote NO_3^- removal, the $\delta^{34}S$ and $\delta^{18}O$ of SO_4^{2-} showed that NO_3^- reduction is not controlled by the oxidation of pyrites but rather by organic matter oxidation, although this could not be confirmed by the $\delta^{13}C_{HCO3}$ data. Since the role of organic matter in NO_3^- attenuation is still an on-going research, further studies on the $\delta^{13}C$ of local contaminant sources should provide a better understanding of the electron donors involved in the natural denitrification processes. Furthermore, mixing of polluted local groundwater and deep regional flows (containing low NO_3^- and oxygen concentrations, or influenced by CO_2-rich waters) can result in the observed

reduction of anthropogenic NO_3^- concentrations through both dilution and denitrification.

4) Statistical techniques based on compositional data analysis have been applied in five NO_3^- vulnerable zones: Baix Ter, Selva, Lluçanès, Maresme and Osona, and using three distinct scenarios: only geochemical data, only isotope data, and both data sets together. These procedures have allowed representing the association between variables and sample groups, and analyzing which variables or combination of variables achieve the optimal separation between the groups, i.e. determining which explanatory variables present the largest discriminant power. The optimal separation of sample groups has been obtained using both geochemical and isotope data subsets. This result ascertains that areas affected by different NO_3^- sources are better discriminated by means of the statistical analysis of multi-isotope and hydrochemical data sets together. Moreover, in the direction defined by the variables $\delta^{13}C_{HCO3}$, $\delta^{34}S$ and $\delta^{18}O_{SO4}$, a separation of sample groups depending on the reactions associated with denitrification processes is suggested. Another important result is that the discrimination power when using only the isotope data set is higher than when using the sole hydrochemical data set. With only isotope data, it is possible to distinguish the sample groups by the NO_3^- source influence, but some difficulties arise interpreting the areas affected by multiple NO_3^- sources. The discriminant plot entering only geochemical data does not allow an easy distinction of the five vulnerable zones according to the main NO_3^- source.

Therefore, the statistical approach that integrates isotope with geochemical data together is a valuable treatment to be considered when comparing NO_3^- vulnerable zones, because it can give a rapid graphical reading of the differences between these zones in terms of sources of pollution and attenuation processes. However, these statistical techniques can be further improved by testing and applying them to more compositional data sets, specially focusing on the assessment and discrimination of NO_3^- natural attenuation processes and on the geochemical reactions involved.

5) To sum up, results obtained in this study of regional-scale areas with different sources of NO_3^- pollution show that multi-isotopic, hydrochemical and statistical approaches, in relation with the corresponding hydrogeological framework, are able to provide a useful insight into sources and processes controlling NO_3^- evolution, and generate scientific criteria for water resources planning and management of

groundwater bodies under human pressures. For this reason, these methodologies can be routinely applied in samplings of groundwater quality networks.

From here, future research intended to understand the mechanisms that control groundwater NO_3^- contamination in regional aquifer systems can take benefit of the approaches used in this study. In regional-scale areas where the conceptual flow model is well known, multi-isotopic data can be used to monitor and quantify NO_3^- natural attenuation, as well as to control induced NO_3^- attenuation strategies. Furthermore, mixing processes between local shallow polluted groundwater and regional deeper free-NO_3^- flows with reducing conditions could be taken into account as a hydrogeological key factor that can promote, apart from dilution, NO_3^- natural denitrification processes. For instance, in areas hydrogeologically related to fault zones and fracture networks, where mixing of groundwater from different flow systems is occurring and denitrification processes are known to be taking place, some representative wells could be hydrogeologically, hydrochemically and isotopically monitored in order to quantify the role of denitrification and dilution processes in relation to NO_3^- evolution.

5.BIBLIOGRAPHY

REFERENCES

ACA. 2007. Diagnosis de la causalidad de la contaminación por nitratos de algunos abastecimientos públicos en las zonas vulnerables de Cataluña, análisis de alternativas, medidas de prevención y corrección. Área vulnerable 1 Girona. Estudio 1: Llanura aluvial de los ríos Ter y Daró, provincia de Girona. ACA (Water Catalan Agency) Internal Report. 168 pp.

ACORD, GOV/128/2009, de 28 de juliol, de revisió i designació de noves zones vulnerables en relació amb la contaminació per nitrats procedents de fonts agràries. Diari Oficial de la Generalitat de Catalunya. Núm. 5435 – 04.08.2009.

Aitchison, J. 1982. The statistical analysis of compositional data (with discussion). *J. R. Stat. Soc.*, Series B (Statistical Methodology). 44, (2), 139-177.

Aitchison, J., Greenacre, M. 2002. Biplots of compositional data. *Appl. Statist.* 51, 375-392.

Amberger, A., Schmidt, H.-L. 1987. "Naturliche Isotopengehalte von Nitrat als Indikatoren fur dessen Herkunft" (Natural isotope abundance of nitrate as an indicator of its origin). *Geochim. et Cosmochim. Acta,* 51, 2699-2705.

Aravena, R., Mayer, B. 2010. Isotopes and processes in the nitrogen and sulfur cycles. In: Aelion, C.M., Höhener, P., Hunkeler, D., Aravena, R. (Eds.), Environmental Isotopes in Biodegradation and Bioremediation. CRC Press, pp. 203–246.

Bacon-Shone, J. 2011. A short history of compositional data analysis. In: Compositional data analysis: theory and applications, First Edition. Edited by Vera Pawlowsky-Glahn and Antonella Buccianti. John Wiley & Sons, Ltd.

Barth, S. 1998. Application of boron isotopes for tracing sources of anthropogenic contamination in groundwater. *Water Res.* 32, 685– 690.

Basset, R.L., Buszka, P.M., Davidson, G.R., Chong-Diaz, D. 1995. Identification of groundwater solute sources using boron isotopic composition. *Environ. Sci. Technol.* 29, 2915–2922.

Bateman, A,S., Kelly, S.D., Jickells, T.J. 2005. Nitrogen isotope relationships between crops and fertilizer: implications for using nitrogen isotope analysis as an indicator of agricultural regime. *J. Agric. Food Chem.* 53, 5760-5765

Bateman, A.S., Kelly, S.D. 2007. Fertilizer nitrogen isotope signatures. *Isot. Environ. Healt. S.* 43, 237-247.

Beaucaire, N., Gassama, N., Tresonne, N., Louvat, N. 1999. Saline groundwaters in the hercynian granites (Chardon Mine, France): geochemical evidence for the salinity origin. *Appl. Geochem.* 14, 67–84.

Böhlke, J.K., 2002. Groundwater recharge and agricultural contamination. *Hydrogeol. J.* 10, 53–179.

Bonton, A., Rouleau, A., Bouchard, C., Rodriguez, M.J. 2010. Assessment of groundwater quality and its variations in the capture zone of a pumping well in an agricultural area. *Agric. Water Manage*., 97: 824-834.

Borch, T., Kretzschmar, R., Kappler, A., Van Cappellen, P., Ginder-Vogel, M., Voegelin, A., Campbell, K. 2010. Biogeochemical redox processes and their impact on contaminant dynamics. *Environ. Sci. Technol.* 44, 15–23.

Böttcher, J., Strebel, O., Voerkelius, S., Schmidt, H.L. 1990. Using isotope fractionation of nitrate-nitrogen and nitrate-oxygen for evaluation of microbial denitrification in sandy aquifer. *J. Hydrol.* 114, 413-424.

Bryan, N.S., Alexander, D.D., Coughlin, J.R., Milkowski, A.L., Boffetta, P. 2012. Ingested nitrate and nitrite and stomach cancer risk: An updated review. *Food Chem. Toxicol.* 50, 3646–3665.

Brunner, B., Contreras, S., Lehmann, M.F., Matantseva, O., Rollog, M., Kalvelage, T., Klockgether, G., Lavik, G., Jetten, M.S.M., Kartal, B., Kuypers, M.M.M. 2013. Nitrogen isotope effects induced by anammox bacteria. Proceedings of the National Academy of Sciences of the United States of America. www.pnas.org/cgi/doi/10.1073/pnas.1310488110

Burgin, A. J., Hamilton, S. K. 2007. Have we overemphasized the role of denitrification in aquatic ecosystems? A review of nitrate removal pathways. *Front. Ecol. Environ.* 5, (2), 89-96.

Carrillo-Rivera, J.J., Irén Varsányi, I., Kovács, L.O., Cardona, A. 2007. Tracing groundwater flow systems with hydrogeochemistry in contrasting geological environments. *Water Air Soil Poll.* 184, 77–103.

Carucci, V., Petitta, M., Aravena, R. 2012. Interaction between shallow and deep aquifers in the Tivoli Plain (Central Italy) enhanced by groundwater extraction: A multi-isotope approach and geochemical modeling. *Appl. Geochem.* 27, (1), 266-280.

Casciotti, K.L., Sigman, D.M., Galanter Hastings, M., Böhlke, J.K., Hilkert, A. 2002. Measurement of the oxygen isotopic composition of nitrate in seawater and freshwater using the denitrifier method. *Anal. Chem.* 74, (19), 4905–4912

Cey, E. E., Rudolph, D. L., Aravena, R., Parkin, G. 1999. Role of the riparian zone in controlling the distribution and fate of agricultural nitrogen near a small stream in southern Ontario. *J. Contam. Hydrol.* 37, (1-2), 45–67.

Clark, I.D., Fritz, P. 1997. Environmental isotopes in hydrogeology. Lewis Publishers, New York. 352 pp.

Cravotta, C.A. 1997. Use of stable isotopes of carbon, nitrogen and sulphur to identify sources of nitrogen in surface waters in the lower Susquehanna River Basin, Pennsylvania. U.S. Geological Survey Water-Supply Paper 2497.

Curt, M.D., Aguado, P., Sánchez, G., Bigeriego, M., Fernández, J. 2004. Nitrogen isotope ratios of synthetic and organic sources of nitrate water contamination in Spain. *Water Air Soil Pollut.* 151, (1), 135-142.

Custodio, E., 2002. Aquifer overexploitation: what does it mean? *Hydrogeol. J.* 10, 254–277.

DECRET 220/2001, d'1 d'agost, de gestió de les dejeccions ramaderes. Diari Oficial de la Generalitat de Catalunya. Núm. 3447 - 07.08.2001

DECRET 283/1998, de 21 d'octubre, de designació de les zones vulnerables en relació amb la contaminació de nitrats procedents de fonts agràries. Diari Oficial de la Generalitat de Catalunya. Núm. 2760 - 06.11.1998

DECRET 476/2004, de 28 de desembre, pel qual es designen noves zones vulnerables en relació amb la contaminació de nitrats procedents de fonts agràries. Diari Oficial de la Generalitat de Catalunya. Núm.4292 – 31.12.2004

Devlin, J.F., Sophocleos, M. 2005. The persistence of the water budget myth and its relationship to sustainability. *Hydrogeol. J.* 13, 549–554.

EC (European Communities). 1991. Council Directive 91/676/EC concerning the protection of waters against pollution caused by nitrates from agricultural sources (Nitrate Directive). Official Journal of the European Communities, OJ L 375.

EC (European Communities). 1998. Council Directive 98/83/EC, of 3 November 1998, on the quality of water intended for human consumption.

EC (European Communities). 2000. Directive 2000/60/EC of the European Parliament and of the Council establishing a framework for the Community action in the field of water policy (Water Framework Directive). Official Journal of the European Communities, OJ L 327.

EC (European Communities). 2006. Directive 2006/118/EC of the European Parliament and of the Council on the protection of groundwater against pollution and deterioration (Groundwater Directive). Official Journal of the European Communities, OJ L 372.

EEA (European Environment Agency). 2012. European waters: assessment of status and pressures. EEA Report Nº 8. Published: Nov 13, 2012. Copenhagen, Denmark.

Fenech, C., Rock, L., Nolan, K., Tobin, J., Morrissey, A. 2012. The potential for a suite of isotope and chemical markers to differentiate sources of nitrate contamination: A review. *Water Res.* 46, (7), 2023–2041

Folch, A., Mas-Pla, J. 2008. Hydrogeological interactions between fault zones and alluvial aquifers in regional flow systems. *Hydrol. Process.* 22, 3476-3487.

Folch, A., 2010. Geological and human influences on groundwater flow systems in range-and-basin areas: the case of the Selva Basin (Catalonia, NE Spain). PhD Dissertation. Universitat Autònoma de Barcelona.

Folch, A., Menció, A., Puig, R., Soler, A., Mas-Pla, J. 2011. Groundwater development effects on different scale hydrogeological systems using head, hydrochemical and isotopic data and implications for water resources management: The Selva basin (NE Spain). *J. Hydrol.* 403, (1–2), 83–102.

Foster, S., Chilton, J., Nijsten, G.J., Richts, A. 2013. Groundwater – a global focus on the 'local resource'. Current Opinion in Environmental Sustainability. 5, 685-695.

Fukada, T., Hiscock, K., Dennis, P.F., Grischek, T. 2003. A dual isotope approach to identify denitrification in groundwater at a river-bank infiltration site. *Water Res.* 37, 3070–3078.

Gabriel, K.R. 1971. The biplot graphic display of matrices with application to principal component analysis. *Biometrika.* 58, (3), 453–467.

Galloway, J.N., Dentener, F.J., Capone, D.G., Boyer, E.W., Howarth, R.W., Seitzinger, S.P., Asner, G.P., Cleveland, C.C., Green, P.A., Holland, E.A., Karl, D.M., Michaels, A.F., Porter, J.H., Townsend, A.R., Vörösmarty, C.J. 2004. Nitrogen cycles: past, present, and future. *Biogeochemistry.* 70, 153–226.

Gascoyne, M., Davison, C.C., Ross, J.D., Pearson, R. 1987. Saline groundwaters and brines in plutons in the Canadian Shield. In: Fritz, P., and Frape, S.K. (eds.) Saline Water and Gases in Crystalline Rocks. Geological Association of Canada Special Paper. 33, 53-68.

Heaton, T.H.E. 1986. Isotopic studies of nitrogen pollution in the hydrosphere and atmosphere: a review. *Chem. Geol.* 59, 87–102.

Karr, J.D., Showers, W.J., Wendell Gilliam, J., Scott Andres, A. 2001. Tracing nitrate transport and environmental impact from intensive swine farming using delta nitrogen-15. J. *Environ. Qual.* 30, 1163–1175.

Kendall, C. 1998. Tracing nitrogen sources and cycling in catchments. In: Isotope Tracers in Catchment Hydrology, C. Kendall and J. J. McDonnell (Eds.). Elsevier Science B.V., Amsterdam, 839 p., 519-576.

Kendall, C., Elliott, E.M., Wankel, S.D. 2007. Tracing anthropogenic inputs of nitrogen to ecosystems, Chapter 12. In: R.H. Michener and K. Lajtha (Eds.), Stable Isotopes in Ecology and Environmental Science, 2nd edition, Blackwell Publishing, pp. 375-449.

Komor, S.C. 1997. Boron contents and isotopic compositions of hog manure, selected fertilizers, and water in Minnesota. *J. Environ. Qual.* 26, 1212–1222.

Kroopnick, P.M. and Craig, H. 1972. Atmospheric oxygen: Isotopic composition and solubility fractionation. *Science*. 175, 54-55.

Krouse, H.R., Van Everdingen, R.O. 1986. Interpretation of oxygen isotope data for sulphate in subsurface waters. In *5th International Symposium on Water-Rock interactions. Extended Abstratcts,* Reykjavik, pp 663-666. International Association of Geochemistry and Cosmochemistry.

Krouse, H.R., Gould, W.D., McCready, R.G.L., Raja, S., 1991. O incorporation into sulphate during the bacterial oxidation of sulphide minerals and the potential for oxygen isotope exchange between O2, H2O and oxidized sulphur intermediates. *Earth Planet. Sc. Lett*. 107, 90-94.

Laegreid, M., Bockman, O.C., Kaarstad, O. 1999. Agriculture, fertilizers and the environment. Norsk Hydro ASA, Porsgruun, Norway.

Li, X., Zhang, L., Hou, X. 2008. Use of hydrogeochemistry and environmental isotopes for evaluation of groundwater in Qingshuihe Basin, northwestern China. *Hydrogeol. J.* 16, 335–348.

Llamas, M.R., Martínez-Santos, P. 2004. Ethical issues in relation to intensive groundwater use. In: Selected Papers of the Symposium on Intensive Groundwater Use (SINEX). Balkema Publishers, The Netherlands, pp. 17–36.

Mahlknecht, J., Gárfias-Solis, J., Aravena, R., Tesch, R. 2006. Geochemical and isotopic investigations on groundwater residence time and flow in the Independence Basin, Mexico. *J. Hydrol.* 324, 283–300.

Mariotti, A., Germon, J.C., Hubert, P., Kaiser, P., Letolle, R., Tardieux, P. 1981. Experimental determination of nitrogen kinetic isotope fractionation: some principles, illustration for the denitrification and nitrification processes. *Plant Soil*. 62, 413–430.

McCready, R.G.L., Gould, W.D., Barendregt R.W. 1983. Nitrogen isotope fractionation during the reduction of NO_3^- to NH_4^+ by *Desulfovibrio sp*. *Can. J. Microbiol*. 29, 231–234.

McIlvin, M.R., Altabet, M.A. 2005. Chemical conversion of nitrate and nitrite oxide for nitrogen and oxygen isotope analysis in freshwater and seawater. *Anal. Chem.* 77, (17), 5589-5595

Menció, A. 2006. Anàlisi multidisciplinària de l'estat de l'aigua a la depressió de la Selva. PhD Dissertation. Universitat Autònoma de Barcelona.

Menció, A., Mas-Pla, J., Otero N., Soler, A. 2011. Nitrate as a tracer of groundwater flow in a fractured multilayered aquifer. *Hydrolog. Sci. J.* 56 (1), 108-122. DOI: 10.1080/02626667.2010.543086.

Mizutani, Y., Rafter, T.A., 1973. Isotopic behaviour of sulphate oxygen in the bacterial reduction of sulphate. *Geochem.* J. 6, 183-191.

Moore, K.B., Ekwurzel, B., Esser, B.K., Hudson, G.B. Moran, J.E. 2006. Sources of groundwater nitrate revealed using residence time and isotope methods. *Appl. Geochem.* 21, 1016-1029.

Neal, C., Neal, M., Warrington, A., Àvila, A., Piñol, J., Rodà, F. 1992. Stable hydrogen and oxygen isotope studies of rainfall and streamwaters for two contrasting holm oak areas of Catalonia, northeastern Spain. *J. Hydrol.* 140, 163–178.

Nolan, B. T., Hitt, K. J. 2006. Vulnerability of shallow groundwater and drinking-water wells to nitrate in the United States. *Environ. Sci. Technol.* 40, 7834–7840.

Otero, N., Canals, A., Soler, A. 2007. Using dual-isotope data to trace the origin and processes of dissolved sulphate: a case study in Calders stream (Llobregat basin, Spain). *Aquat. Geochem.* 13, 109-126.

Otero, N., Torrentó, C., Soler, A., Menció, A., Mas-Pla, J. 2009. Monitoring groundwater nitrate attenuation in a regional system coupling hydrogeology with multi-isotopic methods: the case of Plana de Vic (Osona, Spain). *Agr. Ecosyst. Environ.* 133, (1-2), 103-113.

Palmer, P.C., Gannett, M.W., Stephen, R., Hinkle, S.R. 2007. Isotopic characterization of three groundwater recharge sources and inferences for selected aquifers in the upper Klamath Basin of Oregon and California, USA. *J. Hydrol.* 336, 17–29.

Piqué, A. 2008. Insights into the geochemistry of F, Ba and Zn-(Pb) hydrothermal systems: examples from northern Iberian Peninsula. PhD Dissertation. Universitat de Barcelona.

Postma, D, Boesen, C., Kristiansen, H., Larsen, F. 1991. Nitrate reduction in an unconfined sandy aquifer – water chemistry, reduction processes, and geochemical modeling. *Water Resources Res.* 27, 2027-2045.

Real Decreto 261/1996, de 16 de febrero, sobre protección de las aguas contra la contaminación producida por los nitratos procedentes de fuentes agrarias. BOE num. 61. 11 de marzo de 1996

Rivett, M.O., Buss, S.R., Morgan, P., Smith, J.W.N., Bemment, C.D. 2008. Nitrate attenuation in groundwater: a review of biogeochemical controlling processes. *Water Res.* 42, 4215–4232.

Rockström, J. 2009. A safe operating space for humanity. Nature. 461, 472-475.

Schwientek, M., Einsiedl, F., Stichler, W., Stögbauer, A., Strauss, H., Maloszewski, P. 2008. Evidence for denitrification regulated by pyrite oxidation in a heterogeneous porous groundwater system. *Chem. Geol.* 255, 60–67.

Sebilo, M., Mayer, B., Nicolardot, B., Pinay, G., Mariotti, A. 2013. Long-term fate of nitrate fertilizer in agricultural soils. PNAS (Proceedings of the National Academy of Sciences of the United States of America). www.pnas.org/cgi/doi/10.1073/pnas.1305372110

Seiler, R. L. 2005. Combined use of ^{15}N and ^{18}O of nitrate and 11B to evaluate nitrate contamination in groundwater. *Appl. Geochem.* 20, 1626-1636.

Silva, S.R., Kendall, C., Wilkison, D.H., Ziegler, A.C., Chang, C.C.Y., Avanzino, R.J. 2000. A new method for collection of nitrate from fresh water and the analysis of nitrogen and oxygen isotope ratios. *J. Hydrol.* 228, 22–36.

Sigman, D.M., Casciotti, K.L., Andreani, M., Barford, C., Galanter, M., Böhlke, J.K. 2001. A bacterial method for the nitrogen isotopic analysis of nitrate in seawater and freshwater. *Anal. Chem.* 73, (17), 4145-4153.

Stevenson, F.J., Cole, M.A. 1999. Cycles of soil. Carbon, Nitrogen, Phosphorus, Sulfur, Micronutrients. John Wiley & Sons, 427 pp.

Sutton, M.A., Howard, C.M., Erisman, J.W. 2011. The European nitrogen assessment: sources, effects and policy perspectives. Cambridge University Press, 612 pp.

Tirez, K., Brusten, W., Widory, D., Petelet, E., Bregnot, A., Xue, D., Boeckx, P., Bronders, J. 2010. Boron Isotope Ratio (δ11B) Measurements in Water Framework Directive Programs: Comparison between Double Focusing Sector Field ICP and Thermal Ionization Mass Spectrometry. *J. Anal. At. Spectrom.* 25, 964-974.

Tóth, J. 1995. Hydraulic continuity in large sedimentary basins. *Hydrogeol. J*. 3, 4–16.

Tóth, J. 2000. Las aguas subterráneas como agente geológico: Causas, procesos y manifestaciones. Boletín Geológico y Minero, 111, (4), 9–26.

U.S. Environmental Protection Agency Ground Water and Drinking Water. 2006. Consumer Factsheet on: Nitrates/Nitrites.

Utrilla, R., Pierre, C., Ortí, F., Pueyo, J.J. 1992. Oxygen and sulphur isotope compositions as indicators of the origin of Mesozoic and Cenozoic evaporites from Spain. *Chem. Geol. Isotopes Geosci*. 102, 229–244.

Vengosh, A., Heumann, K.G., Juraske, S., Kasher, R. 1994. Boron isotope application for tracing sources of contamination in groundwater. *Environ. Sci. Technol.* 28, 1968-1974.

Vilanova, E. 2004. Anàlisi dels sistemes de flux a l'àrea Gavarres-Selva-Baix Empordà. Proposta de model hidrodinàmic regional. PhD Dissertation. Universitat Autònoma de Barcelona.

Vilanova, E. and Mas-Pla, J. 2004. Identificación de sistemas de flujo en base a datos isotópicos en el área Gavarres-Baix Empordà-Selva (CIC). *Geotemas*, 6, (4), 197-202.

Vitòria, L. 2004. Estudi multi-isotòpic ($\delta^{15}N$, $\delta^{34}S$, $\delta^{13}C$, $\delta^{18}O$, δD i $^{87}Sr/^{86}Sr$) de les aigües subterrànies contaminades per nitrats d'origen agrícola i ramader. Translated title: Multi-isotopic approach ($\delta^{15}N$, $\delta^{34}S$, $\delta^{13}C$, $\delta^{18}O$, δD and $^{87}Sr/^{86}Sr$) of nitrate contaminated groundwaters by agricultural and stockbreeder activities. PhD Thesis. Universitat de Barcelona, 188 pp.

Vitòria, L., Otero, N., Canals, A., Soler, A. 2004b. Fertilizer characterization: isotopic data (N, S, O, C and Sr). *Environ. Sci. Technol.* 38, 3254–3262.

Vitòria, L., Soler, A., Aravena, R., Canals, A. 2005. Multi-isotopic approach ^{15}N, ^{13}C, ^{34}S, ^{18}O and D) for tracing agriculture contamination in groundwater (Maresme, NE Spain). In: Environmental Chemistry (Eds. E. Lichtfouse, J. Schwarzbauer and D. Robert). Springer-Verlag, Heidelberg, 43-56.

Vitòria, L., Soler, A., Canals, A., Otero, N. 2008. Environmental isotopes (N, S, C, O, D) to determine natural attenuation processes in nitrate contaminated waters: example of Osona (NE Spain). *Appl. Geochem.* 23, 3597–3611.

Ward, M.H., deKok, T.M., Levallois, P., Brender, J., Gulis, G., Nolan, B.T., VanDerslice, J., 2005. Workgroup report: drinking-water nitrate and health—recent findings and research needs. *Environ. Health Perspect.* 113, 1607–1614.

Wassenaar, L. I., 1995. Evaluation of the origin and fate of nitrate in the Abbotsford aquifer using the isotopes of ^{15}N and ^{18}O in NO_3. *Appl. Geochem.* 10, 391–405.

Wassenaar, L. I., 2006. Decadal Geochemical and Isotopic Trends for Nitrate in a Transboundary Aquifer and Implications for Agricultural Beneficial Management Practices. *Environ. Sci. Technol*. 40, 4626-4632

White, A.F., Schulz, M.S., Lowenstern, J.B., Vivit, D.V., Bullen, T.D. 2005. The ubiquitous nature of accessory calcite in granitoid rocks: implications for weathering, solute evolution, and petrogenesis. Geochimica Cosmochimica Acta, 69 (6), 1455–1471.

WHO, 1993. Guidelines for Drinking Water Quality. 1. Recommendations, 2nd Edition. World Health Organisation, Geneva.

WHO, 2008. Guidelines for drinking-water quality (3rd ed., pp. 417–419). Geneva: WHO Press publishing.

Widory, D., Kloppmann, W., Chery, L., Bonnin, J., Rochdi, H., Guinamant, J.L. 2004. Nitrate in groundwater: an isotopic multi-tracer approach. *J. Contam. Hydrol.* 72, 165-188.

Widory, D., Petelet-Giraud, E., Négrel, P., Ladouche, B. 2005. Tracking the sources of nitrate in groundwater using coupled nitrogen and boron isotopes: a synthesis. *Environ. Sci. Technol.* 39, 539-548.

Widory, D., Petelet-Giraud, E., Brenot, A., Bronders, J., Tirez, K., Boeckx, P. 2013. Improving the management of nitrate pollution in water by the use of isotope monitoring: the $\delta^{15}N$, $\delta^{18}O$ and $\delta^{11}B$ triptych. *Isot. Environ. Healt. S.* 48, 1-19.

Xue, D., Botte, J., De Baets, B., Accoe, F., Nestler, A., Taylor, P., Van Cleemput, O., Berglund, M., Boeckx, P. 2009. Present limitations and future prospects of stable isotope methods for nitrate source identification in surface- and groundwater. *Water Res.* 43, 1159-1170.

Yun, S.I., Ro, H.M., Choi, W.J., Chang, S.X.. 2006. Interactive effects of N fertilizer source and timing of fertilization leave specific N isotopic signatures in Chinese cabbage and soil. *Soil Biol. Biochem*., 38, 1682–1689.

6. ANNEXES

ANNEX A

Folch, A., Menció, A., Puig, R., Soler, A., Mas-Pla, J. (**2011**) Groundwater development effects on different scale hydrogeological systems using head, hydrochemical and isotopic data and implications for water resources management: the Selva basin (NE Spain). *Journal of Hydrology* 403, 83–102.

Impact factor: 2.656 (2011)
Quartile and category: Q1 (5/118), Civil Engineering; Q1 (25/170), Multidisciplinary Geosciences; Q1 (4/78), Water Resources

Journal of Hydrology 403 (2011) 83–102

Contents lists available at ScienceDirect

Journal of Hydrology

journal homepage: www.elsevier.com/locate/jhydrol

Groundwater development effects on different scale hydrogeological systems using head, hydrochemical and isotopic data and implications for water resources management: The Selva basin (NE Spain)

A. Folch [a,*], A. Menció [b], R. Puig [c], A. Soler [c], J. Mas-Pla [b]

[a] Unitat de Geodinàmica Externa i Hidrogeologia. Departament de Geologia, Universitat Autònoma de Barcelona, 08193 Bellaterra, Spain
[b] Grup de Geologia Aplicada i Ambiental (GAiA), Centre de Recerca de Geologia i Cartografia Ambiental (Geocamb), Departament de Ciències Ambientals, Universitat de Girona, 17071 Girona, Spain
[c] Grup de Mineralogia Aplicada i Medi Ambient, Departament de Cristal·lografia, Mineralogia i Dipòsits Minerals, Facultat de Geologia, Universitat de Barcelona (UB), 08028 Barcelona, Spain

ARTICLE INFO

Article history:
Received 12 August 2010
Received in revised form 10 February 2011
Accepted 24 March 2011
Available online 3 April 2011
This manuscript was handled by P. Baveye Editor-in-Chief

Keywords:
Human pressure
Range-and-basin
Groundwater level
Fluoride
Nitrate
Stable isotopes

SUMMARY

Hydrogeological resources in regional, large-scale groundwater systems are conditioned by their specific geological setting, which defines their capacity to supply human demand and their potential to recover from human-induced stress factors such as water withdrawal. In this paper, the hydrogeology of a range-and-basin hydrogeological system is described, based on potentiometric, hydrochemical and isotopic data, in order to fulfill a twofold objective: to characterize the alteration brought about in the hydrogeological system by intensive groundwater withdrawal, where tectonic elements such as fault zones play a significant role in the flow behaviour, and to define groundwater hydrodynamics under current human pressures as a necessary step to achieve appropriate groundwater management. Hydraulic head data indicate the relationships between geological formations in the range areas and the sedimentary infill of the basin. In this set-up, fault zones and a fracture network have a direct effect on the recharge, and allow upward vertical flow from the basement to the sedimentary aquifers. Hydrochemical and isotopic data support this observation. The use of fluoride and nitrate as tracers for the contribution of deep and shallow flow systems provides a detailed portrait of the effects of pumping on the flow path distribution. Isotopic data depict seasonal trends in the water captured by wells. In this connection, we can differentiate between two distinct flow systems: a regional, large-scale, longer residence time system, originating in the surrounding ranges, and a local flow system constituted by infiltration in the lower areas of the basin. The two systems, with specific water qualities, contribute differently to the resources that are withdrawn, and their specific contributions, in the frame of the basin water budget, determine the potential for present sustainable water exploitation.

1. Introduction

In many areas, groundwater has become a primary resource for supplying human demand. In some cases, a continuous growth in demand has modified the natural water balance that defines the amount of available resources (Devlin and Sophocleos, 2005). From a holistic perspective, a conceptual approach that encompasses such human pressures must recognize the hydrogeological heterogeneity provided by the complexity of the geological scenario and the potential contributions of distinct recharge areas once groundwater withdrawal has begun (Mahlknecht et al., 2006; Palmer et al., 2007; Li et al., 2008). Indeed, development usually takes place before appropriate hydrogeological studies have determined the suitability of the aquifer system for groundwater withdrawal. As a consequence, research in these areas lacks the aid of historical data records and, frequently, the occurrence of a reliable sample network which has to be substituted by data from private wells. More importantly, groundwater exploitation may have already disturbed the natural flow system, even at a regional scale. Therefore, hydrogeologists must cope with datasets that already reflect the effects of human pressures upon flow fields.

Water balances are undoubtedly a delicate matter in hydrogeological research. In particular, the occurrence of groundwater flows from neighboring basins, in the form of subsurface recharge or discharge, is usually indirectly inferred or deduced through numerical simulations. Field determinations based on potentiometric, hydrochemical or isotopic data are therefore fundamental in depicting groundwater flows within aquifers, and between distinct geological formations (e.g., Cunningham et al., 1998; Chen et al., 2004; Sukhija et al., 2006; Demlie et al., 2007; Aji et al., 2008;

* Corresponding author. Tel.: +34 581 2556; fax: +34 581 1263.
E-mail address: albert.folch@uab.cat (A. Folch).

0022-1694/$ - see front matter © 2011 Elsevier B.V. All rights reserved.
doi:10.1016/j.jhydrol.2011.03.041

among others). These attempts, however, encounter additional difficulties where tectonic structures add complexity to the regional geological setting, and when, as mentioned, intensive groundwater exploitation, characterized by seasonal withdrawal regimes, different exploitation depths, sparse well distribution, and so on, modifies the naturally steady flow systems under predevelopment

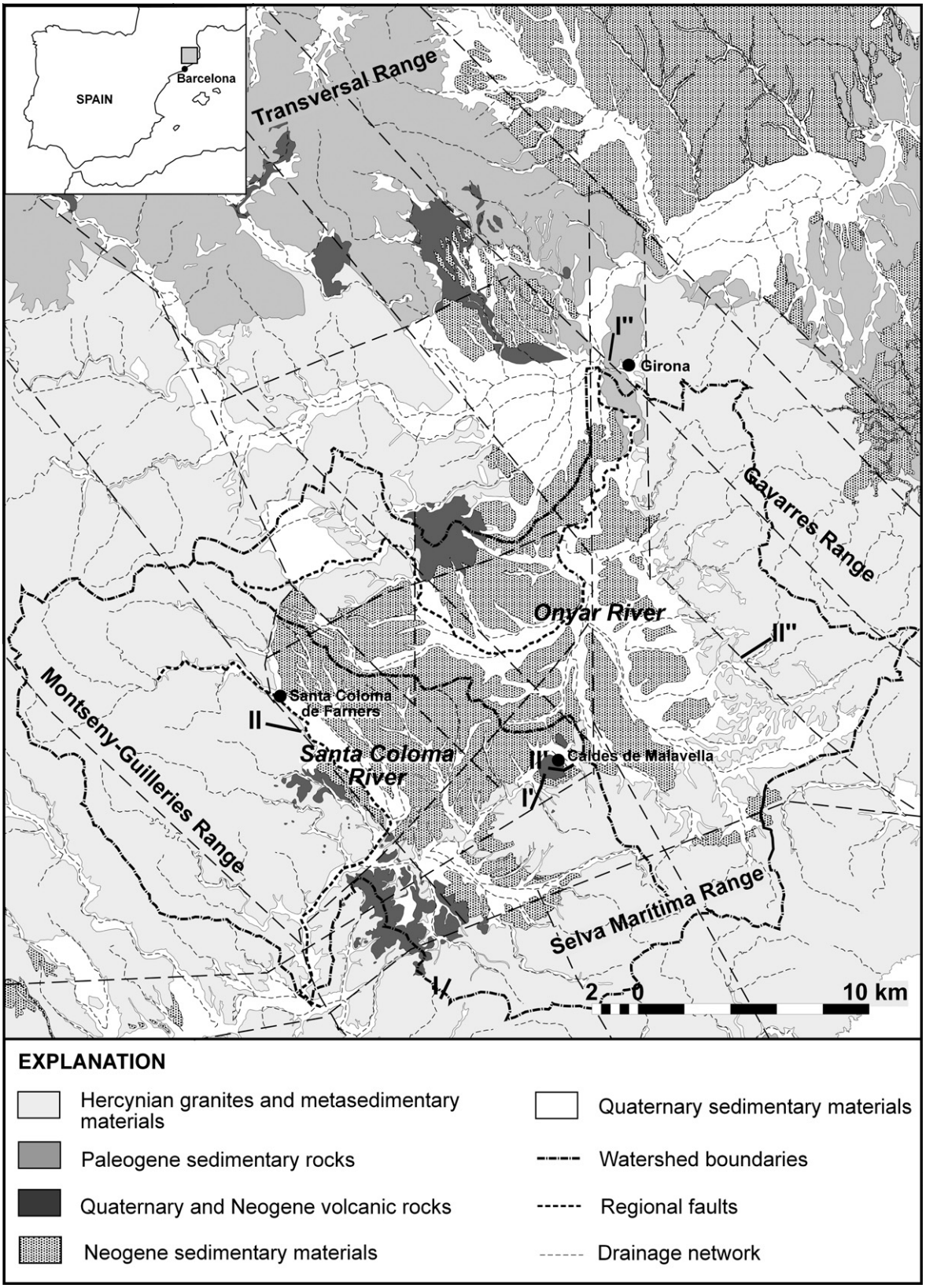

Fig. 1. Geographical situation and geological setting of the Selva basin. I and II refer to geological cross-sections shown in Fig. 2.

conditions. It is in this context where a multiparametric approach is required to provide a primary sound hydrogeological description and diagnosis for a hydrogeological system under recent development with severe exploitation rates.

All these aspects coexist in the Selva basin (NE Spain, Fig. 1), where the recent development of agricultural and industrial activity and a growing urban sprawl have called into question the future availability of water resources and their sustainable management under foreseeable water demand (Menció, 2006). The Selva basin is a range-and-basin area of an approximate extension of 565 km^2, where groundwater exploitation meets most of the human demand (Menció et al., 2010).

Tectonic structures exert an important role in this hydrogeological system, as indicated by the naturally occurring thermal and/or CO_2-rich springs exploited since the Roman period. Previous research in the study area has shown that tectonic elements are responsible for a significant recharge towards the sedimentary infilling of the basin, and flow systems of different spatial magnitude have been described (Vilanova, 2004; Menció, 2006; Folch and Mas-Pla, 2008). Nevertheless, these studies do not address the effect of groundwater withdrawal on the forced recharge towards the aquifer, and therefore the role of distinct recharge areas on the water balance of the basin. Furthermore, groundwater exploitation takes place during the irrigation season when recharge is almost nil. In this scenario, the distortion of flow systems caused by water withdrawal is relevant as it may limit inflow magnitudes leaked from other geological formations. Such alterations, described within the appropriate hydrogeological framework, are therefore of major interest in defining the availability of groundwater resources in the face of potential future demand.

The objective of this paper is to characterize the alteration of a hydrogeological system located in a range-and-basin area by intensive groundwater withdrawal, where tectonic elements such as fault zones are expected to contribute to the overall recharge of the aquifers. Within this context, we seek to construct a conceptual hydrodynamic framework, supported by potentiometric, hydrochemical and isotopic data. This model must provide a suitable explanation of the seasonal variations in the system due to groundwater extraction, during withdrawal as well as recovery periods, that fit with the behaviour observed under the present exploitation regime. Our contention is that understanding the alteration of natural flow systems at a seasonal frequency will reveal their hydrodynamics under current human pressures, and therefore, provide criteria for the groundwater management of these water resources.

2. Study area and geological setting

The Selva basin is a tectonic area surrounded by the Montseny–Guilleries (1202 m asl), Gavarres (535 m asl), Selva Marítima (519 m asl) and Transversal (998 m asl) mountain ranges in the province of Girona (NE Spain) (Fig. 1). There are two main watersheds in the study area, those of the Santa Coloma River and Onyar River basins. The Santa Coloma River Basin (SCRB) extends along the entire length of the south-western side of the Selva basin, with part of its headwaters in the Montseny–Guilleries mountains. The Onyar River basin (ORB) occupies the north-eastern side of the basin, and its headwaters are in the Gavarres and Selva Marítima ranges. Topography within the basin ranges from 65 m asl at the northern and southern limits, to 145 and 220 m asl in the highest hills of the ORB and SCRB, respectively.

An annual human demand of 27.1 h m^3 (1 h m^3 = 10^6 m^3) is supplied mainly by groundwater, with 16.0 h m^3 devoted to agricultural uses, primarily during the summer. Mean annual rainfall is approximately 705 mm; that is, about 398 h m^3 for the entire ORB and SCRB basins. Menció et al. (2010) propose a water budget approach that allows the contribution of groundwater inputs into the hydrogeological system to be estimated based on the surface water budget (i.e., the average rainfall, evapotranspiration and surface runoff parameters) and the human groundwater exploitation. According to this, a net annual groundwater inflow from the nearby basins of between 19.8 and 46.6 h m^3 is needed to compensate human exploitation and natural discharge towards streams and surrounding aquifers. Such a wide inflow rate range is due to the different ways of estimating actual evapotranspiration values.

Geomorphologically, the Selva basin constitutes a type of range-and-basin structural area (Pous et al., 1990). It was created during the distensive period following the Alpine orogeny during the Neogene. The main fault direction in the area is NW–SE, with other significant faults, oriented NE–SW and N–S, being responsible for the tectonic and morphological evolution of the area (Duran, 1985). The surrounding ranges consist of Paleozoic igneous and metamorphic rocks in the Montseny–Guilleries, Selva Marítima and Gavarres, and pre-Alpine Paleogene sedimentary rocks (mainly limestone and sandstone) in the Transversal range. The basin sedimentary infill consists of a layer of unconsolidated gravel, coarse and medium sand and layers of silt, deposited by alluvial fan systems during the basin formation (Fig. 2). They can reach a total thickness of more than 200 m in the western area, varying according to the tectonic blocks that form the basin basement.

Groundwater occurs in unconfined conditions in shallow sedimentary formations, such as alluvial and weathered zones, and in confined and leaky conditions at deeper levels. Hydrogeologically, three main units can be determined: (1) the upper aquifer formed by alluvial materials associated with the main rivers, surface Neogene sedimentary layers, and weathered igneous rocks outcropping in the basin; (2) an alternation of silts, arkosic sands, gravels and conglomerates with low clay content of Neogene sediment, resulting in an intermediate multilayer aquifer with thicknesses from 20 to 300 m (MOPU, 1985; Pous et al., 1990); and (3) a deep aquifer, formed by the granite basement affected by local and regional faults and by a weathering cap in the upper zones. Wells located in the foothills of the ranges exploit weathered granite layers under unconfined conditions or, if drilled in unaltered rock, benefit from the occurrence of fractures. In particular, the Santa Coloma fault zone (Fig. 2), located on the western boundary of the basin, has a strong regional geological, as well as hydrogeological, significance.

3. Methodology and analytical procedures

Field surveys in the Selva basin were conducted from 2000 to 2006. Groundwater hydraulic head was measured in successive years: 2000 (December), 2002 (September), 2003 (February, July and December), 2004 (May and October), 2005 (May and October), 2006 (May). The number of head data measured was between 156 and 366, depending on the season and year. Hydraulic heads were measured under non-pumping conditions.

Hydrochemical data from 60 water samples were collected in May 2006. Sampling points were in the Selva basin sedimentary infill and in the surrounding ranges (Fig. 3). Fifty-five wells between 7 and 150 m deep were sampled. In addition, three springs (SCFP, SCFSS, SG0200) in different geological settings coinciding with fault zones were analyzed, and two surface water samples from the Santa Coloma River complemented the dataset. Hydrochemical data from previous surveys are provided by Menció (2006). The isotopic data used in this study were collected in three different seasons in 2003 (May, September, and December), and in May 2006 (Fig. 3). Environmental isotopes, oxygen-18 ($\delta^{18}O$), deuterium

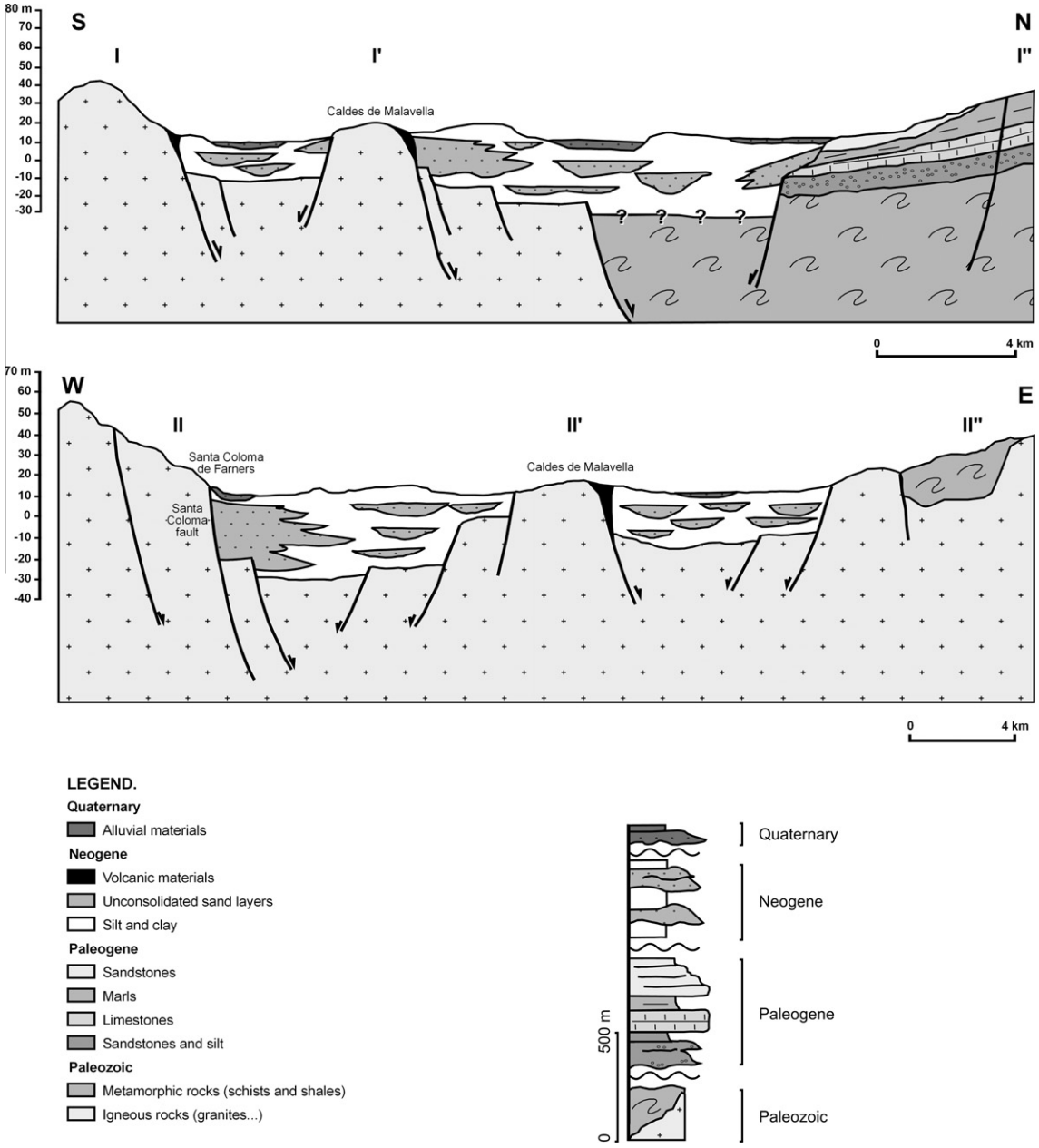

Fig. 2. Schematic cross-sections of the Selva basin. See Fig. 1 for cross-section locations.

(δD), were analyzed. Sample numbers increased from 20 in 2003, to 60 in 2006, to enable better characterization of the hydrogeological system.

Samples for hydrochemical and isotopic analysis were taken under pumping conditions. We ensured that at least three casing volumes of groundwater were removed from each bore prior to sampling. Physicochemical parameters (pH, electrical conductivity (EC), Eh, dissolved O_2 and temperature) were measured *in situ* using a flow cell to avoid contact with the atmosphere. After filtration (0.45 μm), the samples were processed in the field and stored at 4 °C in a dark environment for subsequent chemical and isotopic analyses.

In the laboratory, pH and conductivity at 25 °C were measured again. Alkalinity (HCO_3^-) was measured by titration (METROHM 702SM Titrino) and F^- by the ion selective electrode method (Orion 901 ion selective electrode). The anion (NO_3^-, SO_4^{2-} and Cl^-) content was measured by Capillary Electrophoresis (Agilent Technologies) using indirect UV detection; concentrations of Na^+, K^+, Ca^{2+} were measured by Inductively Coupled Plasma-Optical Emission Spectrometry (ICP-OES, Perkin Elmer 4300 DV). The quality of the chemical analysis was checked by performing an ionic mass balance, with an error lower than 5% accepted.

Deuterium and O isotopes of water were analyzed in a Finnigan Matt Delta S Isotope Ratio Mass Spectrometer (IRMS) coupled to an automated line based on the equilibration between H-water and H_2 gas with a Pt catalyst, and between O-water and CO_2 gas following standard methods (Epstein and Mayeda, 1953). Notation is expressed in terms of δ‰ relative to the international standards V-SMOW (Vienna Standard Mean Oceanic Water) for δD and $\delta^{18}O$. The precision ($\equiv 1\sigma$) of the samples calculated from international and internal standards systematically interspersed in the analytical batches was ±1.5‰ for δD and ±0.2‰ for $\delta^{18}O_{H2O}$.

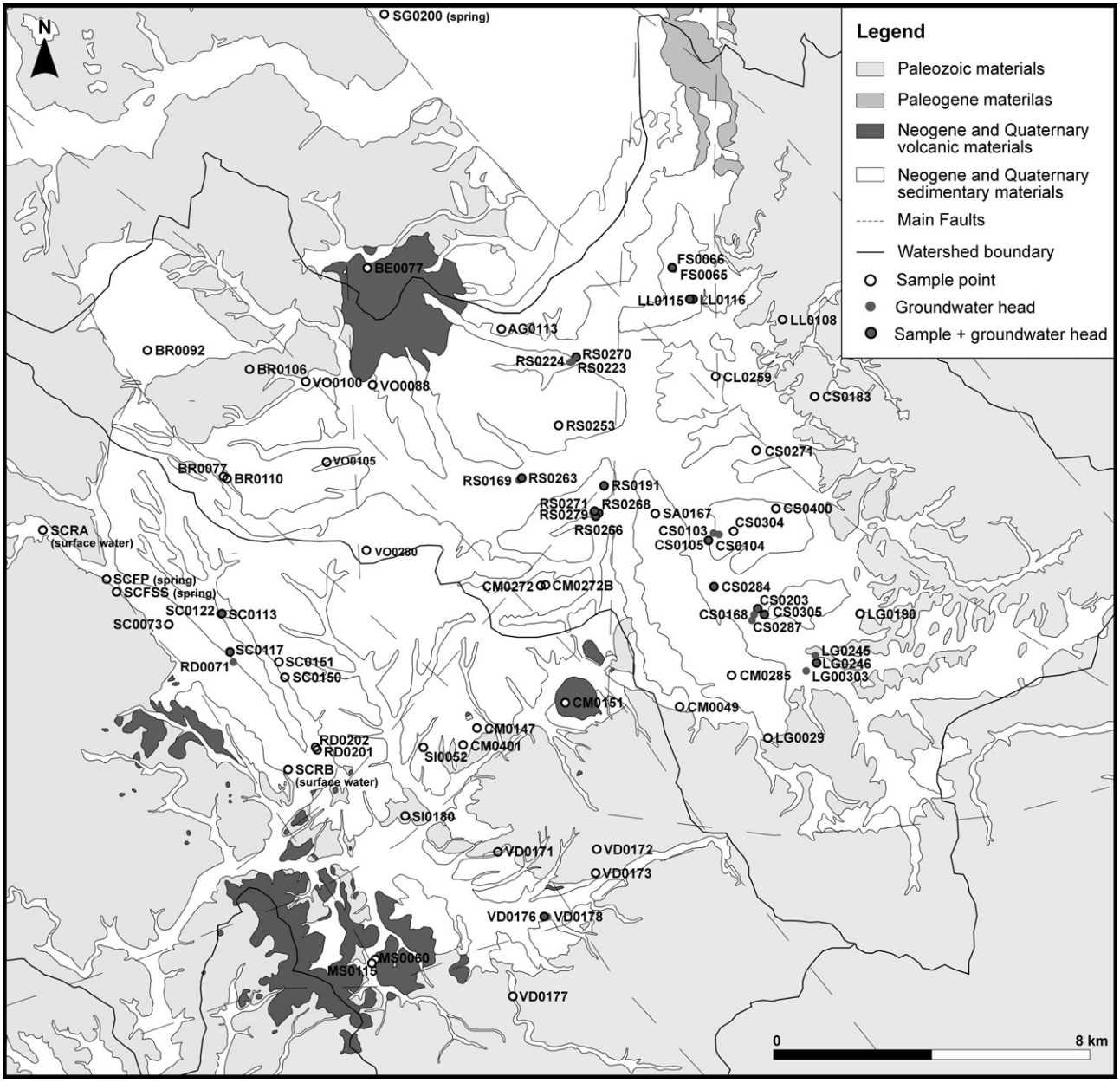

Fig. 3. Sample points used for hydraulic head evolution and/or hydrochemical and isotopic data collection. If not specified, codes in the figure refer to wells. Other wells used for head measurements are not shown for the sake of simplicity. Sampled points refer to wells, surface water and springs sampled for hydrochemistry and/or isotopes shown in Tables 2 and 4. Groundwater head refers to the hydraulic head evolution of wells shown in Table 1.

All chemical and isotopic analyses were prepared in the Mineralogia Aplicada i Medi Ambient Research Group laboratory. Major ions were analyzed at the Servei d'Anàlisi Química (SAQ) of the Autonomous University of Barcelona. The other chemicals and the isotopic compounds were analyzed at the Scientific Services of the University of Barcelona (UB).

Groundwater hydraulic head, hydrochemical and isotopical data were all collected from private wells. These wells seek maximum productivity and some of them are therefore screened at unknown multiple depths. However, most deep wells are cased in the upper 10–20 m limiting the influence of the shallowest aquifer formations. Apart from the most productive level, some water samples are not always taken from the desired aquifer level, and in these cases they may represent a mixture of water from different layers. However, groundwater pumped from each well, whether the result of mixing or not, will show the real features of the water withdrawn from the flow system.

Because of the complexity of the available sampling points, we focused our efforts on grouping samples by their geological and hydrochemical features in an attempt to identify distinct hydrogeological systems, and to provide a complete description of the range-and-basin hydrodynamics.

4. Results and discussion

4.1. Piezometric data

Potentiometric lines were drawn separately for the upper unconfined aquifer, which includes alluvial formations and the uppermost Neogene sedimentary units, and the confined and leaky aquifers underneath (Fig. 4). The boundary for both aquifer systems is set at a depth of 30 m, the maximum depth that can reach shallow unconfined aquifer formations in accordance with local

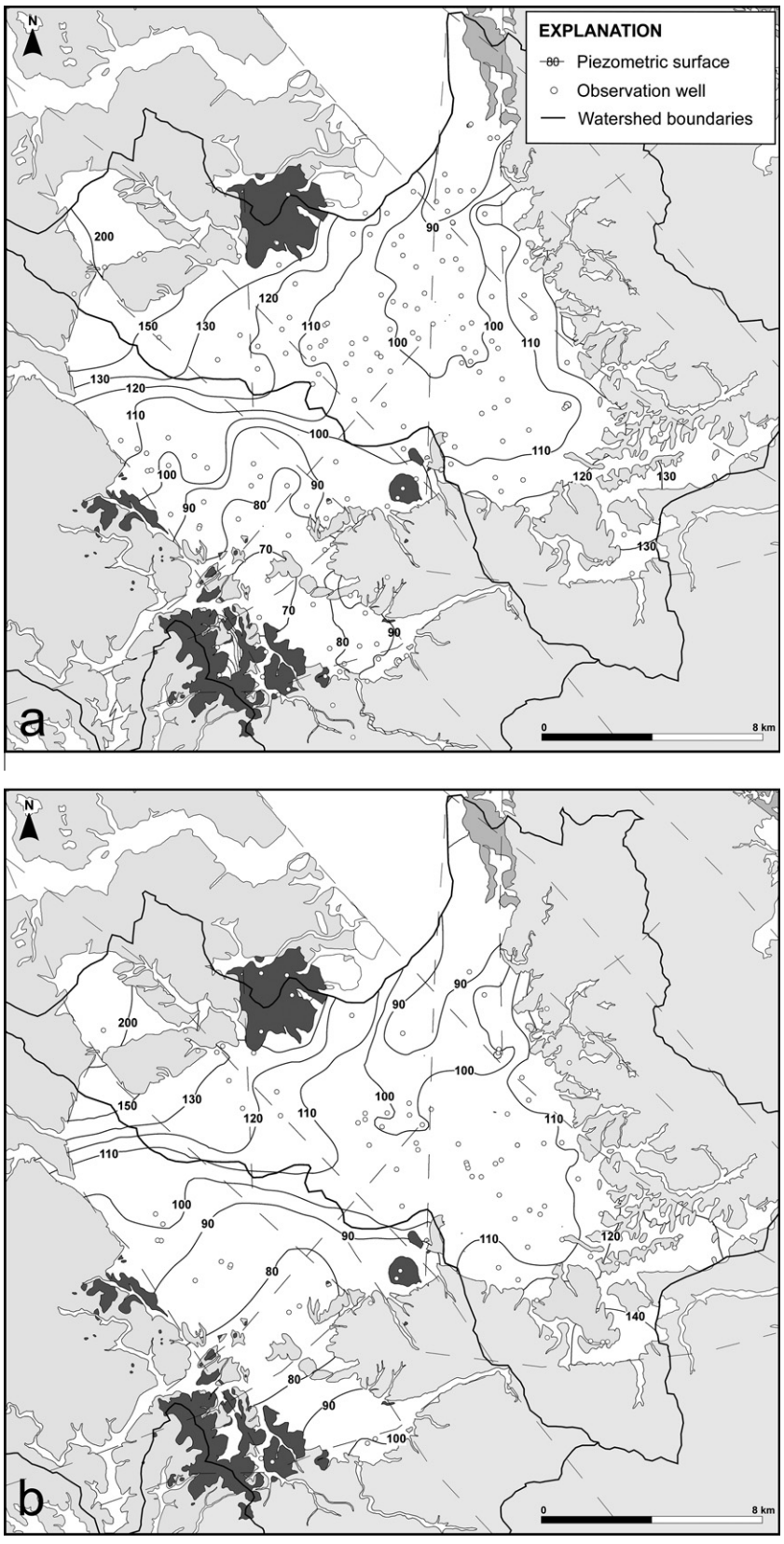

Fig. 4. Potentiometric contour map May 2004. a) Upper unconfined aquifers (around 190 wells less than 30 m deep). b) Deep confined or semi-confined aquifer (around 70 wells over 30 m deep).

sedimentary records. In both maps, flow lines define two main hydrogeological units, in agreement with the hydrographic boundaries of the SCRB and ORB. According to them, the main recharge areas are located in the Montseny–Guilleries and Selva Marítima

ranges for the SCRB, and the Gavarres and Selva Marítima ranges for the ORB. Rainfall infiltration from the basin sedimentary infill surface is also significant in the upper formations.

Groundwater flow systems are south-oriented in the SCRB, and north-oriented in the ORB. Between them, a groundwater divide oriented WNW-ESE appears in the central part of the Selva basin, within the Neogene sedimentary formation, which coincides with the surface limits of both watersheds. This setting reflects a geological control of the head distribution that results in separated flow systems draining in opposite directions, controlled by the drainage pattern of the basin on the surface and by structural elements at depth. It is worth noting that altitude at the northern and southern exits of the two drainage networks is similar (approximately 65 m asl).

River-aquifer interaction changes along the basin with some areas behaving as gaining streams (mainly in the upper parts of the basin) and other areas as losing streams (Folch et al., 2010). Hydrological cross-sections, transversal to the watercourse, show that the water table gradient towards the stream diminishes during dry periods, and in some locations it may even reverse, creating a losing stream scenario. In any case, summer seasons, when major extractions occur, are characterized by a very low or null groundwater contribution to base-flow. Stream discharge does not recover until the October and November rainfall events, which also contribute to the raising of the water table (Menció and Mas-Pla, 2008).

Major head decline in both surface and deep aquifer levels occurs during the driest months (July and August), because of low recharge (Fig. 5) and maximum groundwater extractions (Fig. 6; Table 1). As a result, a reduction in the water stored in the aquifer takes place. Nevertheless, head variations over time reveal specific hydrological behaviour as a response to intense groundwater withdrawal. To discern the behaviour of the flow system under such a development scenario, groundwater head evolution was considered in representative wells between 2000 and 2006.

Because of intensive pumping, deep wells (i.e., those of a depth greater than 30 m) show larger head drawdowns than shallow wells in the upper unconfined formation as expected in leaky and/or confined aquifers. Such large drawdowns occur despite all the Neogene sedimentary infilling, tens of meters thick, and the high hydraulic conductivity of the sandy layers which, *a priori*, should allow significant flow rates, suggesting limited hydraulic connectivity between aquifer layers. However, they recover well at the end of the irrigation season (Fig. 6b, f and Table 1 well zone 1, 4, 7 ,10, 11) indicating induced recharge from the surrounding ranges where, given the structural setting, fluxes take place through fracture networks and fault zones. Such behaviour illustrates the significant influence of pumping on the natural flow fields, forcing discharge from the range areas towards the intensively exploited sedimentary aquifers within the basin by a shift in the water isotopic composition as shown later on in this paper.

Different vertical relationships between surface and deep aquifer levels can be established depending on the location and the geological setting. For instance, close drawdowns are observed in both shallow and deep wells in specific areas, suggesting an effective connection between sedimentary layers that end up behaving as a single hydrogeological unit (Fig. 6c). In other locations, distinct behaviours are identified at depth, depending on the degree of vertical connectivity between Neogene sand layers. For instance, limited connectivity results in distinct hydraulic heads but similar evolution over time (Fig. 6d and Table 1 well zone 7), while in some places deep layers act as confined aquifers with head levels above (Table 1 well zone 1) or below (Fig. 6e and Table 1well zone 5) those of the unconfined aquifers. The latter case is usually found where the upper aquifers are located in topographically elevated areas. In such cases, head differences reflect a practically nil vertical downward leakage between the aquifers.

Head distribution points to there being a lateral hydraulic connection between the range-front areas and the basin aquifers, which indicates an effective recharge through fault zones and fracture networks within the basement (Fig. 4). Similar behaviour can also be said to occur at the contact between the sedimentary infill of the basin and the basement, although the magnitude of the recharge will depend on distinct geological features such as the hydraulic conductivity of the lowest Neogene sediments, the thickness of the weathered granite on the top of the basement, the

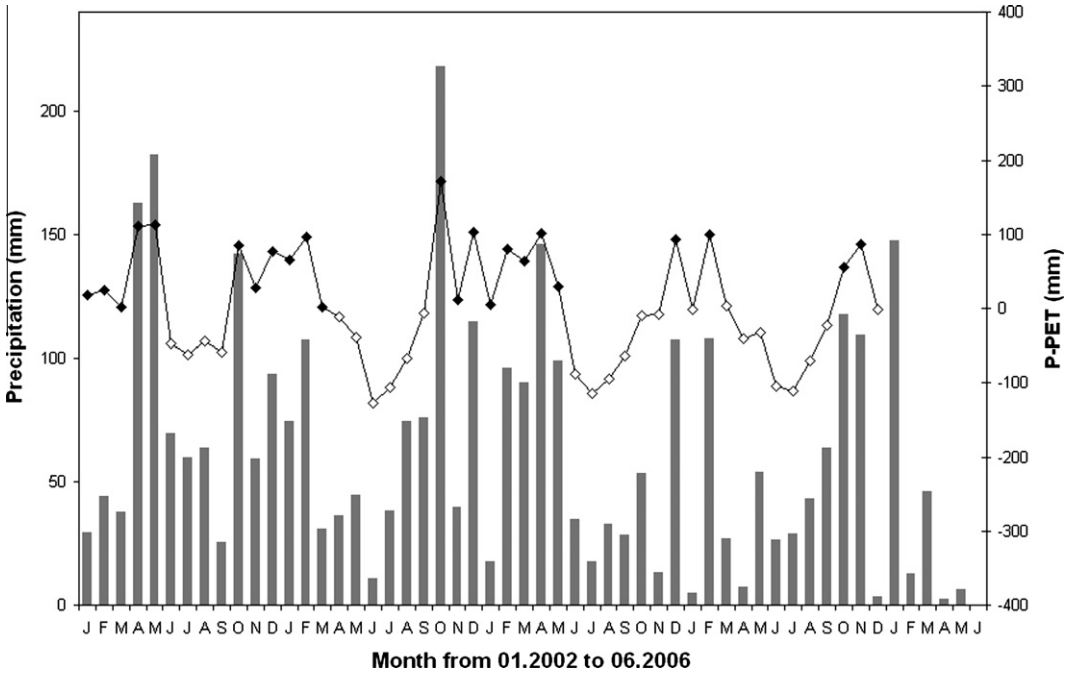

Fig. 5. Precipitation and effective rainfall (i.e., rainfall minus potential evapotranspiration; P-PET) at the Fornells weather station. Data from Servei Meteorològic de Catalunya (http://www.meteocat.com).

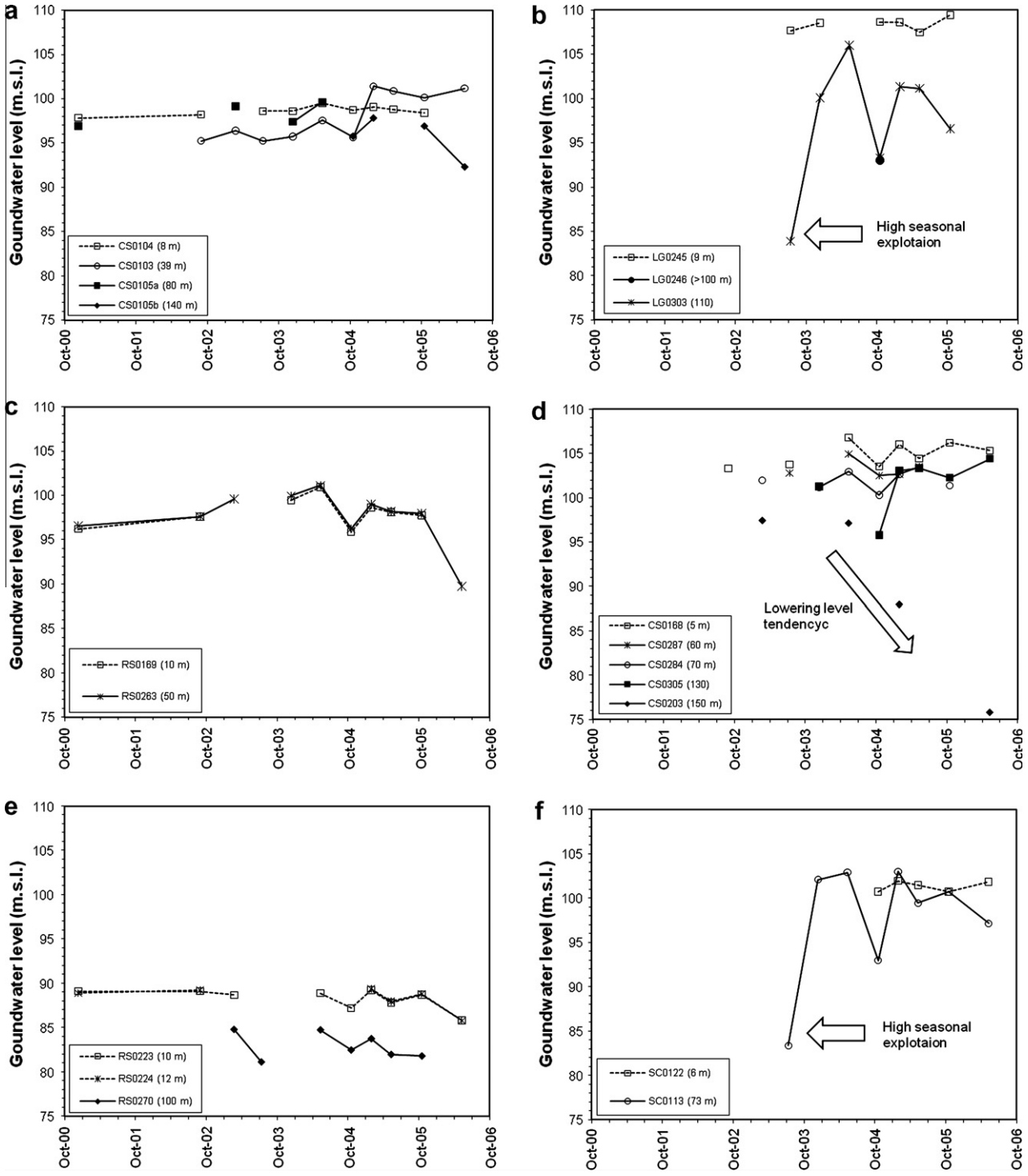

Fig. 6. Groundwater head evolution at different wells in the Selva basin. Each plot represents two or more wells located close to each other. See Fig. 2 for well locations in the Selva basin.

fracture networks, and the vertical head gradient generated by pumping rates. This means that deep wells located in the vicinity of regional fault zones (e.g., CS0203 in Fig. 6d, and LG0303 in Fig. 6b) are the most productive, and will even have a distinct hydrochemical facies. In particular, well CS0203 showed a lowering tendency during the later surveys that was related to fault zones with high storage capacity, but limited recharge.

Wells CS0103, CS0104 and CS0105 (Fig. 6a), with a well depth ranging from 8 to 140 m and ca. 250 meters distance from each other, also reflect the spatial heterogeneity that controls the relationship between the basement (located at a depth of 80 m in this area) and the overlying sedimentary layers. For instance, well CS0105 exploited the sedimentary layers at a depth of 80 m until October 2004 (named CS0105a in the plot) having a yield of 80 m^3/h. Afterwards, the borehole was drilled 60 m into the granitic basement (renamed CS0105b in the plot), increasing its yield to more than 200 m^3/h. This significant change in well yield indicated the significant productivity of the basement fracture and fault networks in comparison with the Neogene sedimentary layers.

Table 1
Geology and hydraulic head (a.s.l) evolution of some representative wells for each field campaign. *Well zone* indicates the nearby location of wells. See Fig. 2 for well locations in the Selva basin.

Code	Well zone	Geology	Depth (m)	December-00	September-02	February-03	July-03	December-03	May-04	October-04	February-05	May-05	October-05	May-06
FS0065	1	Neogene + Granite	26	83.4	84.1	83.9	84.6	84.1	87.1	84.8	84.6	84.6	84.1	
FS0066		Neogene	102	85.2		89.4		88.8	88.4	84.1	89.9	89.5	89.2	88.2
CS0168	2	Quaternary	5		103.3		103.8		106.8	103.5	106.0	104.4	106.2	105.3
CS0203		Neogene + Granite	150			97.4			97.1		88.0			75.8
CS0305		Neogene + Granite	130					101.3		95.8	103.1	103.3	102.3	104.4
CS0284		Neogene	70			102.0		101.2	103.0	100.3	102.7		101.4	
CS0287		Neogene	60				102.8		105.0	102.5	102.7	103.5		
CS0103	3	Neogene	39		95.2	96.4	95.2	95.7	97.6	95.7	101.4	100.9	100.1	101.2
CS0104		Neogene	8	97.8	98.2		98.6	98.6	99.5	98.7	99.1	98.8	98.4	
CS0105a		Neogene	80	96.9		99.2		97.4	99.6					
CS0105b		Neogene + granite	140							95.8	97.8		96.9	92.3
LG0245	4	Quaternary	9				107.7	108.5		108.6	108.6	107.5	109.4	
LG0246		Granit	>100							93.0				
LG0303		Granit	110				83.9	100.1	106.0	93.3	101.4	101.2	96.6	
LL0115	5	Neogene	80			99.4	99.6	99.8	100.4	100.0	100.5	100.5	100.3	
LL0116		Neogene	12				111.0	110.7	111.4	111.3	110.9	110.8	110.6	109.6
RS0223	6	Quaternary	10	89.1	89.1	88.7			88.9	87.2	89.2	87.8	88.7	85.8
RS0224		Quaternary	12	88.9	89.2						89.4	88.0	88.8	85.8
RS0270		Neogene	100			84.8	81.1		84.7	82.5	83.8	82.0	81.8	
RS0191	7	Neogene	105	95.6	94.7	98.0	91.9	97.7	99.3	95.7				
RS0266		Neogene	120			99.6		99.4	101.0	97.9	99.6	97.8	98.6	
RS0268		Neogene	65			98.9		97.6		96.4	97.9	97.5		
RS0271		Quaternary + Neogene	65			98.1			99.6	96.8	98.2	97.0	97.4	96.8
RS0279		Neogene	18				93.6			99.3	100.9	100.5	99.7	
RS0169	8	Quaternary + Neogene	10	96.2	97.6			99.5	100.9	95.9	98.6	98.1	97.7	
RS0263		Quaternary + Neogene	50	96.5	97.6	99.6		99.9	101.1	96.2	99.0	98.2	98.0	89.7
VD0178	9	Neogene	13							82.5	85.6	84.5	86.2	84.5
VD0176		Neogene	69					86.1		83.8	85.4	85.5	83.5	
SC0113	10	Neogene	73				83.4	102.1	102.9	93.0	103.0	99.5	100.7	97.2
SC0122		Quaternary	6							100.7	102.0	101.5	100.7	101.9
SC0117	11	Neogene	65				91.2	94.1	94.2	92.5	94.0	93.0	93.1	93.4
RD0071		Neogene	16		92.3	93.5	93.9	94.0	95.3	93.5	93.9	94.0	93.2	94.2

After extraction in the granitic basement began, well CS0103 (depth of 39 m in the sedimentary infilling) raised its hydraulic head by approximately 10 m (Fig. 6a). As this well maintained its pumping rates during the studied period, this observed head increase after October 2004 suggests that the basement rocks may endure intensive pumping rates with an almost nil hydraulic influence on the overlying sedimentary layers, indicating a limited vertical hydraulic conductivity between the granite and the overlying sedimentary formation in this area.

Water-table in the unconfined aquifer (CS0104) remained fairly steady during the studied period, being unaffected by higher piezometric levels of deeper sedimentary aquifers after October 2004. This behaviour suggests an efficient recharge of deeper Neogene sedimentary layers that did not originate at the basin surface. It is therefore possible to conclude that non local flow systems originating in the surrounding ranges, and flowing through the main tectonic elements that define the geological setting of the system, have a major influence on the recharge of the basin sedimentary infill. This local context indicates that these tectonic elements provide an efficient recharge of the basin sedimentary layers and, at the same time, allow significant exploitation rates within the basement (CS0105b).

The last type of interaction is the seasonal change in the relative groundwater level between surface and deep aquifers (Fig. 6f and Table 1 well zone 1, 9, 10, 11). Throughout the wet season, deep aquifers show higher water levels than shallow ones. Upward vertical flows towards the upper formations depend on leakage magnitude across the overlying aquitards. Conversely, at the end of the dry season, deep aquifer levels decrease because of intensive groundwater withdrawal and show a water level below the upper unconfined aquifers.

To summarize, the two hydrogeological units show differences in the origin of their recharge. The upper unconfined aquifer unit receives superficial recharge through direct rainfall and river infiltration, while deeper aquifer levels are recharged by lateral flow systems and, more importantly, by upward vertical flows from the basement. In addition, lateral flow from the surrounding range areas is also significant. At the same time, hydraulic head data indicate a vertical connection between sedimentary aquifer levels at various depths, which allow distinct vertical connections between the Neogene sedimentary aquifer layers.

Discharge from the system is also different in both units. The upper aquifer mainly drains through the river network as base flow from the alluvial formations (Fig. 1 and Fig. 4) and as a result of pumping. Deep aquifer discharge is also related to water withdrawal, although potentiometric data from the deepest wells suggest an efficient outflow from the basin through regional faults at its south-eastern margin. Evidence of such deep flows is encountered in CO_2-rich springs located on the tectonic boundary between the Selva Marítima and Gavarres ranges (Vilanova, 2004; Vilanova et al., 2008).

The behaviour of and the interactions between distinct hydrogeological units are thus seen to be diverse and dependent on location, geological setting, seasonal variation, and pumping rate. The differences observed between aquifer head levels and productivity indicate the occurrence of recharge fluxes from the range front and the basement. Groundwater capture by pumping modifies natural flow paths and the recharge/discharge relationships between large-scale hydrogeological units. Such a degree of interaction affects groundwater quantity as well as its quality, and ultimately the vulnerability of the Selva basin water resources.

4.2. Hydrochemistry

Each geological environment in the Selva basin has a different hydrochemical facies based on its rock lithology and hydrogeological flow path (Fig. 7). Stiff diagrams (Fig. 8) corresponding to the May 2006 survey identify low salinity groundwater samples on the western side of the SCRB with a mean electrical conductivity of 618 ± 99 μS/cm, whereas those samples from the ORB and eastern SCRB commonly show a higher salinity, with an electrical conductivity mean value of 879 ± 29 μS/cm. Such a general difference can be attributed to the fingerprint of distinct recharge areas, as already suggested by hydraulic head data and potentiometric maps (Fig. 4).

Specifically, groundwater samples from aquifers in Neogene sediments, regardless of their depth, have a Ca–HCO_3 facies (VO0280, SC0117, RS0191, RS0263, CM0272), some of them with a significant chloride content of up to 30–40%, as indicated in the Piper diagram (Fig. 7). Samples from wells in weathered or fractured igneous rocks also have a Ca–HCO_3 facies (e.g., CS0304, SC0117, and SC0113), although in some cases, especially in those wells that are totally or partially drilled in granite, the chloride content increases up to 60%, which defines a Ca–HCO_3–Cl facies (VD0173; VD0172, CS0183).

Sodium content is about 20–40% of the cation proportion in many samples (Fig. 8). Sodium-rich hydrochemical facies, such as Na–HCO_3 and Ca–Na–HCO_3, are thus encountered in deep wells in Neogene materials (RS0270, VD0176) and in granites (VD0177, LG0246, BR0092), provided they are in the vicinity of main fault zones. Some of these samples, for instance, have high chloride concentrations (up to 221 mg/L) without being Na–Cl rich, (FS0066, LG0190, VD0172). Some springs located at the basin border also have sodium-rich hydrochemical facies (SCFP, SG0200).

Hydrochemical facies allow distinct groundwater sources to be differentiated in the main aquifers of the Selva basin (Figs. 7 and 8). Based on their chemical composition, Na–HCO_3 and chloride-rich facies can be attributed to regional flow systems with longer residence times at the subsurface (Gascoyne et al., 1987; Tóth, 1995, 2000; Beaucaire et al., 1999; and Carrillo-Rivera et al., 2007). These samples also have low nitrate concentrations and high fluoride content of up to 15 mg/L, indicating high water–rock interaction (Piqué et al., 2008). In the SCRB, a potential input of deep CO_2 modifying the calcite–fluorite equilibrium may also be controlling the fluoride concentration in groundwater (Table 2). Conversely, local flow systems have Ca–HCO_3 facies with high nitrate, sulphate and chloride concentrations related to pollution sources. This type of facies indistinctively shows a low fluoride content (<2.0 mg/L). Among them, Ca–HCO_3 facies with significant sodium content may be attributed to intermediate flow systems, with sulphate and nitrate concentrations lower than samples from local flow regimes. Some enrichment in chloride may be related to evaporation processes in the unsaturated zone, as revealed by isotopic data shown later in the paper.

Considering that only a few wells drilled in igneous rocks over 100 m deep show redox conditions for denitrification (Table 2), fluoride and nitrate act as valuable tracers that define the origin of groundwater recharge within the basin. High nitrate samples seldom coincide with high fluoride content, and thus define distinct end-members in the recharge of the Selva basin: inflow from rainfall infiltration within the basin will present nitrate pollution, while vertical upward inflow from the granitic basement, or lateral inflow from the range-front as in the Santa Coloma fault zone, will present a significant fluoride concentration (Table 2). It is worth noting that the occurrence of fluoride is limited to wells located along the main fault areas, suggesting an efficient flow path through tectonic structures. Most samples located in these fault areas also show high concentrations of HCO_3^- being saturated or close to saturation with calcite indicating a potential deep CO_2 input or mixing with thermal waters.

Previous studies indicated the occurrence of mixing processes between distinct flow systems (Vilanova, 2004; Menció, 2006;

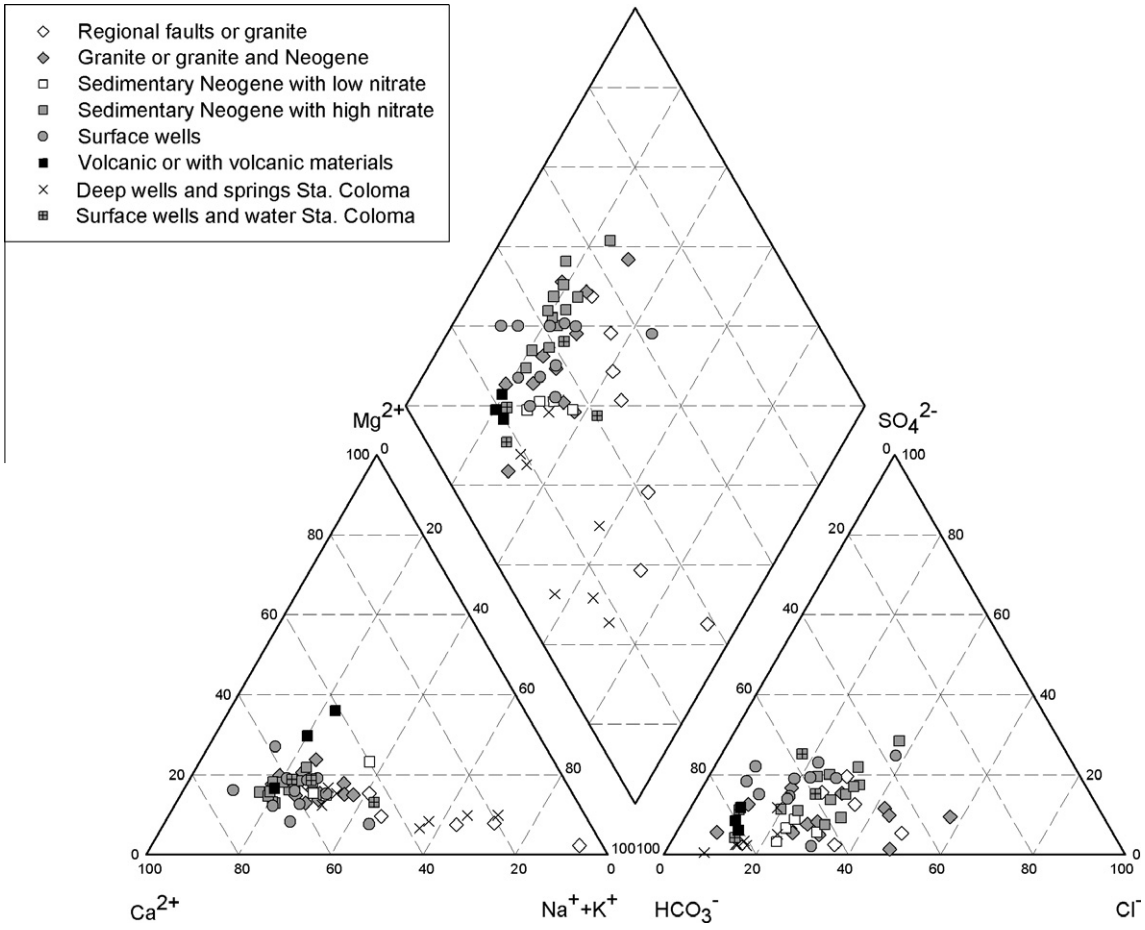

Fig. 7. Piper diagram of May 2006 survey showing hydrochemical groups. See text for explanation.

Folch and Mas-Pla, 2008). In this dataset, some wells present high fluoride concentrations as well as moderated nitrate content (CM0151, SC0117, and CS0304; Table 2). Such hydrochemical composition could also be attributable to mixing caused by the cones of depression inside the aquifer, or simply to the existence of several screened intervals in the borehole. All the same, these samples illustrate the impact of withdrawal on the quality of pumped groundwater.

In summary, hydrochemical facies permit a classification of groundwater samples in different groups according to their geological origin in the ORB and eastern SCRB (Table 3):

1. Samples related to *regional fault zones and granitic aquifers* with fluoride concentrations higher than 2 mg/L, except in the case of SG0200 which, being located on the northern edge of the study area, can be understood to have a hydrochemistry mainly affected by the sedimentary formations of the Transversal range, which do not contain fluoride-rich minerals.
2. Samples from wells in *granitic rocks that may also exploit Neogene sedimentary formations*, usually have a Ca–HCO_3 facies, some of them with high chloride content.
3. Samples from *Neogene sedimentary layers with low nitrate content*, below 37.5 mg/L NO_3, indicate sources from regional or intermediate flow systems, and a minimum contribution from local recharge. Nitrate threshold values of 37.5 mg/L NO_3, and 50.0 mg/L in Group 4, are set based on actual field data values, although they coincide, respectively, with the standard point for pollution trend reversal actions and the quality standard for nitrate defined in the European Groundwater Directive (Directive 2006/118/EC).
4. Samples from *Neogene sedimentary layers with high nitrate content*, usually above 50.0 mg/L NO_3, show the influence of groundwater withdrawal at moderate depth from or below shallow aquifer units. Pumping in the Neogene layers forces a downward flow that conveys nitrate from the surface soil. Such hydrochemical features are common in areas where the Neogene sedimentary unit is homogeneous in its depth, i.e. with insignificant aquitard formations as depicted by well cores and also reflected by potentiometric data.
5. Samples from *surface wells*, whether in alluvial, in the uppermost Neogene layers, or in weathered granite outcrops, have a characteristic Ca–HCO_3 facies, and are likely to present high nitrate concentrations in the eastern SCRB and in the ORB.
6. Samples located totally or partially in *volcanic rock,* with Ca–HCO_3 and/or Ca–Mg–HCO_3, may reach a depth of 80 m and be related to local aquifers and/or deeper system flows.

Finally, two types of wells can be distinguished in the western SCRB with features different to those already described, such as lower salinity content. Accordingly, we differentiate between:

1. Samples from *surface wells and stream water in the SCRB,* with a lower nitrate content than those of the ORB, as a result of various human pressures and agricultural land-use distribution, and
2. Samples from *deep wells and springs in the Santa Coloma River basin,* also with a significant fluoride content and low nitrate concentration.

One of the main outcomes of the dataset is that surface wells are seen to have a wide range of hydrochemical facies. This can

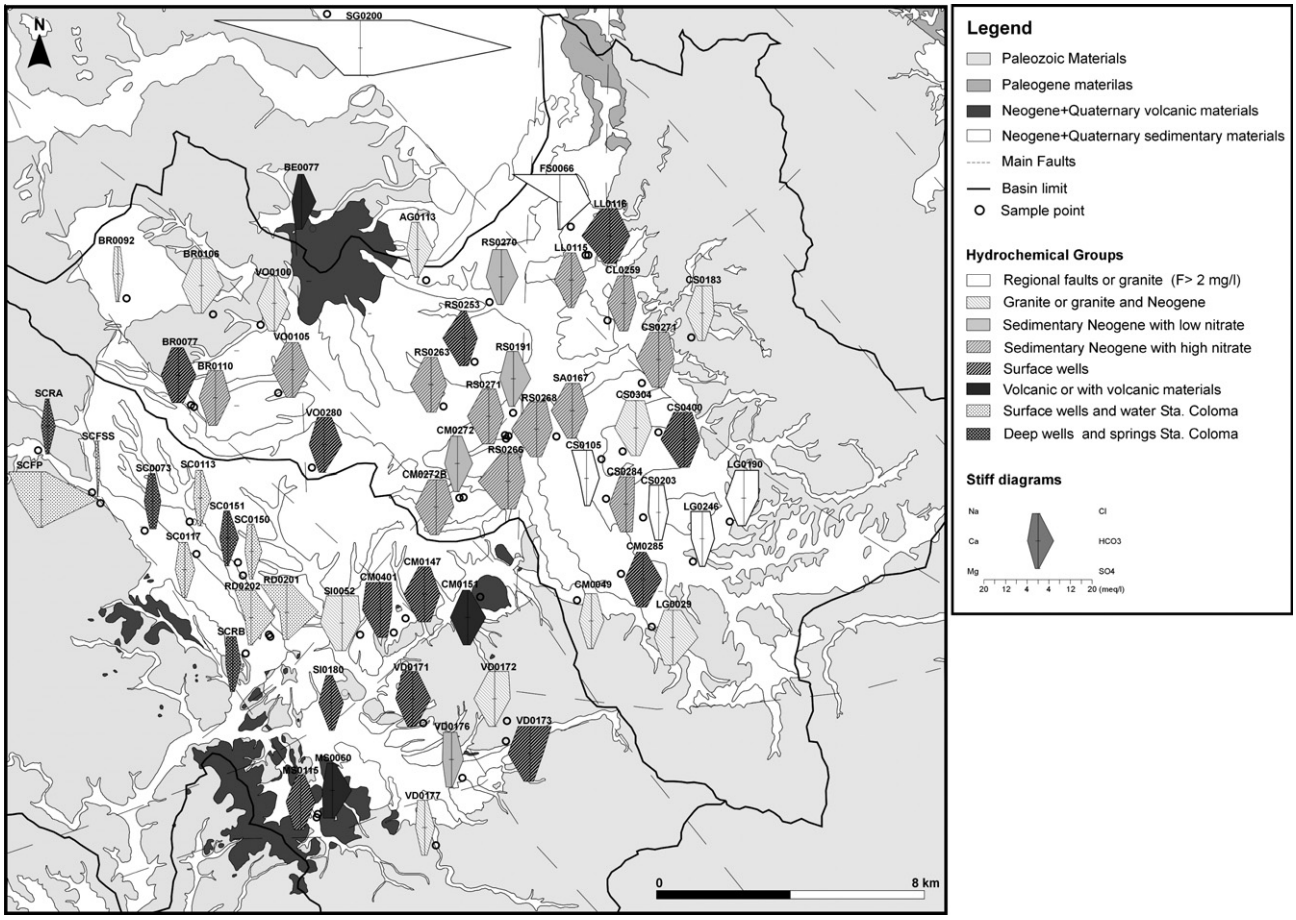

Fig. 8. Stiff diagram distribution in the May 2006 field campaign. Refer to text for hydrochemical groups description.

be attributed to the effect of aquifer lithology and pollution impacts, mainly from the intensive use of manure as fertilizer. Specifically, groundwater samples from the Santa Coloma River unconfined aquifer have a similar hydrochemistry to that of stream waters, corroborating the effective hydrological connectivity between river and aquifer. Stream recharge to the aquifer also explains the low nitrate content observed in the aquifer (in all samples but one, less than 20 mg/L). Samples from the unconfined aquifer have a Ca–HCO_3 facies, although deep wells and springs associated with fault zone hydraulics are characteristically of the Na–HCO_3 type.

Nitrate is also found in some deep wells in the ORB, which indicates the occurrence of a continuous hydrogeological unit consisting of the surface layers and the underlying Neogene sedimentary formations.

Wells placed in granitic rocks may present distinct mineralization levels according to residence time and the extent of granite weathering processes. Nitrate may occasionally occur, although in these cases it is attributable to a downward flux from the surface caused by pumping in the igneous unit.

Fluoride, as a specific component of this hydrogeological system, is found in specific locations within the Selva basin, in particular in the vicinity of the main fault zones (e.g., FS0066, CS0105, LG0190, and others in the ORB; and SCFP and RD0201 in the SCRB; Table 2). As fluoride origin is related to fluoride-bearing minerals recognized in veins in the Montseny–Guilleries range (Piqué et al., 2008), its occurrence must be related to upward vertical flows occurring from the basin basement whose recharge areas are located at the summit of the surrounding ranges and have acquired the required hydraulic gradient. However, not all the samples from springs or wells associated with fault zones present noteworthy fluoride concentrations. Some of the samples at the SCR watershed are low in fluoride, and therefore their origin must be linked to a distinct flow path with a different mineralogical composition. Based on the location of fluoride-rich groundwater samples, it can be assumed that fluoride mineralization is probably associated with particular fracture networks, especially those of most regional significance, developed during specific stages of the basement's geological history. This may explain why only samples from the basement have high fluoride content despite all of them being related to flow into fractures.

Flow systems of different magnitude and scale (regional, intermediate, and local) are thus identified in the Selva basin according to their hydrochemical facies and the geological location where they occur. The SCRB presents a major recharge associated with the Montseny–Guilleries range, governed by the Santa Coloma fault zone that controls the flow towards the Neogene sedimentary materials that fill the basin as well as to the upper surface (alluvial) aquifers (Folch and Mas-Pla, 2008). In the ORB, two recharge poles are identified. One of them represents infiltration from rainfall recharge within the lower basin area. This pole is defined by high nitrate content. The second pole is related to fault zones within the basement, which contribute through a recharging flow path originating far away, on a regional scale, in the Transversal range, and also possibly in the Montseny–Guilleries range. Faults located in the E and SE of the basin limits, on the boundaries with the Gavarres and Selva Marítima ranges, also represent flow zones that provide a lateral, intermediate-scale flow contribution to the basin's Neogene

sedimentary aquifers. These regional and intermediate flow systems are frequently characterized by significant fluoride content.

4.3. Environmental Isotopes (δD, $\delta^{18}O$)

The contribution of isotopic data to the understanding of the hydrogeological system in the Selva basin is considered in four field surveys depicting seasonal evolution in recharge processes. Three surveys were conducted in 2003 (May, September and December), and a fourth in May 2006, which coincides with the previously discussed hydrochemical dataset. Some of the sampling locations were the same in the different surveys, whereas others were changed depending on their accessibility. The most complete dataset is that of May 2006, coinciding with the beginning of the exploitation period of the study area.

In the study area, isotopic composition of rainfall can mainly be of two different origins: Mediterranean or Atlantic fronts (Vandenschrick et al., 2002; Araguas-Araguas and Diaz Teijeiro, 2005; and Jiménez-Martínez and Custodio, 2008). While a slope around 8 is found in different zones of the Iberian Peninsula for Local Meteoric Water Lines, the deuterium excess undergoes major changes depending on the origin of the rainfall. So, rainfalls coming from the Atlantic usually show a deuterium excess around 10‰, while fronts coming from the western Mediterranean have a deuterium excess of around 15‰ (Vandenschrick et al., 2002 and Jiménez-Martínez and Custodio, 2008).

A local meteoric water line (LMWL-R) was presented by Neal et al. (1992) for the Montseny–Guilleries and another range in NE Spain. This meteoric water line corresponds to $\delta D = 7.9\ \delta^{18}O + 9.8$, which is considered representative of the range areas surrounding the Selva basin. Deuterium excess indicates an Atlantic origin, in agreement with the limited influence of western Mediterranean air masses, limited to short distances from the coastline (Araguas-Araguas and Diaz Teijeiro, 2005). This limited influence of Mediterranean fronts in the study areas is also evident considering the meteoric water line proposed by Carmona et al. (2000), who describe a local meteoric water line of precipitation ($\delta D = 8\ \delta^{18}O + 14$) for the Corredor Range, a few kilometers away from the coast line.

Recharge water in the Selva basin is characterized using the precipitation data from the the IAEA/WMO for the "*Gerona aeropuerto*" station in the central part of the Selva basin. The regression line ($n = 20$) of these samples collected monthly over two years show similar slopes (around 8) but lower deuterium excess than the LMWL-R. Even the values weighted with the amount of precipitation, which are −5.3‰ of $\delta^{18}O$ of and −35.5‰ of δD (Araguas-Araguas and Diaz Teijeiro, 2005) is far from the LMWL-R. Precipitation samples presented by Vilanova (2004), collected in the neighboring basins show similar trends indicating the characteristics of the recharge in the basin areas. The most feasible explanation for the lower deuterium excess found in the precipitation in Selva basin is the partial evaporation of raindrops of the Atlantic fronts before their arrival on the land surface. Secondary evaporation during precipitation has been described in other studies in the Iberian Peninsula (Andreo et al. 2004).

Groundwater samples are plotted in Fig. 9 according to the hydrochemical categories established in the previous section. Samples are dispersed along local meteoric line and heavier values indicating different areas and altitudes of recharge. In particular, groundwater from regional fault zones, granite areas and springs show low isotopic content near to LMWL-R, indicating recharge to the surrounding basin from higher altitudes. Specifically, samples straight from fault zones (i.e. SG0200, FS0066 and SCFP) show the lowest isotopic values and, therefore, confirm a relationship with regional, fluoride-rich (except SG0200, as discussed), longer-residence time flow systems, and a control of the fault zones upon the flow line distribution. According to the study by Carmona et al. (2000), relating recharge altitude and δD and $\delta^{18}O$ content (based on springs with well defined recharge altitudes) in the Montnegre-Corredor and Montseny–Guilleries ranges, the lightest samples have to be infiltrated at altitudes between 500 and 800 m. Therefore, considering the altitudes of the range areas surrounding the Selva basin, the lightest samples have to be infiltrated in the upper lands of the Montseny–Guilleries range and/or Transversal ranges.

Conversely, most of the samples from wells in the Neogene sedimentary formations show more enriched values of $\delta^{18}O$ and δD than LMWL-R, denoting recharge at the Selva basin. With these isotopic values, wells with higher nitrate content also show Ca–HCO_3; and samples in deep Neogene with low nitrate also show Na–Ca–HCO_3 facies.

Isotopic content that varies within a similar geological environment in the same survey reflects the presence of different recharge flow systems, controlled by the hydraulic conductivity and storage capacity of distinct hydrogeological units, especially in the fault zones and in the coarse sediment layers of the Neogene infilling of the basin.

Seasonal variability is also encountered, as samples tend to lie around the LMWL-R in the September and December surveys, and then shift to heavier values in both May surveys, with some evidence of evaporation processes in the non saturated zone in the larger May 2006 dataset. The most obvious displacements affect samples from deep wells, and from the Neogene sedimentary layers (RS0266, VO0105, CM0272 and CS0183).

As previously mentioned, wells located in the regional fault zones present the lightest values, and therefore the highest altitudes of recharge (FS0066, SG0200, SCFP, SC0113). However, sampling point FS0066, located in the central part of the ORB, showed light values in 2003, although its isotopic content was enriched in May 2006, suggesting that mixing processes of different flow systems may occur within the fault zones, probably induced by water withdrawal pressures. Despite this, its values are some of the lightest in the dataset, indicating that fault zones do act as interceptors of regional, large-scale flow systems. In addition, sample SG0200, placed at the northern limit of the Selva basin, presents similar isotopic values to those of FS0066, which indicates a common recharge origin for both groundwater samples regardless of their hydrochemical differences.

In the same geochemical group as FS0066 (i.e. samples from regional fault zones and granitic aquifers) there are samples with higher isotopic values (e.g., LG0190 and LG0246). Such values denote a gradation of regional flow systems from distinct recharge areas at different altitudes in the surrounding ranges. As shown by piezometric data, wells in regional faults are also affected by seasonal withdrawals but the later recovery indicates the efficient contribution of these tectonic elements to the basin recharge (Fig. 6d). In particular, isotopic values in wells located downstream along the flow line in the Neogene sediments and granite basement (CS0105 and CS0203) are interpreted as the result of mixing processes from different screened intervals in the borehole, as also indicated by the moderate nitrate content (around 30 mg/L) and significant fluoride concentrations (over 2 mg/L) (Table 2).

In the western SCRB, samples with the lightest isotopic values are indicative of high altitude recharge from the surrounding range areas, namely the Montseny–Guilleries range (SCFP, RD0201). While some samples exhibit steady isotopic content in all surveys (SC0113) and show a recharge from a steady flow system, other samples, like SC117, vary through the seasons (Table 4). Considering that this well is cased in the upper 20 m, a shifting isotopic content suggests that sampled water originated from distinct flow systems, whose contributions vary throughout

Table 2
Hydrochemical data of the May 2006 field campaign. See Fig. 2 for well locations in the Selva basin.

Sample	Group	Geology	Depth (m)	Date	Cond. µS	T (°C)	pH	Eh (mV)	O_2 (mg/L)	Alkalinity as mg/L HCO3	Cl (mg/L)	SO_4 (mg/L)	NO_3 (mg/L)	F (mg/L)	Ca (mg/L)	Mg (mg/L)	Na (mg/L)	K (mg/L)	SI Calcite	SI Fluorite
CS0105b	Regional faults or granite	Neogene + granite	80	06/05/2006	767	16.8	7.31	403.7	0.9	274.3	73.0	58.1	30.0	6.2	50.8	8.0	125.0	3.6	−0.13	0.51
CS0203	Regional faults or granite	Neogene + granite	150	09/05/2006	751	17.2	7.04			205.0	70.7	62.8	34.8	2.0	76.0	16.0	76.2	7.6	−0.39	−0.31
FS0066	Regional faults or granite	Neogene + granite	102	06/05/2006	1533	19.7	7.78	243.8	0.2	653.9	221.1	21.0	<0.5	15.4	18.7	5.3	397.8	1.8	0.22	0.75
LG0190	Regional faults or granite	Granite	120	05/05/2006	963	17.4	7.25	18.1	0.1	314.8	196.1	29.6	0.5	2.3	133.7	24.8	71.8	1.4	0.23	0.01
LG0246	Regional faults or granite	Granite	>100	05/05/2006	786	17.7	7.27	22.2		263.5	103.0	50.3	13.4	3.0	81.5	10.7	94.7	4.3	−0.02	0.07
SG0200	Regional faults or granite	Spring not determined	0	05/05/2006	4790	17.2	6.49			3220.8	651.9	238.4	<0.5	0.13	319.5	74.1	1249.8	30.1	0.54	−2.51
AG0113	Granite or granite and Neo.	Neogene + granite	70	16/05/2006	556	18.2	7.21	343.4	2.3	329.4	19.7	17.1	4.5	0.7	77.7	11.6	47.8	1.5	0.04	0.58
BR0092	Granite or granite and Neo.	Quaternari + granite	80	16/05/2006	361	17	6.28	456.8	4.3	122.0	29.8	11.3	24.4	0.2	36.1	8.1	29.0	<1	−1.61	0.71
BR0106	Granite or granite and Neo.	Granite	83	23/05/2006	974	16.8	7.01			478.2	136.2	30.0	9.0	0.5	143.7	32.3	68.3	2.1	0.18	0.32
CM0049	Granite or granite and Neo.	Granite	121	19/05/2006	681	17.2	7.19			270.8	73.9	28.1	26.9	0.5	89.9	15.8	50.8	1.2	−0.03	0.48
CS0183	Granite or granite and Neo.	Granite	60	06/05/2006	825	–	6.9			251.3	133.1	49.8	30.7	1.3	117.6	17.6	55.2	1.2	−0.22	0.47
CS0304	Granite or granite and Neo.	Neogene + granite	116	06/05/2006	1046	17.7	6.96		6.3	344.0	115.6	77.7	119.8	2.8	156.8	20.9	84.6	1.1	0.01	0.50
LG0029	Granite or granite and Neo.	Wheathered granite + granite	110	09/05/2006	970	17.3	7.43	−76.5	0.1	541.7	114.9	33.7	<0.5	0.5	135.8	38.3	74.0	2.4	0.62	0.51
SI0052	Granite or granite and Neo.	Wheathered granite	50	10/05/2006	1217	16.3	6.87	343.6	5.5	385.5	213.6	64.7	79.0	0.5	159.3	29.4	129.5	1.4	−0.05	0.65
VD0172	Granite or granite and Neo.	Wheathered granite + granite	50	23/05/2006	921	19.3	7.22			329.4	184.1	7.5	0.5	0.4	153.0	25.7	50.6	<1	0.30	0.52
VD0173	Granite or granite and Neo.	Wheathered granite	20	23/05/2006	1136	–	7.24			275.7	277.7	62.1	7.1	0.2	162.4	27.6	101.0	1.4	0.25	0.43
VD0177	Granite or granite and Neo.	Granite	80	10/05/2006	612	16.5	7.04	351.0	0.1	214.7	37.9	44.2	66.7	0.2	66.9	12.8	60.2	<1	−0.42	0.39
VO0100	Granite or granite and Neo.	Quaternary + granite	80	16/05/2006	783	16.9	7.06	464.9	3.8	317.2	29.6	42.0	155.9	0.3	126.8	25.0	44.4	1.5	0.00	0.40
CM0272	S. Neogene with low nitrate	Neogene	90	23/05/2006	682	18	6.76			322.1	62.2	24.3	32.6	0.3	94.0	15.6	54.9	<1	−0.36	0.59
RS0191	S. Neogene with low nitrate	Neogene	90	11/05/2006	765	18.6	6.87	423.6	6.1	370.9	67.0	13.1	20.5	0.3	99.8	20.2	55.3	1.9	−0.16	0.72
RS0270	S. Neogene with low nitrate	Neogene	100	23/05/2006	803	16.9	6.93			361.1	75.3	37.8	37.3	0.9	109.7	18.4	73.3	1.2	−0.11	0.70
VD0176	S. Neogene with low nitrate	Neogene + volcanic	69	10/05/2006	710	17.9	7.37	348.9	0.1	256.2	71.0	17.9	<0.5	0.7	67.7	23.9	70.4	1.8	0.02	0.64
BR0110	S. Neogene with high nitrate	Quaternary + Neogene	70	11/05/2006	894	17.0	6.93			319.6	94.8	30.9	86.7	0.6	118.0	28.7	58.6	1.4	−0.15	0.50
CL0259	S. Neogene with high nitrate	Neogene	75	06/05/2006	891	17.2	6.92			244.0	85.7	54.8	104.4	0.4	130.0	24.4	57.5	<1	−0.24	0.50
CM0272B	S. Neogene with high nitrate	Neogene	40	09/05/2006	1004	16.9	6.86	344.1	5.1	380.6	131.8	49.3	78.3	0.2	154.2	24.9	66.3	<1	−0.05	0.52
CS0271	S. Neogene with high nitrate	Neogene	80	09/05/2006	1049	16.3	6.76	337.1	5.2	334.3	134.6	94.5	113.8	0.2	163.1	28.2	74.8	<1	−0.21	0.33

CS0284	S. Neogene with high nitrate	Neogene	70	09/05/2006	856	16.2	6.55	326.8	4.0	178.6	110.7	115.7	87.9	0.5	122.3	23.7	55.5	3.2	−0.79	0.51
LL0115	S. Neogene with high nitrate	Neogene	80	06/05/2006	763	17.2	6.96	371.3	7.0	319.6	53.6	41.4	67.4	0.2	125.1	14.9	46.7	<1	−0.08	0.47
RS0263	S. Neogene with high nitrate	Neogene	50	10/05/2006	887	16.5	6.79	325.5	0.9	329.4	79.5	89.4	70.3	0.2	151.9	18.4	54.4	1.1	−0.19	0.43
RS0266	S. Neogene with high nitrate	Neogene	120	23/05/2006	1171	–	6.87			368.4	143.0	135.4	138.4	0.2	221.2	31.1	62.8	<1	0.10	0.50
RS0268	S. Neogene with high nitrate	Neogene	65	23/05/2006	1045	16	6.79			341.6	129.3	91.1	97.5	0.2	183.5	24.7	59.4	2.7	−0.12	0.57
RS0271	S. Neogene with high nitrate	Neogene	65	23/05/2006	948	15.9	6.89			327.0	91.6	96.0	94.6	0.2	156.6	27.2	52.3	<1	−0.10	0.59
SA0167	S. Neogene with high nitrate	Neogene	80	19/05/2006	895	–	6.89			329.4	98.9	62.5	114.7	0.1	154.9	22.7	51.1	1.1	−0.04	0.54
VO0105	S. Neogene with high nitrate	Neogene	150	11/05/2006	916	16.5	6.8	396.1	6.2	366.0	77.1	48.5	94.2	0.2	147.7	26.5	56.5	<1	−0.15	0.58
BR0077	Surface wells	Quaternary	11.3	11/05/2006	999	16.4?	6.84			373.3	66.0	90.0	99.9	0.2	128.9	28.1	53.6	38.9	−0.12	0.25
CM0147	Surface wells	Neogene	7	10/05/2006	1011	14.7	6.79	352.0	3.6	336.7	78.6	111.2	128.0	0.2	151.8	24.6	50.0	34.7	−0.23	0.44
CM0285	Surface wells	Neogene	14.7	09/05/2006	835	15.4	7.82	440.9	6.6	402.6	43.0	66.8	88.0	0.4	133.7	25.8	52.0	2.8	0.88	0.57
CM0401	Surface wells	Neogene	14.6	10/05/2006	1124	14.8	6.83	348.3	6.0	248.9	147.5	130.3	170.4	0.2	132.3	12.8	122.5	31.1	−0.39	0.54
CS0400	Surface wells	Neogene	12	09/05/2006	1078	15.3	6.86	341.4	3.2	339.2	104.0	96.8	138.9	0.1	170.8	21.7	86.5	1.5	−0.10	0.52
LL0116	Surface wells	Neogene	11.8	06/05/2006	1148	15	7.42		6.8	424.6	93.9	110.4	200.5	0.2	206.5	23.0	75.4	1.0	0.60	0.49
MS0115	Surface wells	Quaternary + volcanic	21.9	11/05/2006	735	16.7	6.84	324.4	2.4	312.3	55.9	55.1	46.6	0.2	106.9	30.0	30.2	<1	−0.28	0.77
RS0253	Surface wells	Neogene	17.1	11/05/2006	864	17.0	6.9	482.7	8.1	278.2	21.0	70.1	217.2	0.2	160.8	21.6	27.2	<1	−0.14	0.51
SI0180	Surface wells	Weathered Granite	12	11/05/2006	612	15	7.15	329.2	2.6	261.1	18.6	51.9	18.4	0.4	91.5	7.1	42.0	3.3	−0.11	0.49
VD0171	Surface wells	Quaternary	80	11/05/2006	909	16.4	7.11	377.9	4.7	385.5	67.5	64.0	59.7	0.4	125.4	21.7	84.8	<1	0.12	0.58
VO0280	Surface wells	Neogene	8	12/05/2006	805	17.0	7.03	357.7	6.8	366.0	98.4	9.3	14.7	0.5	111.5	22.6	58.0	1.4	0.01	0.65
RD0201	D. wells and springs Sta. Col.	Neogene	75	16/05/2006	1093	18.2	6.79	270.7	0.7	675.9	70.2	16.3	<0.5	3.2	51.7	16.5	221.9	3.7	−0.30	0.81
RD0202	D. wells and springs Sta. Col.	Neogene	65	16/05/2006	839	17.2	7.15			500.2	50.3	12.1	4.3	1.0	48.0	11.3	138.4	2.5	−0.05	0.80
SC0113	D. wells and springs Sta. Col.	Neogene	73	11/05/2006	440	16	7.11	496.7	5.0	226.9	27.6	5.1	5.7	0.3	51.3	9.3	38.8	<1	−0.40	0.64
SC0117	D. wells and springs Sta. Col.	Neogene	65	11/05/2006	533	17.4	6.7	391.4	3.7	214.7	33.8	28.7	35.5	2.6	69.3	9.4	45.4	<1	−0.71	0.53
SC0150	D. wells and springs Sta. Col.	Neogene	80	22/05/2006	447	16.9	6.93			212.3	24.0	7.1	16.3	0.5	52.3	10.2	35.7	<1	−0.59	0.65
SCFP	D. wells and springs Sta. Col.	Spring granite	0	22/05/2006	1471	17.1	6.41			1207.8	66.2	5.8	<0.5	3.4	161.4	17.4	273.9	4.2	−0.03	0.75
SCFSS	D. wells and springs Sta. Col.	Spring granite	0	22/05/2006	131	17	6.08			51.2	9.1	2.9	<0.5	0.8	8.9	1.3	16.9	<1	−2.71	0.75
SC0073	S. wells and waters Sta. Col.	Quaternary	9.5	22/05/2006	502	15.6	6.6			175.7	31.2	60.9	8.5	0.2	61.3	12.8	33.2	1.1	−0.98	0.25
SC0151	S. wells and waters Sta. Col.	Neogene	20	22/05/2006	466	–	6.93			234.2	22.1	9.5	20.1	0.5	59.8	12.3	33.1	<1	−0.45	0.57
SCRA	S. wells and waters Sta. Col.	Stream	0	22/05/2006	358	19.2	8.07			164.5	13.3	18.7	7.7	0.4	47.4	9.2	19.8	1.1	0.43	0.35

(*continued on next page*)

Table 2 (*continued*)

Sample	Group	Geology	Depth (m)	Date	Cond. µS	*T* (°C)	pH	Eh (mV)	O_2 (mg/L)	Alkalinity as mg/L HCO3	Cl (mg/L)	SO_4 (mg/L)	NO_3 (mg/L)	F (mg/L)	Ca (mg/L)	Mg (mg/L)	Na (mg/L)	K (mg/L)	SI Calcite	SI Fluorite
SCRB	S. wells and waters Sta. Col.	Stream	0	22/05/2006	524	22.3	8.79			183.0	45.5	36.8	10.7	0.6	51.3	9.3	55.4	3.1	1.17	0.25
BE0077	Volcanic or with vol. materials	Volcanic + Neogene	80	11/05/2006	588	17.9	7.15	409.1	1.3	307.4	29.3	18.3	11.3	0.3	71.6	25.7	30.6	3.8	−0.09	0.39
CM0151	Volcanic or with vol. materials	Volcanic	75	19/05/2006	764	18.7	7.15			390.4	31.9	46.9	67.7	1.2	127.4	20.2	42.7	3.3	0.21	0.56
MS0060	Volcanic or with vol. materials	Volcanic	60	11/05/2006	693	18.3	6.95	263.8	1.1	412.4	34.1	34.6	0.7	0.2	75.8	40.4	44.8	6.6	−0.16	0.79

the year depending on natural rainfall recharge and the effect of withdrawal regimes. This behaviour is also indicated by hydrochemical data; well SC0113 shows low concentrations of fluoride and nitrate while well SC0117 has more than 30 mg/L of nitrate and over 2.5 mg/L of fluoride. This seasonal behaviour is difficult to depict from groundwater head evolution alone as both wells show seasonal head variations (Table 1, Well zones 10, 11). However, the different groundwater origin of both wells (SC0113 and SC0117) may indicate why wells located in relatively close areas (Fig. 3) and of similar depths and geologies show different seasonal withdrawals.

During the summer season, an evolution to lighter isotopic values coincides with a decrease in nitrate and an increase in fluoride, when rainfall recharge is almost nil (Menció, 2006). Isotopic values reverse in fall and winter when rainfall events are intense, with hydrochemical data showing a similar seasonal trend. This series of results confirms that distinct, independent flow systems concur in a single aquifer, and alternate as a consequence of groundwater withdrawal regimes.

The decrease in $\delta^{18}O$ observed in some wells related with regional faults (for instance, SCFP, RD201, RD0202 and SG0200; Fig. 9d), which is displaced to the left of the LMWL-R, should be interpreted as an isotopic equilibrium with carbon dioxide of thermal origin. This assumption is also supported by hydrochemical data, showing $Na–HCO_3$ facies with high concentrations of HCO_3^- to be saturated or close to saturation with calcite.

Isotopic values in samples from the Neogene sedimentary aquifers move closer to the evaporated rain values, representing the recharge in the Selva basin, during the spring surveys (May 2003 and 2006; Fig. 9a and d; Table 4), while in surveys conducted in fall and winter (Fig. 9b and c) they are placed on the LMWL-R and show lighter isotopic values. Some samples from wells in granite terrain also show a similar seasonal displacement.

Additionally, samples from the May surveys, notably May 2006 (Fig. 9d), follow a line with a slope of ≈4.0 that is consistent with the occurrence of evaporation processes in the non saturated zone (Clark and Fritz, 1997). The most evaporated samples are found in granitic areas in the southeastern corner of the Selva basin, where there are weathered or partially weathered granite outcrops and the unsaturated zone depth is up to 25 m.

The occurrence of partially evaporated samples enables the identification of seasonal hydrodynamics. Water withdrawn at the end of the summer season, i.e. in September or October, shows higher recharge altitudes and isotopic values aligned according to the LMWL-R. During May surveys, following the wet season that lasts from October to May, groundwater samples exhibit more enriched isotopic values that have shifted to local recharge in the basin surface. Moreover, specific samples located in the ORB are distinctively aligned along an evaporation line. Such seasonal differences are attributable to local recharge pulses during the wet season, i.e. rainfall in the basin area infiltrating into the Neogene layers after being affected by evaporation processes. Such recharge is therefore the main resource that is captured by pumping wells after the end of the wet season. The most evaporated groundwater samples also exhibit a wide range of nitrate concentration (Table 2), as would be expected from the local recharge pole.

By September, intensive water withdrawal has exhausted such local resources, and the isotopic content reveals the dominant influence of groundwater flow from regional systems on the captured water. That is to say, the lateral and vertical upward recharge from the surrounding ranges and the basement provides water to the sedimentary aquifers of the basin, fulfilling major water needs as most of the wells can therefore maintain their exploitation rates. Such seasonal conduct emphasizes the effect of the groundwater withdrawal regime on the hydrogeological

Table 3
Characteristics of each group of samples.

Group number	Group Name	Geology and type of sample point	Type of source	Sub−basin	Well depth (m)	Hydrochemical facies	F^- (mg/L)	NO_3^- (mg/L)
1	Regional faults or granite	Granite or granites and sedimentary Neogene	Wells and spring	Onyar	0–150	$Na–HCO_3$ $Ca–Na–HCO_3–Cl$	2.01–15.4 SG0200 = 0.13	<0.5–34.8
2	Granite or granite and Neogene	Granite. granite + sedimentary Neogene. weathered granite and/or Quaternary + granite	Wells	Onyar and South Santa Coloma	20–121	$Ca–HCO_3$ $Ca–HCO_3–Cl$	0.18–2.79	<0.5–155.9
3	Sedimentary Neogene with low nitrate	Sedimentary Neogene and sedimentary Neogene + volcanic	Wells	Onyar and South Santa Coloma	69–100	$Ca–HCO_3$ $Ca–Na–HCO_3$	0.28–0.89	<0.5–37.3
4	Sedimentary Neogene with high nitrate	Sedimentary Neogene and quaternary + sedimentary Neogene	Wells	Onyar	40–150	$Ca–HCO_3$	0.14–0.65	67.4–138.4
5	Surface wells	Quaternary. sedimentary Neogene. Neogene + volcaic and weathered granite	Wells	Onyar and South Santa Coloma	7–22	$Ca–HCO_3$	0.15–0.51	14.7–217.2
6	Deep wells and springs Santa Coloma	Neogene and granite (springs)	Wells and springs	North Santa Coloma	0–80	$Na–HCO_3$	0.34–3.42	<0.5–35.5
7	Surface wells and water Santa Coloma	Quaternary and Neogene	Wells and surface waters	North Santa Coloma	0–20	$Ca–HCO_3$	0.22–0.55	7.7–20.1
8	Volcanic or with volcanic materials	Volcanic or volcanic + Neogene	Wells	Onyar and South Santa Coloma	60–80	$Ca–HCO_3$ $Ca–Mg–HCO_3$	0.21–1.15	0.7–67.7

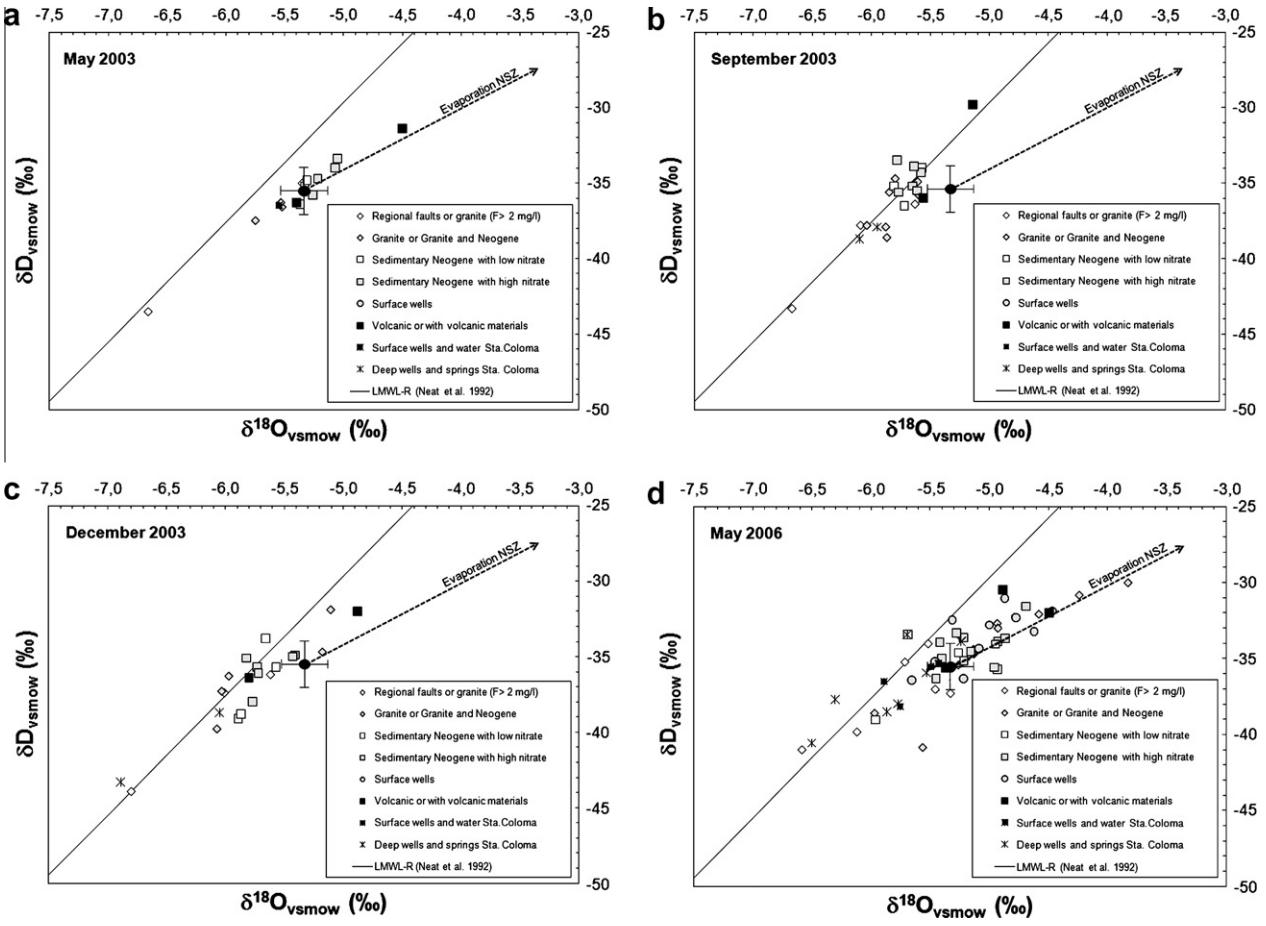

Fig. 9. Environmental isotope distribution (δD, $\delta^{18}O$) in the different field surveys. Error bar indicates analytical error and the value weighted with the amount of precipitation calculated with data from the Global Network of Isotopes in Precipitation (GNIP) from station "Gerona Aeropuerto" located in the Selva Basin (IAEA/WMO, 2006). Evaporation indicates the trend line of groundwater evaporated in the non saturated zone.

Table 4
Environmental isotopes of each field campaign. If no other type of source is specified in the geology column. samples have been collected from wells. See Fig. 2 for well locations in the Selva basin.

Sample	Group	Geology	Deep	May–03		September–03		December–03		May–06	
				$\delta^{18}O$	δD	$\delta^{18}O$	δD	$\delta^{18}O$	δD	$\delta^{18}O$	δD
CS0105a	Regional faults or granites	Neogene	80	−5.3	−35.0	−5.6	−36.4				
CS0105b	Regional faults or granites	Neogene + granite	140							−5.3	−37.3
CS0203	Regional faults or granites	Neogene + granite	150			−6.1	−37.8	−6.0	−37.4	−5.5	−37.0
FS0066	Regional faults or granites	Neogene + granite	102	−6.7	−43.5	−6.7	−43.3	−6.8	−43.9	−6.1	−39.9
LG0190	Regional faults or granites	Granite	120	−5.4	−35.0			−5.6	−36.2	−5.5	−34.0
LG0246	Regional faults or granites	Granite	>100							−5.7	−35.2
SG0200	Regional faults or granites	Source	0							−6.6	−41.0
AG0113	Granite or granite and Neo.	Neogene + granite	70							−5.4	−35.5
BR0092	Granite or granite and Neo.	Quaternary + granite	80	−5.8	−37.5	−6.0	−37.8	−6.0	−37.3	−6.0	−38.6
BR0106	Granite or granite and Neo.	Paleozoic	83	−5.5	−36.6	−5.9	−35.6			−5.3	−35.4
CS0183	Granite or granite and Neo.	Granite	60	−5.5	−36.3	−5.9	−38.6	−6.1	−39.8	−5.1	−34.7
LG0029	Granite or granite and Neo.	Wheath. granite + granite	110							−4.9	−32.7
SI0052	Granite or granite and Neo.	Wheathered granite	50							−5.1	−34.4
VD0172	Granite or granite and Neo.	Wheath. granite + granite	50			−5.9	−37.9	−6.0	−36.3	−5.5	−35.4
VD0173	Granite or granite and Neo.	Wheathered granite	20			−5.6	−35.8			−4.2	−30.8
VD0177	Granite or granite and Neo.	Granite	80			−5.6	−34.9	−5.2	−34.7	−4.6	−32.1
VO0100	Granite or granite and Neo.	Quaternary + granite	80							−5.6	−40.8
CM0049	Granite or granite and Neo.	Granite	121					−5.1	−31.9	−3.8	−30.0
CS0304	Granite or granite and Neo.	Neogenee + granite	116			−5.8	−34.7			−4.9	−33.0
CM0272	S. Neogene with low nitrate	Neogene	90	−5.4	−36.4	−5.7	−36.5	−5.9	−39.1	−4.9	−35.7
RS0191	S. Neogene with low nitrate	Neogene	90	−5.3	−35.2	−5.8	−35.2	−5.9	−38.8	−5.7	−33.4
RS0270	S. Neogene with low nitrate	Neogene	100	−5.3	−34.8	−5.6	−34.0	−5.6	−35.7	−6.0	−39.0
VD0176	S. Neogene with low nitrate	Neogene + volcanic	69							−5.3	−34.6
BR0110	S. Neogene with high nitrate	Quaternary + Neogene	70							−4.9	−33.9
CL0259	S. Neogene with high nitrate	Neogene	75			−5.7	−35.2	−5.7	−35.7	−5.2	−35.2
CM0272B	S. Neogene with high nitrate	Neogene	40							−5.0	−35.6
CS0271	S. Neogene with high nitrate	Neogene	80	−5.3	−35.8	−5.6	−34.3	−5.8	−38.0	−4.9	−33.7
CS0284	S. Neogene with high nitrate	Neogene	70			−5.8	−35.6	−5.8	−35.1	−5.4	−35.0
LL0115	S. Neogene with high nitrate	Neogene	80	−5.2	−34.7	−5.6	−35.5	−5.4	−34.9	−5.2	−34.5
RS0263	S. Neogene with high nitrate	Neogene	50							−5.4	−36.3
RS0266	S. Neogene with high nitrate	Neogene	120	−5.1	−34.0	−5.6	−33.9	−5.4	−35.0	−5.2	−33.6
RS0268	S. Neogene with high nitrate	Neogene	65							−5.3	−33.3
RS0271	S. Neogene with high nitrate	Neogene	65	−5.1	−33.4					−5.4	−33.9
SA0167	S. Neogene with high nitrate	Neogene	80							−4.7	−31.6
VO0105	S. Neogene with high nitrate	Neogene	150	−5.3	−35.8	−5.8	−33.5	−5.7	−36.1	−4.9	−34.1
BR0077	Surface wells	Quaternary	11.3							−5.7	−36.4
CM0147	Surface wells	Neogene	7							−5.1	−34.3
CM0285	Surface wells	Neogene	14.7							−4.6	−33.2
CM0401	Surface wells	Neogene	14.6							−5.2	−36.3
CS0400	Surface wells	Neogene	12							−5.3	−32.5
LL0116	Surface wells	Neogene	11.8							−5.0	−32.8
MS0115	Surface wells	Quaternary + volcanic	21.9							−4.9	−31.0
RS0253	Surface wells	Neogene	17.1							−4.8	−32.3
SI0180	Surface wells	Wheath. granite	12							−5.5	−35.2
VD0171	Surface wells	Quaternary	8							−4.5	−31.9
VO0280	Surface wells	Neogene	8							−5.3	−35.6
RD0201	D. wells and springs Sta. Col.	Neogene	75							−6.3	−37.7
RD0202	D. wells and springs Sta. Col.	Neogene	65							−5.7	−33.4
SC0113	D. wells and springs Sta. Col.	Neogene	73			−6.1	−38.7	−6.1	−38.7	−5.8	−38.0
SC0117	D. wells and springs Sta. Col.	Neogene	65			−6.0	−37.9	−6.9	−43.3	−5.2	−33.9
SC0150	D. wells and springs Sta. Col.	Neogene	80							−5.5	−35.9
SCFP	D. wells and springs Sta. Col.	Spring granite	0							−6.5	−40.6
SCFSS	D. wells and springs Sta. Col.	Spring granite	0							−5.9	−38.5
SC0073	S. wells and waters Sta. Col.	Quaternary	9.5	−5.6	−36.5					−5.8	−38.2
SC0151	S. wells and waters Sta. Col.	Neogene	20							−5.5	−35.5
SCRA	S. wells and waters Sta. Col.	Stream	0							−5.9	−36.5
SCRB	S. wells and waters Sta. Col.	Stream	0							−5.4	−35.3
BE0077	Volcanic or with vol. materials	Volcanic + Neogene	80	−5.4	−36.3	−5.6	−36.0	−5.8	−36.4	−5.4	−35.6
CM0151	Volcanic or with vol. materials	Volcanic	75							−4.5	−32.0
MS0060	Volcanic or with vol. materials	Volcanic	60	−4.5	−31.4	−5.1	−29.8	−4.9	−32.0	−4.9	−30.5

dynamics of this system, with the origin of captured water being modified from local to regional recharge sources. It also reveals the role of fault zones as preferential flow paths that recharge the overlying sedimentary layers from the basement.

In the December 2003 survey, isotopic data show a transitional distribution between the end of the dry season (mainly summer) and the beginning of the recharge period in October and November. In particular, those months had more rainfall than the average (i.e., 220 mm in October 2003; Fig. 5), providing support for the behaviour described.

5. Summary and conclusions

The major features and findings of this hydrogeological research are summarized as follows:

1. Potentiometric, hydrochemical and isotopic data have been used to describe the hydrogeological system of the Selva basin (NE Spain), located in a range-and-basin environment. Structural elements, i.e., fault zones, play an important role in the recharge from the ranges towards the basin's infill aquifers.

2. Water withdrawal, mainly from the basin sediments, exerts a significant influence upon the hydrogeology of the system, producing a modification of regional and local scale flow paths in accordance with natural recharge periods and seasonal exploitation regimes.
3. Potentiometric data measured over a six-year period reveal distinct flow dynamics within the sedimentary infilling of the basin. They indicate the degree of vertical connectivity in this leaky multilayered aquifer system, as well as the existence of a lateral inflow from the range-front and, more importantly, a vertical upward flow from the granitic basement. They also indicate that fault zones act as specific recharge spots, controlling the hydraulic efficiency of wells and, overall, the recharge flows.
4. Hydrochemical facies support the observations derived from potentiometric data. The occurrence of sodium and chloride-rich facies points to the contribution of groundwater flow from the basement to the basin sedimentary infill.
5. Fluoride and nitrate concentrations are taken as tracer components of, respectively, a regional end-member, defined by large-scale, longer residence time flows from the range areas to the basin, and a local end-member, caused by rainfall infiltration in the basin surface. Variations in the content of both components are attributable to the capture of distinct flow paths, as stored resources decline during intensive pumping (irrigation) periods.
6. The local meteoric water line of the range areas and the evaporation that characterize the rain in the Selva basin show different recharge flow systems. In this sense, the Selva basin recharge takes place from the basin surface, creating a local flow system, and from the surrounding ranges as regional flow systems originated at higher altitude and with a longer residence time.
7. Seasonal isotopic data shift between both local meteoric water lines and the fact that fractionation processes related to evaporation are identified during the spring (May) surveys also indicate that the amount of captured water resources from the two flow systems may vary along the year.
8. Meeting water demand in the Selva basin does in fact depend on the seasonal exploitation of regional and local flow systems. In particular, regional flow systems related to fractures and major fault zones supply current demands that could not be satisfied by only the local rainfall recharge.

These main outcomes conclude that hydrogeological systems are greatly disturbed by groundwater withdrawal regimes, which modify natural flow paths. Such modifications, which govern the water balance within the basin and, therefore, the amount of available water resources, can be identified with the aid of potentiometric, hydrochemical and isotopic data. Furthermore, structural elements, such as fault zones, represent a significant, preferential flow path whose contribution is fundamental to completely meeting water demand and, more importantly, the recovery of the resources stored in periods of low demand. Data from surveys covering only the most recent years after intense development, and a multiparametric analysis, provide a crucial contribution to the depiction of spatial heterogeneity in groundwater dynamics under human pressures.

Despite their negative impact, human alterations enable us to identify some of the flow field characteristics, such as the occurrence of nitrate at depth as indicative of vertical downward induced recharge, or the spatial distribution of fluoride indicating those areas where wells are fed by recharge from the basement. This hydrochemical information, together with head data, defines the behaviour of the distinct hydrogeological units and the contribution of the tectonic structure to the overall flow system, and especially to the conceptual design of the water balance. These are necessary to go a step further in hydrogeological basin management: the location of the main hydrogeological trends such as vertical recharge from faults, downward flow due to pumping, the relation between sedimentary units, etc., are necessary to build numerical models of hydrological basins to improve water management (Kalf and Woolley, 2005).

Furthermore, the large-scale geological approach applied to this paper shows the effectiveness of implicitly recognizing that many hydrogeological systems consist of distinct interrelated geologic formations. Such an assumption is of relevance to the establishment of water bodies and their available water resources, according to the Water Framework Directive (Directive 2000/60/EC). In addition, quality issues are also better understood if this regional perspective is used, by providing helpful explanations for the occurrence of natural or human introduced pollutants, such as fluoride and nitrate, respectively. The occurrence of regional flows that contribute to the overall recharge of the basin aquifer system represents the surplus of groundwater inflow necessary to balance the hydrogeological mass balance in the basin, as estimated in the water budget (Menció et al., 2010). Such an analytical approach, combining field data and current groundwater exploitation within the appropriate geological context, contributes to the management of groundwater bodies under the demand of human pressures by preserving their resources as enforced by the Water Framework Directive (Directive 2000/60/EC).

Acknowledgements

This work was funded by the projects CICYT-CGL2008-06373-C03-03; 01/BTE of the Spanish Government and the projects 2009SGR00103 and 2009SGR1199 from the Catalan Government. We would like to thank the Serveis Científics Tècnics of the Universitat de Barcelona. We acknowledge the contributions from Mike Edmunds from the Oxford Centre for Water Research and those from anonymous reviewers.

References

Aji, K., Tang, C., Song, X., Kondoh, A., Sakura, Y., Yu, J., Kaneko1, S., 2008. Characteristics of chemistry and stable isotopes in groundwater of Chaobai and Yongding River basin, North China Plain. Hydrological Processes 22, 63–72.

Andreo, B., Liñan, C., Carrasco, F., Jiménez de Cisneros, C., Caballero, F., Mudry, J., 2004. Influence of rainfall quantity on the isotopic composition (^{18}O and ^{2}H) of water in mountainous areas. Application for groundwater research in the Yunquera–Nieves karst aquifers (S Spain). Applied Geochemistry 19, 561–574.

Araguas-Araguas, L.J., Diaz Teijeiro, M.F., 2005. Isotope composition of precipitation and water vapour in the Iberian Peninsula. In: Goucy, L. (Ed.), Isotopic Composition of Precipitation in the Mediterranean Basin in Relation to Air Circulation Patterns and Climate, IAEA-TECDOC-1453, Vienna.

Beaucaire, N., Gassama, N., Tresonne, N., Louvat, N., 1999. Saline groundwaters in the hercynian granites (Chardon Mine, France): geochemical evidence for the salinity origin. Applied Geochemistry 14, 67–84.

Carmona, J.M., Bitzer, K., López, E., Bouazza, M., 2000. Isotopic composition and origin of geothermal waters at Caldetes (Maresmes-Barcelona). Journal of Geochemical Exploration 69–70, 441–447.

Carrillo-Rivera, J.J., Irén Varsányi, I., Kovács, L.O., Cardona, A., 2007. Tracing groundwater flow systems with hydrogeochemistry in contrasting geological environments. Water Air and Soil Pollution 184, 77–103.

Chen, J., Tang, C., Sakura, Y., Kondoh, A., Yu, J., Shimada, J., Tanaka, T., 2004. Spatial geochemical and isotopic characteristics associated with groundwater flow in the North China Plain. Hydrological Processes 18, 3133–3146.

Clark, I.D., Fritz, P., 1997. Environmental Isotopes in Hydrogeology. Lewis Publishers, New York. 329 pp.

Cunningham, E.E.B., Long, A., Eastoe, C., Basset, R.L., 1998. Migration of recharge waters downgradient from the Santa Catalina Mountains into the Tucson basin aquifer, Arizona, USA. Hydrogeology Journal 6, 94–103.

Demlie, M., Wohnlich, S., Gizaw, B., Stichler, W., 2007. Groundwater recharge in the Akaki catchment, central Ethiopia: evidence from environmental isotopes ($\delta^{18}O$, $\delta^{2}H$ and ^{3}H) and chloride mass balance. Hydrological Processes 21, 807–818.

Devlin, J.F., Sophocleos, M., 2005. The persistence of the water budget myth and its relationship to sustainability. Hydrogeology Journal 13, 549–554.

Duran, H. 1985. El paleozoico de Les Guilleries. PhD thesis, Departament de Geologia, Universitat Autònoma de Barcelona.

Folch, A., Mas-Pla, J., 2008. Hydrogeological interactions between fault zones and alluvial aquifers in regional flow systems. Hydrological Processes 22, 3476–3487.

Folch, A., Casadellà, L., Astui, O., Menció, A., Massana, J., Vidal-Gavilan, G., Pérez-Paricio, A., Mas-Pla, J., 2010. Verifying conceptual flow models in river-connected alluvial aquifers for management purposes using numerical modeling. In: XVIII International Conference on Computational Methods in Water Resources (CMWR 2010), Barcelona, Spain.

Gascoyne, M., Davison, C.C., Ross, J.D., Pearson, R., 1987. Saline groundwaters and brines in plutons in the Canadian Shield. In: Fritz, P., Frape, S.K. (Eds.), Saline Water and Gases in Crystalline Rocks. Geological Association of Canada Special Paper 33, pp. 53–68.

IAEA/WMO. International Atomic Energy Agency in Colaboration with the World Meteorological Organization. Global Network of Isotopes in Precipitation. The GNIP Database. <http://isohis.iaea.org> (accessed 12.06.06).

Jiménez-Martínez, J., Custodio, E., 2008. El exceso de deuterio en la lluvia y en la recarga a los acuíferos en el área circum-mediterránea y en la costa mediterránea española. Boletín Geológico y Minero 119, 21–32.

Kalf, F.R.P., Woolley, D.R., 2005. Applicability and methodology of determining sustainable yield in groundwater systems. Hydrogeology Journal 13, 295–312.

Li, X., Zhang, L., Hou, X., 2008. Use of hydrogeochemistry and environmental isotopes for evaluation of groundwater in Qingshuihe Basin, northwestern China. Hydrogeology Journal 16, 335–348.

Mahlknecht, J., Gárfias-Solis, J., Aravena, R., Tesch, R., 2006. Geochemical and isotopic investigations on groundwater residence time and flow in the Independence Basin, Mexico. Journal of Hydrology 324, 283–300.

Menció, A., 2006. Anàlisi multidisciplinària de l'estat de l'aigua a la depressió de la Selva. PhD Thesis, Universitat Autònoma de Barcelona, Spain.

Menció, A., Mas-Pla, J., 2008. Assessment by multivariate analysis of groundwater-surface water interactions in urbanized Mediterranean streams. Journal of Hydrology 362, 355–366.

Menció, A., Folch, A., Mas-Pla, J., 2010. Analyzing Hydrological Sustainability Through Water Balance. Environmental Management 45, 1175–1190.

MOPU, 1985. Plan Hidrológico del Pirineo Oriental. EE2 Estudio complementario sobre aguas subterráneas. Zona5-La Selva. Síntesis Hidrogeológica. Ministerio de Obras Públicas y Urbanismo, Dirección General de Obras Hidráulicas, Spain.

Neal, C., Neal, M., Warrington, A., Avila, A., Pinol, J., Roda, F., 1992. Stable hydrogen and oxygen isotope studies of rainfall and streamwaters for two contrasting holm oak areas of Catalonia, northeastern Spain. Journal of Hydrology 140, 163–178.

Palmer, P.C., Gannett, M.W., Stephen, R., Hinkle, S.R., 2007. Isotopic characterization of three groundwater recharge sources and inferences for selected aquifers in the upper Klamath Basin of Oregon and California, USA. Journal of Hydrology 336, 17–29.

Piqué, A., Canals, A., Grandia, F., Banks, D.A., 2008. Mesozoic fluorite veins in NE Spain record regional base metal-rich brine circulation through basin and basement during extensional events. Chemical Geology 257, 139–152.

Pous, J., Solé Sugrañes, L., Badiella, P., 1990. Estudio geoeléctrico de la depresión de La Selva (Girona). Acta Geológica Hispánica 25, 261–269.

Sukhija, B.S., Reddy, D.V., Nagabhushanam, P., Nagabhushanam, P., Bhattacharya, S.K., Jani, R.A., Kumar, D., 2006. Characterization of recharge processes and groundwater flow mechanisms in weathered-fractured granites of Hyderabad (India) using isotopes. Hydrogeology Journal 14, 663–674.

Tóth, J., 1995. Hydraulic continuity in large sedimentary basins. Hydrogeology Journal 3, 4–16.

Tóth, J., 2000. Las aguas subterráneas como agente geológico: Causas, procesos y manifestaciones. Boletín Geológico y Minero 111 (4), 9–26.

Vandenschrick, G., Van Wesemael, B., Frot, E., Pulido-Bosch, A., Molina, L., Stievenenard, M., Souchez, R., 2002. Using stable isotope analysis to characterize the regional hydrology of the Sierra de Gador, S–E Spain. Journal of Hydrology 265, 43–55.

Vilanova, E., 2004. Ànalisi dels sistemes de flux a l'àrea Gavarres-Selva-Baix Empordà, Proposta de model hidrodinàmic regional. PhD thesis Universitat Autònoma de Barcelona, Spain.

Vilanova, E., Menció, A., Mas-Pla, J., 2008. Determinación de sistemas de flujo regionales y locales en las depresiones tectónicas del Baix Empordà y la Selva (NE de España) en base a datos hidroquímicos e isotópicos. Boletín Geológico y Minero, vol. 119, no. 1. Instituto Geológico y Minero de España, Spain, pp. 51–62.

ANNEX B

Puig, R., Folch, A., Menció, A., Soler, A. and Mas-Pla, J. (**2013**) Multi-isotopic study (^{15}N, ^{34}S, ^{18}O, ^{13}C) to identify processes affecting nitrate and sulfate in response to local and regional groundwater mixing in a large-scale flow system. *Applied Geochemistry* 32, 129–141.

Impact factor: 1.708 (2012)
Quartile and category: Q2 (33/76), Geochemistry and Geophysics

Applied Geochemistry 32 (2013) 129–141

Contents lists available at SciVerse ScienceDirect

Applied Geochemistry

journal homepage: www.elsevier.com/locate/apgeochem

Multi-isotopic study (^{15}N, ^{34}S, ^{18}O, ^{13}C) to identify processes affecting nitrate and sulfate in response to local and regional groundwater mixing in a large-scale flow system

R. Puig [a,*,1], A. Folch [b,1], A. Menció [c], A. Soler [a], J. Mas-Pla [c]

[a] Grup de Mineralogia Aplicada i Medi Ambient, Departament de Cristal·lografia, Mineralogia i Dipòsits Minerals, Facultat de Geologia, Universitat de Barcelona, Spain
[b] Grup d'Hidrologia Subterrània, Departament d'Enginyeria del Terreny, Cartogràfica i Geofísica, Universitat Politècnica de Catalunya-Barcelona Tech, Spain
[c] Grup de Geologia Aplicada i Ambiental (GAiA), Centre de Geologia i Cartografia Ambiental (Geocamb), Universitat de Girona, Spain

ARTICLE INFO

Article history:
Available online 2 November 2012

ABSTRACT

The integrated use of hydrogeologic and multi-isotopic approaches ($\delta^{15}N$, $\delta^{18}O_{NO3}$, $\delta^{34}S$, $\delta^{18}O_{SO4}$ and $\delta^{13}C_{HCO3}$) was applied in the Selva basin area (NE Spain) to characterize NO_3^- and SO_4^{2-} sources and to evaluate which geochemical processes affect NO_3^- in groundwater. The studied basin is within a basin-and-range physiographic province where natural hydrodynamics have been modified and different scale flow systems converge as a consequence of recent groundwater development and exploitation rates. As a result, groundwaters related to the local recharge flow system (affected by anthropogenic activities) and to the generally deeper regional flow system (recharged from the surrounding ranges) undergo mixing processes. The $\delta^{15}N$, $\delta^{18}O_{NO3}$ and $\delta^{34}S$ indicated that the predominant sources of contamination in the basin are pig manure and synthetic fertilizers. Hydrochemical data along with $\delta^{15}N$, $\delta^{18}O_{NO3}$, $\delta^{34}S$, $\delta^{18}O_{SO4}$ and $\delta^{13}C_{HCO3}$ of some wells confirmed mixing between regional and local flow systems. Apart from dilution processes that can contribute to the decrease of NO_3^- concentrations, the positive correlation between $\delta^{15}N$ and $\delta^{18}O_{NO3}$ agreed with the occurrence of denitrification processes. The $\delta^{34}S$ and $\delta^{18}O_{SO4}$ indicated that pyrite oxidation is not linked to denitrification, and $\delta^{13}C_{HCO3}$ did not clearly point to a role of organic matter as an electron donor. Therefore, it is proposed that the mixing processes between deeper regional and local surface groundwater allow denitrification to occur due to the reducing conditions of the regional groundwater. Thus, isotopic data add useful complementary information to hydrochemical studies, especially in those areas where hydrochemical data is not conclusive.

1. Introduction

Groundwater development and agricultural, livestock and industrial activities have increased during the second half of the last century. These human activities have affected the rates and quality of groundwater recharge and particularly aquifer biogeochemistry. Factors that are known to contribute to the degradation of groundwater quality are excessive groundwater withdrawal in relation to average natural recharge, infiltration of surplus of N coming from synthetic and organic fertilizers, surface water irrigation, leakage from urban sewers, wastewater ponds, septic tanks, urban solid waste landfills, abandoned wells, mine tailings, etc. (Llamas and Martínez-Santos, 2004; Arvena and Mayer, 2010). According to the European Commission, groundwater pollution is the most serious problem noted in the EU water resources policy that is managed through Member States implementation of the Nitrates, Water Framework and Groundwater Directives (Rivett et al., 2008). The development of effective management practices to preserve water quality and the design of remediation plans for sites that are already polluted requires the identification of actual pollution sources and an understanding of the processes affecting local contaminant concentrations (Kendall et al., 2007).

In most regional hydrogeological systems, the main sources of contamination are related to the application of synthetic and manure-based fertilizers, municipal sewage effluent and septic system seepage. Contamination from these origins usually produces a NO_3^- non-point source leading to degradation of water quality and the eutrophication of surface waters. Nitrate in aquifers frequently exceeds legal drinking water thresholds (50 mg L^{-1} NO_3^-; EC, 1998). Additionally, dissolved SO_4^{2-} in groundwater may originate from dissolution of evaporitic rocks (mainly gypsum), oxidation of reduced S minerals, atmospheric deposition and saline water intrusion, as well as from anthropogenic sources such as fertilizers, manure, sewage and mine drainage, among others.

* Corresponding author.
E-mail address: rpuig@ub.edu (R. Puig).
[1] These authors contributed equally to this article.

0883-2927/$ - see front matter © 2012 Elsevier Ltd. All rights reserved.
http://dx.doi.org/10.1016/j.apgeochem.2012.10.014

Stable isotope ratios of NO_3^- ($\delta^{15}N$, $\delta^{18}O_{NO3}$), SO_4^{2-} ($\delta^{34}S$, $\delta^{18}O_{SO4}$) and C ($\delta^{13}C$) have been successfully used to characterize the predominant sources of pollution (Cravotta, 1997; Aravena and Robertson, 1998; Vitòria et al., 2008) in a variety of settings, and to determine the physicochemical processes that can affect pollutant transport and fate (Otero et al., 2009). The isotopic composition of these elements measured in groundwater not only reflects the original source (either natural or anthropogenic), but can be influenced by source mixing or by isotopic fractionation during the transport and chemical transformation of N, S and C compounds. For example, trends in NO_3^- isotopes are capable of indicating denitrification (Aravena and Mayer, 2010), while SO_4^{2-} and C isotopes can help to evaluate which reactions (and which electron donors) are linked to denitrification (Schwientek et al., 2008; Otero et al., 2009).

Therefore, physicochemical processes that can occur during NO_3^- transport, producing the increase or reduction of its concentration and its isotopic composition, must be considered. Four major physicochemical processes are: (1) dilution by means of mixing with pristine or NO_3^--poor surface water or groundwater; (2) volatilization of NH_3 after organic and/or inorganic fertilizers are spread onto the fields; (3) nitrification of NH_4^+; and (4) natural attenuation processes such as denitrification. The most significant natural attenuation reaction in the saturated zone is denitrification, which occurs under reducing conditions, and is mediated through denitrifying bacterial activity. Two distinct classes of denitrifying bacteria are distinguished: (1) *heterotrophic denitrifiers*, that use organic compounds as electron donors and C sources, and (2) *(chemolitho)autotrophic denitrifiers*, that use inorganic compounds (minerals containing reduced Fe or S, such as pyrite) as electron donors, and CO_2 as a C source (Rivett et al., 2008). On the other hand, the isotopic composition of SO_4^{2-} is controlled by: (1) the isotopic signature of SO_4^{2-} sources, (2) isotope exchange reactions, and (3) kinetic isotope fractionation during S and O transformations. With regard to changes in the isotopic composition, the most important process affecting S is the reduction or oxidation of S compounds. Variations in the isotopic ratio of groundwater SO_4^{2-} depend on mixing processes and chemical and microbial reactions (Krouse and Mayer, 2000).

Multi-isotopic approaches have been applied to characterize diffuse pollution at a regional scale in hydrogeological basins where local and large-scale flow systems converge (Palmer et al., 2007; Demlie et al., 2008; Folch and Mas-Pla, 2008; Stuart et al., 2010; Abid et al., 2012; among others). Local flow systems, made up of groundwater supplied by the local recharge infiltrated in the basin, are the most affected by pollution and processes occurring at the basin surface. In contrast, large-scale flow systems are made up of older groundwater supplied by recharge areas at greater elevation. Regional large-scale flow systems are characterized by deeper, usually higher temperature flows with no, or limited, interaction with the atmosphere (i.e. less dissolved O_2 and less CO_2 than local flows) and longer timescales of water–rock interaction. These differences between flow paths give waters in regional flow systems different compositions and physicochemical parameters compared to those of local groundwater.

Human activity changes groundwater quality of local flow systems by introducing pollutants from different sources. Moreover, these areas usually undergo intense groundwater exploitation which, in turn, modifies the natural flow conditions of the hydrogeological basin through drawdown (Mahlknecht et al., 2006; Palmer et al., 2007; Li et al., 2008; Folch et al., 2011; Carucci et al., 2012; among others). Groundwater pumped from wells located in these basins may be a mixture of groundwater from different origins, of different qualities, and affected by different processes.

This paper characterizes the sources and fate of NO_3^- and SO_4^{2-} by means of the analysis of stable isotopes ($\delta^{15}N$, $\delta^{34}S$ and $\delta^{13}C_{HCO3}$) in a basin-and-range area, where local and regional flow systems converge due to the disturbance exerted by groundwater exploitation. The aims are: (1) to confirm that the mixing between local polluted and regional pristine groundwater flow systems can influence the isotopic signatures found in contaminated groundwater, and (2) to study whether this mixing process allows denitrification to occur given the reducing conditions of the regional groundwater.

2. Study area

The Selva basin (NE, Spain) is a 565 km^2 area that has experienced considerable tectonic activity, and is surrounded by Montseny–Guilleries, Selva Marítima, Gavarres and Transversal mountain ranges that can reach an altitude of 1202 masl. Two main watersheds are found within these ranges: Santa Coloma River Basin (SCRB) and Onyar River Basin (ORB) (Fig. 1). Geomorphologically, the Selva basin constitutes a type of basin-and-range structural area (Menció, 2006; Folch, 2010) with a main NW–SE fault direction, and other significant faults oriented NE–SW and N–S. The surrounding ranges consist of Paleozoic igneous and metamorphic rocks in the Montseny–Guilleries, Selva Marítima and Gavarres ranges and pre-Alpine Paleogene sedimentary rocks (mainly limestone and sandstone) in the Transversal range. The basin sedimentary infill consists of a layer of unconsolidated gravel, coarse and medium sand and layers of silt, deposited by Neogene alluvial fan systems during basin formation. These layers can reach a total thickness of more than 300 m in the western area, varying according to the tectonic blocks that form the basin basement. Outcrops of Quaternary and Neogene volcanic material related to some of the main faults are found in the north and south, respectively.

Hydrogeologically, three main units can be determined: (1) the upper unconfined aquifer, less than 30 m deep, formed by alluvial materials associated with the main rivers, surficial Neogene sedimentary layers, and weathered igneous rocks outcropping in the basin; (2) an alternation of silts, arkosic sands, gravels and conglomerates with low clay content of Neogene sediment, resulting in an intermediate multilayer aquifer system with thicknesses from 10 to more than 200 m in the Santa Coloma basin, and more than 300 m in the Onyar basin (Menció, 2006; Folch, 2010); and (3) a deep aquifer, formed by the granite basement affected by local and regional faults and by a weathering layer in the upper zones. Wells located in the foothills of the ranges exploit weathered granite layers under unconfined conditions or, if drilled in unaltered rock, benefit from the occurrence of fractures. The degree of connectivity between hydrogeological formations changes along the basin depending on the geological setting at a small scale. For instance, in some areas of the Onyar basin the sedimentary formations act as a unique aquifer, while in other areas the three units show different hydraulic head evolution (Folch et al., 2011).

The Selva basin is classified as a *vulnerable zone to nitrate pollution from agricultural sources* following the European Union nitrate directive (EEC, 1991) and its adaptation in Catalunya (NE Spain) (Decret 283/1998 and Decret 476/2004). The human pressures that contribute to groundwater N compounds in the study area are: (1) livestock activity; (2) agricultural activity; (3) wastewater treatment plants; (4) industrial and urban areas; and (5) wastewater collectors (Luna et al., 2008). The application of organic animal waste (mainly pig manure) on the fields is a common activity, since an excess of manure is produced in the farms and, apart from its application as a fertilizer, illegal dumping may take place. Generally, animal residues are applied at the same municipality where the farms are located, but manure from neighboring areas can also be added to the local deposits. Moreover, most of the crop fields receive synthetic fertilizers once a year and the irrigated areas are

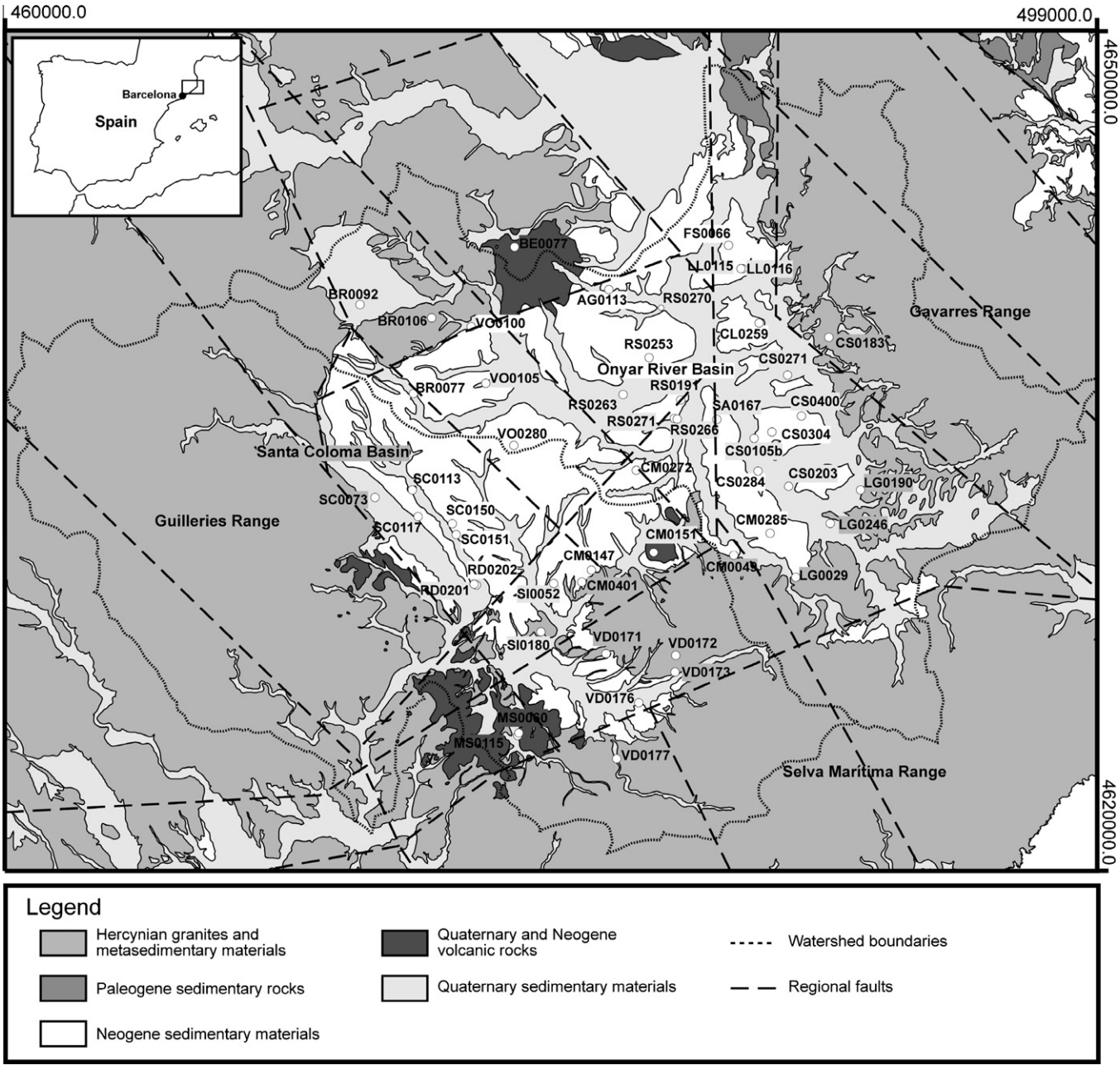

Fig. 1. The Selva basin area with the sample points used for hydrochemical and isotopic data collection.

susceptible to leaching of N to groundwater. The remaining potential N sources (i.e. wastewater treatment plants, industrial and urban areas, and wastewater collectors) usually have point-source effects in accordance with the land use distribution, and their expected contribution is orders of magnitude lower than that of pig manure and inorganic fertilizers. Only dumping from urban areas into the streams could constitute a notable NO_3^- source due to the frequency of this activity.

Hydrochemical facies analysis (Table 1) allows distinct groundwater sources to be differentiated in the main aquifers of the Selva basin (Folch et al., 2011). Based on their chemical composition, Na–HCO_3 and Cl-rich facies can be attributed to regional flow systems with longer residence times in the subsurface. These samples also have low NO_3^- concentrations and a high F^- content of up to 15 mg L^{-1}, indicating protracted water–rock interaction. Conversely, local flow systems belong to the Ca–HCO_3 facies, most of them having high NO_3^-, SO_4^{2-} and Cl^- concentrations related to pollution sources. This facies generally has a low F^- content (<2.0 mg L^{-1}). The Ca–HCO_3 facies containing significant Na^+ content and with sulfate and nitrate concentrations lower than those of samples from local flow regimes can be attributed to intermediate flow systems.

Fault zones and a fracture network have a direct effect on recharge, and allow for upward vertical flow from the basement to the sedimentary aquifers (Vilanova, 2004; Menció, 2006; Folch and Mas-Pla, 2008). Intensive seasonal withdrawal regimes from different depths and within sparse wells yield water with high F^- concentrations as well as significant NO_3^- content (Menció et al., 2010). This composition is attributable to mixing of different layers or flow systems, caused by pumping within the aquifer and/or the existence of several screened intervals in the borehole (or even the absence of well casing).

Table 1
Hydrochemical data of the May 2006 field sampling.

Sample	Group	Hydrochemical facies	HCO_3^- (mg L^{-1})	Cl^- (mg L^{-1})	SO_4^{2-} (mg L^{-1})	NO_3^- (mg L^{-1})	Na^+ (mg L^{-1})	K^+ (mg L^{-1})	Ca^{2+} (mg L^{-1})	Mg^{2+} (mg L^{-1})	Fe (mg L^{-1})	Mn (mg L^{-1})	F (mg L^{-1})
CS0105	Regional faults or granite	Ca–Na–HCO_3–Cl	302	73	58	30	125	4	51	8	0.05	0.031	6.2
FS0066	Regional faults or granite	Na–HCO_3	719	221	21	<0.5	398	2	19	5	0.26	0.062	15.4
LG0190	Regional faults or granite	Ca–Na–HCO_3–Cl	346	196	30	0.5	72	1	134	25	0.63	0.233	2.3
LG0246	Regional faults or granite	Ca–Na–HCO_3–Cl	290	103	50	13	95	4	81	11	n.d.	0.045	3.0
AG0113	Granite or Granite and Neogene	Ca–HCO_3	362	20	17	5	48	2	78	12	0.03	0.026	0.7
BR0092	Granite or Granite and Neogene	Ca–HCO_3–Cl	134	30	11	24	29	0	36	8	n.d.	0.002	0.2
CS0183	Granite or Granite and Neogene	Ca–HCO_3–Cl	276	133	50	31	55	1	118	18	0.08	0.002	1.3
LG0029	Granite or Granite and Neogene	Ca–HCO_3–Cl	596	115	34	0	74	2	136	38	1.18	0.250	0.5
SI0052	Granite or Granite and Neogene	Ca–HCO_3–Cl	424	214	65	79	130	1	159	29	0.21	0.009	0.5
VD0177	Granite or Granite and Neogene	Ca–HCO_3	236	38	44	67	60	0	67	13	0.04	0.016	0.2
VO0100	Granite or Granite and Neogene	Ca–HCO_3	349	30	42	156	44	1	127	25	n.d.	0.001	0.3
RS0191	Sedimentary Neogene with low nitrate	Ca–Na–HCO_3	408	67	13	20	55	2	100	20	0.04	0.002	0.3
VD0176	Sedimentary Neogene with low nitrate	Ca–Na–HCO_3	282	71	18	0	70	2	68	24	1.27	0.129	0.7
BR0110	Sedimentary Neogene with high nitrate	Ca–HCO_3	352	95	31	87	59	1	118	29	0.03	0.002	0.6
CL0259	Sedimentary Neogene with high nitrate	Ca–HCO_3	268	86	55	104	58	0	130	24	0.06	0.002	0.4
CM0272B	Sedimentary Neogene with high nitrate	Ca–HCO_3	419	132	49	78	66	0	154	25	0.04	0.001	0.2
CS0271	Sedimentary Neogene with high nitrate	Ca–HCO_3	368	135	94	114	75	0	163	28	0.07	0.007	0.2
CS0284	Sedimentary Neogene with high nitrate	Ca–HCO_3	196	111	116	88	56	3	122	24	0.06	0.026	0.5
CS0304	Sedimentary Neogene with high nitrate	Ca–HCO_3	378	116	78	120	85	1	157	21	0.06	0.003	2.8
LL0115	Sedimentary Neogene with high nitrate	Ca–HCO_3	352	54	41	67	47	0	125	15	0.06	0.004	0.2
RS0263	Sedimentary Neogene with high nitrate	Ca–HCO_3	362	79	89	70	54	1	152	18	0.02	0.002	0.2
VO0105	Sedimentary Neogene with high nitrate	Ca–HCO_3	403	77	48	94	57	0	148	26	0.05	0.002	0.2
CM0147	Surface wells	Ca–HCO_3	370	79	111	128	50	35	152	25	n.d.	0.001	0.2
CM0285	Surface wells	Ca–HCO_3	443	43	67	88	52	3	134	26	0.03	0.001	0.4
CM0401	Surface wells	Ca–HCO_3	274	148	130	170	122	31	132	13	0.03	0.001	0.2
CS0400	Surface wells	Ca–HCO_3	373	104	97	139	86	2	171	22	0.05	0.002	0.1
LL0116	Surface wells	Ca–HCO_3	467	94	110	201	75	1	206	23	0.03	0.002	0.2
MS0115	Surface wells	Ca–HCO_3	344	56	55	47	30	0	107	30	0.03	0.001	0.2
RS0253	Surface wells	Ca–HCO_3	306	21	70	217	27	0	161	22	0.04	0.001	0.2
SI0180	Surface wells	Ca–HCO_3	287	19	52	18	42	3	92	7	0.07	0.004	0.4
VD0171	Surface wells	Ca–HCO_3	424	67	64	60	85	0	125	22	0.05	0.001	0.4
VO0280	Surface wells	Ca–HCO_3	403	98	9	15	58	1	111	23	0.04	0.002	0.5
RD0201	Deep wells Sta. Coloma	Na–HCO_3	743	70	16	<0.5	222	4	52	17	0.16	0.077	3.2
SC0113	Deep wells Sta. Coloma	Na–HCO_3	250	28	5	6	39	0	51	9	0.04	0.001	0.3
SC0117	Deep wells Sta. Coloma	Na–HCO_3	236	34	29	35	45	0	69	9	0.04	0.001	2.6
BE0077	Volcanic or with volcanic materials	Ca–Mg–HCO_3	338	29	18	11	31	4	72	26	0.02	0.001	0.3
MS0060	Volcanic or with volcanic materials	Ca–Mg–HCO_3	454	34	35	1	45	7	76	40	0.05	0.239	0.2

3. Methodology

3.1. Sampling and analysis

Groundwater samples for chemical and isotopic analysis were collected in May 2006 from 37 private wells (mainly pumped for domestic, agriculture and cattle-raising uses), that represent the different geologic units and groundwater flow systems in the Selva basin. These wells were chosen from 60 wells previously studied by Folch et al. (2011) in order to analyze the effect of groundwater development on the head, hydrochemical, $\delta^{18}O_{H2O}$ and δD data. Physicochemical parameters (pH, temperature, conductivity, Eh and dissolved O_2) were measured *in situ*, using a flow cell to avoid contact with the atmosphere. Eh was measured with a WTW SenTix® Plus electrode (consisting of a Pt measuring electrode and a Ag/AgCl reference electrode) connected to a WTW pH 330i pH/mV meter. All Eh measurements were corrected to the standard hydrogen electrode system (UH) by adding the reference electrode potential at the groundwater temperature to the measured potential. The concentration of dissolved O_2 was measured with a DO meter (Hach® LDO/HQ10). Samples were collected after wells had been continuously pumped until Eh values were stabilized.

Samples were kept at 4 °C in a dark environment for their subsequent chemical and isotopic analyses. In the laboratory, pH and conductivity at 25 °C were measured again. Alkalinity (HCO_3^-) was determined by titration (METROHM 702SM Titrino) and F^- by an ion selective electrode method (Orion 901 ion selective electrode). Afterwards an aliquot of the sample was filtered through a 0.45 μm Millipore® filter. The anion (NO_3^-, SO_4^{2-} and Cl^-) content was measured by High Performance Liquid Chromatography (WATERS 515 HPLC), concentrations of Na^+, K^+, Ca^{2+}, Mg^{2+} and Fe, were measured by Inductively Coupled Plasma-Optical Emission Spectrometry (ICP-OES, Thermo Jarell ASH 61-E), and concentrations of Mn, by Inductively Coupled Plasma-Mass Spectrometry (ICP-MS, Perkin Elmer Elan 6000). The quality of the chemical analysis was checked by performing an ionic mass balance, accepting an error lower than 5%.

For the SO_4^{2-} isotopic analysis ($\delta^{34}S_{SO4}$ and $\delta^{18}O_{SO4}$), dissolved SO_4^{2-} was precipitated as $BaSO_4$ by adding $BaCl_2{\cdot}2H_2O$ after acidifying the sample with HCl and boiling it to prevent $BaCO_3$ precipitation following standard methods (e.g. Dogramaci et al., 2001). Unfiltered aliquots were treated with NaOH solution to give a pH above 11, and $BaCl_2$ solution was added to precipitate carbonates together with sulfates and phosphates. Later, they were filtered at 3 μm and the $\delta^{13}C$ of the total dissolved inorganic C, mainly HCO_3^-, was determined. $\delta^{18}O_{H2O}$ was determined with a Finnigan Matt Delta S Isotope Ratio Mass Spectrometer (IRMS) coupled to an automated line based on the equilibration between O–water and CO_2 gas. For the $\delta^{15}N_{NO3}$ and $\delta^{18}O_{NO3}$ analysis, dissolved NO_3^- was concentrated using anion-exchange columns Bio Rad® AG 1-X8 (Cl^-) 100–200 mesh resin after extracting the SO_4^{2-} and PO_4^{3-} by precipitation with $BaCl_2{\cdot}2H_2O$ and filtration. Next the dissolved NO_3^- was eluted with HCl and converted to $AgNO_3$ by adding Ag_2O. The $AgNO_3$ solution was then freeze-dried to purify the $AgNO_3$ for analysis (collection and purification procedures modified from Silva et al., 2000). The $\delta^{15}N_{NO3}$, $\delta^{34}S_{SO4}$ and $\delta^{13}C_{HCO3}$ were determined in a Carlo Erba Elemental Analyzer (EA) coupled in continuous flow to a Finnigan Delta C IRMS. The $\delta^{18}O_{NO3}$ and $\delta^{18}O_{SO4}$ were determined in duplicate with a ThermoQuest TC/EA (high Temperature Conversion/Elemental Analyzer) unit coupled with a Finnigan Matt Delta C IRMS. Notation is expressed in terms of δ ‰ relative to that of the international standards V-SMOW (Vienna Standard Mean Oceanic Water) for $\delta^{18}O_{H2O}$, AIR (atmospheric N_2) for $\delta^{15}N$, V-CDT (Vienna Canyon Diablo Troilite) for $\delta^{34}S$, and V-PDB (Vienna Peedee Belemnite) for $\delta^{13}C$. Precision ($\equiv 1\sigma$) of the samples calculated from international and internal standards systematically interspersed in the analytical batches was ±0.2‰, ±0.3‰, ±0.4‰, ±0.4‰, ±0.5‰ and ±0.2‰ for $\delta^{18}O_{H2O}$, $\delta^{15}N_{NO3}$, $\delta^{18}O_{NO3}$, $\delta^{34}S_{SO4}$, $\delta^{18}O_{SO4}$ and $\delta^{13}C_{HCO3}$, respectively. All samples for chemical and isotopic analyses were prepared in the Mineralogia Aplicada i Medi Ambient Research Group laboratory and analyzed at the Centres Científics i Tecnològics of the University of Barcelona.

4. Results and discussion

Before isotope data interpretation, samples were classified in groups such as those proposed by Folch et al. (2011), according to basin (Onyar or Santa Coloma), hydrogeological unit (shallow aquifer exploited by surface wells, Neogene multilayer aquifer or wells tapping granite) and hydrochemistry (F^- and NO_3^- concentration, and also hydrochemical facies). Thus, the studied samples were divided into the following groups:

1. Samples related to *regional fault zones and granitic aquifers*, mainly having a F^- content greater than 2 mg L^{-1}.
2. Samples from *wells in granitic rocks that may also exploit Neogene sedimentary formations*, usually with Ca–HCO_3 facies and some with high Cl^- content.
3. Samples from Neogene sedimentary layers with low nitrate content (below 38 mg L^{-1} NO_3^-).
4. Samples from *Neogene sedimentary layers with high nitrate content* (usually above 50 mg L^{-1} NO_3^-) showing the influence of groundwater withdrawal at moderate depth from or below shallow aquifer units.
5. Samples from *surface wells*, either in alluvial, or in the uppermost Neogene layers, or in weathered granite outcrops, having a characteristic Ca–HCO_3 facies, and likely to have high NO_3^- concentrations in the eastern SCRB and in the ORB.
6. Samples located totally or partially in *volcanic rocks*, with Ca–HCO_3 and/or Ca–Mg–HCO_3 facies, reaching a possible depth of 80 m and being related to local aquifers and/or deeper system flows.

Finally, two types of wells can be distinguished in the western SCRB with features different from those already described above, for example, lower salinity content. Accordingly, these two groups are differentiated:

1. Samples from *surface wells in the SCRB* with lower NO_3^- content than those of the ORB.
2. Samples from *deep wells and springs in the SCRB*, with a significant F^- content and low NO_3^- concentrations.

Chemical parameters and stable isotopes of dissolved NO_3^- ($\delta^{15}N$, $\delta^{18}O_{NO3}$), dissolved SO_4^{2-} ($\delta^{34}S$, $\delta^{18}O_{SO4}$), and HCO_3^- ($\delta^{13}C$) are summarized in Tables 1 and 2, where the samples are classified taking into account the groups described above.

4.1. Redox conditions

Dissolved O_2 values of the Selva sampled wells ranged between 0.1 and 8.1 mg L^{-1}, with a median value of 3.9 mg L^{-1} ($n = 34$), almost all below saturation concentration (8 mg L^{-1}). Eh values ranged between −76 and 497 mV, with a median value of 349 mV ($n = 33$). These physicochemical parameters related to redox conditions indicate that most of the studied samples are oxic groundwater (Table 3).

It is worth noting that several samples linked to regional flow (LG0190, LG0246 and FS0066) or fracture and fault systems

Table 2
Environmental isotopes data of the May 2006 field sampling ("Animal manure" means that near the well there are fields related with farms and/or areas where pig manure has been applied; and "Synthetic fertilizers" means that near the well there are areas with fruit trees and plant nurseries n.d. = not determined).

Sample	Group	Geology	Main NO_3^- source	$\delta^{18}O_{H2O}$ (‰)	$\delta^{34}S$ (‰)	$\delta^{18}O_{SO4}$ (‰)	$\delta^{15}N$ (‰)	$\delta^{18}O_{NO3}$ (‰)	$\delta^{13}C_{HCO3}$ (‰)
CS0105	Regional faults or granite	Neogene + granite	Animal manure	−5.3	6.8	6.3	18.9	10.6	−12.5
FS0066	Regional faults or granite	Neogene + granite	Unknown	−6.1	28.7	14.4	n.d.	n.d.	−9.8
LG0190	Regional faults or granite	Granite	Unknown	−5.5	n.d.	n.d.	n.d.	n.d.	−15.2
LG0246	Regional faults or granite	Granite	Unknown	−5.7	5.6	7.2	15.4	9.5	−13.7
AG0113	Granite or Granite and Neogene	Neogene + granite	Unknown	−5.4	14.4	7.1	n.d.	n.d.	−14.5
BR0092	Granite or Granite and Neogene	Quaternary + granite	Synthetic fertilizer	−6.0	10.0	7.6	6.2	4.0	−19.7
CS0183	Granite or Granite and Neogene	Granite	Animal manure	−5.1	5.7	4.8	12.0	3.4	−17.5
LG0029	Granite or Granite and Neogene	Wheathered granite + granite	Unknown	−4.9	n.d.	n.d.	n.d.	n.d.	−11.5
SI0052	Granite or Granite and Neogene	Wheathered granite	Animal manure	−5.1	7.5	5.4	9.9	5.4	−11.6
VD0177	Granite or Granite and Neogene	Granite	Unknown	−4.6	3.8	7.1	10.5	7.4	−17.3
VO0100	Granite or Granite and Neogene	Quaternary + granite	Animal manure	−5.6	5.2	5.5	10.4	4.7	−15.6
RS0191	Sedimentary Neogene with low nitrate	Neogene	Unknown	−5.7	11.2	6.7	8.3	5.0	−14.8
VD0176	Sedimentary Neogene with low nitrate	Neogen + volcanic	Unknown	−5.3	n.d.	n.d.	n.d.	n.d.	−14.6
BR0110	Sedimentary Neogene with high nitrate	Quaternary + Neogene	Unknown	−4.9	9.0	6.1	12.7	5.6	−15.1
CL0259	Sedimentary Neogene with high nitrate	Neogene	Synthetic fertilizer	−5.2	7.2	5.0	8.2	5.3	−15.5
CM0272B	Sedimentary Neogene with high nitrate	Neogene	Animal manure	−5.0	7.3	6.8	10.4	4.9	−14.1
CS0271	Sedimentary Neogene with high nitrate	Neogene	Animal manure	−4.9	9.0	7.3	14.0	7.4	−14.8
CS0284	Sedimentary Neogene with high nitrate	Neogene	Animal manure/synthetic fertilizer	−5.4	2.2	3.2	13.0	8.1	−15.8
CS0304	Sedimentary Neogene with high nitrate	Neogene + granite	Synthetic fertilizer	−4.9	7.2	5.8	9.3	6.8	−15.6
LL0115	Sedimentary Neogene with high nitrate	Neogene	Synthetic fertilizer	−5.2	7.6	4.2	9.2	6.6	−14.0
RS0263	Sedimentary Neogene with high nitrate	Neogene	Animal manure	−5.4	5.9	8.9	12.8	8.6	−13.2
VO0105	Sedimentary Neogene with high nitrate	Neogene	Animal manure	−4.9	7.1	6.7	10.2	5.5	−14.0
CM0147	Surface wells	Neogene	Unknown	−5.1	6.9	6.7	10.8	6.2	−14.5
CM0285	Surface wells	Neogene	Unknown	−4.6	7.2	4.8	8.3	5.8	−14.7
CM0401	Surface wells	Neogene	Unknown	−5.2	7.4	5.6	13.5	6.5	−14.4
CS0400	Surface wells	Neogene	Animal manure	−5.3	7.1	4.7	11.4	5.8	−15.0
LL0116	Surface wells	Neogene	Synthetic fertilizer	−5.0	8.1	4.8	7.4	5.5	−13.7
MS0115	Surface wells	Quaternary + volcanic	Animal manure	−4.9	7.2	8.8	13.5	8.0	−11.2
RS0253	Surface wells	Neogene	Unknown	−4.8	5.1	6.7	6.9	4.7	−14.0
SI0180	Surface wells	Wheathered granite	Unknown	−5.5	7.3	6.5	14.6	8.8	−16.9
VD0171	Surface wells	Quaternary	Unknown	−4.5	6.4	7.6	8.6	5.0	−14.3
VO0280	Surface wells	Neogene	Unknown	−5.3	12.2	5.8	6.3	3.8	−11.9
RD0201	Deep wells Sta. Coloma	Neogene	Non applied	−6.3	n.d.	n.d.	11.9	10.5	−5.4
SC0113	Deep wells Sta. Coloma	Neogene	Synthetic fertilizer	−5.8	n.d.	n.d.	n.d.	n.d.	−14.8
SC0117	Deep wells Sta. Coloma	Neogene	Synthetic fertilizer	−5.2	10.1	7.5	8.6	6.3	−12.8
BE0077	Volcanic or with volcanic materials	Volcanic + Neogene	Unknown	−5.4	7.6	9.5	10.3	5.3	−15.7
MS0060	Volcanic or with volcanic materials	Volcanic	Animal manure	−4.9	n.d.	n.d.	n.d.	n.d.	−9.3

(LG0029, RD0201) had the lowest values of dissolved O_2 (0–1 mg L^{-1}), together with the lowest values of Eh (<300 mV), and the lowest concentrations of SO_4^{2-}, together with the absence of NO_3^- and the highest values of Fe and Mn. The redox conditions suggested by these parameters are quite favorable to denitrification processes, and in some cases, SO_4^{2-} reduction.

4.2. Sulfate isotopes

Dissolved SO_4^{2-} in Selva basin groundwater may have several origins: (a) SO_4^{2-} from livestock manure, synthetic fertilizers or sewage leaking (anthropogenic sources related to land use and human pressure) and (b) oxidation of reduced S compounds, dissolution of evaporites, soil-derived SO_4^{2-} or CO_2-rich thermal waters (natural sources linked to hydrogeological conditions). The contribution of rainwater SO_4^{2-} is negligible, since the measured SO_4^{2-} concentration in rainwater samples collected near the basin is around 0.7 mg L^{-1} (Àvila et al., 2010) and the mean annual precipitation is 706 mm. The resulting SO_4^{2-} flux of 0.5 g m^{-2} y^{-1} can be considered low SO_4^{2-} input in terms of mass balance. As for other natural SO_4^{2-} sources, the oxidation of sulfides in the metamorphic basement rocks and the oxidation of magmatic H_2S would lead to dissolved SO_4^{2-} with a similar $\delta^{34}S$ to that of the precursor magmatic sulfide (0 ± 5‰) (Piqué, 2008). In the case of sulfide oxidation, the $\delta^{18}O$ of the newly formed SO_4^{2-} would be controlled either by the O source (H_2O or O_2) or by O isotope exchange between the intermediate species sulfite and water (Van Stempvoort and Krouse, 1994). The outcropping marine evaporites in the massifs from the north of the basin (Beuda gypsum formation) have $\delta^{34}S$ values between +20.2‰ and +21.8‰, and $\delta^{18}O_{SO4}$ values between +11.1‰ and +14.7‰ (Utrilla et al., 1992; Carrillo and Rossell, pers. comm.). Since gypsum dissolution does not result in isotopic fractionation, dissolved SO_4^{2-} derived from gypsum would preserve its S isotopic signature. The influence of soil-derived SO_4^{2-} would result in groundwater with $\delta^{34}S$ ranging between 0‰ and 6‰, and $\delta^{18}O_{SO4}$ between 0‰ and 6‰ (Krouse and Mayer, 2000).

Table 3
Physicochemical parameters data of the May 2006 field sampling (n.d. = not determined).

Sample	Group	Geology	Deep (m)	Cond. (μS/cm)	pH	Eh (mV)	T (°C)	O_2 (mg L^{-1})
CS0105	Regional faults or granite	Neogene + granite	100.0	767	7.3	403.7	16.8	0.9
FS0066	Regional faults or granite	Neogene + granite	102.0	1533	7.8	243.8	19.7	0.2
LG0190	Regional faults or granite	Granite	120.0	963	7.3	18.1	17.4	0.1
LG0246	Regional faults or granite	Granite	>100	786	7.3	22.2	17.7	n.d.
AG0113	Granite or Granite and Neogene	Neogene + granite	70.0	556	7.2	343.4	18.2	2.3
BR0092	Granite or Granite and Neogene	Quaternary + granite	80.0	361	6.3	456.8	17.0	4.3
CS0183	Granite or Granite and Neogene	Granite	60.0	825	6.9	n.d.	n.d.	n.d.
LG0029	Granite or Granite and Neogene	Wheathered granite + granite	110.0	970	7.4	−76.5	17.3	0.1
SI0052	Granite or Granite and Neogene	Wheathered granite	50.0	1217	6.9	343.6	16.3	5.5
VD0177	Granite or Granite and Neogene	Granite	80.0	612	7.0	351.0	16.5	0.1
VO0100	Granite or Granite and Neogene	Quaternary + granite	80.0	783	7.1	464.9	16.9	3.8
RS0191	Sedimentary Neogene with low nitrate	Neogene	90.0	765	6.9	423.6	18.6	6.1
VD0176	Sedimentary Neogene with low nitrate	Neogen + volcanic	69.0	710	7.4	348.9	17.9	0.1
BR0110	Sedimentary Neogene with high nitrate	Quaternary + Neogene	70.0	894	6.9	n.d.	17.0	n.d.
CL0259	Sedimentary Neogene with high nitrate	Neogene	75.0	891	6.9	n.d.	17.2	n.d.
CM0272B	Sedimentary Neogene with high nitrate	Neogene	40.0	1004	6.9	344.1	16.9	5.1
CS0271	Sedimentary Neogene with high nitrate	Neogene	80.0	1049	6.8	337.1	16.3	5.2
CS0284	Sedimentary Neogene with high nitrate	Neogene	70.0	856	6.6	326.8	16.2	4.0
CS0304	Sedimentary Neogene with high nitrate	Neogene + granite	116.0	1046	7.0	n.d.	17.7	6.3
LL0115	Sedimentary Neogene with high nitrate	Neogene	80.0	763	7.0	371.3	17.2	7.0
RS0263	Sedimentary Neogene with high nitrate	Neogene	50.0	887	6.8	325.5	16.5	0.9
VO0105	Sedimentary Neogene with high nitrate	Neogene	150.0	916	6.8	396.1	16.5	6.2
CM0147	Surface wells	Neogene	7.0	1011	6.8	352.0	14.7	3.6
CM0285	Surface wells	Neogene	14.7	835	7.8	440.9	15.4	6.6
CM0401	Surface wells	Neogene	14.6	1124	6.8	348.3	14.8	6.0
CS0400	Surface wells	Neogene	12.0	1078	6.9	341.4	15.3	3.2
LL0116	Surface wells	Neogene	11.8	1148	7.4	n.d.	15.0	6.8
MS0115	Surface wells	Quaternary + volcanic	21.9	735	6.8	324.4	16.7	2.4
RS0253	Surface wells	Neogene	17.1	864	6.9	482.7	17.0	8.1
SI0180	Surface wells	Wheathered granite	12.0	612	7.2	329.2	15.0	2.6
VD0171	Surface wells	Quaternary	80.0	909	7.1	377.9	16.4	4.7
VO0280	Surface wells	Neogene	8.0	805	7.0	357.7	17.0	6.8
RD0201	Deep wells Sta. Coloma	Neogene	75.0	1093	6.8	270.7	18.2	0.7
SC0113	Deep wells Sta. Coloma	Neogene	73.0	440	7.1	496.7	16.0	5.0
SC0117	Deep wells Sta. Coloma	Neogene	65.0	533	6.7	391.4	17.4	3.7
BE0077	Volcanic or with volcanic materials	Volcanic + Neogene	80.0	588	7.2	409.1	17.9	1.3
MS0060	Volcanic or with volcanic materials	Volcanic	60.0	693	7.0	263.8	18.3	1.1

Agrochemical products and pig manure are spread as fertilizers on the fields of the studied area, so they must be considered as potential anthropogenic SO_4^{2-} sources. The isotopic composition of fertilizers covers a wide range of values, with a mean isotopic composition of $\delta^{34}S$ = +5‰ and $\delta^{18}O_{SO4}$ = +12‰ (Vitòria et al., 2004b). Cravotta (1997) reported S isotopic values of pig manure ranging from −0.9‰ to +5.8‰, with a mean value of +3.7‰; and Otero et al. (2007) obtained $\delta^{34}S$ values between 0‰ and +5‰ for pig manure from a region near the studied area. The O isotopic composition of dissolved SO_4^{2-} derived from pig manure is not reported in the literature, hence, as a reference the estimated range of +3.8‰ to +6‰, corresponding to the $\delta^{18}O_{SO4}$ of groundwater polluted beyond doubt by pig manure (Vitòria, 2004; Otero et al., 2007) is assumed. Sewage, characterized by a mean $\delta^{34}S$ = +9.6‰ and $\delta^{18}O_{SO4}$ = +10‰ (Otero et al., 2008), could be another potential anthropogenic source, considering that the seven water treatment plants in the Selva basin usually discharge water into the rivers (Menció and Mas-Pla, 2008, 2010), and the outflow water can have SO_4^{2-} concentrations ranging from 100 to 850 mg L^{-1} (Otero et al., 2008). Furthermore, dumping from urban areas into the streams in areas that are not connected to the sewer system must be taken into account as another feasible SO_4^{2-} source. Therefore, since river–aquifer interaction changes throughout the basin with some areas behaving as gaining streams (mainly in the upper parts of the basin) and other areas as losing streams (Folch et al., 2010), the contribution of SO_4^{2-} from sewage cannot be disregarded at sites near streams. However, the influence of seepage from the sewer network can be considered negligible compared with the extent of the other SO_4^{2-} sources (Luna et al., 2008).

The $\delta^{34}S$ of groundwater samples ranged between +2.2‰ and +28.7‰, with a median value of +7.2‰ (n = 33), and $\delta^{18}O_{SO4}$ ranged between +3.2‰ and +14.4‰, with a median value of +6.7‰ (n = 33). The concentration of dissolved SO_4^{2-} varied from 5 to 238 mg L^{-1} with a median value of 49.3 mg L^{-1} (n = 39). Regarding the S isotope values, most of the Selva samples with SO_4^{2-} concentration between 50 and 150 mg L^{-1} had $\delta^{34}S$ between +5.0‰ and +9.0‰, in agreement with anthropogenic source values (inorganic fertilizers and pig manure) (Fig. 2). It is worth noting that most of these samples correspond to shallow wells or deep Neogene wells with high NO_3 concentrations, and therefore the high SO_4^{2-} concentrations are likely due to human contamination as well. Those samples with SO_4^{2-} concentration below 50 mg L^{-1} had higher isotopic variability, with $\delta^{34}S$ ranging from +3.8‰ to +28.7‰. The higher $\delta^{34}S$ values corresponding to lower SO_4 concentrations could be linked either to bacteriogenic SO_4^{2-} reduction processes or to the influence of CO_2-rich thermal waters.

The $\delta^{34}S$ and $\delta^{18}O_{SO4}$ values measured for groundwater samples are plotted in Fig. 3 together with those of the main SO_4^{2-} end-members, so that the contribution of the different potential sources can be assessed. As shown in Fig. 3, most of the samples fall in the mixing area defined by the isotopic ranges of fertilizers, pig manure and sewage, indicating that groundwater SO_4^{2-} is mainly controlled by anthropogenic sources. The general absence of pyrite in the Selva basin, and the fact that only two samples (CS0284 and VD0177) had $\delta^{34}S$ values below 5‰, make sulfide oxidation an unlikely process in the studied area. On the other hand, the lack of correlation between S and O isotopic compositions of dissolved SO_4^{2-} in groundwater (Fig. 3) indicates that SO_4^{2-} reduction is not generally occur-

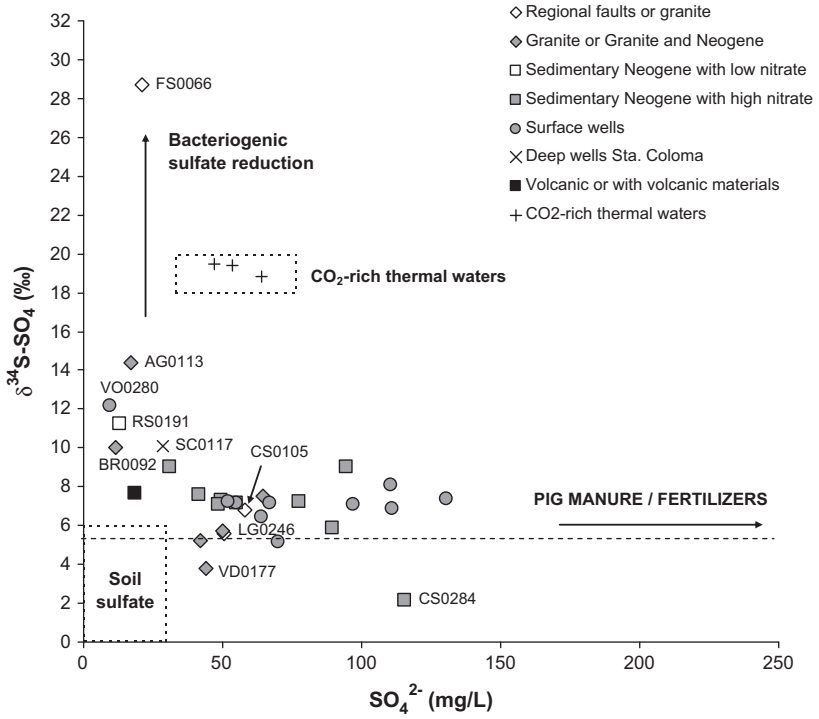

Fig. 2. SO_4^{2-} concentrations vs. $\delta^{34}S$ of the studied samples. The isotopic signatures of the main SO_4^{2-} sources and the trend of SO_4^{2-} reduction are also depicted.

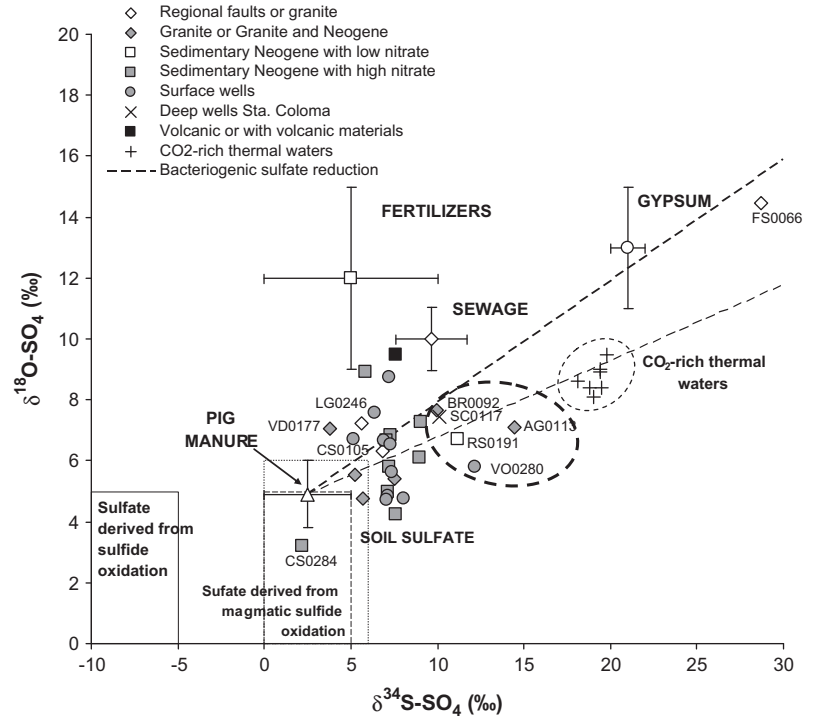

Fig. 3. $\delta^{34}S$ vs. $\delta^{18}O_{SO4}$ of dissolved SO_4^{2-} with the representation of natural and anthropogenic source isotopic ranges. Values for pig manure are taken from Otero et al. (2007) and Cravotta (1997), soil SO_4^{2-} data from Clark and Fritz (1997), fertilizer data from Vitòria et al. (2004b), and gypsum values from Utrilla et al. (1992). Dashed lines define the isotopic fractionation range ($\varepsilon^{34}S/\varepsilon^{18}O_{SO4}$) in SO_4^{2-} reduction reactions, which is between 2.5 and 4 (Mizutani and Rafter, 1973). Dashed bold circle indicates samples of intermediate flow system and/or mixing between local and regional flow systems.

ring. Only SO_4^{2-} in sample FS0066 could be explained as residual from bacteriogenic SO_4^{2-} reduction, since it has the highest $\delta^{34}S$ and $\delta^{18}O_{SO4}$ values and plots in the area defined by the extreme enrichment ratios of that process. Moreover, sample FS0066 is linked to regional flows and, as Einsiedl and Mayer (2005) observed in groundwaters with mean residence times of more than 60 a, a

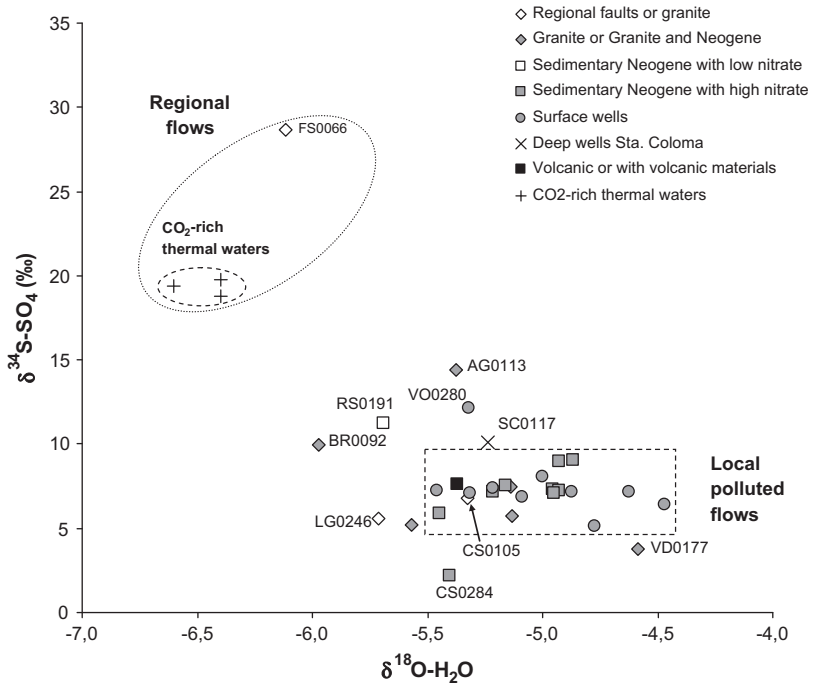

Fig. 4. $\delta^{34}S$–$\delta^{18}O_{H2O}$ diagram, where local recharge (affected by contamination) and regional flow samples are distinguished.

trend of increasing $\delta^{34}S$ and $\delta^{18}O_{SO4}$ values coupled with decreasing SO_4 concentrations can be explained by the occurrence of bacterial (dissimilatory) SO_4^{2-} reduction.

A comparison between the $\delta^{34}S$ in groundwater and the isotopic values of the outcropping marine evaporites from the north of the basin shows that all the samples differ from the expected values for the dissolution of gypsum (Fig. 3). Thus, the input of this natural SO_4^{2-} is unlikely to occur. Besides, the dissolution of marine gypsum is often accompanied by a dramatic increase in SO_4^{2-} concentration (Nriagu et al., 1991), and the values measured in this study were too low to suggest control by gypsum dissolution. In contrast, SO_4^{2-} derived from magmatic sulfide oxidation could exert some influence, although only one sample plots in its isotopic range: sample CS0284, with the lowest $\delta^{34}S$ and $\delta^{18}O_{SO4}$ values, might be linked to a ^{34}S-depleted source of reduced S associated with volcanic rocks. According to Rock and Mayer (2002), if groundwater SO_4^{2-} was partly derived from soil SO_4^{2-}, samples with low SO_4 concentrations and $\delta^{34}S$ between 0‰ and +6‰ would have been obtained (Fig. 3). Moreover, the substantial NO_3^- concentrations observed, in addition to a slight correlation between SO_4^{2-} and NO_3^-, suggest the influence of anthropogenic sources rather than a soil organic contribution.

Five samples (AG0113, BR0092, RS0191, SC0117 and VO0280) had greater values of $\delta^{34}S$, lower SO_4^{2-} concentrations and were slightly displaced from the clustered samples near the isotopic range of pig manure and fertilizers (mainly shallow wells and deep Neogene wells with high NO_3; Figs. 2 and 3). These samples are all located on the northern side of the water divide. They can be interpreted either as an intermediate flow or as mixtures between the local recharge and a ^{34}S-enriched source, like a regional long residence-time flow or CO_2-rich thermal waters.

Regional flow samples (FS0066, and CO_2-rich thermal waters analyzed by Piqué (2008) in the Caldes de Malavella geothermal field, located at the SE of the study area) had more negative $\delta^{18}O_{H2O}$ in accordance with a higher altitude of recharge in the surrounding ranges (Folch et al., 2011). These samples also had the greatest $\delta^{34}S$ values and relatively low SO_4^{2-} concentrations indicating the existence of SO_4^{2-} reduction processes (Fig. 4). On the other hand, the samples affected by local polluted flows had lesser $\delta^{34}S$ and greater $\delta^{18}O_{H2O}$ values, respectively, because they are controlled by an anthropogenic SO_4^{2-} isotopic signature (mainly inorganic fertilizers), and the origin of their recharge is local infiltration. From Fig. 4, it can be observed that the previously mentioned five samples followed a trend towards CO_2-rich thermal and/or regional groundwater, indicating they might be the result of mixing processes between contaminated and CO_2-rich thermal waters.

4.3. Dissolved inorganic carbon isotopes

Measured $\delta^{13}C_{HCO3}$ varied from −19.7‰ to −5.4‰, with a median value of −14.5‰ ($n = 38$) in the range of $\delta^{13}C_{HCO3}$ in groundwater (from −16‰ to −14‰, Clark and Fritz, 1997). In the study area, groundwater had HCO_3^- concentrations ranging between 134 mg L^{-1} and 743 mg L^{-1}, with a median value of 362.3 mg L^{-1}. Hence, the measured inorganic C isotopic composition is mainly controlled by the C signature of groundwater HCO_3^- in equilibrium with soil $CO_{2(g)}$, as well as by the secondary calcite linked to granites (White et al., 2005; Fig. 5). However, the influence of pig manure can account for the C isotopic composition of some of the samples, considering that Cravotta (1997) measured a manure $\delta^{13}C$ value in total C of −16.4‰, and Vitòria et al. (2004) obtained a pig manure $\delta^{13}C$ value of −23.8‰. Organic C in pig manure could lend its isotopic composition to the inorganic C pool, if denitrification was occurring by means of organic matter oxidation, and assuming that pig manure organic matter could act as an electron donor. Regarding the possible influence of synthetic fertilizers, it is considered that their C isotope ratio in total C ranges between −24‰ and −35‰ (Vitòria et al., 2004b). On the other hand, the higher concentrations of HCO_3^- in the Selva basin groundwater are linked to the interaction with CO_2-rich thermal waters. The isotopic composition of dissolved inorganic C in CO_2-rich thermal waters was determined by Vilanova (2004) in various CO_2-rich springs, and the median $\delta^{13}C$ ranged between −7.9‰ and −6.6‰.

Samples RD0201 and FS0066, related to the fracture network and regional flow system, had high values of $\delta^{13}C_{HCO3}$ (−5.4‰

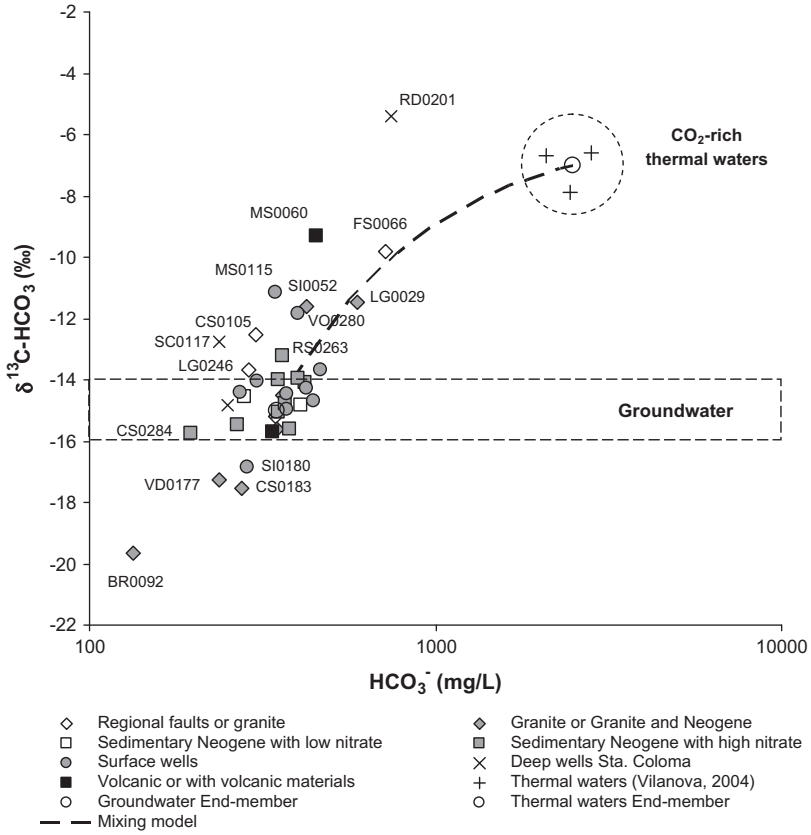

Fig. 5. $\delta^{13}C$–HCO_3 plot of the studied samples. The usual range of $\delta^{13}C_{HCO3}$ in groundwater in equilibrium with soil CO_2 (from −14‰ to −16‰; Clark and Fritz, 1997) and the sparkling spring samples analyzed by Vilanova (2004) are also plotted. Dashed bold curve indicates the two end-member mixing model trend.

and −9.8‰, respectively) and the highest values of HCO_3^- (above 700 mg L^{-1}) (Fig. 5), which can be interpreted as a result of the influence of CO_2-rich thermal waters and also longer water–rock interaction. Three other samples linked to long residence times (SC0117, CS0105 and LG0246) had lesser HCO_3^- concentrations, and lesser $\delta^{13}C$ values (although slightly greater than the typical isotope signatures of groundwater). Moreover, samples LG0029, MS0060, SI0052, VO0280, MS0115 and RS0263 had $\delta^{13}C$ values greater than −14‰ and HCO_3^- concentrations greater than the median value. Furthermore, the calcite saturation index (SI) of all these mentioned samples (except SC0017) is almost zero or positive (Folch et al., 2011). These results suggest that groundwater samples with $\delta^{13}C$ greater than −14‰, HCO_3^- concentrations greater than 300 mg L^{-1} and calcite SI > 0 may be accounted for by a contribution from CO_2-rich thermal waters and/or long residence time along flowpaths. In order to support this explanation, a theoretical mixing model has been calculated assuming two end-members: (1) the CO_2-rich thermal waters, represented by the average values of $\delta^{13}C$ = −7.0‰ and HCO_3^- = 2500 mg L^{-1}, and (2) groundwater, with the average values of $\delta^{13}C$ = −15.0‰ and HCO_3^- = 347 mg L^{-1}. The mixing model trend shown in Fig. 5 plots close to the greater $\delta^{13}C$ and HCO_3^- groundwater values and fits well with a few samples (RS0263, LG0029 and FS0066). Sample RD0201 is clearly not related to the mixing model trend because it belongs to another thermal water zone characterized by lower mineralization. Therefore, groundwater samples associated with the local flow system can be derived by mixing with CO_2-rich regional flow system groundwater, as pointed out by Folch et al. (2011).

The samples that had the lesser $\delta^{13}C$ values (below −16‰) and the lesser HCO_3^- concentrations (below 300 mg L^{-1}) (BR0092, CS0183, VD0177 and SI0180) had a calcite SI < 0 (Folch et al., 2011), indicating a potential lower influence of the natural C sources (soil CO_2 and the secondary calcite linked to granites). Thus, according to the C-source isotopic signatures, the inorganic C of these samples could be partly derived from C related to contamination, i.e. from pig manure or mixing between anthropogenic sources (manure and synthetic fertilizers) and groundwater HCO_3^-.

4.4. Nitrate isotopes

The $\delta^{15}N$ and $\delta^{18}O$ isotopic signatures of NO_3^- in groundwater can help identify different sources of NO_3^- and provide evidence of denitrification. Whereas denitrification causes a decrease in the amount of NO_3^-, dilution can likewise produce a decrease in NO_3^- concentration, but the total contaminant load remains in the aquifer. In order to elucidate which of these processes control NO_3^- concentrations in the Selva basin, where mixing between regional and local flow systems can make an adequate interpretation based only on hydrochemistry data difficult, the $\delta^{15}N$ and $\delta^{18}O$ of dissolved NO_3^- in groundwater were also determined.

For $\delta^{15}N_{NO3}$, groundwater samples ranged between +6.2‰ and +18.9‰, with a median value of +10.4‰ (n = 32), and for $\delta^{18}O_{NO3}$, between +3.4‰ and +28.0‰, with a median value of +5.8‰ (n = 32). The concentration of dissolved NO_3^- varied from 0 to 217 mg L^{-1} with a median value of 47 mg L^{-1} (n = 39). Isotopic composition ranges of potential NO_3^- sources in the Selva basin were obtained from previous studies in nearby areas with similar vulnerabilities to NO_3^- contamination (Otero et al., 2009; Vitòria et al., 2004b; Vitòria et al., 2008) and from the literature (Aravena and Mayer, 2010). Isotopic values of dissolved NO_3^- in groundwater are plotted in Fig. 6 together with those of the main NO_3^- sources in the study area. Values of $\delta^{18}O$ in NO_3^- derived from nitrification of NH_4^+ of fertilizers and manure were estimated following the

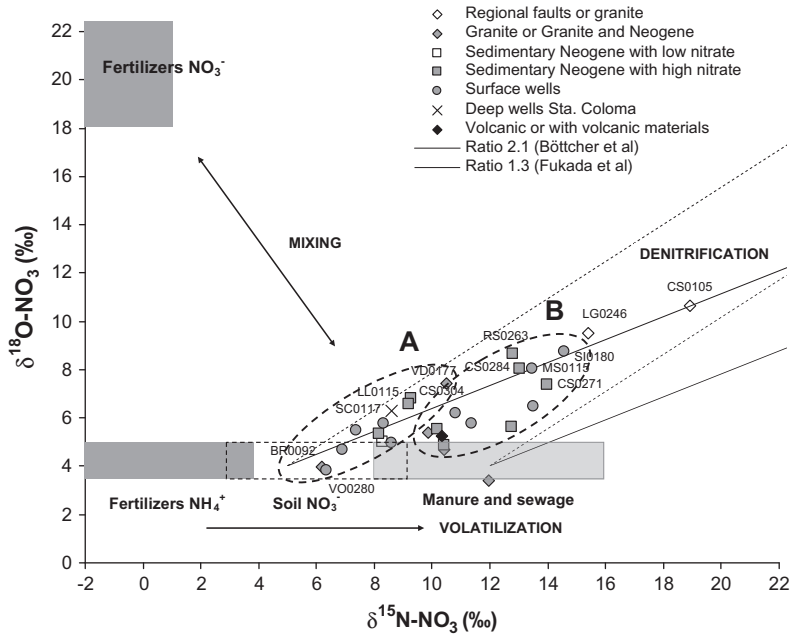

Fig. 6. Isotopic values of groundwater dissolved NO_3^- plotted with the ranges of the potential NO_3^- sources in the study area (Vitòria et al., 2004b; Vitòria et al., 2008).

experimental expression: $\delta^{18}O_{NO3} = 2/3(\delta^{18}O_{H2O}) + 1/3(\delta^{18}O_{O2})$ (Kendall et al., 2007), where the $\delta^{18}O_{H2O}$ is assumed to be that of the Selva basin groundwater and the $\delta^{18}O_{O2}$ is assumed to be that of atmospheric O_2 (+23.5‰).

The lowest $\delta^{15}N$ values were in the range of soil organic N ($\delta^{15}N$ between +3‰ and +8‰; Kendall et al., 2007). However, this source cannot be considered to be the main origin of NO_3^- because some NO_3^- concentrations (in some cases, up to around 200 mg L^{-1} NO_3^-) were much higher than those produced by the mineralization of soil organic N. Thus, the origin of NO_3^- for these samples might be ammonium fertilizers that, in addition to nitrification, have undergone processes such as volatilization or partial denitrification plus assimilation. This is consistent with the fact that some of these samples were collected in areas with fruit trees and plant nurseries, as, for instance, BR0092 and VO0280. In the same way, Vitòria et al. (2005) observed that $\delta^{15}N$ and $\delta^{18}O_{NO3}$ in groundwater from a zone influenced only by ammonium synthetic fertilizers fell in the range of soil organic N due to the effect of volatilization of NH_3.

For samples with $\delta^{15}N$ in the range of manure ($\delta^{15}N_{NH4}$ between +8‰ and +16‰; Vitòria, 2004) and/or sewage, and $\delta^{18}O_{NO3}$ up to +5‰ (the highest estimated $\delta^{18}O_{NO3}$), NO_3^- is the result of volatilization and nitrification processes affecting the NH_4 of pig manure, in agreement with the land use, the extent and pressure of livestock activities. Nevertheless, the impact of NO_3^- derived from sewage can also be significant, since frequent urban dumping attributed to areas not connected to the sewer system is occurring. In this case, NO_3^- would behave as a point-source pollution, and would not have the distribution pattern resulting from the application of synthetic and organic fertilizers. In order to distinguish between samples contaminated by pig manure or sewage, it could be worthwhile to analyze B isotopes in the groundwaters (Widory et al., 2012).

On the other hand, the influence of NO_3^- coming directly from nitrate synthetic fertilizers (KNO_3, etc.) was not noticed. Even the NO_3^- found in some fertilizers as a NO_3^- source taking into account the process of mineralization–immobilization-turnover (Mengis et al., 2001), where NO_3^- is immobilized as organic N by microbial incorporation, then mineralized to NH_4^+ and finally nitrified again to NO_3^- could be considered. This last process could also explain why most of the $\delta^{18}O_{NO3}$ values obtained were slightly greater than the estimated $\delta^{18}O_{NO3}$ values of NO_3^- resulting from the nitrification of manure and/or fertilizer NH_4^+.

In the case of samples with $\delta^{15}N$ in the range of manure and/or sewage, and with $\delta^{18}O_{NO3}$ values greater than +5‰, NO_3^- isotopic values displayed a positive trend in a plot of $\delta^{15}N$ vs. $\delta^{18}O_{NO3}$ (Fig. 6) indicating that denitrification processes could be taking place. Furthermore, attention should be drawn to the fact that samples RD0201 and FS0066 had physicochemical parameters typical of anaerobic conditions suitable for NO_3^- reduction, i.e. low O_2 content and moderate or low Eh values, as well as a very low NO_3^- content (<0.5 mg L^{-1}) that prohibited analysis of NO_3^- isotopic composition. Despite this lack of isotope data, denitrification is a reasonable explanation for the low NO_3^- concentrations of samples RD0201 and FS0066. Moreover, two other samples related to the regional groundwater flow, CS0105 and LG0246, had similar anoxic conditions to the two previous samples, whereas they had a NO_3^- content of 30 mg L^{-1} and 13 mg L^{-1}, respectively, and the greatest values of $\delta^{15}N$ and $\delta^{18}O_{NO3}$, in agreement with a denitrification trend. Hence, the samples linked to the regional flow system having sufficient NO_3^- concentration to allow isotopic analysis appeared to be clearly affected by natural attenuation processes of NO_3^-.

Based on the field campaign information and isotopic data, the samples have been separated into two groups (A and B in Fig. 6) according to the most likely source of NO_3^- (ammonium synthetic fertilizers or pig manure, see Table 2). As shown in Fig. 6, a coupled increase of $\delta^{15}N$ with $\delta^{18}O_{NO3}$ was observed for each group of samples suggesting that denitrification was taking place. The samples most affected by this natural attenuation process of NO_3^- were VD0177, CS0304, LL0115 and SC0117 (fertilizers-derived NO_3^-) (group A), and SI0180, RS0263, MS0115, CS0284 and CS0271 (pig manure-derived NO_3^-) (group B). They are all characterized by being associated with deep Neogene wells and/or surface wells in granite or volcanic materials. Moreover, some samples of group B had F^- contents around 0.5 mg L^{-1}, greater than the average for local flow systems (Folch et al., 2011). A clear example of this behavior is sample CS0284, collected from a 70 m deep well finished at the contact between Neogene sediments and granite, with a F^- content of 0.5 mg L^{-1}, as mentioned. Thus, all these wells seem to be influenced by mixing with regional flows with reducing conditions, represented mainly by samples CS0105 and LG0246.

Therefore, the assessment of processes involved in the transport and fate of NO_3^- by means of the dual NO_3^- isotopes approach seems to indicate that the reducing conditions of long residence time and deep flows favor NO_3^- reduction of polluted local recharge groundwater. Consistent mixing between the regional deeper groundwater and local groundwater plus denitrification superimposes the effects of dilution and consumption on NO_3^- concentrations. This is coherent with $\delta^{34}S$, $\delta^{18}O_{SO4}$ and $\delta^{13}C_{HCO3}$ data, as they also indicate mixing processes between deep and shallow flows.

Natural attenuation of NO_3^- can occur by means of heterotrophic and/or autotrophic denitrification. Studying the isotopic composition of dissolved HCO_3^- and SO_4^{2-} in groundwater can reveal whether or not organic matter and/or sulfides play a significant role as electron donors when denitrification processes are occurring. Denitrification by oxidation of organic matter should result in a decrease of NO_3^- and $\delta^{13}C_{HCO3}$ together with an increase of HCO_3^-. The sample trend in the $\delta^{13}C_{HCO3}$ vs. HCO_3^- plot (Fig. 5) was the opposite to the expected trend if denitrification linked to organic matter oxidation was occurring. This result, however, does not conclusively mean that NO_3^- was not being reduced by means of heterotrophic denitrification, because the influence of regional CO_2-rich flows and/or other C sources could have been masking it. It does not appear from the isotopes that significant pyrite oxidation was occurring. Therefore, either autotrophic denitrification is not occurring or sulfide is not a significant electron donor.

5. Conclusions

The multi-isotopic approach allowed determining the main sources of pollution in the Selva basin, a large hydrogeological system containing distinct but interrelated groundwater flow systems. The isotopic composition of dissolved SO_4^{2-} revealed that the origin of the SO_4^{2-} is related to a ternary mixing between synthetic fertilizers, pig manure and some influence from regional flow systems linked to CO_2-rich waters. The isotopic composition of dissolved NO_3^- confirmed that the main contribution to N in the Selva basin comes from pig manure (mainly in surface and sedimentary Neogene wells) and synthetic fertilizers (with perhaps minor contributions from sewage point-pollution), and that natural attenuation processes (denitrification) are occurring.

Furthermore, mixing between the polluted local groundwater and deep regional flows, containing low NO_3^- and O_2 concentrations, results in reduction of anthropogenic NO_3^- concentrations through both dilution and denitrification. While sulfide is not a significant electron donor, denitrification through the oxidation of organic matter cannot be ruled out.

Acknowledgements

This work was financed by the CICYT projects CGL2008-06373-C03-01 and CGL2011-29975-C04-01 from the Spanish Government, and partially by the project 2009SGR 103 from the Catalan Government. We would like to thank the Centres Científics i Tecnològics of the Universitat de Barcelona for the analysis.

References

Abid, K., Dulinski, M., Ammar, F.H., Rozanski, K., Zouari, K., 2012. Deciphering interaction of regional aquifers in Southern Tunisia using hydrochemistry and isotopic tools. Appl. Geochem. 27, 44–55.

Aravena, R., Robertson, W., 1998. The use of multiple isotope tracers to evaluate denitrification in groundwater: a case study in a large septic system plume. Ground Water 36, 975–982.

Aravena, R., Mayer, B., 2010. Isotopes and processes in the nitrogen and sulfur cycles. In: Aelion, C.M., Höhener, P., Hunkeler, D., Aravena, R. (Eds.), Environmental Isotopes in Biodegradation and Bioremediation. CRC Press, pp. 203–246.

Àvila, A., Molowny-Horas, R., Gimeno, B.S., Peñuelas, J., 2010. Analysis of decadal time series in wet N concentrations at five rural sites in NE Spain. Water Air Soil Pollut. 207, 123–138.

Carucci, V., Petitta, M., Aravena, R., 2012. Interaction between shallow and deep aquifers in the Tivoli Plain (Central Italy) enhanced by groundwater extraction: a multi-isotope approach and geochemical modeling. Appl. Geochem. 27, 266–280.

Clark, I.D., Fritz, P., 1997. Environmental Isotopes in Hydrogeology. Lewis Publishers, New York.

Cravotta, C.A., 1997. Use of Stable Isotopes of Carbon, Nitrogen, and Sulfur to Identify Sources of Nitrogen in Surface Waters in the Lower Susquehanna River Basin, Pennsylvania. U.S. Geol. Surv, Water-Supply Paper 2497.

Demlie, M., Wohnlich, S., Ayenew, T., 2008. Major ion hydrochemistry and environmental isotope signatures as a tool in assessing groundwater occurrence and its dynamics in a fractured volcanic aquifer system located within a heavily urbanized catchment, central Ethiopia. J. Hydrol. 353, 175–188.

Dogramaci, S.S., Herczeg, A.L., Schiff, S.L., Bone, Y., 2001. Controls on $\delta^{34}S$ and $\delta^{18}O$ of dissolved SO_4 in aquifers of the Murray Basin (Australia) and their use as indicators of flow processes. Appl. Geochem. 16, 475–488.

EC, 1998. Council Directive 98/83/EC, of 3 November 1998, on the Quality of Water Intended for Human Consumption.

EEC, 1991. Council Directive 91/676/EEC, of 12 December 1991, Concerning the Protection of Waters Against Pollution Caused by Nitrates from Agricultural Sources.

Einsiedl, F., Mayer, B., 2005. Sources and processes affecting sulfate in a Karstic groundwater system of the Franconian Alb, Southern Germany. Environ. Sci. Technol. 39, 7118–7125.

Folch, A., 2010. Geological and Human Influences on Groundwater Flow Systems in Range-and-basin Areas: The Case of the Selva Basin (Catalonia, NE Spain). PhD Dissertation, Universitat Autònoma de Barcelona.

Folch, A., Mas-Pla, J., 2008. Hydrogeological interactions between fault zones and alluvial aquifers in regional flow systems. Hydrol. Process. 22, 3476–3487.

Folch, A., Casadellà, L., Astui, O., Menció, A., Massana, J., Vidal-Gavilan, G., Pérez-Paricio, A., Mas-Pla, J., 2010. Verifying conceptual flow models in river-connected alluvial aquifers for management purposes using numerical modeling. In: Proc. XVIII Internat. Conf. Computational Methods in Water Resources (CMWR 2010), Barcelona, Spain.

Folch, A., Menció, A., Puig, R., Soler, A., Mas-Pla, J., 2011. Groundwater development effects on different scale hydrogeological systems using head, hydrochemical and isotopic data and implications for water resources management: the Selva basin (NE Spain). J. Hydrol. 403, 83–102.

Kendall, C., Elliott, E.M., Wankel, S.D., 2007. Tracing anthropogenic inputs of nitrogen to ecosystems. In: Michener, R.H., Lajtha, K. (Eds.), Stable Isotopes in Ecology and Environmental Science, second ed. Blackwell Publishing, pp. 375–449 (Chapter 12).

Krouse, H.R., Mayer, B., 2000. Sulfur and oxygen isotopes in sulfate. In: Cook, P.G., Herczeg, A.L. (Eds.), Environmental Tracers in Subsurface Hydrology. Kluwer Academic Press, Boston, pp. 195–231.

Li, X., Zhang, L., Hou, X., 2008. Use of hydrogeochemistry and environmental isotopes for evaluation of groundwater in Qingshuihe Basin, northwestern China. Hydrogeol. J. 16, 335–348.

Llamas, M.R., Martínez-Santos, P., 2004. Ethical issues in relation to intensive groundwater use. In: Selected Papers of the Symposium on Intensive Groundwater Use (SINEX). Balkema Publishers, The Netherlands, pp. 17–36.

Luna, M., Guimerà, J., Bruno, J., ACA, 2008. Diagnosis de la causalidad de la contaminación por nitratos de algunos abastecimientos públicos en las zonas vulnerables de Cataluña, análisis de alternativas, medidas de prevención y corrección. Área vulnerable 8. ACA (Water Catalan Agency) Internal Report, 218 pp.

Mahlknecht, J., Gárfias-Solis, J., Aravena, R., Tesch, R., 2006. Geochemical and isotopic investigations on groundwater residence time and flow in the Independence Basin, Mexico. J. Hydrol. 324, 283–300.

Menció, A., 2006. Anàlisi multidisciplinària de l'estat de l'aigua a la depressió de la Selva. PhD Dissertation, Universitat Autònoma de Barcelona.

Menció, A., Mas-Pla, J., 2008. Assessment by multivariate analysis of groundwater–surface water interactions in urbanized Mediterranean streams. J. Hydrol. 362, 355–366.

Menció, A., Mas-Pla, J., 2010. Influence of groundwater exploitation on the ecological status of streams in Mediterranean systems (Selva Basin, NE Spain). Ecol. Indic. 10, 915–926.

Menció, A., Folch, A., Mas-Pla, J., 2010. Analyzing hydrological sustainability through water balance. Environ. Manage. 45, 1175–1190.

Mengis, M., Walther, U., Bernasconi, S.M., Wehrli, B., 2001. Limitations of using $\delta^{18}O$ for the source identification of nitrate in agricultural soils. Environ. Sci. Technol. 35, 1840–1844.

Mizutani, Y., Rafter, T.A., 1973. Isotopic behaviour of sulfate oxygen in the bacterial reduction of sulfate. Geochem. J. 6, 183–191.

Nriagu, J.O., Rees, C.E., Mekhtiyeva, V.L., Lein, A. Yu., Fritz, P., Drimmie, R.J., Pankina, R.G., Robinson, B.W., Krouse, H.R., 1991. Hydrosphere. In: Krouse, H.R., Grinenko, V.A. (Eds.), Stable Isotopes: Natural and Anthropogenic Sulphur in the Environment. Wiley, Chichester, pp. 177–265.

Otero, N., Canals, A., Soler, A., 2007. Using dual-isotope data to trace the origin and processes of dissolved sulphate: a case study in Calders stream (Llobregat basin, Spain). Aquat. Geochem. 13, 109–126.

Otero, N., Soler, A., Canals, A., 2008. Controls of $\delta^{34}S$ and $\delta^{18}O$ in dissolved sulphate: learning from a detailed survey in the Llobregat River (Spain). Appl. Geochem. 23, 1166–1185.

Otero, N., Torrentó, C., Soler, A., Menció, A., Mas-Pla, J., 2009. Monitoring groundwater nitrate attenuation in a regional system coupling hydrogeology with multi-isotopic methods: the case of Plana de Vic (Osona, Spain). Agric. Ecosyst. Environ. 133, 103–113.

Palmer, P.C., Gannett, M.W., Stephen, R., Hinkle, S.R., 2007. Isotopic characterization of three groundwater recharge sources and inferences for selected aquifers in the upper Klamath Basin of Oregon and California, USA. J. Hydrol. 336, 17–29.

Piqué, A., 2008. Insights into the Geochemistry of F, Ba and Zn-(Pb) Hydrothermal Systems: Examples from Northern Iberian Peninsula. PhD Dissertation, Universitat de Barcelona.

Rivett, M.O., Buss, S.R., Morgan, P., Smith, J.W.N., Bemment, C.D., 2008. Nitrate attenuation in groundwater: a review of biogeochemical controlling processes. Water Res. 42, 4215–4232.

Rock, L., Mayer, B., 2002. Isotopic assessment of sources and processes affecting sulfate and nitrate in surface water and groundwater of Luxembourg. Isotopes Environ. Health Stud. 38, 191–206.

Schwientek, M., Einsiedl, F., Stichler, W., Stögbauer, A., Strauss, H., Maloszewski, P., 2008. Evidence for denitrification regulated by pyrite oxidation in a heterogeneous porous groundwater system. Chem. Geol. 255, 60–67.

Silva, S.R., Kendall, C., Wilkinson, D.H., Zieglerc, A.C., Chang, C.C.Y., Avanzino, R.J., 2000. A new method for collection of nitrate from fresh water and the analysis of nitrogen and oxygen isotope ratios. J. Hydrol. 228, 22–36.

Stuart, M.E., Maurice, L., Heaton, T.H.E., Sapiano, M., Micallef Sultana, M., Gooddy, D.C., Chilton, P.J., 2010. Groundwater residence time and movement in the Maltese islands: a geochemical approach. Appl. Geochem. 25, 609–620.

Utrilla, R., Pierre, C., Ortí, F., Pueyo, J.J., 1992. Oxygen and sulphur isotope compositions as indicators of the origin of Mesozoic and Cenozoic evaporites from Spain. Chem. Geol. Isotope Geosci. 102, 229–244.

Van Stempvoort, D.R., Krouse, H.R., 1994. Controls of $\delta^{18}O$ in sulphate. In: Alpers, C.A., Blowes, D.W. (Eds.), Environmental Geochemistry of Sulphide Oxidation. Am. Chem. Soc. Symp. Ser., vol. 550, pp. 446–480.

Vilanova, E., 2004. Anàlisi dels sistemes de flux a l'àrea Gavarres-Selva-Baix Empordà. Proposta de model hidrodinàmic regional. PhD Dissertation, Universitat Autònoma de Barcelona.

Vitòria, L., 2004. Estudi multi-isotòpic ($\delta^{15}N$, $\delta^{34}S$, $\delta^{13}C$, $\delta^{18}O$, δD i $^{87}Sr/^{86}Sr$) de les aigües subterrànies contaminades per nitrats d'origen agrícola i ramader. Translated title: multi-isotopic study ($\delta^{15}N$, $\delta^{34}S$, $\delta^{13}C$, $\delta^{18}O$, δD i $^{87}Sr/^{86}Sr$) of nitrate polluted groundwater from agricultural and livestock sources. PhD Thesis, Univ. Barcelona.

Vitòria, L., Otero, N., Canals, A., Soler, A., 2004. Fertilizer characterization: isotopic data (N, S, O, C and Sr). Environ. Sci. Technol. 38, 3254–3262.

Vitòria, L., Soler, A., Aravena, R., Canals, A., 2005. Multi-isotopic approach ^{15}N, ^{13}C, ^{34}S, ^{18}O and D) for tracing agriculture contamination in groundwater (Maresme, NE Spain). In: Lichtfouse, E., Schwarzbauer, J., Robert, D. (Eds.), Environmental Chemistry. Springer-Verlag, Heidelberg, pp. 43–56.

Vitòria, L., Soler, A., Canals, A., Otero, N., 2008. Environmental isotopes (N, S, C, O, D) to determine natural attenuation processes in nitrate contaminated waters: example of Osona (NE Spain). Appl. Geochem. 23, 3597–3611.

White, A.F., Schulz, M.S., Lowenstern, J.B., Vivit, D.V., Bullen, T.D., 2005. The ubiquitous nature of accessory calcite in granitoid rocks: implications for weathering, solute evolution, and petrogenesis. Geochim. Cosmochim. Acta 69, 1455–1471.

Widory, D., Petelet-Giraud, E., Brenot, A., Bronders, J., Tirez, K., Boeckx, P., 2012. Improving the management of nitrate pollution in water by the use of isotope monitoring: the $\delta^{15}N$, $\delta^{18}O$ and $\delta^{11}B$ triptych. Isotopes Environ. Health Stud. 48, 1–19.

ANNEX C

Puig, R., Soler, A., Widory, D. and Mas-Pla, J. (**2014**) Characterizing sources and natural attenuation of nitrate contamination in the Baix Ter aquifer system (Spain) using a multi-isotope approach ($\delta^{15}N$ and $\delta^{18}O$ of NO_3^-, $\delta^{34}S$ and $\delta^{18}O$ of SO_4^{2-}, $\delta^{11}B$, δD and $\delta^{18}O$ of H_2O, and $\delta^{13}C$ of HCO_3^-). Accepted for revision in *Journal of Hydrology* on March 2014.

Impact factor: 2.964 (2012)
Quartile and category: Q1, Civil Engineering; Q1, Multidisciplinary Geosciences; Q1, Water Resources

Characterizing sources and natural attenuation of nitrate contamination in the Baix Ter aquifer system (Spain) using a multi-isotope approach ($\delta^{15}N$ and $\delta^{18}O$ of NO_3, $\delta^{34}S$ and $\delta^{18}O$ of SO_4, $\delta^{11}B$, δD and $\delta^{18}O$ of H_2O, and $\delta^{13}C$ of HCO_3)

Roger Puig[a], Albert Soler[a], David Widory[b] and Josep Mas-Pla[c, d]

[a]Grup de Mineralogia Aplicada i Medi Ambient, Dept. de Cristal·lografia, Mineralogia i Dipòsits Minerals, Facultat de Geologia, Universitat de Barcelona, c/ Martí i Franquès s/n, 08028 Barcelona, Spain. rpuig@ub.edu

[b]Département des Sciences de la Terre et de l'Atmosphère, Geotop/UQAM, Montréal, Canada.

[c]Grup de Geologia Aplicada i Ambiental, Centre de Geologia i Cartografia Ambiental, Dept. de Ciències Ambientals, Universitat de Girona, 17071 Girona, Spain.

[d]Catalan Institute for Water Research, c/ Emili Grahit 101, 17003 Girona, Spain.

Abstract

The Baix Ter basin (NE Spain) is a regional large-scale aquifer system under heavy anthropogenic pressures from both agricultural and farming practices and industrial and urban activities. This leads to nitrate (NO_3) contamination and groundwater exploitation, ultimately resulting in local drinking water supply wells often exceeding the sanitary 50 mg NO_3 L^{-1} threshold. Local sources of NO_3 are dominated by organic and mineral fertilizers. In this context, identifying sources, major biogeochemical processes and sinks of dissolved NO_3 in groundwater is mandatory for improving policies regarding water resource quality and for addressing solutions to the impact of anthropogenic activities. Here, we sampled groundwater during two field campaigns in January (wet season) and August (dry season), and characterized them using a chemical and multi-isotope approach. Results show that NO_3 is not homogeneously distributed in groundwater and presents a large range of values, from no NO_3 to up to 480 mg NO_3 L^{-1}. NO_3 isotopes ($\delta^{15}N$ and $\delta^{18}O$) prove that natural denitrification is occurring in our study site, and in combination with boron isotopes ($\delta^{11}B$) confirm that pig manure application is the main vector of NO_3 pollution, although sewage and mineral fertilizers can also be isotopically detected. The natural reduction of NO_3 happens in near-river environments or in areas hydrologically related to fault zones. Sulfate isotopes ($\delta^{34}S$ and $\delta^{18}O$) indicate that denitrification is not linked to the pyrite oxidation but rather to the oxidation of organic matter. The multi-isotope approach in the Baix Ter basin allowed

characterizing the origin and natural attenuation of NO_3 contamination, and demonstrated its added value, compared to the study of the sole hydrochemical data. Obtaining this information can help to understand the mechanisms that control groundwater NO_3 contamination, and to evaluate the influence of anthropogenic activities and pressures to the aquifer system at a local as well as regional scale, as a basis for adopting a comprehensive water management strategy.

Keywords: Stable isotopes, nitrate contamination, boron, denitrification, groundwater, manure.

1. Introduction

Groundwater contamination arising from long-standing agricultural practices is a global water resources problem with adverse economic and health effects. Modern-day agriculture often entails the intense use of mineral and organic fertilizers, leading to high nutrient surpluses that are transferred to water bodies. Agriculture is the largest contributor of nitrogen pollution in Europe (EEA, 2012), with nitrate (NO_3) being the most widespread contaminant usually leading groundwaters to exceed the 50 mg L^{-1} legal threshold value for drinking water (EC, 1998). High NO_3 concentrations in groundwater are considered a threat for water bodies, since: 1) they damage the quality of aquifer resources and groundwater withdrawn from wells in public supply and capture areas, and 2) they lead to the eutrophication of surface waters. Moreover, the linkage between NO_3 ingestion and infant methaemoglobinaemia (the "blue baby" syndrome), or diseases like cancer of the digestive tract, has been reported (Bryan et al., 2012; Ward et al., 2005).

NO_3 is one of the main contaminants that could hinder the achievement of the goals of the Water Framework Directive (EC, 2000) and the European Groundwater Directive (EC, 2006). Current efforts in environmental management and research are focused on recovering groundwater quality, either by reducing NO_3 inputs into aquifers or remediate it from groundwater in order to reach drinking water levels. Mineral fertilizers account for almost half of all nitrogen input into European agricultural soils, while manure is the other major input (EEA, 2012). Leakage of sewage from sewer networks is also causing significant NO_3 contamination in urban environments (Aravena and Mayer, 2010).

When nitrogen enters the soil it is biologically modified through redox transformations (nitrogen fixation, nitrification, denitrification, dissimilatory NO_3 reduction to ammonium and anammox) mediated by microorganisms (Borch et al., 2010), so that nitrogen cannot be considered conservative. Most of the nitrogen that reaches groundwater appears in the oxidized form of NO_3, since the availability of oxygen in the unsaturated zone allows nitrification to occur. Nitrification and denitrification reactions, both taking place during infiltration of the water and in the groundwater body, produce isotope fractionation and finally a change in the isotope signature of the dissolved nitrogen species (Kendall, 1998). Denitrification is a microbially mediated redox process that reduces NO_3 to nitrogen gas (N_2) under anaerobic conditions and abundant NO_3 input, though it has been reported that some organisms can denitrify even in the presence of some oxygen (Rivett et al., 2008). Denitrification is the main natural attenuation process of NO_3 contamination in groundwater. Two main mechanisms have been proposed in soils and aquifers:

1) *Heterotrophic denitrification*, which is linked to the oxidation of organic compounds:

$$4NO_3^- + 5CH_2O \rightarrow 2N_2 + 4HCO_3^- + CO_2 + 3H_2O \quad (1)$$

2) *Autotrophic denitrification*, which is favoured by the oxidation of inorganic compounds such as sulfide minerals (by the *Thiobacillus denitrificans* bacteria):

$$14NO_3^- + 5FeS_2 + 4H^+ \rightarrow 7N_2 + 10SO_4^{2-} + 5Fe^{2+} + 2H_2O \quad (2)$$

Recently another redox process has emerged as significant nitrogen sink: *anaerobic ammonium oxidation* (anammox), which consists in the direct bacterial conversion of nitrite and ammonium into dinitrogen gas (Brunner et al., 2013; Devol, 2003):

$$NH_4^+ + NO_2^- \rightarrow N_2 + 2H_2O \quad (3)$$

In areas characterized by a complexity of groundwater flow systems and exposed to multiple potential sources of nitrogen, it is usually difficult to conclusively identify the main origin and processes controlling the nitrogen budget based only on hydrogeological and hydrochemical data. While dilution, dispersion and natural

denitrification processes result in a decrease in nitrogen concentrations, only natural denitrification leads to the reduction of the contaminant mass within the aquifer and has well known effects on NO_3 isotopes. The nitrogen ($\delta^{15}N$) and oxygen ($\delta^{18}O$) isotope compositions of the NO_3 molecule have shown their added value to assess sources and processes affecting nitrogen compounds in agricultural areas (Aravena et al., 1993; Aravena and Mayer, 2010; Clark and Fritz, 1997; Kendall, 1998, 2007; Panno et al., 2001). The significant isotope differences that exist between inorganic and organic fertilizers (Kendall et al., 2007) allow distinguishing between NO_3 coming from one source or another. On the other hand, $\delta^{15}N$ and $\delta^{18}O$ of NO_3 are useful to confirm the occurrence of natural denitrification in aquifers thanks to the isotopic fractionation induced by this process, which results in an enrichment in the heavy isotopes (^{15}N and ^{18}O) in the residual NO_3 (Aravena and Robertson, 1998; Fukada et al., 2003; Kendall et al., 2007; Mariotti et al., 1988). However, when the isotope signatures of some potential NO_3 sources overlap (e.g. animal manure and sewage), and the effects of mixing processes and transformation reactions are superimposed, discriminating multiple NO_3 sources based on the coupled use of $\delta^{15}N$ and $\delta^{18}O$ of NO_3 may become somewhat difficult. To alleviate this difficulty several studies have proposed a multi-isotope approach coupling hydrochemical data and $\delta^{15}N$ and $\delta^{18}O$ of NO_3 with the isotope compositions of ions involved in denitrification reactions ($\delta^{34}S$, $\delta^{18}O_{SO4}$ and $\delta^{13}C_{HCO3}$; Aravena and Robertson, 1998; Cravotta, 1997; Otero et al., 2009; Rock and Mayer, 2002; Saccon et al., 2013; Vitòria, 2004; Vitòria et al., 2005, 2008).

Moreover, in the last decade some studies have shown that the coupled use of $\delta^{15}N$ and $\delta^{18}O$ of NO_3 along with $\delta^{11}B$ is another successful approach to trace the origin of NO_3 in water (Seiler, 2005; Widory et al., 2004, 2005, 2013). While boron (B) is usually found in natural ground- and surface water as a minor constituent (<0.05 mg B L^{-1}), contaminant sources are enriched in B (>0.1 mg B L^{-1}; Tirez et al., 2010). Therefore, groundwater affected by anthropogenic activities may present elevated B contents (Vengosh et al., 1994). The main human application of B is the use of sodium perborate ($NaBO_3 \cdot nH_2O$) as an oxidation bleaching agent in domestic and industrial cleaning products (detergents, soaps, toothpaste, etc.). B is thus commonly detected in anthropogenic wastewater (Barth, 1998).

B has two stable isotopes, ^{10}B and ^{11}B, whose abundances are 19.9 and 80.1%, respectively. Based on the large relative mass difference between these isotopes and the

high geochemical reactivity of B, a wide range of $\delta^{11}B$ is expected in natural samples from different geological environments (Barth, 1993). This wide range of $\delta^{11}B$ may result in significant contrasts between B sources in groundwater. The main processes that can shift the concentration and $\delta^{11}B$ of dissolved B are aquifer matrix interaction (with dissolution of B-bearing silicates) and adsorption-desorption interactions with clay minerals, iron and aluminum oxide surfaces, and organic matter (Yingkai and Lan, 2001). When adsorption to clay particles occurs, the lighter ^{10}B isotope is favoured leaving water enriched in ^{11}B. However, B isotopes can be used as a co-migrating tracer of NO_3 in aquatic systems due to the lack of isotopic effects on B induced by evaporation, volatilization, and oxidation-reduction reactions (Bassett et al., 1995).

Komor (1997), Seiler (2005) and Widory (2004, 2005 and 2013) used $\delta^{11}B$ data combined with $\delta^{15}N$ and $\delta^{18}O$ of NO_3 in order to distinguish contributions from animal manure, sewage and mineral fertilizers. Hence, B isotopes can be useful in semirural zones where agricultural and farming practices cohabitate with industrial and urban activities. This is the case in the Baix Ter aquifers (Baix Empordà region; Catalonia, NE Spain), which were declared vulnerable to NO_3 pollution in 1998 by the local government following the 91/676/EC European Nitrate Directive (EC, 1991). Local sources of NO_3 pollution are dominated by a large amount of fertilizers (Mas Pla et al., 1998). This surplus has resulted, within the last years, in some drinking water supply wells exceeding the 50 mg NO_3 L^{-1} threshold (ACA, 2007). Trends in NO_3 contents are mainly related to agriculture and cattle raising practices that started in the 80's and have been intensified during the last decades (ACA, 2007; EEA, 1999). The Baix Ter aquifer is subjected to heavy anthropogenic pressures: 1) NO_3 contamination from various nitrogen sources, and 2) groundwater exploitation, which can alter the hydrodynamics of local and regional groundwater flows and induce groundwater mixing by means of seasonal withdrawal regimes. In this context, studying the origin, transport and fate of groundwater NO_3 is mandatory for improving water resource quality policies and for minimizing the impact of anthropogenic activities, which have become important objectives for stakeholders. To achieve this, a multi-isotope approach has demonstrated its added value compared to the study of the sole hydrochemical data (Kendall et al., 2007). The main purposes of our study were to:

1) Identify the dominant source(s) of NO_3 in the Baix Ter aquifer using a multi-isotope approach in a large-scale flow system disturbed by numerous anthropogenic pressures.

2) Include the study of $\delta^{11}B$ for the first time in the area in order to unambiguously discriminate NO_3 coming from animal manure from that coming from sewage.

3) Determine whether natural denitrification processes are occurring.

4) Assess the impact of geochemical reactions, geological settings and hydrodynamical processes on the occurrence of NO_3 natural attenuation.

2. Study area

2.1. Geological setting

The Baix Ter basin is located in the Baix Empordà tectonic basin (NE Catalonia, Spain) (Fig. 1). The study zone encompasses a 200 km^2 area characterized by the Ter River alluvial plain that turns into a fluvio-deltaic environment in its eastern margin. This plain is delimited by the Montgrí Range at the north, formed by Mesozoic limestone formations, and by the Gavarres Range at the south, composed of igneous and metamorphic rocks of Paleozoic age. The foothills of the Gavarres Range, as well as the basin basement, present Paleogene sedimentary materials (sandstone and limestone formations) that are severely affected by fractures (Mas-Pla and Vilanova, 2001).

The Baix Empordà tectonic graben was formed during the distensive period of the Alpine orogenesis. It is followed by the sedimentation of detritic, fine-grained and silty formations during the Neogene. The Quaternary fluvio-deltaic deposits, which constitute the main aquifers of the area, lay on the Neogene sediments in the western area, and on the Paleogene in the eastern part of the basin.

Fluvial deposits originate from the Ter River, as well as from some minor tributaries from the Gavarres Range (i.e., Daró River). Fluvial deposits reach a maximum depth of 50-60 m in the central part of the basin and are constituted by three main distinguishable units according to the Holocene sedimentary sequence (Montaner, 2010): 1) a deep level formed by alluvial coarse detritic material, gravel and sand, covered by a higher level of fine sediments, 2) an intermediate level, formed by sandy lenticular bodies in a silty-sandy level, also covered by a level of fine sediments, and 3) a shallow level,

mainly sandy with a thickness of 10 to 20 m, formed by the present prograding alluvial deposits that transform to marsh and coastal deposits near the coast line.

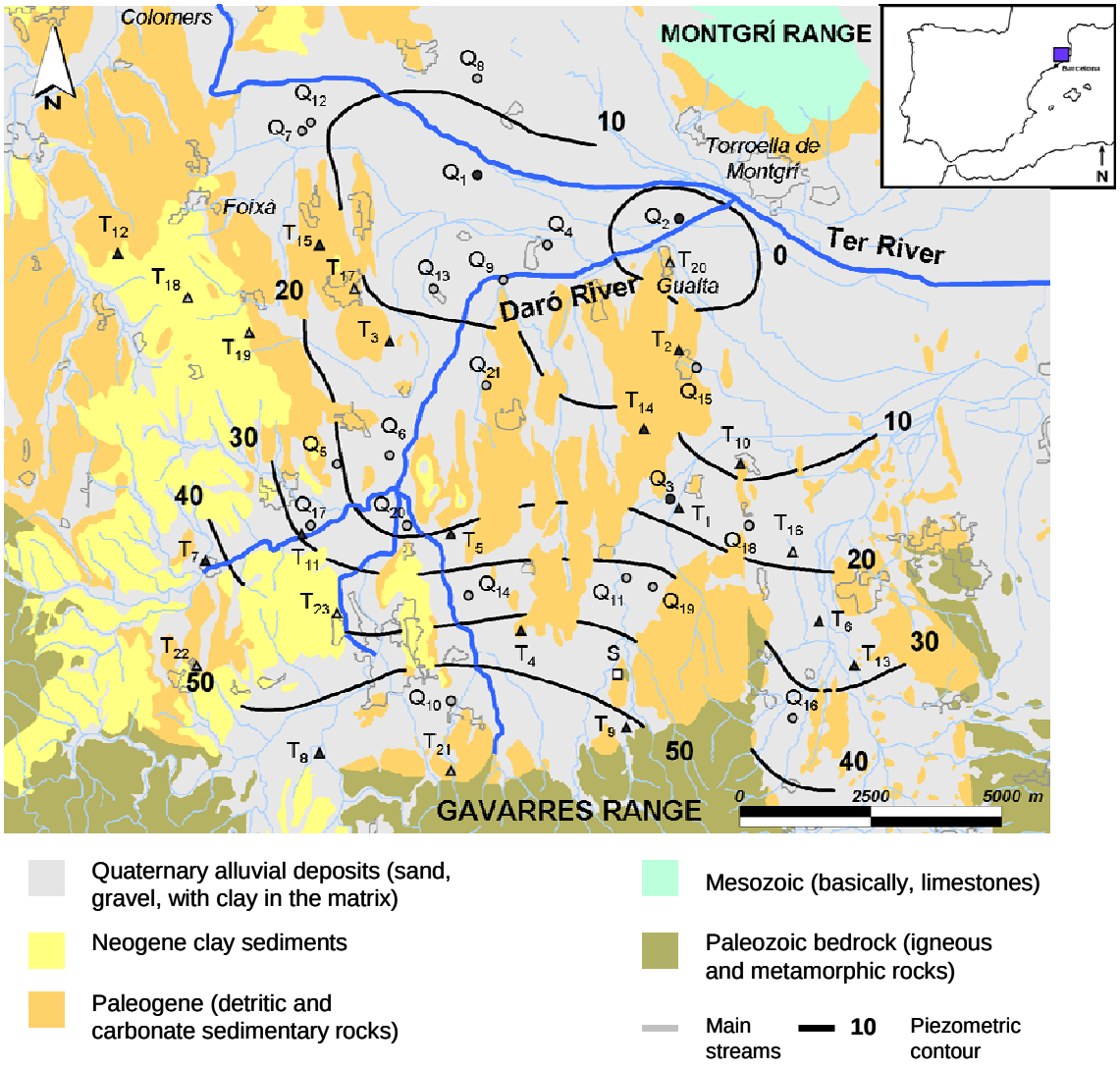

Figure 1. Baix Ter basin map showing the geology and sampling points, labeled according to their hydrogeological formation (round and triangle shapes distinguish between Quaternary and Tertiary aquifers, respectively, and light and bold points, between shallow and deep formations, respectively). Potentiometric contourlines correspond to the water table measurements of the Quaternary unit (August 2004).

2.2. Hydrogeological dynamics

The Quaternary fluvio-deltaic deposits of the Ter River constitute the main hydrogeological system in the study area. Because of its lithological diversity, distinct aquifer levels are differentiated, from bottom to top (Montaner, 2010): 1) a leaky aquifer formed by the deeper coarse sediment layer, lying on the Paleogene basement, 2) an upper leaky aquifer formed by the intermediate sandy layer, and 3) an upper unconfined aquifer formed by the prograding deposits. All of them present significant

lateral variations, especially the upper aquifer that reflects the geomorphological units presently occurring in the plain: fluvio-deltaic, marsh and coastal areas. Groundwater withdrawal from these aquifers supplies the main water demand for agricultural and urban uses.

Main recharge is related to local precipitation, seasonal contribution from the Ter and Daró rivers (whether natural or induced by pumping), and to irrigation returns (Montaner, 2010). Locally, leakage from the municipal water supply network may also contribute to groundwater recharge. Nevertheless, the fractured nature of the Paleogene sedimentary basement overlying the metamorphic rocks of the Gavarres Range allows an upward vertical flux that also recharges the aquifers constituted by Quaternary formations, especially in the southern border of the basin (Vilanova and Mas-Pla, 2004; Vilanova et al., 2008). Hence, igneous and metamorphic rocks at the Gavarres Range act as regional recharge areas that discharge into the fluvio-deltaic Quaternary aquifers through the preferential flow paths of the limestone and carbonate Paleogene aquifers and, more importantly, through the fractures that affect them.

This hydrogeological flow model is corroborated by potentiometric, hydrochemical and isotope data (Vilanova, 2004). Hydraulic head, for instance, is some meters higher in the Paleogene foothills than in the nearby alluvial plain. Potentiometric maps reveal an influent (losing stream) behavior of the Ter River in its western reach, between Colomers and Foixà, before entering the fluvio-deltaic plain. Downstream, both the Ter and Daró rivers show an effluent (gaining stream) behavior until the coast line.

Nevertheless, groundwater withdrawal in the fluvio-deltaic formation, which started in the 60's with the agricultural development of the area, modified the natural flow field. A noticeable depression cone in the center of the formation, between the villages of Gualta and Torroella de Montgrí, was first reported in 1969. It grew during the 80's and is now constant (ACA, 2007). This severe depression cone, that in its central part may reach several meters below sea level, has created a downward flow from the upper unconfined aquifer. It has also captured the Ter River discharge and induced seawater intrusion that severely affects groundwater.

Samples will thus be distinguished according to their hydrogeological formation: shallow Quaternary, including wells in the upper unconfined aquifer (Q_S); deep Quaternary, including wells in the lower leaky aquifers (Q_D); and shallow (T_S) and deep (T_D) Tertiary for wells located in the Paleogene materials according to the their depth (the limit to distinguish them is arbitrarily set at 30 m depth).

2.3. Anthropogenic activities and soil uses

The Baix Ter basin area is marked by the influence of 1) rural agriculture and livestock activities, 2) industrial activity, and 3) several small to medium-sized urban areas that drastically increase their population during summer due to the intense touristic activity. Herbaceous dry-farmed and irrigated crops (mainly maize, sunflower and rice) cover a 60% of the surface, forest and pasture 20%, and 7% of the area is used for fruit growing (ACA, 2007). The agricultural activity developed in the alluvial plains uses preferentially mineral fertilizers, but animal manure is also applied due to large amount of organic residues generated by the important cattle farming activity. The total nitrogen produced by livestock in the study zone is around 500 tones of N $year^{-1}$. 60% of this amount is from intensive pig raising (460 pigs/km^2; 50 m^3 ha^{-1} $year^{-1}$ of pig manure are applied onto maize crops; ACA, 2007). Leakage from manure ponds or inappropiate spillages may be another source of nitrogen. This surplus of nitrogen unassimilated by crops is leached into the aquifer during precipitation or irrigation periods, and incorporated in the saturated zone elevating NO_3 concentrations in groundwater. Agricultural return water must thus be considered influential for pollution dynamics. Therefore, groundwater contamination is directly related to the organic residues management, but also to agricultural practices. Finally, the La Bisbal water treatment plant should also be considered as a potential nitrogen source. It discharges downstream of Daró River and produces mud that is sometimes applied onto the fields. Recently, some corrective measures were adopted to avoid release of wastewater effluents from the plant.

In the Baix Ter alluvial plain, the total groundwater abstraction is around 21 Hm^3/yr: 62% for domestic use (including the touristic season), 36% for agriculture activities and 2% for the industry (ACA, 2007). The combination of periods of low precipitation and low aquifer recharge with the increase of groundwater withdrawal in summer (crop irrigation period from May to August) has led to water table decreasings and periods of groundwater shortage (Montaner et al., 2010).

2.4. Isotope characterization of NO_3 sources

The multi-isotope approach consists in coupling isotope data of elements related to the origin and fate of the contaminant. In order to use this approach, we need NO_3, SO_4, B and dissolved inorganic carbon (HCO_3) isotopic composition ranges of the potential

Table 1. Nitrate, sulfate, boron and dissolved inorganic carbon isotope ranges of the potential nitrate sources obtained from the literature.

NO_3^- source	Pig manure	Mineral fertilizers	Sewage	Soil
Isotope ratio (‰)				
$\delta^{15}N$	+8 — +16	-4 — +4	+8 — +20	+3 — +8
	Vitòria (2004)	*Bateman and Kelly (2007), Kendall et al. (2007), Vitòria et al. (2004b)*	*Aravena and Mayer (2010), Curt el al. (2004)*	*Aravena and Mayer (2010), Heaton (1986), Kendall et al. (2007)*
$\delta^{18}O_{NO3}$	+3,4 — +4,6	+17 — +25	+3,4 — +4,6	+3,4 — +4,6
	This study	*Aravena and Mayer (2010), Vitòria et al. (2004b), Xue et al. (2009)*	*ºThis study*	*This study*
$\delta^{34}S$	-0,9 — +5,8	0 — +10	+7,6 — +11,7	0 — +6
	Cravotta (1997)	*Vitòria et al. (2004b)*	*Otero et al. (2008)*	*Krouse and Mayer (2000)*
$\delta^{18}O_{SO4}$	+3,8 — +6	+9 — +15	+9 — +11,1	0 — +6
	Otero et al. (2007), Vitòria (2004)	*Vitòria et al. (2004b)*	*Otero et al. (2008)*	*Krouse and Mayer (2000)*
$\delta^{11}B$	+19,5 — +42,4	-9 — +15	-7,7 — +12,9	-
	Widory et al. (2005)	*Komor (1997), Widory et al. (2005), (2013)*	*Bassett et al. (1995), Vengosh et al. (1994), Widory et al. (2013), Xue et al. (2009)*	-
$\delta^{13}C_{HCO3}$	-23,8 — -16,4	-35 — -24	-25 — -13	-23
	Cravotta (1997), Vitòria (2004)	*Vitòria et al. (2004b)*	*Jurado et al. (2013), Li et al. (2010), Waldron et al. (2001)*	*Clark and Fritz (1997)*

3. Methodology

3.1. Sampling

Two sampling campaigns were conducted in the Baix Ter basin, which are specifically located in the right bank alluvial plain: 1) in January 2004 (24 wells), during the wet season, fertilization and growing of dry land cereals and 2) in August 2004 (40 wells), during the dry season and cultivation of spring cereals. Groundwater hydraulic head, hydrochemical and isotope data (Tables 2, 3 and 4) were obtained mainly from private wells. Most of the sampling locations were common in both campaigns. Wells were pumped until the water Eh stabilized and groundwater samples were then collected in bottles that were first rinsed several times with groundwater. Samples were collected and stored at 4ºC in a dark environment before analysis.

3.2. Analytical techniques

Temperature, pH, electrical conductivity (EC) and Eh were measured in situ, using a flow cell to avoid contact with the atmosphere. Cl^-, NO_2^-, NO_3^-, SO_4^{2-}, HCO_3^-, Na^+, K^+, Ca^{2+}, Mg^{2+}, NH_4^+, total Fe, total Mn, B and total organic carbon (TOC) were determined by standard analytical techniques.

The multi-isotope approach includes the stable isotope compositions of: hydrogen (δD) and oxygen ($\delta^{18}O$) of water, nitrogen ($\delta^{15}N$) and oxygen ($\delta^{18}O$) of dissolved NO_3, sulfur ($\delta^{34}S$) and oxygen ($\delta^{18}O$) of dissolved sulfate, boron ($\delta^{11}B$) of dissolved boron, and carbon ($\delta^{13}C$) of dissolved inorganic carbon (HCO_3). δD and $\delta^{18}O$ of water were measured by the H_2 and CO_2 equilibration technique, respectively, and isotope ratio mass spectrometry (IRMS) with a Delta S Finnigan Mat. $\delta^{15}N$ and $\delta^{18}O$ of dissolved NO_3 were measured using the $AgNO_3$ method (modified from Silva et al. (2000)). $\delta^{15}N$ was analysed using an Elemental Analyser (Carlo Erba 1108) coupled with an Isochrom Continuous Flow IRMS. For $\delta^{34}S$ and $\delta^{18}O$, the dissolved SO_4 was precipitated as $BaSO_4$, first acidifying the sample with HCl and boiling it, and then adding an excess of $BaCl_2 \cdot 2H_2O$. $\delta^{34}S$ was measured using an Elemental Analyser (Carlo Erba 1108) coupled with a Delta C Finnigan Mat. $\delta^{18}O$ of NO_3 and SO_4 were analysed in duplicate with a Thermo-Chemical Elemental Analyser (TC/EA Thermo-Quest Finnigan) coupled with a Delta C Finnigan Mat. $\delta^{11}B$ was determined on the Cs_2BO^{2+} ion (Spivack and Edmond, 1986) by negative-ion Thermal-Ionization Mass Spectrometry (TIMS) at the BRGM (France). Reproducibility was obtained by repeated measurements of the

NBS951, and the accuracy was controlled with the analysis of the IAEA-B1 seawater standard ($\delta^{11}B$ = 38.6 ± 1.7‰). For dissolved inorganic carbon, liquid samples were acidified with ortho-phosphoric acid and shaken for at least two hours to convert all bicarbonate into CO_2 and to reach equilibrium between the dissolved and gaseous phases. Gas samples were diluted with helium to facilitate analysis. $\delta^{13}C$ of inorganic carbon was measured on a Gas Chromatograph-Combustion-Isotopic Ratio Mass Spectrometer (GC-C-IRMS) at the Environmental Isotope Laboratory (EIL) of the University of Waterloo (Canada).

All isotope notations are expressed in terms of δ per mil relative to their respective international standards: Vienna Standard Mean Ocean Water (V-SMOW), atmospheric N_2 (AIR), Vienna Canyon Diablo Troilite (V-CDT), NBS951 and Vienna Pee Dee Belemnite (V-PDB) standards. Reproducibility is ±1.5‰ for δD, ±0.2‰ for $\delta^{18}O_{H2O}$, ±0.3‰ for $\delta^{15}N$, ±0.2‰ for $\delta^{34}S$, ±0.5‰ for both $\delta^{18}O_{NO3}$ and $\delta^{18}O_{SO4}$, ±0.3‰ for $\delta^{11}B$, and ±0.3‰ for $\delta^{13}C_{HCO3}$. Except for $\delta^{11}B$ and $\delta^{13}C_{HCO3}$ measurements, samples were prepared at the laboratory of the Mineralogia Aplicada i Medi Ambient research group and performed at the Centres Científics i Tecnològics of the Universitat de Barcelona.

4. Results and discussion

4.1. Hydrodynamics

Potentiometric contourlines correspond to hydraulic head measurements in the Quaternary aquifer conducted during the second field campaign (Fig. 1). The amount of hydraulic head measurements in this second survey was higher than in the first allowing a more reliable potentiometric layout. In agreement with the conceptual flow model described in previous studies (Vilanova and Mas-Pla, 2004), the Quaternary piezometry showed groundwater flow lines oriented south to north (from the Gavarres massif to the Ter River) (Fig. 1). Near the Ter River, groundwater flow changes to a west-to-east direction towards the sea, showing the influence of the Ter River, except close to the pumping area of the Gualta supply wells. The exploitation of these wells produces a depression cone around this municipality. Groundwater withdrawal activity near Gualta village modifies the behavior of the Ter River, inducing surface water to drain into the alluvial aquifer, and making the Ter River a losing stream where the depression cone appears. Vilanova (2004) and Vilanova and Mas-Pla (2004) also pointed out an upward vertical flow line from the underlying confined fractured Tertiary unit to the shallow

Quaternary aquifer, but due to the few sampled wells that reached the Tertiary aquifer in our hydrogeological study, we could not consistently plot a Tertiary potentiometric map in order to depict such hydrogeological relationship.

4.2. Sources of the recharge

$\delta^{18}O$ and δD of groundwater mainly plot at the right side of the annual and winter local meteoric water lines (LMWL, W-LMWL; Vilanova, 2004; Fig. 2). The isotope values of samples collected from wells in the Quaternary and Tertiary aquifers were mostly lighter than those of the weighted mean precipitation (δD = -33.5‰, $\delta^{18}O$ = -5.2‰; calculated from Mas Badia station data, located in the Baix Ter basin). This indicates that recharge of these aquifers is not only attributable to the infiltration of rainfall within the basin but also to other sources of recharge. Quaternary groundwater samples align better with the annual LMWL than the Tertiary groundwaters. Both aquifers had groundwater $\delta^{18}O$ values higher than the winter LMWL. The slight enrichment in ^{18}O exhibited by both deep and shallow Quaternary groundwaters can be interpreted as a result of evaporation processes, in agreement with Vilanova (2004). The wide range of $\delta^{18}O$ and δD values in the shallow Quaternary aquifer, even within the same sampling campaign, denotes the influence of different recharge flow systems with distinct hydrogeological characteristics, and the mixing among them:

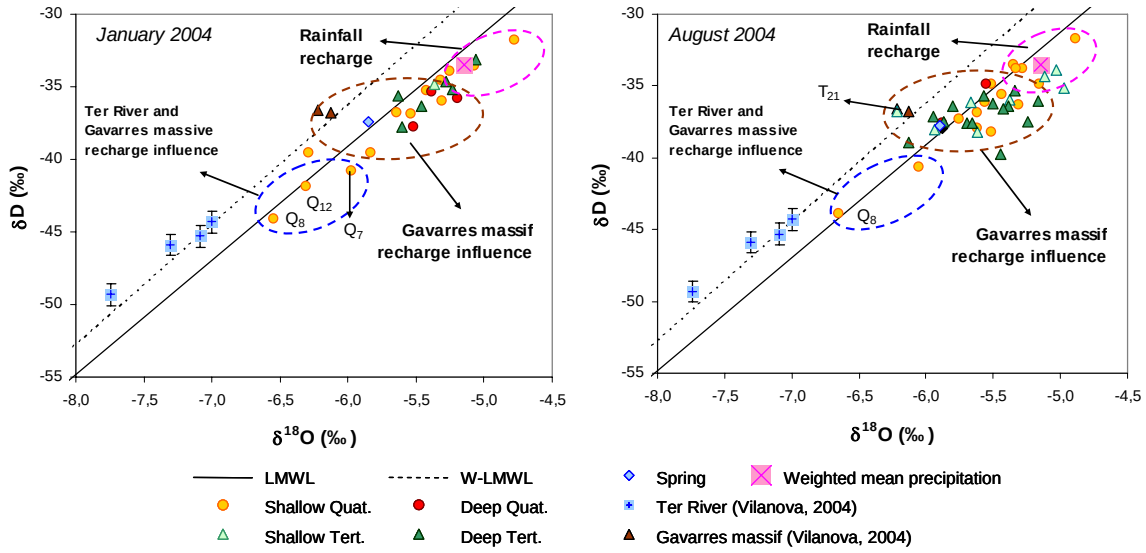

Figure 2. $\delta^{18}O_{H2O}$ and δD of the Baix Ter groundwater samples collected in January and August 2004. The annual-Local Meteoric Water Line (LMWL) follows the equation $\delta D = 7.9\ \delta^{18}O + 8.0$, whose slope is equal to that of the neighboring range areas ($\delta D = 7.9\ \delta^{18}O + 9.8$; Neal et al., 1992). The Winter-Local Meteoric Water Line (W-LMWL) ($\delta D = 8.3\ \delta^{18}O + 13.4$) minimizing potential evaporation effects is also represented as most of the effective surface recharge takes place during winter (Vilanova, 2004).

1) The Ter River

At the NW of the area, three samples in the shallow Quaternary aquifer (Q_7, Q_8 and Q_{12}) yielded lighter isotope signatures (Fig. 2), with values similar to those of the Ter River, which range between -8 and -7‰, for $\delta^{18}O$, and between -50 and -45‰, for δD (Vilanova et al., 2008). These $\delta^{18}O$ and δD from the Ter River waters are the lightest in the area since the Ter River originates at a higher recharge altitude (Ulldeter, Pyrenees, 2400 m.a.s.l.). Thereby, a contribution from the Ter River to the alluvial aquifer groundwater is possible in the NW part of the study zone.

2) Local rainfall

Other shallow Quaternary groundwater samples fell near the isotope signature of the weighted mean precipitation (Fig. 2), indicating they are clearly influenced by the infiltration of rainfall in the basin. All these samples presented NO_3 concentrations higher than 50 mg NO_3^- L^{-1}.

3) The Gavarres massif

Sample T_{21} is located in the south part of the study area, in the Gavarres massif foothill. It corresponds to a very low mineralized groundwater that shows a low NO_3 concentration (6 mg NO_3^- L^{-1}) and isotope compositions similar to groundwater from Paleozoic materials in the Gavarres massif (Vilanova, 2004). Thus, T_{21} sample can be geochemically and isotopically considered as a natural end-member linked to the recharge from the Gavarres massif.

The contributions of these sources of recharge change during the hydrological cycle depending on rainfall events and the effect of groundwater withdrawal regimes. The remaining Quaternary groundwater samples plot between the samples more influenced by rainfall in the basin and those influenced by the Ter River, showing a groundwater isotope composition similar to the Tertiary groundwaters. This overlap between the isotope compositions of the Quaternary and Tertiary groundwater suggests that both aquifers share a common source of recharge or are somehow connected. This is consistent with the conceptual model described by Vilanova and Mas-Pla (2004), who hypothesized an upward groundwater flow from the Tertiary aquifer to the deep Quaternary aquifer in the northern part of the area. Therefore, this contribution from the Tertiary units should be considered as another recharge of the Quaternary aquifer. On

the other hand, most of the samples from shallow and deep Tertiary aquifers fell between the weighted mean precipitation signature and the isotope compositions of groundwaters collected at the Gavarres massif (Vilanova, 2004), indicating that this massif is a source of recharge for the Tertiary unit, in addition to local rainfall. The $\delta^{18}O$ variability displayed by deep Tertiary aquifer samples is likely a consequence of evaporation processes occurring in the non-saturated zone.

4.3. Hydrochemistry

Chemical data for groundwater samples collected in the Baix Ter basin (Table 3) showed a HCO_3^--Ca facies, in accordance with a hydrochemistry controlled by carbonate dissolution reactions that occur throughout the Tertiary materials and alluvial formations. The rapid kinetic of carbonate dissolution hides the hydrochemical characteristics acquired from the igneous and metamorphic rocks of the Gavarres massif (Vilanova et al., 2008). Groundwater pH values were all above 7.4 and EC varied from 552 $\mu S\ cm^{-1}$ (for the most pristine groundwater) to 2993 $\mu S\ cm^{-1}$ (for the most polluted). NO_3^- concentrations presented a wide range of values in both aquifers, from samples with no NO_3 to concentrations up to 480 mg L^{-1}, with an average value of 109 mg L^{-1} (n = 64). 60% of the studied samples had NO_3 levels above the legal threshold of 50 mg L^{-1} for drinking water. No NO_2^- was detected. Groundwater SO_4 varied between 29 and 371 mg L^{-1}, with an average value of 108 mg L^{-1} (n = 64). The monthly NO_3 average for the Ter River was 15 mg NO_3 L^{-1} (σ = 5.1, n = 37) in the NW of the study zone (Colomers) between 2003 and 2006 (from Water Catalan Agency data). In our study, the NO_3 concentrations of two river samples, collected at the Colomers station and at a sampling site located downwards, presented values of 8.8 and 7.0 mg NO_3^- L^{-1}, respectively.

Table 2. Hydrogeological formation, depth (m), hydraulic head (m.a.s.l.), and physico-chemical parameters measured in situ of the sampled points for each field campaign. See Fig. 1 for sampling locations in the Baix Ter basin.

Sample	*Field campaign*	*Hydrogeological formation*	*Depth (m)*	*Hydraulic head (m.a.s.l.)*	*T (ºC)*	*EC (25 ºC) (mS/cm)*	*pH*	*Eh (mV)*
Q_1	1	Q_D	28	13.1	14.0	787	7.9	89
Q_2	1	Q_D	46	-1.4	14.4	596	8.0	46
Q_3	1	Q_D	72	16.9	16.7	955	7.7	397
Q_2	2	Q_D	46	-3.0	18.3	812	7.8	188
Q_3	2	Q_D	72	15.6	18.2	1225	7.7	393
Q_4	1	Q_S	7	10.8	15.0	1594	7.4	276

Table 2. (continued)

Sample	*Field campaign*	*Hydrogeological formation*	*Depth (m)*	*Hydraulic head (m.a.s.l.)*	*T (ºC)*	*EC (25 ºC) (mS/cm)*	*pH*	*Eh (mV)*
Q_5	1	Q_S	10	27.4	16.0	1640	7.6	376
Q_6	1	Q_S	10	22.4	14.6	899	7.6	332
Q_7	1	Q_S	21	13.4	17.0	843	7.7	368
Q_8	1	Q_S	20	10.9	16.9	862	7.9	366
Q_9	1	Q_S	10	12.6	14.0	772	7.9	267
Q_{10}	1	Q_S	8	60.3	16.3	1180	7.7	425
Q_{11}	1	Q_S	6	32.0	13.3	722	8.2	361
Q_{12}	1	Q_S	20	12.3	16.1	773	7.9	340
Q_{13}	1	Q_S	16	13.1	14.9	836	7.8	449
Q_{14}	1	Q_S	6	37.7	13.2	886	8.2	378
Q_{15}	1	Q_S	6	5.2	15.3	2523	7.6	409
Q_{16}	1	Q_S	6	36.4	14.7	1004	7.8	392
Q_5	2	Q_S	10	24.8	16.8	2359	7.6	386
Q_6	2	Q_S	10	*n.d.*	17.3	1125	7.8	318
Q_7	2	Q_S	21	10.2	17.1	1164	7.5	413
Q_8	2	Q_S	20	10.7	17.7	1383	7.8	332
Q_9	2	Q_S	10	*n.d.*	16.2	1070	7.7	395
Q_{10}	2	Q_S	8	60.4	16.2	1320	7.4	428
Q_{13}	2	Q_S	16	8.7	16.2	1219	7.4	395
Q_{14}	2	Q_S	12	36.1	17.6	949	7.5	365
Q_{15}	2	Q_S	6	3.8	17.3	2993	8.0	388
Q_{16}	2	Q_S	6	35.7	22.9	1007	7.8	443
Q_{17}	2	Q_S	*n.d.*	29.5	17.6	809	7.9	386
Q_{18}	2	Q_S	6	14.2	17.9	875	7.7	408
Q_{19}	2	Q_S	12	32.8	16.4	999	7.6	348
Q_{20}	2	Q_S	17	19.0	15.8	661	7.8	727
Q_{21}	2	Q_S	17	15.0	16.2	980	7.5	445
S	1	spring	0	55.0	15.0	629	7.7	319
S	2	spring	0	55.0	15.4	748	7.9	334
T_1	1	T_D	90	21.6	19.5	552	8.0	348
T_2	1	T_D	100	7.2	14.9	908	8.0	369
T_3	1	T_D	100	27.7	17.5	1176	7.8	378
T_4	1	T_D	110	27.4	16.6	725	8.1	*n.d.*
T_5	1	T_D	125	27.1	16.5	1325	7.8	343
T_6	1	T_D	110	-4.5	18.5	736	7.8	362
T_1	2	T_D	90	21.6	20.0	935	7.7	366
T_2	2	T_D	100	11.4	19.8	1095	7.7	426
T_3	2	T_D	100	22.1	17.2	1500	7.7	370
T_5	2	T_D	125	24.4	19.1	1330	7.9	301
T_6	2	T_D	110	-4.5	19.0	600	8.2	326
T_7	2	T_D	70	42.0	21.2	1164	7.7	425
T_8	2	T_D	156	*n.d.*	18.1	1374	8.0	357
T_9	2	T_D	85	53.9	18.4	971	7.9	157
T_{10}	2	T_D	125	*n.d.*	20.7	1053	7.9	183
T_{11}	2	T_D	130	23.8	19.4	824	8.0	916

Table 2. (continued)

Sample	*Field campaign*	*Hydrogeological formation*	*Depth (m)*	*Hydraulic head (m.a.s.l.)*	*T (ºC)*	*EC (25 ºC) (mS/cm)*	*pH*	*Eh (mV)*
T_{12}	2	T_D	110	*n.d.*	19.3	994	7.8	456
T_{13}	2	T_D	175	*n.d.*	17.1	1137	7.6	393
T_{14}	2	T_D	60	19.3	17.0	1449	7.6	159
T_{15}	2	T_D	80	*n.d.*	19.1	1389	7.8	331
T_{16}	1	T_S	22	-6.5	16.1	1006	7.9	363
T_{16}	2	T_S	22	-5.8	16.8	1219	7.5	408
T_{17}	2	T_S	40	23.7	19.2	2414	7.6	321
T_{18}	2	T_S	34	126.0	18.0	837	8.0	357
T_{19}	2	T_S	10	106.3	17.8	944	8.0	352
T_{20}	2	T_S	9	9.0	17.7	1528	7.7	357
T_{21}	2	T_S	5	102.5	22.2	649	7.7	385
T_{22}	2	T_S	*n.d.*	*n.d.*	17.9	1055	7.6	327
T_{23}	2	T_S	40	35.0	17.5	1438	7.5	372
R_1	-	Ter River	-	-	*n.d.*	636	7.8	*n.d.*
R_2	-	Ter River	-	-	*n.d.*	664	7.8	*n.d.*

Table 3. Hydrochemical data of the January and August 2004 field campaigns ("*" = DOC concentrations instead of TOC concentrations).

Sample	*Field campaign*	*Hydrogeological formation*	HCO_3^-	SO_4^{2-}	Cl^-	NO_3^-	Na^+	K^+	Ca^{2+}	Mg^{2+}	NH_4^+	*TOC*	*Mn*	*Fe*	*B*
			(mg/L)												
Q_1	1	Q_D	413	66	138	*b.d.l.*	43	*b.d.l.*	157	23	0.15	1.2	0.056	0.015	*b.d.l.*
Q_2	1	Q_D	349	48	51	*b.d.l.*	44	3	90	19	0.47	1.0	0.289	0.020	*b.d.l.*
Q_3	1	Q_D	361	117	79	115	37	*b.d.l.*	181	18	0.15	1.2	0.002	0.010	*b.d.l.*
Q_2	2	Q_D	341	41	61	*b.d.l.*	45	3	99	19	0.41	0.6	0.335	0.016	*b.d.l.*
Q_3	2	Q_D	335	129	79	144	36	*b.d.l.*	184	17	0.14	0.9	0.002	*b.d.l.*	*b.d.l.*
Q_4	1	Q_S	473	227	269	6	92	4	239	40	0.25	2.3	4.380	0.019	0.127
Q_5	1	Q_S	463	223	200	215	88	*b.d.l.*	291	28	0.13	2.1	0.002	0.019	*b.d.l.*
Q_6	1	Q_S	388	71	62	88	31	2	153	18	0.15	1.6	0.003	0.015	*b.d.l.*
Q_7	1	Q_S	353	111	76	48	30	*b.d.l.*	159	22	0.13	1.0	0.001	0.013	*b.d.l.*
Q_8	1	Q_S	347	136	99	13	60	3	128	25	0.12	1.4	0.783	0.016	*b.d.l.*
Q_9	1	Q_S	372	86	84	25	63	4	122	17	0.16	1.2	0.002	0.012	0.217
Q_{10}	1	Q_S	384	114	60	325	41	*b.d.l.*	245	15	0.18	1.3	0.001	0.014	0.113
Q_{11}	1	Q_S	253	60	52	31	31	3	94	13	0.17	3.3	0.003	0.018	*b.d.l.*
Q_{12}	1	Q_S	324	134	81	12	43	2	141	20	0.18	1.1	0.001	0.011	0.055
Q_{13}	1	Q_S	401	89	106	51	44	*b.d.l.*	167	20	0.15	1.9	0.001	0.017	0.089
Q_{14}	1	Q_S	210	77	52	147	29	*b.d.l.*	128	12	0.15	1.7	0.002	*b.d.l.*	*b.d.l.*
Q_{15}	1	Q_S	427	277	294	387	94	72	283	76	0.14	3.2	0.001	0.011	0.168
Q_{16}	1	Q_S	351	124	76	168	57	*b.d.l.*	183	19	0.17	1.9	0.001	*b.d.l.*	*b.d.l.*
Q_5	2	Q_S	483	321	226	328	123	*b.d.l.*	331	30	0.14	1.6	0.001	*b.d.l.*	*b.d.l.*
Q_6	2	Q_S	366	88	59	129	28	2	165	18	0.16	0.6	0.006	*b.d.l.*	*b.d.l.*

Table 3 (continued)

Sample	Field campaign	Hydrogeological formation	HCO_3^-	SO_4^{2-}	Cl^-	NO_3^-	Na^+	K^+	Ca^{2+}	Mg^{2+}	NH_4^+	TOC	Mn	Fe	B
			(mg/L)												
Q_7	2	Q_S	399	112	79	122	30	*b.d.l.*	201	26	0.11	0.5	0.001	0.011	*b.d.l.*
Q_8	2	Q_S	337	204	139	51	71	3	174	31	0.08	1.1	0.971	*b.d.l.*	*b.d.l.*
Q_9	2	Q_S	358	86	84	26	58	4	130	17	0.11	0.6	0.002	*b.d.l.*	0.209
Q_{10}	2	Q_S	440	76	50	241	45	*b.d.l.*	225	13	0.12	0.9	0.002	0.012	0.189
Q_{13}	2	Q_S	405	120	86	66	44	2	178	21	0.08	1.2	0.001	*b.d.l.*	0.123
Q_{14}	2	Q_S	195	66	55	201	29	*b.d.l.*	140	13	0.08	0.5	0.002	0.011	*b.d.l.*
Q_{15}	2	Q_S	413	371	362	480	111	68	345	85	0.14	3.4	0.001	*b.d.l.*	0.150
Q_{16}	2	Q_S	356	93	55	65	47	*b.d.l.*	143	14	0.14	0.6	0.001	*b.d.l.*	*b.d.l.*
Q_{17}	2	Q_S	301	29	28	60	18	*b.d.l.*	116	12	0.13	0.4	0.001	*b.d.l.*	*b.d.l.*
Q_{18}	2	Q_S	390	102	47	83	38	6	163	14	0.13	0.6	0.001	*b.d.l.*	*b.d.l.*
Q_{19}	2	Q_S	304	55	52	205	24	*b.d.l.*	166	14	0.15	0.7	0.001	0.022	*b.d.l.*
Q_{20}	2	Q_S	177	52	52	50	29	5	83	11	0.12	0.9	0.001	0.012	0.082
Q_{21}	2	Q_S	313	95	71	45	55	4	124	16	0.21	0.6	0.002	0.011	0.232
S	1	spring	298	64	47	37	29	*b.d.l.*	110	12	0.18	1.4	0.001	0.011	*b.d.l.*
S	2	spring	268	58	50	68	31	*b.d.l.*	117	13	0.15	1.0	0.001	0.013	*b.d.l.*
T_1	1	T_D	417	68	43	10	42	3	131	13	0.13	0.8	0.001	0.012	*b.d.l.*
T_2	1	T_D	470	156	87	9	51	3	129	54	0.13	1.3	0.018	0.019	*b.d.l.*
T_3	1	T_D	276	116	123	222	55	*b.d.l.*	185	22	0.15	1.9	0.001	0.014	*b.d.l.*
T_4	1	T_D	383	110	60	15	33	49	118	24	0.16	1.2	0.025	0.016	0.071
T_5	1	T_D	430	152	119	222	105	12	178	36	0.20	2.8	0.007	0.012	0.066
T_6	1	T_D	382	59	76	46	57	3	118	20	0.14	1.2	0.007	0.014	*b.d.l.*
T_1	2	T_D	402	55	41	23	35	3	136	12	0.16	0.4	0.001	*b.d.l.*	*b.d.l.*
T_2	2	T_D	435	157	74	11	44	3	127	51	0.12	0.7	0.026	*b.d.l.*	0.081
T_3	2	T_D	376	91	180	221	68	4	214	30	0.12	1.7	0.001	*b.d.l.*	0.065
T_5	2	T_D	514	118	99	61	162	11	94	23	0.18	0.6	0.010	*b.d.l.*	0.104
T_6	2	T_D	354	34	70	3	54	3	100	18	0.14	0.3	0.007	*b.d.l.*	0.051
T_7	2	T_D	368	83	66	139	32	*b.d.l.*	183	14	0.14	0.9	0.001	*b.d.l.*	*b.d.l.*
T_8	2	T_D	222	107	135	265	58	9	181	24	0.12	1.1	0.007	0.016	*b.d.l.*
T_9	2	T_D	384	31	118	*b.d.l.*	75	5	81	39	0.16	0.9	0.197	0.013	0.055
T_{10}	2	T_D	533	74	52	*b.d.l.*	63	2	168	16	0.10	0.4	0.064	0.013	0.053
T_{11}	2	T_D	323	32	46	69	41	3	106	16	0.11	0.8	0.001	0.013	*b.d.l.*
T_{12}	2	T_D	379	52	62	71	33	3	104	45	0.12	0.4	0.002	0.013	*b.d.l.*
T_{13}	2	T_D	392	86	96	46	55	2	146	28	0.12	0.7	0.001	0.010	0.051
T_{14}	2	T_D	619	87	126	*b.d.l.*	74	4	102	94	0.33	0.5	0.042	0.016	0.061
T_{15}	2	T_D	401	95	130	152	114	3	110	42	0.21	1.2	0.002	0.014	0.095
T_{16}	1	T_S	388	149	93	63	55	2	162	37	0.12	1.4	0.002	0.014	*b.d.l.*
T_{16}	2	T_S	371	146	102	71	49	*b.d.l.*	169	32	0.23	0.9	0.002	0.012	*b.d.l.*
T_{17}	2	T_S	372	245	231	419	122	59	223	70	0.11	2.6	0.003	*b.d.l.*	0.084
T_{18}	2	T_S	249	30	31	147	15	*b.d.l.*	121	19	0.14	0.6	0.001	*b.d.l.*	*b.d.l.*
T_{19}	2	T_S	348	56	39	89	33	7	137	13	0.14	1.2	0.003	*b.d.l.*	*b.d.l.*

Table 3 (continued)

Sample	Field campaign	Hydrogeological formation	HCO_3^-	SO_4^{2-}	Cl^-	NO_3^-	Na^+	K^+	Ca^{2+}	Mg^{2+}	NH_4^+	TOC	Mn	Fe	B
			(mg/L)												
T_{20}	2	T_S	350	210	108	212	56	6	200	38	0.17	2.2	0.001	*b.d.l.*	0.123
T_{21}	2	T_S	300	30	36	6	22	*b.d.l.*	104	9	0.14	1.0	0.002	0.012	*b.d.l.*
T_{22}	2	T_S	371	81	49	153	29	*b.d.l.*	193	8	0.16	1.1	0.002	0.012	*b.d.l.*
T_{23}	2	T_S	355	66	181	190	75	*b.d.l.*	216	24	0.26	0.7	0.004	0.010	*b.d.l.*
R_1	-	Ter River	194	73	50	7	38	5	75	11	*n.d.*	4,3*	0.029	0.010	0.075
R_2	-	Ter River	204	74	50	9	40	5	78	12	*n.d.*	4,5*	0.025	0.012	0.090

A spatially complex distribution following a diffuse regional pattern was observed for groundwater NO_3. The average NO_3 of Q_S and T_S aquifers is 136 mg L^{-1} (n = 37), and 74 mg L^{-1} (n = 25) for Q_D and T_D aquifers. While the highest NO_3 concentrations occurred in shallow wells, several wells with depths above 70 m (T_3, T_5, T_7, T_8, and T_{15}) were also notably contaminated, with NO_3 levels between 139 and 265 mg L^{-1}, denoting that NO_3 is not correlating with well depth. Furthermore, the spatial variation of NO_3 concentrations did not fit with any specific groundwater flow direction or limit of the aquifer units. This NO_3 distribution pattern may be explained by the highly complex hydrogeology of the study zone and by the mixing of waters from distinct origins and qualities within the well borehole. This latter process can be caused by: 1) the intended exploitation of several levels to increase the well efficiency, 2) the possible lack of well casing derived from an incomplete borehole construction, and 3) the presence of preferential flow paths through fractures or fault zones that connect local and regional flow systems, i.e. Quaternary and Tertiary aquifers. Where these conditions take place, simultaneously or not, groundwater mixing of deep and superficial layers is induced. Moreover, the intensive pumping during irrigation and low rainfall periods can also enhance this re-circulation between aquifer levels, mainly from shallow to deeper ones, resulting in inputs of low quality water and quality declining of water resources stored in the deeper aquifer layers.

The lowest NO_3 contents in the Quaternary aquifer were observed near the Ter River. In the Tertiary aquifer the lowest NO_3 values were measured in the SE area, near the Gavarres Range. In the first sampling campaign, Q_4 and Q_8 samples, collected in the shallow alluvial formation near the Ter River, presented NO_3 concentrations of 6 mg L^{-1} and 13 mg L^{-1}, respectively, as well as high levels of Mn (4.4 and 0.8 mg Mn L^{-1}) and around 2 mg L^{-1} of total organic carbon. Five samples in the Q_D (Q_1 and Q_2) and T_D

aquifers (T_9, T_{10} and T_{14}) contain no NO_3, have an Eh below 200 mV and show the highest ammonium and manganese concentrations (Fig. 3, Tables 2 and 3). These characteristics are typical of groundwater under reducing conditions, which would agree with the occurrence of denitrification processes. NO_3 in Q_2 has been monitored through time and no NO_3 content has ever been detected. In our study, its ammonium content displayed the highest value (0.5 mg NH_4 L^{-1}). TOC concentrations for these unpolluted samples ranged between 0.4 and 1.2 mg L^{-1}, values that are not high enough to stoichiometrically allow the reduction of NO_3 by oxidation of organic matter in anaerobic conditions (Rivett et al., 2008), but indicate the presence of an organic matter that could be a residual content after previous consumption by heterotrophic denitrifying bacteria.

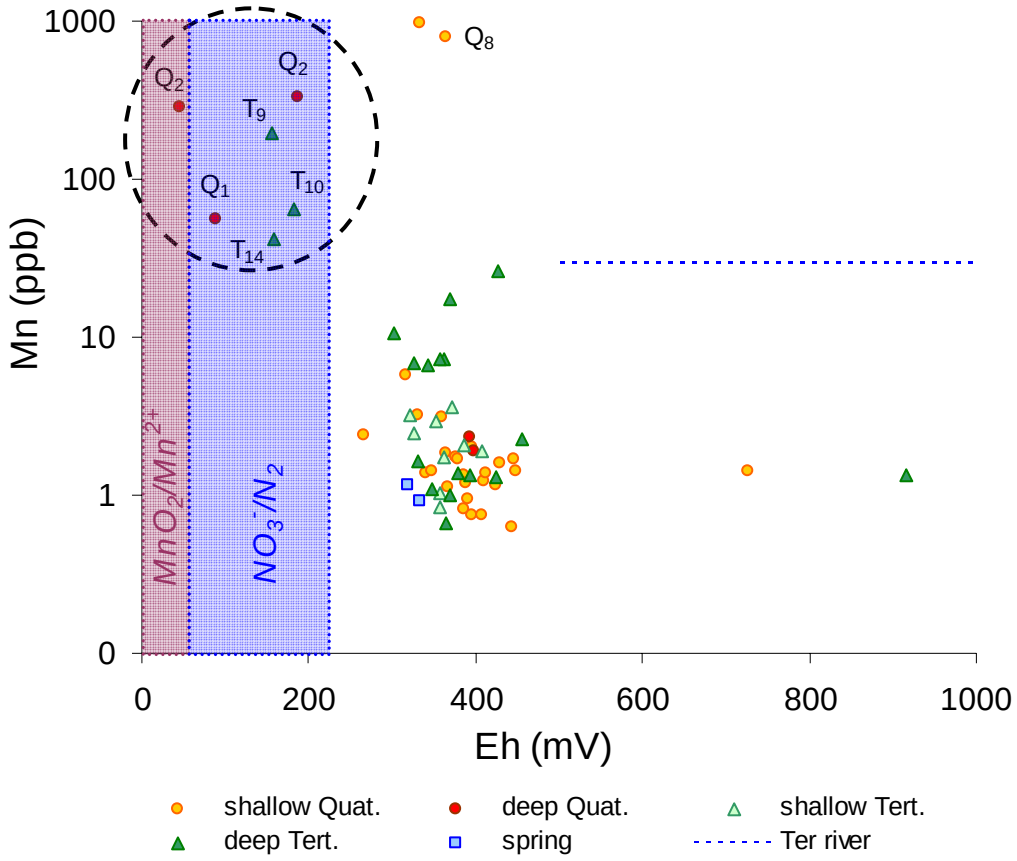

Figure 3. Mn concentrations plotted against Eh values of groundwater samples. Eh ranges of MnO_2/Mn^{2+} and $NO_3^-/N_{2(g)}$ redox pairs are taken from Rivett et al. (2008).

Samples with high NO_3 concentrations tended to be Cl-SO_4-Ca type waters, in agreement with a contribution of anthropogenic contaminant sources (manure, synthetic fertilizers or sewage). Since no evaporitic or gypsum outcrops nor disseminate pyrite

exist in the studied area, the highest SO_4 concentrations must originate from anthropogenic sources. Accordingly, although NO_3 and SO_4 are not strongly correlated (Fig. 4b), some wells that showed high SO_4 contents coupled with elevated NO_3 concentrations (Q_5, Q_{10}, Q_{15} and Q_{16} from Q_S, T_{17} and T_{20} from T_S, and T_3, T_5 and T_8 from T_D) are likely to be affected by human activities. The same trend is observed in the NO_3 vs. Cl plot (Fig. 4a), with the previously mentioned samples also having high Cl contents, which can be caused by the input of organic fertilizers since they generally show elevated chloride concentrations (Karr et al., 2001). Some samples polluted by NO_3 have high B concentrations up to 232 μg B L^{-1} (e.g. Q_{21} sample, with a corresponding 45 mg NO_3 L^{-1}). This makes sewage another NO_3 and SO_4 potential source. All these observations suggest that mineral and organic fertilizers both are major vectors of contamination. Considering that Cl is a conservative element largely unaffected by physical, chemical and microbiological processes occurring in groundwater (Altman and Parizek, 1995), we used the (NO_3/Cl) ratio in order to eliminate the potential effect of dilution. Groundwater samples with $1<(NO_3/Cl)<2$ presented high NO_3 and SO_4 concentrations, whereas samples with $(NO_3/Cl)>2$ had high NO_3 but lower SO_4 concentrations (Fig. 4c). The presence of B in groundwater was not necessarily linked to high NO_3 concentrations; e.g. some samples with $(NO_3/Cl)<1$ showed high B contents (Fig. 4d).

Our results show that groundwater is affected by more than one source of contamination, but an unambiguous identification of these sources based on the sole hydrochemical data is somewhat difficult, as the signal may be hindered by the mixing of groundwaters from different layers and flow systems.

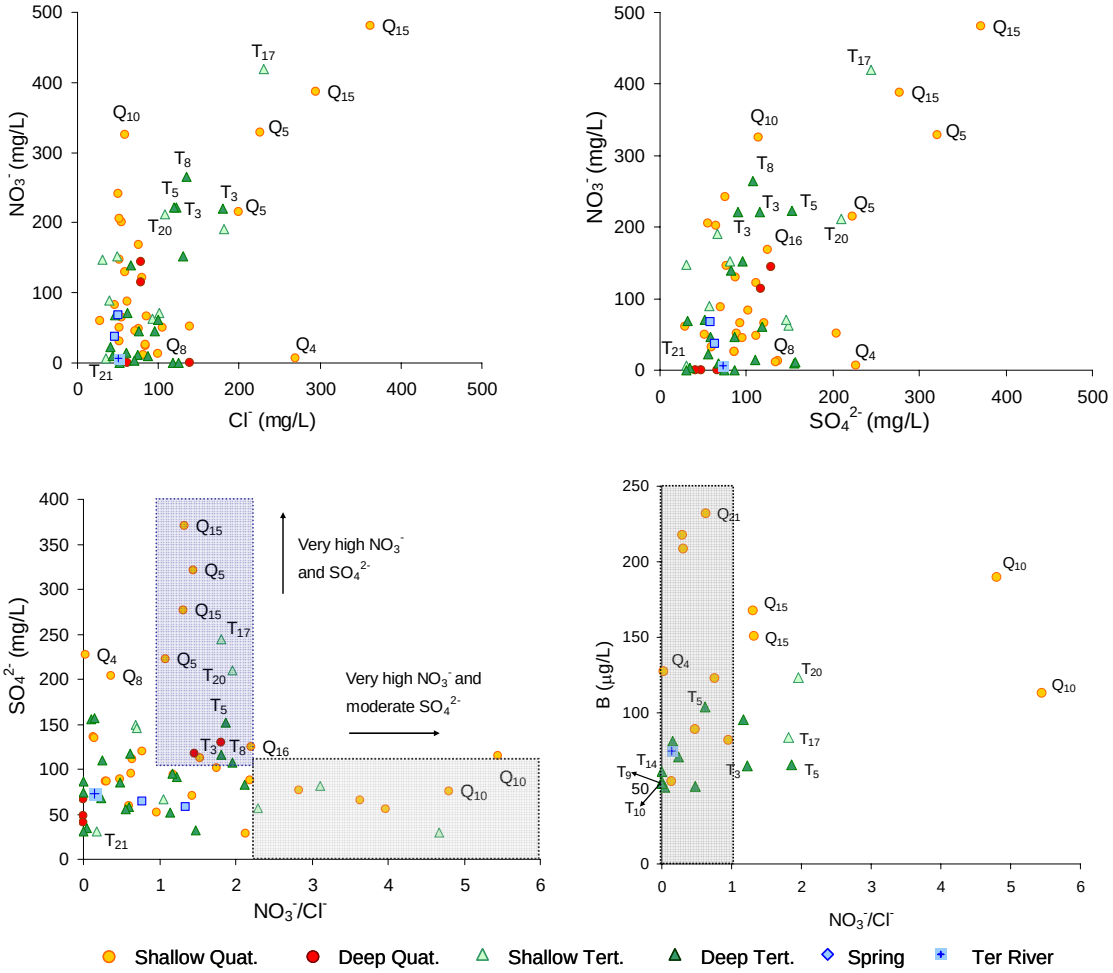

Figure 4. a) NO_3^- concentration versus Cl^- concentration, b) NO_3^- concentration versus SO_4^{2-} concentration, c) SO_4^{2-} concentration versus (NO_3^-/Cl^-) ratio, and d) B concentration versus (NO_3^-/Cl^-) ratio.

4.4. Isotope identification of the sources of contamination

4.4.1. $\delta^{15}N$ and $\delta^{18}O$ of NO_3

NO_3 isotope composition in groundwater ranged between +5.0 and +32.5‰ for $\delta^{15}N$, with an average value of +13.0‰ (n = 58), and between +1.8 and +18.1‰ for $\delta^{18}O$, with an average value of +7.1‰ (n = 58) (Table 4). Since NO_2^- concentrations were below detection limit (0.1 mg L^{-1}) fractionation caused by incomplete nitrification is not affecting our $\delta^{15}N$ values. The range of $\delta^{18}O$ of NO_3 coming from the oxidation of ammonium in the unsaturated zone (ammonium from synthetic fertilizers, soil nitrogen or manure) was estimated according to the experimental expression: $\delta^{18}O_{NO3} = 2/3(\delta^{18}O_{H2O}) + 1/3(\delta^{18}O_{O2})$ (Anderson and Hooper, 1983; Hollocher, 1984; Kendall et al., 2007), where the $\delta^{18}O_{H2O}$ values are the highest and lowest groundwater $\delta^{18}O$

measured in the Baix Ter basin, and the $\delta^{18}O_{O2}$ is that of the atmospheric O_2 (+23.5‰; Horibe et al., 1973).

Five groundwater samples (Q_{14} and Q_{16} from Q_S, T_3 from T_D, and T_{18} and T_{21} from T_S) presented $\delta^{15}N$ values comparable to soil organic nitrogen (from +3 to +8‰) (Fig. 5a), but the origin of the NO_3 for these samples cannot be mainly attributed to this source, because, except for sample T_{21}, their NO_3 contents (from 65 to 222 mg NO_3^- L^{-1}) were too high for having only been produced by mineralization of soil nitrogen. Therefore, though a small contribution of soil organic nitrogen is possible (Wassenaar, 1995), other sources of NO_3 must be considered to explain Q_{14}, Q_{16}, T_3 and T_{18} samples, like e.g. synthetic ammonium fertilizers, whose $\delta^{15}N$ (around 0‰) is enriched in ^{15}N by volatilization processes and can then reach values in the range of soil nitrogen (Vitòria, 2004). Then, since reaction kinetics is rapid and leads to a complete oxidation of ammonium to NO_3 in the presence of oxygen, the NO_3 produced after nitrification has the same $\delta^{15}N$ value than the former ammonium molecule affected by volatilization. On the other hand, sample T_{21} was lowly mineralized (6 mg L^{-1} of NO_3, 36 mg L^{-1} of Cl and 30 mg L^{-1} of SO_4), had the lowest $\delta^{15}N$ (+5.0‰) and showed δD and $\delta^{18}O$ similar to those of the Gavarres massif (Fig. 2). Our results show that sample T_{21} derives from soil nitrogen, and could thus be assumed to represent the local NO_3 background.

When comparing $\delta^{15}N$ of dissolved NO_3 in our groundwater samples to those of potential sources of contamination (Fig. 5a), results show that most of the $\delta^{15}N$ ranged between +8 and +16‰, indicating that NO_3 has probably a pig manure and/or wastewater ammonium origin. While, for most of them, corresponding $\delta^{18}O$ comfort this conclusion, some samples show significant ^{18}O enrichment. It is thus difficult to discriminate between manure and sewage ammonium based only on NO_3 stable isotopes and hydrochemical data. In order to alleviate this difficulty, $\delta^{11}B$ was measured for representative groundwater samples (section 4.4.3.). $\delta^{15}N$ values higher than +16‰ observed in eleven samples suggest either the occurrence of ammonium volatilization or the reduction of NO_3 in groundwater yielding to N_2 gas (Kendall, 2007). Four of these samples with $\delta^{15}N > +16$‰ (Q_5 and Q_{15} from Q_S, and T_{17} and T_{23} from T_S) can be the result of volatilization because they showed high NO_3 concentrations (between 190 and 480 mg L^{-1}) and $\delta^{18}O_{NO3}$ values up to +6‰. In exchange, five other samples with also $\delta^{15}N > +16$‰ (Q_4, Q_8 and Q_9, from Q_S, and T_2 from T_D) are more likely to be affected

by denitrification since their NO_3 contents were low (between 6 and 26 mg L^{-1}) and the $\delta^{18}O_{NO3}$ higher than +10‰.

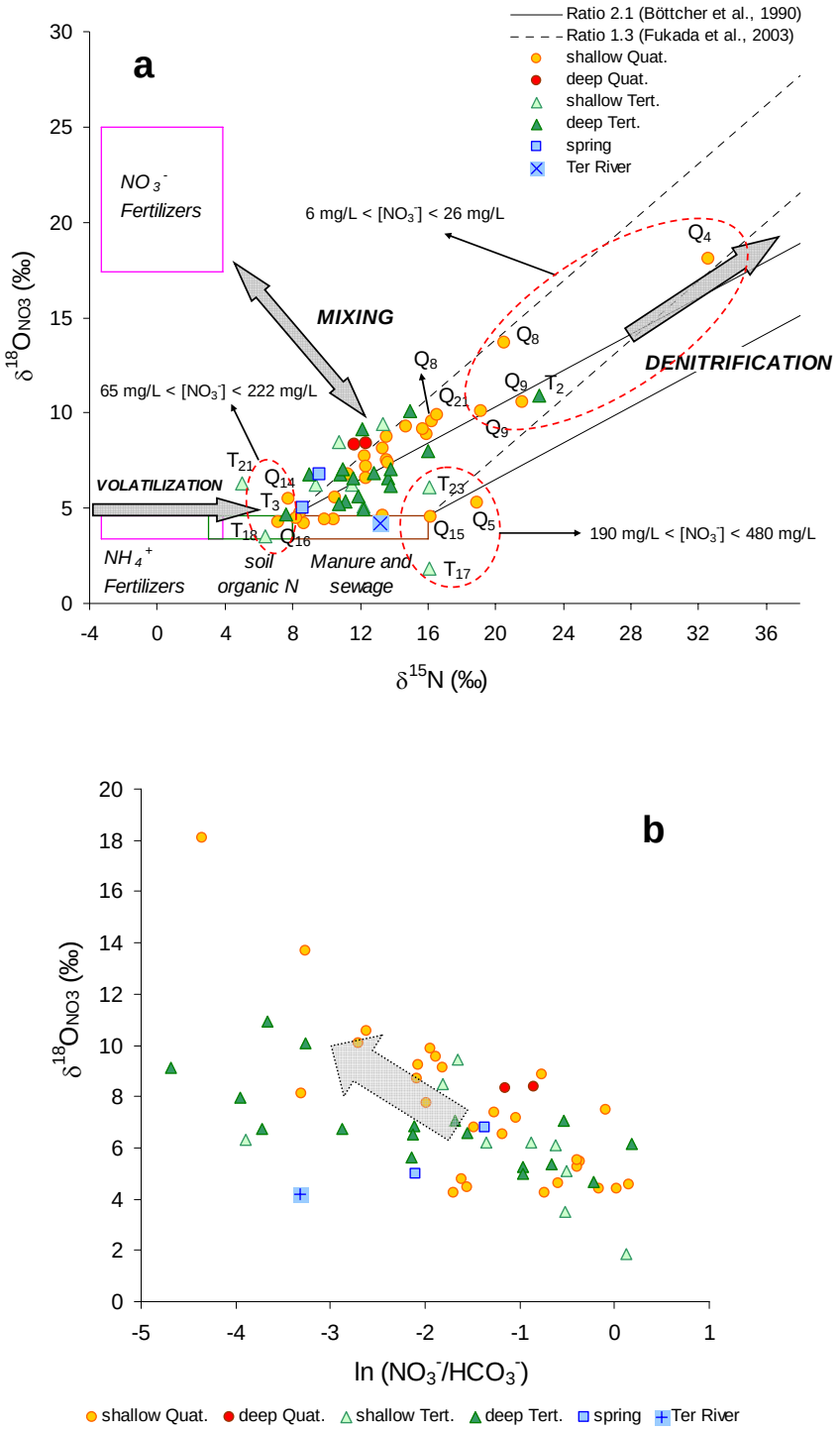

Figure 5. a) Variations of the $\delta^{15}N$ and $\delta^{18}O$ of dissolved NO_3 in groundwater according to their hydrogeological unit. Isotope ranges of the main NO_3 sources from the literature as well as local sources (Vitòria, 2004; Vitòria et al., 2004b, 2008) are also represented. The extreme isotopic fractionation ratios from the literature are $\varepsilon_N/\varepsilon_O$ = 2.1 (Böttcher et al., 1990) and $\varepsilon_N/\varepsilon_O$ = 1.3 (Fukada et al., 2003). $\delta^{18}O$ of NO_3 deriving from nitrification of fertilizers and manure NH_4 were calculated following the experimental expression: $\delta^{18}O_{NO3} = 2/3(\delta^{18}O_{H2O}) + 1/3(\delta^{18}O_{O2})$ (Kendall et al., 2007), where the $\delta^{18}O_{H2O}$ is assumed to be that of the Baix Ter basin groundwater and the $\delta^{18}O_{O2}$ that of atmospheric O_2 (+23.5‰; Horibe et al., 1973). b) $\delta^{18}O_{NO3}$ values plotted against ln (NO_3^-/HCO_3^-).

Based on $\delta^{18}O$ from NO_3, the following observations can be made: 1) While NO_3-bearing mineral fertilizers are actually applied onto local crops, fertilizer NO_3 did not show their direct influence in groundwater, and 2) most of the samples had $\delta^{18}O$ higher than the maximum expected value. Both results can be interpreted as a consequence of:

1) The mineralization-immobilization-turnover (MIT) process, which consists on the microbial-mediated immobilization of N-NO_3 as organic nitrogen, the subsequent mineralization of this organic nitrogen to ammonium, and finally the nitrification of this ammonium back to NO_3 (Mengis et al., 2001). This process would result in a depletion of ^{18}O of the initial $\delta^{18}O$ of synthetic fertilizers (~ +20‰) due to the incorporation of two groundwater oxygen atoms during nitrification. If this process was dominant in the Baix Ter basin some groundwater samples would have fallen in the isotope range of synthetic fertilizers. Our results show that MIT is not an active process in our study site.

2) Evaporation or respiration (or unknown isotope effects occurring during nitrification) that produce an enrichment of $^{18}O_{H2O}$. This enrichment is slightly observed in the δD-$\delta^{18}O_{H2O}$ diagram (Fig. 2)

3) A higher consumption of NO_3 from mineral fertilizers than of ammonium in the root zone. The fact that pig manure is mainly liquid and synthetic fertilizers are solid favours faster infiltration of the former through the non-saturated zone. Pig manure ammonium, after a quick and complete nitrification in the non-saturated zone, can easily be leached towards the saturated zone and incorporated as NO_3 into groundwaters. Conversely, N-NO_3 from synthetic fertilizers has more time to be absorbed by plants and, if not, it is incorporated and stored in the soil organic matter pool, and then slowly rereleased for either uptake in crops or export into the hydrosphere (Sebilo et al., 2013).

4) The reduction of NO_3 via denitrifying bacteria, which is characterized by an enrichment of both $\delta^{15}N$ and $\delta^{18}O_{NO3}$. This process is superimposed to the mixing of potential end-members and modifies both the NO_3 concentration (i.e. attenuation) and isotope compositions.

4.4.2. $\delta^{34}S$ and $\delta^{18}O$ of SO_4

SO_4 isotope compositions ranged between -16.0 and +14.7‰ for $\delta^{34}S$, with an average value of +4.5‰ (n = 64), and between +3.8 and +16.1‰ for $\delta^{18}O_{SO4}$, with an average value of +7.2‰ (n = 64). Most of the groundwater samples from the Q_S aquifer unit fall within the area defined by the isotope signatures of local anthropogenic sources, showing that SO_4 in the Baix Ter groundwater can be explained by a ternary mixing between 1) mineral fertilizers, 2) sewage and 3) pig manure (Fig. 6). Moreover, SO_4 and NO_3 concentrations from these samples, as well as the slight correlation between both anions (Fig. 4b), also corroborate contributions from these three sources. Still, some samples having a $\delta^{34}S$ and a $\delta^{18}O_{SO4}$ between 0 and +6‰ (Q_{17}, T_{11}, T_{18} and T_{21}) could also indicate a soil origin (Table 1), in agreement with their low SO_4 concentrations (around 30 mg SO_4^{2-} L^{-1}). But samples with a $\delta^{34}S$ in the range of soil SO_4 and/or pig manure, with corresponding SO_4 concentrations >200 mg L^{-1} (Q_{15}, T_{17} and T_{20}), could be explained by the influence of SO_4 assimilated by the soil and subsequently remineralized (their SO_4 concentrations are too high for coming from a pig manure contribution; Otero, personal communication). Two sampling sites (T_2 and T_{14}) yielded the lowest negative $\delta^{34}S$ and had $\delta^{18}O_{SO4}$ around +5‰, revealing a SO_4 contribution from a ^{34}S-depleted source of reduced S. Moreover, both T_2 and T_{14} showed no to low (9-11 mg L^{-1}) NO_3 concentrations, respectively. Other samples with no NO_3 exhibited the highest $\delta^{34}S$ and $\delta^{18}O_{SO4}$ values. These no-NO_3 samples, along with T_2 and T_{14}, and some other samples with NO_3^- < 25 mg L^{-1} and $\delta^{18}O_{SO4}$ > +8‰, define a linear trend with a slope ($\varepsilon^{34}S/\varepsilon^{18}O_{SO4}$ = 3.3) compatible with bacteriogenic SO_4 reduction (Mizutani and Rafter, 1973) (Fig. 6). $\delta^{34}S$ and $\delta^{18}O_{SO4}$ of the Ter River samples indicated that the dissolved SO_4 in surface waters originated from wastewater, in agreement with their $\delta^{15}N$ and $\delta^{18}O_{NO3}$. This has to be linked with reported occasional episodes of wastewater discharge near the Ter River.

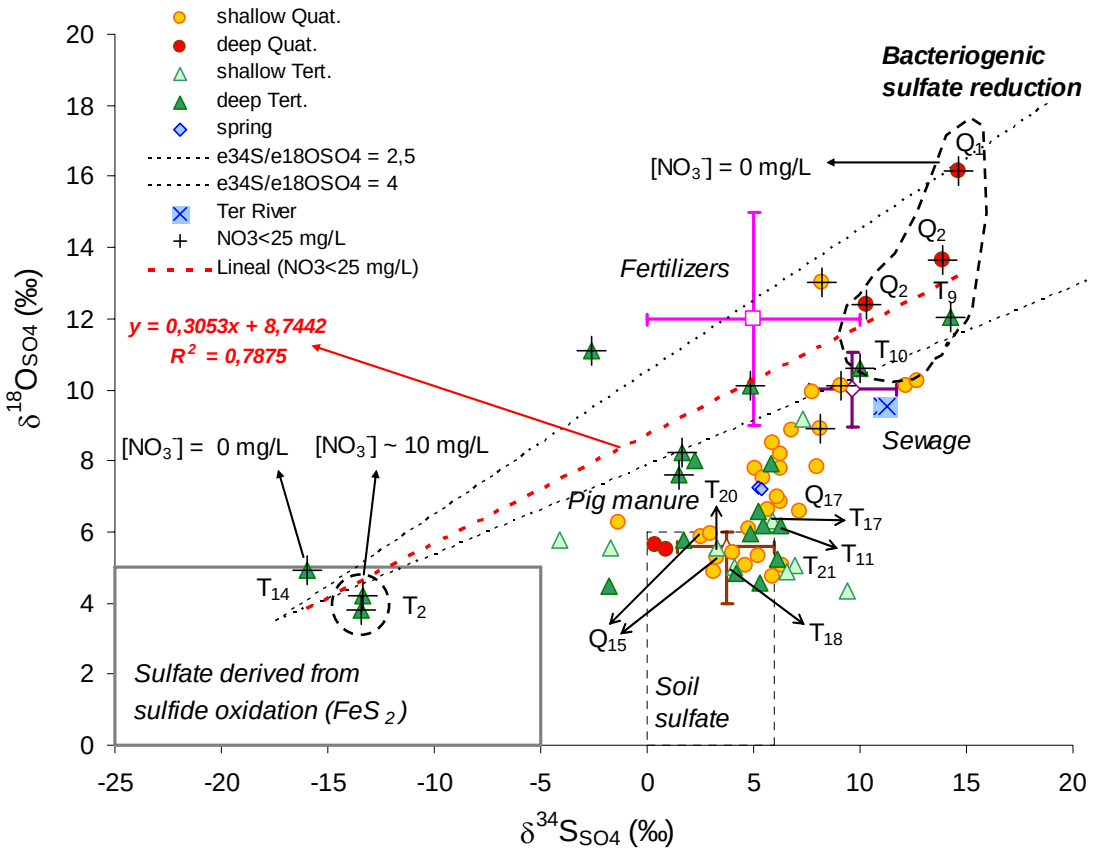

Figure 6. $\delta^{34}S$ and $\delta^{18}O$ of dissolved SO_4 in groundwater according to their hydrogeological unit. Isotope ranges of natural and anthropogenic SO_4 sources and SO_4 reduction are also represented. Values for pig manure are taken from Otero et al. (2007) and Cravotta (1997), soil SO_4 data from Clark and Fritz (1997), and fertilizer data from Vitòria et al. (2004b). Dashed lines define the isotopic fractionation range ($\varepsilon^{34}S/\varepsilon^{18}O_{SO4}$) in SO_4 reduction reactions, which is between 2.5 and 4 (Mizutani and Rafter, 1973).

4.4.3. Boron isotopes

While NO_3 isotopes efficiently discriminate mineral fertilizers from manure, the distinction between manure and sewage becomes impossible due to the overlapping between their respective $\delta^{15}N$ and $\delta^{18}O_{NO3}$ ranges (Curt et al., 2004). Moreover, processes such as volatilization and natural denitrification significantly shift the original isotope compositions of the NO_3 sources involved. However, considering that: 1) NO_3 and B co-migrate in many environmental settings, 2) $\delta^{11}B$ differentiate manure from wastewater, and 3) the fractionation of NO_3 and B isotopes is caused by different processes, the combined use of $\delta^{15}N$, $\delta^{18}O_{NO3}$ and $\delta^{11}B$ may be a useful approach for identifying sources of dissolved NO_3 (Saccon et al., 2013; Seiler, 2005; Widory, 2004, 2005, 2013). We selected 12 groundwater samples taking into account their NO_3 and B contents, and making sure that some of them were in the vicinity of pig farms or urban areas in order to discriminate between these two origins.

The combination of B content with a readily distinguished $\delta^{11}B$ makes B a good tracer for identifying sources of anthropogenic contaminants. Pig manure has low B concentrations (<0.1 mg L^{-1}) and a wide range of positive $\delta^{11}B$ values (Table 1); urban wastewater has higher B concentrations (0.5-1.1 mg L^{-1}) (Vengosh et al., 1994) and lower $\delta^{11}B$ values (Table 1); and mineral fertilizers are characterized by a $\delta^{11}B$ range similar to sewage (Table 1), and although they can present a wide range of B concentrations, usually have lower B contents than pig manure. Baix Ter groundwater $\delta^{11}B$ ranged between +1.4‰ and +34.5‰, with an average value of +24.1‰ (n = 12), and B concentrations ranged between 0.051 and 0.232 mg L^{-1}. If significant B adsorption onto clay minerals had occurred, we would have observed a ^{11}B enrichment with decreasing B content, along with groundwater pH values higher than 8, which was not the case. The $\delta^{11}B$ versus 1/B (Fig. 7a) and $\delta^{11}B$ versus $\delta^{15}N$ (Fig. 7b) diagrams show that most samples fell in the isotope ranges of pig manure, in agreement with the NO_3 and SO_4 isotope data. Only two samples showed $\delta^{11}B$ values consistent with a wastewater origin. They correspond to groundwaters collected in La Bisbal (Q_{20}) and Ullastret (Q_{21}) water supply wells, located downstream the discharge of the La Bisbal water treatment plant into the Daró River. Despite the low number of groundwater samples analyzed, most of them have significantly high $\delta^{11}B$ that can only be explained by a pig manure input, suggesting that the influence of sewage and mineral fertilizers is lesser than the contribution from organic residues.

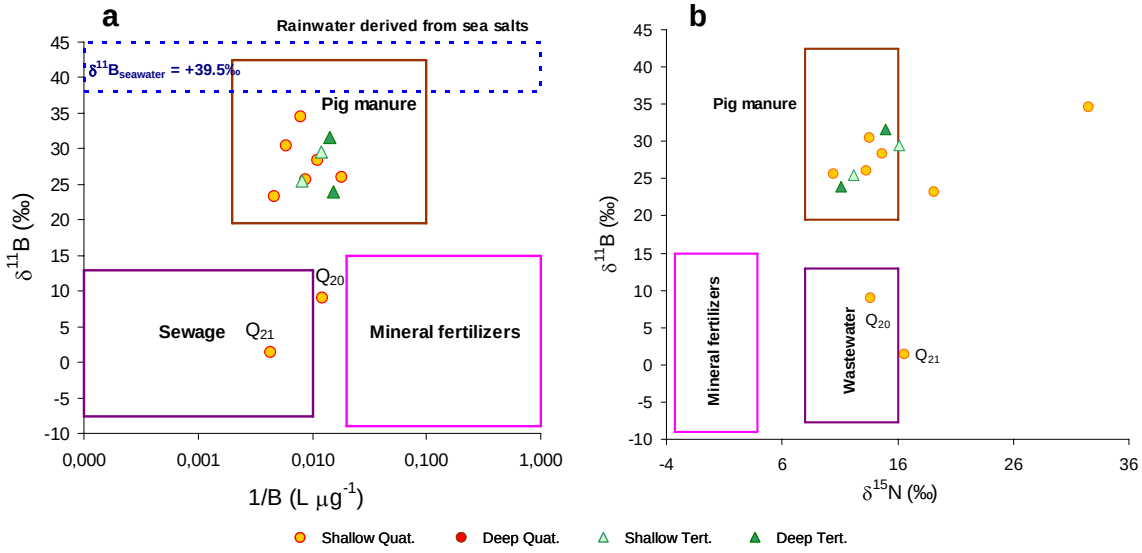

Figure 7. $\delta^{11}B$ values plotted against 1/B (a) and $\delta^{15}N$ values (b).

4.5 Evaluation of natural attenuation

NO_3 in groundwater can be reduced to N_2 via biological denitrification, resulting in a nitrogen loss from aquifers to the atmosphere. The required conditions for natural denitrification include the presence of denitrifying bacteria and electron donors (organic carbon, reduced sulphur and/or reduced iron), an anaerobic environment (dissolved oxygen concentrations below 2 mg L^{-1}), and favorable ranges of temperature (between 0 and 50ºC), pH (between 6.2 and 10.2) and Eh (between -200 and 665 mV) (Rivett et al., 2008). Furthermore, denitrification can occur in anaerobic microsites in an otherwise oxygenated water body (Koba et al., 1997). The denitrification reaction follows a Rayleigh distillation process:

$$\delta^{15}N_{residual} = \delta^{15}N_{initial} + \varepsilon_N \ln ([NO_3^-]_{residual}/[NO_3^-]_{initial})$$
$$\delta^{18}O_{residual} = \delta^{18}O_{initial} + \varepsilon_O \ln ([NO_3^-]_{residual}/[NO_3^-]_{initial})$$

A linear relationship is thus expected when plotting $\delta^{15}N$ or $\delta^{18}O_{NO3}$ against ln ($[NO_3]$) (Böttcher et al., 1990; Fukada et al., 2003; Mariotti et al., 1981), where the slope represents ε, the isotopic fractionation which depends on the aquifer characteristics (Mariotti et al., 1981).

In the Baix Ter groundwaters, some of the highest $\delta^{15}N$ were coupled to elevated $\delta^{18}O_{NO3}$: 10 samples had $\delta^{15}N$ and $\delta^{18}O_{NO3}$ higher than +15‰ and +8‰, respectively. Fig. 5a shows that these samples roughly aligned following a 1:2 slope, consistent with natural denitrification (Kendall, 2007). The highest denitrified samples were observed either in the shallow Quaternary levels near the Ter River or in deep layers of Quaternary and Tertiary aquifers (e.g. Q_4, Q_8, Q_9 and T_2; Fig. 5a). The absence of NO_3 in the samples Q_1, Q_2, T_9, T_{10} and T_{14} is also interpreted as a consequence of the natural attenuation of NO_3.

During the second campaign, 19 samples from the previous campaign were resampled, and among those, 15 wells showed either a significant increase or no significant changes in NO_3 concentration, while 4 samples showed a significant decrease. Among the latter, only two showed shifts in the isotope and chemical compositions in agreement with natural denitrification. This suggests that natural denitrification had a moderate activity and/or that NO_3 attenuation was balanced by the input of new NO_3 into the aquifer.

4.5.1 Biogeochemical processes linked to natural denitrification

The energy required to reduce NO_3^- into N_2 can be released via the oxidation of labile organic carbon or inorganic compounds (electron donors) mediated by microorganisms (Borch et al., 2010). In order to assess how natural attenuation occurs, stable isotopes of the ions involved in the reactions (1) and (2) (SO_4 and HCO_3) were analyzed.

Most of the $\delta^{34}S$ measurements did not present the negative values typical of sedimentary pyrites (Otero et al., 2009), and only two sampling points (T_2 and T_{14}) lied in its isotope range (Fig. 6). This result is consistent with the little presence of sulphides such as pyrites in the study zone. Autotrophic denitrification can be eliminated as the main denitrifying process, although a pair of denitrified samples is explained by this mechanism. $\delta^{13}C_{HCO3}$ values ranged between -6.5‰ and -16.2‰, with an average value of -13.1‰ (n = 64), and HCO_3 concentrations between 177 and 619 mg L^{-1}, with an average value of 367 mg L^{-1} (n = 64). Denitrification catalyzed by organic matter oxidation induces a decrease in $\delta^{13}C_{HCO3}$, and NO_3 and total organic carbon concentrations, along with an increase of $\delta^{15}N$ and $\delta^{18}O_{NO3}$, and dissolved inorganic carbon concentration (reaction 1). We did not observe these trends in our results. This probably has to be linked to distinct sources of dissolved inorganic carbon that may buffer our $\delta^{13}C_{HCO3}$ values: marine marls in the study zone ($\delta^{13}C \sim 0‰$), CO_2 dissolved in the soil (between -14 and -16‰) (Clark and Fritz, 1997), and pig manure ($\delta^{13}C_{total}$ = -16.4‰; Cravotta, 1997). Nevertheless, heterotrophic denitrification cannot be ruled out as some of the rough trends we observed, e.g. high $\delta^{18}O_{NO3}$ coupled to low ln (NO_3/HCO_3) (Fig. 5b), are in agreement with natural denitrification catalyzed by organic matter oxidation.

Recent studies (Brunner et al., 2013; Burgin and Hamilton, 2007) have highlighted the significance of alternative N loss pathways, such as anammox, to enhance the net isotope effect due to natural denitrification. Although further research is needed, anammox is improbable in our study area due to the very low concentrations of ammonium and the absence of nitrite in the Baix Ter groundwater.

4.5.2 Hydrogeological conditions linked to natural denitrification

Groundwater samples affected the most by natural denitrification were collected in areas with optimal conditions for this process. Taking into account that natural denitrification is probable in near-river environments (Rivett et al., 2008) and also

through mixing with groundwaters associated with reducing environments and deep regional flow systems (Puig et al., 2013), two different hydrogeological conditions can be considered as determining factors for our identified denitrified samples.

In the shallow Quaternary aquifer, near the Ter River (Q_4, Q_8 and Q_9), NO_3 natural attenuation may have been favored by the aquifer-river interaction, i.e. the infiltration of surface waters in the losing stream areas. In an air-saturated groundwater (10.3 mg L^{-1} O_2 at 12ºC), the lowest DOC concentration required to reach anaerobic conditions suitable for the natural denitrification is 3.8 mg L^{-1} C (Rivett et al., 2008). Since the DOC concentration in the Ter River was 4.3 mg L^{-1}, we can hypothesize that the transfer of Ter River water to the alluvial aquifer may have induced heterotrophic denitrification at some stretches, apart from mixing and dilution processes. Natural denitrification could also happen under the wooded areas at the Ter riverside, which would behave as riparian zones, or thanks to disseminated organic matter layers in the alluvial aquifer.

For sites sampled in the deep Quaternary and Tertiary aquifers (Q_1, Q_2, T_2, T_9, T_{10} and T_{14}), the NO_3 reduction can be attributed to their location in fault areas, where local and regional flowpaths converge, and the mixing between shallow and deep groundwaters is favored by fractures. The reducing conditions of these deep groundwaters, acquired after crossing reducing environments, can lead to the total removal of NO_3 coming from the more surficial groundwaters. Another favoring characteristic for the occurrence of natural attenuation in Q_D and T_D groundwaters is the presence of abundant organic matter in the floodable endhorreic zones between Ullastret and Fontanilles (ACA, 2007).

5. Conclusions

Our results show that the combined study of hydrochemical and multi-isotope data in relation with the local hydrogeological framework provides a valuable insight into sources and processes controlling the NO_3 budget in the Baix Ter basin. We demonstrated that dissolved NO_3 in groundwater in the study area results mainly from pig manure application onto the fields, although smaller but non-negligible contributions from sewage and mineral fertilizers have been isotopically identified. The study of $\delta^{11}B$ confirmed pig manure as the main vector of pollution but also fingerprinted an urban origin for two of the analyzed wells.

The dual-isotope ($\delta^{15}N$ and $\delta^{18}O$ of NO_3) approach indicated that natural denitrification processes are occurring in the study area. The $\delta^{34}S$ and $\delta^{18}O$ of SO_4 showed that NO_3 reduction is not controlled by the oxidation of pyrites but rather by organic matter oxidation (although this could not be confirmed by the $\delta^{13}C_{HCO3}$ data). The consumption of organic matter in anaerobic environments is favored by 1) the river-aquifer connection, 2) the existence of some organic layers in the Ter riversides, and 3) mixing between polluted groundwaters and deep regional flows with reducing conditions. Since the role of organic matter in the NO_3 reduction is still an on-going research, further studies on the $\delta^{13}C$ of local contaminant sources should provide a better understanding of the electron donors involved in the natural attenuation processes.

Acknowledgements

This research was funded by the CGL2011-29975-C04-01 and 2009SGR103 projects from the Spanish and Catalan Governments, respectively. We would like to thank the Centres Científics i Tecnològics of the Universitat de Barcelona for its laboratory help.

References

ACA, 2007. Diagnosis de la causalidad de la contaminación por nitratos de algunos abastecimientos públicos en las zonas vulnerables de Cataluña, análisis de alternativas, medidas de prevención y corrección. Área vulnerable 1 Girona. Estudio 1: Llanura alluvial de los ríos Ter y Daró, provincia de Girona. ACA (Water Catalan Agency) Internal Report. 168 pp.

Altman, S.J. and Parizek, R.R., 1995. Dilution of non-point source nitrate in ground water. J. Environ. Qual. 24, 707-718.

Anderson, K. K. and Hooper, A. B., 1983. O_2 and H_2O are each the source of one O in NO_2^- produced from NH_3 by Nitrosomas-^{15}N-NMR evidence. FEBS Letters, 64, 236–40.

Aravena, R., Evans, M.L., Cherry, J.A., 1993. Stable isotopes of oxygen and nitrogen in source identification of nitrate from septic tanks. Ground Water, 31, 180–186.

Aravena, R. and Robertson, W.D., 1998. Use of Multiple Isotope Tracers to Evaluate Denitrification in Ground Water: Study of Nitrate from a Large-Flux Septic System Plume. Ground Water, 36, 975-982.

Aravena, R., Mayer, B., 2010. Isotopes and Processes in the Nitrogen and Sulfur Cycles. In: Aelion, C.M., Höhener, P., Hunkeler, D., Aravena, R. (Eds.), Environmental Isotopes in Biodegradation and Bioremediation. CRC Press, pp. 203–246.

Barth, S., 1993. Boron isotope variations in nature: a synthesis. Geol Rundsch, 82, 640-651.

Barth, S., 1998. Application of boron isotopes for tracing sources of anthropogenic contamination in groundwater. Water Res. 32, 685– 690.

Basset, R.L., Buszka, P.M., Davidson, G.R., Chong-Diaz, D., 1995. Identification of groundwater solute sources using boron isotopic composition. Environ. Sci. Technol. 29, 2915–2922.

Bateman, A.S. and Kelly, S.D., 2007. Fertilizer nitrogen isotope signatures. Isotopes in Environmental and Health Studies, 43, 237-247.

Borch, T., Kretzschmar, R., Kappler, A., Van Cappellen, P., Ginder-Vogel, M., Voegelin, A., Campbell, K., 2010. Biogeochemical Redox Processes and their Impact on Contaminant Dynamics. Environmental Science and Technology, 44, 15–23.

Böttcher, J., Strebel, O., Voerkelius, S., Schmidt, H.L., 1990. Using isotope fractionation of nitrate-nitrogen and nitrate-oxygen for evaluation of microbial denitrification in sandy aquifer. Journal of Hydrology, 114, 413-424.

Brunner, B., Contreras, S., Lehmann, M.F., Matantseva, O., Rollog, M., Kalvelage, T., Klockgether, G., Lavik, G., Jetten, M.S.M., Kartal, B., Kuypers, M.M.M., 2013. Nitrogen isotope effects induced by anammox bacteria. Proceedings of the National Academy of Sciences of the United States of America. www.pnas.org/cgi/doi/10.1073/pnas.1310488110

Bryan, N.S., Alexander, D.D., Coughlin, J.R., Milkowski, A.L., Boffetta, P., 2012. Ingested nitrate and nitrite and stomach cancer risk: An updated review. Food and Chemical Toxicology, 50, 3646–3665.

Burgin, A.J. and Hamilton, S.K., 2007. Have we overemphasized the role of denitrification in aquatic ecosystems? A review of nitrate removal pathways. Frontiers in Ecology and the Environment. 5 (2), 89-96.

Clark, I.D. and Fritz, P., 1997. Environmental Isotopes in Hydrogeology. Lewis Publishers, New York. 352 pp.

Cravotta, C.A., 1997. Use of Stable Isotopes of Carbon, Nitrogen and Sulphur to Identify Sources of Nitrogen in Surface Waters in the Lower Susquehanna River Basin, Pennsylvania. U.S. Geological Survey Water-Supply Paper 2497.

Curt, M.D., Aguado, P., Sánchez, G., Bigeriego, M. and Fernández, J., 2004. Nitrogen isotope ratios of synthetic and organic sources of nitrate water contamination in Spain. Water, Air and Soil Pollution, 151, 135-142.

Devol, A.H., 2003. Nitrogen cycle: Solution to a marine mystery. Nature, 422 (6932), 575-576.

EC (European Communities), 1991. Council Directive 91/676/EC, of 12 December 1991, concerning the protection of waters against pollution caused by nitrates from agricultural sources.

EC (European Communities), 1998. Council Directive 98/83/EC, of 3 November 1998, on the quality of water intended for human consumption.

EC (European Communities), 2000. Directive 2000/60/EC of the European Parliament and of the Council establishing a framework for the Community action in the field of water policy (Water Framework Directive). Official Journal of the European Communities, OJ L 327.

EC (European Communities), 2006. Directive 2006/118/EC of the European Parliament and of the Council on the protection of groundwater against pollution and deterioration (Groundwater Directive). Official Journal of the European Communities, OJ L 372.

EEA (European Environment Agency), 1999. Nutrients in European Ecosystems. Environmental assessment report Nº 4.

EEA (European Environment Agency), 2012. European waters: assessment of status and pressures. EEA Report Nº 8. Published: Nov 13, 2012. Copenhagen, Denmark.

Fukada, T., Hiscock, K., Dennis, P.F., Grischek, T., 2003. A dual isotope approach to identify denitrification in groundwater at a river-bank infiltration site. Water Res. 37, 3070–3078.

Heaton, T.H.E., 1986. Isotopic studies of nitrogen pollution in the hydrosphere and atmosphere: a review. Chem. Geol. 59, 87–102.

Hollocher, T. C., 1984. Source of oxygen atoms in nitrate in the oxidation of nitrite by *Nitrobacter agilis* and evidence against a P-O-N anhydride mechanism in oxidative phosphorylation. Archives of Biochemistry and Biophysics, 233, 721–27.

Horibe, Y., Shigehara, K., and Takakuwa, Y., 1973. Isotope separation factors of carbon dioxide-water system and isotopic composition of atmospheric oxygen. Journal of Geophysical Research, 78, 2625-2629.

Jurado, A., Vàzquez-Suñé, E., Soler, A., Tubau, I., Carrera, J., Pujades, E., Anson, I., 2013. Application of multi-isotope data (O, D, C and S) to quantify redox processes in urban groundwater. Applied Geochemistry, 34, 114–125.

Karr, J.D., Showers, W.J., Wendell Gilliam, J., Scott Andres, A., 2001. Tracing nitrate transport and environmental impact from intensive swine farming using delta nitrogen-15. J. Environ. Qual. 30, 1163–1175.

Kendall, C., 1998. Tracing Nitrogen Sources and Cycling in Catchments. In: Isotope Tracers in Catchment Hydrology, C. Kendall and J. J. McDonnell (Eds.). Elsevier Science B.V., Amsterdam, 839 p., 519-576.

Kendall, C., Elliott, E.M., and Wankel, S.D., 2007. Tracing anthropogenic inputs of nitrogen to ecosystems, Chapter 12. In: R.H. Michener and K. Lajtha (Eds.), Stable Isotopes in Ecology and Environmental Science, 2nd edition, Blackwell Publishing, pp. 375-449.

Koba, K., Tokuchi, N., Wada, E., Nakajima, T., Iwatsubo, G., 1997. Intermittent denitrification: the application of a ^{15}N natural abundance method to a forested ecosystem. Geochim. Cosmochim. Acta, 61, 5043–5050.

Komor, S.C., 1997. Boron contents and isotopic compositions of hog manure, selected fertilizers, and water in Minnesota. J. Environ. Qual. 26, 1212–1222.

Krouse, H.R. and Mayer, B., 2000. Sulphur and oxygen isotopes in sulphate. In: Cook, P.G., Hercseg, A.L. (Eds.), Environmental Tracers in Subsurface Hydrology. Kluwer Academic Press, Boston, pp. 195–231.

Li, X-D, Liu, C-Q, Harue, M., Li, S-L, Liu, X-L, 2010. The use of environmental isotopic (C, Sr, S) and hydrochemical tracers to characterize anthropogenic effects on karst groundwater quality: A case study of the Shuicheng Basin, SW China. Applied Geochemistry, 25, 1924–1936.

Mariotti, A., Germon, J.C., Hubert, P., Kaiser, P., Letolle, R., Tardieux, P., 1981. Experimental determination of nitrogen kinetic isotope fractionation: some principles, illustration for the denitrification and nitrification processes. Plant Soil, 62, 413–430.

Mariotti, A., Landreau, A., Simon, B., 1988. ^{15}N isotope biogeochemistry and natural denitrification process in groundwater: application to the chalk aquifer of northern France. Geochim. Cosmochim. Acta, 52, 1869–1878.

Mas-Pla, J., Bach, J., Montaner J., 1998. Distribución de la concentración de nitratos en el sistema hidrogeológico Baix Ter-Gavarres (Girona). In: La contaminación de las aguas subterráneas: Un problema pendiente. ITGE-AIH, pp. 139–145.

Mas-Pla, J. and Vilanova, E., 2001. Dinámica del sistema hidrogeológico Baix Ter-Gavarres en base a isótopos estables. In: IGME, Las Caras del Agua, Serie Hidrogeología y Aguas Subterráneas n. 1/2001, tomo I, pp. 395-402.

Mengis, M., Walther, U., Bernasconi, S.M., Wehrli, B., 2001. Limitations of using $\delta^{18}O$ for the source identification of nitrate in agricultural soils. Environ. Sci. Technol. 35 (9), 1840–1844.

Mizutani, Y. and Rafter, T.A., 1973. Isotopic behaviour of sulphate oxygen in the bacterial reduction of sulphate. Geochemical Journal, 6, 183-191.

Montaner, J., Pons, P., López, J., 2010. Caracterització del flux hidrològic a la plana litoral del Baix Ter. In: El flux hidrològic de la plana litoral del Baix Ter. Evolució fluvial, caracterització hidrològica i pautes de gestió. Montaner, J. (coord.). Càtedra d'Ecosistemes Litorals Mediterranis. Museu de la Mediterrània (Ed.). Recerca i Territori, 2.

Neal, C., Neal, M., Warrington, A., Àvila, A., Piñol, J., Rodà, F., 1992. Stable hydrogen and oxygen isotope studies of rainfall and streamwaters for two contrasting holm oak areas of Catalonia, northeastern Spain. Journal of Hydrology, 140, 163–178.

Otero, N., Canals, A., Soler, A., 2007. Using dual-isotope data to trace the origin and processes of dissolved sulphate: a case study in Calders stream (Llobregat basin, Spain). Aquat. Geochem. 13, 109–126.

Otero, N., Soler, A., Canals, A., 2008. Controls of $\delta^{34}S$ and $\delta^{18}O$ in dissolved sulphate: Learning from a detailed survey in the Llobregat River (Spain). Applied Geochemistry, 23, 1166-1185.

Otero, N., Torrentó, C., Soler, A., Menció, A., Mas-Pla, J., 2009. Monitoring groundwater nitrate attenuation in a regional system coupling hydrogeology with multi-isotopic methods: the case of Plana de Vic (Osona, Spain). Agr. Ecosyst. Environ. 133 (1-2), 103–113.

Panno, S.V., Hackley, K.C., Hwang, H.H. and Kelly, W.R., 2001. Determination of the sources of nitrate contamination in karst springs using isotopic and chemical indicators. Chemical Geology, 179, 113-128.

Puig, R., Folch, A., Menció, A., Soler, A., Mas-Pla, J., 2013. Multi-isotopic study (^{15}N, ^{34}S, ^{18}O, ^{13}C) to identify processes affecting nitrate and sulfate in response to local and regional groundwater mixing in a large-scale flow system. Applied Geochemistry, 32, 129–141.

Rivett, M.O., Buss, S.R., Morgan, P., Smith, J.W.N., Bemment, C.D., 2008. Nitrate attenuation in groundwater: a review of biogeochemical controlling processes. Water Res. 42, 4215–4232.

Rock, L., Mayer, B., 2002. Isotopic assessment of sources and processes affecting sulphate and nitrate in surface water and groundwater of Luxembourg. Isotopes Environ. Health Stud. 38 (4), 191-206.

Saccon, P., Leis, A., Marca, A., Kaiser, J., Campisi, L., Böttcher, M.E., Savarino, J., Escher, P., Eisenhauer, A., Erbland, J., 2013. Multi-isotope approach for the identification and characterization of nitrate pollution sources in the Marano lagoon (Italy) and parts of its catchment area. Appl. Geochem., 34, 75–89.

Sebilo, M., Mayer, B., Nicolardot, B., Pinay, G., Mariotti, A., 2013. Long-term fate of nitrate fertilizer in agricultural soils. PNAS (Proceedings of the National Academy of Sciences of the United States of America). www.pnas.org/cgi/doi/10.1073/pnas.1305372110

Seiler, R. L., 2005. Combined use of ^{15}N and ^{18}O of nitrate and ^{11}B to evaluate nitrate contamination in groundwater. Applied Geochemistry, 20, 1626-1636.

Silva, S.R., Kendall, C., Wilkison, D.H., Ziegler, A.C., Chang, C.C.Y., Avanzino, R.J., 2000. A new method for collection of nitrate from fresh water and the analysis of nitrogen and oxygen isotope ratios. Journal of Hydrology, 228, 22–36.

Spivack, A.J. and Edmond, J.M., 1986. Determination of boron isotope ratios by thermal ionization mass spectrometry of the dicesium metaborate cation. Anal. Chem., 58, 31-35.

Tirez, K., Brusten, W., Widory, D., Petelet, E., Bregnot, A., Xue, D., Boeckx, P., Bronders, J., 2010. Boron Isotope Ratio ($\delta^{11}B$) Measurements in Water Framework Directive Programs: Comparison between Double Focusing Sector Field ICP and Thermal Ionization Mass Spectrometry, J. Anal. At. Spectrom. 25, 964-974.

Vengosh, A., Heumann, K.G., Juraske, S., Kasher, R., 1994. Boron Isotope Application for Tracing Sources of Contamination in Groundwater. Environmental, Science and Technology, 28, 1968-1974.

Vilanova, E., 2004. Anàlisi dels sistemes de flux a l'àrea Gavarres-Selva-Baix Empordà. Proposta de model hidrodinàmic regional. Ph.D Dissertation. Universitat Autònoma de Barcelona, 337 pp.

Vilanova, E. and Mas-Pla, J., 2004. Identificación de sistemas de flujo en base a datos isotópicos en el área Gavarres-Baix Empordà-Selva (CIC). Geotemas, 6(4), 197-202.

Vilanova, E., Mas-Pla, J., Menció, A., 2008. Determinación de sistemas de flujo regionales y locales en las depresiones tectónicas del Baix Empordà y La Selva (NE de España) en base a datos hidroquímicos e isotópicos. Boletín Geológico y Minero, 119 (1), 51-62.

Vitòria, L., 2004. Estudi multi-isotòpic ($\delta^{15}N$, $\delta^{34}S$, $\delta^{13}C$, $\delta^{18}O$, δD i $^{87}Sr/^{86}Sr$) de les aigües subterrànies contaminades per nitrats d'origen agrícola i ramader. Translated title: Multi-isotopic approach ($\delta^{15}N$, $\delta^{34}S$, $\delta^{13}C$, $\delta^{18}O$, δD and $^{87}Sr/^{86}Sr$) of nitrate contaminated groundwaters by agricultural and stockbreeder activities. PhD Thesis. Universitat de Barcelona, 188 pp.

Vitòria, L., Otero, N., Canals, A., Soler, A., 2004b. Fertilizer characterization: isotopic data (N, S, O, C and Sr). Environ. Sci. Technol. 38, 3254–3262.

Vitòria, L., Soler, A., Aravena, R., Canals, A., 2005. Multi-isotopic approach (^{15}N, ^{13}C, ^{34}S, ^{18}O and D) for tracing agriculture contamination in groundwater (Maresme, NE Spain). In: Environmental Chemistry (Eds. E. Lichtfouse, J. Schwarzbauer and D. Robert). Springer-Verlag, Heidelberg, 43-56.

Vitòria, L., Soler, A., Canals, A., Otero, N., 2008. Environmental isotopes (N, S, C, O, D) to determine natural attenuation processes in nitrate contaminated waters: example of Osona (NE Spain). Appl. Geochem. 23, 3597–3611.

Waldron, S., Tatner, P., Jack, I., Arnott, C., 2001. The Impact of Sewage Discharge in a Marine Embayment: A Stable Isotope Reconnaissance. Estuarine, Coastal and Shelf Science, 52, 111–115. doi:10.1006/ecss.2000.0731

Ward, M.H., deKok, T.M., Levallois, P., Brender, J., Gulis, G., Nolan, B.T., VanDerslice, J., 2005. Workgroup report: drinking-water nitrate and health—recent findings and research needs. Environ. Health Perspect. 113, 1607–1614.

Wassenaar, L. I., 1995. Evaluation of the origin and fate of nitrate in the Abbotsford aquifer using the isotopes of ^{15}N and ^{18}O in NO_3. Applied Geochemistry, 10, 391–405.

Widory, D., Kloppmann, W., Chery, L., Bonnin, J., Rochdi, H., Guinamant, J.L., 2004. Nitrate in groundwater: an isotopic multi-tracer approach. Journal of Contaminant Hydrology, 72, 165-188.

Widory, D., Petelet-Giraud, E., Négrel, P., Ladouche, B., 2005. Tracking the sources of nitrate in groundwater using coupled nitrogen and boron isotopes: a synthesis. Environmental, Science and Technology, 39, 539-548.

Widory, D., Petelet-Giraud, E., Brenot, A., Bronders, J., Tirez, K., Boeckx, P., 2013. Improving the management of nitrate pollution in water by the use of isotope monitoring: the $\delta^{15}N$, $\delta^{18}O$ and $\delta^{11}B$ triptych. Isotopes in Environmental and Health Studies, 48, 1-19.

Xue, D., Botte, J., De Baets, B., Accoe, F., Nestler, A., Taylor, P., Van Cleemput, O., Berglund, M., Boeckx, P., 2009. Present limitations and future prospects of stable isotope methods for nitrate source identification in surface- and groundwater. Water Research, 43, 1159-1170.

Yingkai, X., Lan, W., 2001. The effect of pH and temperature on the isotopic fractionation of boron between saline brine and sediments. Chem. Geol. 171, 253–261.

ANNEX D

Puig, R., Tolosana-Delgado, R., Otero, N. and Folch, A. (**2011**) Combining isotopic and compositional data: a discrimination of regions prone to nitrate pollution. In: Compositional Data Analysis: Theory and Applications. V. Pawlowsky-Glahn, A. Buccianti (Eds.). John Wiley & Sons, Ltd, 303–316.

22

Combining isotopic and compositional data: a discrimination of regions prone to nitrate pollution

Roger Puig[1], Raimon Tolosana-Delgado[2], Neus Otero[1] and Albert Folch[3]

[1] *Faculty of Geology, University of Barcelona (UB), Spain*
[2] *Maritime Engineering Laboratory, Technical University of Catalonia, Spain*
[3] *Department of Geology, Autonomous University of Barcelona, Spain*

22.1 Introduction

In the last few decades, nitrate pollution has become a major threat to groundwater quality, as the threshold value for drinking water [50 mg l^{-1}, Directive 98/83/EC; EC (1998)] is achieved in most of the local and regional aquifers in Europe. High nitrate levels in drinking water poses a health risk, because the ingestion of high nitrate concentration can cause methahemoglobinaemia in children and babies (Magee and Barnes 1956), and some authors pointed out that nitrogen compounds can act as human cancer promoters (Ward *et al*. 2005; Volkmer *et al*. 2005). Nitrate pollution is linked to the intensive use of synthetic and organic fertilizers, as well as to septic systems effluents. In Catalunya (north-east Spain), according to the nitrate directive (91/767/EU), twelve areas have been declared as vulnerable to nitrate

Compositional Data Analysis: Theory and Applications, First Edition. Edited by Vera Pawlowsky-Glahn and Antonella Buccianti.
 Published 2011 by John Wiley & Sons, Ltd.

pollution from agricultural sources (Decrets 283/1998, 436/2004 and 136/2009), covering more than one third of the territory.

To improve water management in these areas, it is essential to determine the origin of pollution and the evolution of nitrogen compounds. Nitrate isotopes are a unique tool for this purpose. Nitrogen and oxygen isotopes of dissolved nitrate can be used as tracers of nitrate pollution, distinguishing between chemical fertilizers and manure/sewage (Wassenaar 1995; Kendall and McDonnell 1998). However, in order to use the isotopic composition of dissolved nitrate as a tracer of nitrate origin, one must bear in mind that several processes (e.g. volatilization, nitrification and denitrification) change the isotopic composition of the sources, leading to overlapping isotopic signatures for different nitrate sources. For example, ammonia volatilization results in an increase of the δ^{15}N residual ammonium (Letolle 1980). In denitrification processes, nitrate is reduced to N_2, increasing the isotopic composition (δ^{15}N and δ^{18}O) of the remaining nitrate in waters (Böttcher *et al*. 1990). This fact, considered a drawback in the application of nitrate isotopes as tracers of sources, can be applied to trace processes themselves, e.g. the isotopic composition of dissolved nitrate is used to distinguish between dilution and denitrification in groundwater samples in areas where a diminution in nitrate concentration is observed (Grischek *et al*. 1998; Cey *et al*. 1999; Mengis *et al*. 1999). In this sense, this approach towards the identification of processes could be later complemented with geochemical and biogeochemical reaction modelling applied to all chemical and isotopic variables (Bethke 2008). A further step in the investigation of denitrification processes is to determine the factors controlling the reaction. This has been done coupling chemical data with the δ^{15}N and/or δ^{18}O of dissolved nitrate and the isotopic composition of the ions involved in denitrification reactions, as δ^{34}S and δ^{18}O of dissolved sulfate, and/or δ^{13}C of dissolved inorganic carbon (Aravena and Robertson 1998; Pauwels *et al*. 2000). This approach was proposed in an ongoing project performed in several areas classified as vulnerable to nitrate pollution in Catalunya. Five of the vulnerable areas (Maresme, Osona, Lluçanès, Empordà and Selva) have been studied coupling classical hydrochemistry data with a comprehensive isotopic characterization, including δ^{15}N and δ^{18}O of dissolved nitrate, δ^{34}S and δ^{18}O of dissolved sulfate, δ^{13}C of dissolved inorganic carbon, and δD and δ^{18}O of water (Vitòria *et al*. 2005, 2008; Puig *et al*. 2007; Otero *et al*. 2009). The key goals of this project were (i) to identify the main sources of nitrate pollution in the areas, (ii) to verify if denitrification (natural attenuation) processes were taking place, and (iii) to determine the factors controlling the denitrification reactions. In this framework, the present chapter aims to put forward a statistical methodology to integrate isotope data together with geochemical data. This methodology will be applied to discriminate sample groups affected by different nitrate pollution sources.

22.2 Study area

The studied areas are located in Barcelona and Girona provinces, four of them belong to the Ter river basin and one is located along the coast (Figure 22.1). The Ter river is a major stream in the area, it crosses the Osona, Lluçanès, Empordà and Selva studied areas. Its mean discharge in the Osona area is 509 hm^3 $year^{-1}$ (at the gauging station of Roda de Ter), in the Empordà area 1026 hm^3 $year^{-1}$ (at the gauging station of Colomers), and in the Selva area 261 hm^3 $year^{-1}$ (at the gauging station of Cellera de Ter). The studied areas have a sub-Mediterranean climate with mean rainfall between 550 and 850 mm $year^{-1}$ for all the areas. The potential evapotranspiration, calculated by the Thornwaite method, is in the

Figure 22.1 Map of Catalunya showing in grey the areas classified as vulnerable to nitrate pollution from agricultural sources. The studied areas are indicated by the first letter of their names (see text).

range of rainfall (570–910 mm year^{-1}). The following sections describe the main geological, hydrogeological and land use characteristics of each studied area.

22.2.1 Maresme

In the Maresme vulnerable zone the studied area is 3 km^2. The geology of the area consists of Holocene alluvial deposits of coarse sands derived from the weathered granodiorite that forms the Catalan Coastal Range. The main hydrogeological units are an unconfined sandy aquifer underlaid by an aquitard composed of silts and clays and a confined sandy aquifer. The thickness of these units is 5–40, 5–15 and 15–20 m, respectively. The unconfined aquifer is the only one affected by groundwater extractions and its water table varies between 4 and 30 m in depth. The Maresme area is characterized by intensive agricultural activity. Flowers, fruit and vegetable crops are the main agricultural products, and about half of them grow under greenhouse conditions. Fertilization is carried out with inorganic fertilizers usually injected through trickle irrigation systems that use groundwater extracted from partially penetrating wells (5–40 m deep). The soil type in this area is usually coarse sand with a low organic matter content (<3% of dry soil) and a low C:N ratio of approximately 1:2 (Guimerà *et al*. 1995). This low natural fertility, together with the low water-holding capacity of the soil, requires high fertilizer and irrigation applications, resulting in high nutrient leaching in the upper zone of the aquifer affected by groundwater withdrawals. Recirculation of the shallow groundwater by the irrigation system causes high concentrations of nitrates (up to 300 mg^{-1}) in the groundwater (ACA 2009). This area, where only chemical fertilizers are used, is considered as representative of nitrate pollution from inorganic fertilizers, as shown by Vitòria *et al*. (2005) using an isotope approach.

22.2.2 Osona

The study performed in the Osona area covers 600 km^2. From a geological perspective, the area is constituted of Paleogene sedimentary materials overlaying hercynian crystalline (igneous and metamorphic) rocks. The stratigraphic sequence primarily consists of carbonate formations, with an alternation of calcareous, marl and carbonate sandstone layers. It is worth noting the presence of disseminated pyrite in marls. These formations show a quite uniform dipping of about 7–10° to the west. The area is hydrogeologically constituted by a series of confined aquifers located in the carbonate and carbonate–sandstone layers. Marl strata act as confining layers. In this area the porosity is mainly related to the fracture network. Main production wells for agriculture and farm demand usually reach depths of more than 100 m, searching for the most productive confined aquifers. Alluvial aquifers are scarce and generally nonproductive in the area; except those located at the Ter river terraces. In the central part of Osona nitrate pollution is widely extended, with a median concentration above 100 mg l^{-1} during the last 5 years. In this region, of 1263.8 km^2, there are more than 1000 pig farms, with 990 000 pigs, 110 000 cows and 67 000 sheep (IDESCAT 1999). This intensive farming activity produces huge amounts of organic residues, 10 900 t $year^{-1}$ of nitrogen. Fertilizers are also applied, but only in the surroundings of the villages, as the use of pig manure close to urban areas is forbidden. 93% of the municipalities are connected to the sewage network; therefore the contribution of sewage to groundwater nitrate pollution is expected to have negligible influence, compared with agricultural sources. In this area, although chemical fertilizers are also applied, the main contribution to nitrate pollution is linked to an excess of manure application as fertilizer or in uncontrolled dumps, as demonstrated by Vitòria *et al*. (2008) and Otero *et al*. (2009) using a multi-isotopic approach. Hence this area is considered as representative of manure nitrate pollution.

22.2.3 Lluçanès

The Lluçanès area is located in the north-west of the Osona area, and the studied area covers 400 km^2. The geology of the area is constituted by Paleogene sedimentary materials, which include continental detritic facies (conglomerates, sandstones and clays) and marine facies (silts, marls and limestones). The lithostratigraphic units configure an upper and lower deltaic complexes whose clastic contributions are from the north. A monoclinal structure shows a regional dip <4° to the south–south-west–west. The main hydrogeological unit in the Lluçanès area consists of sandstones and conglomerates of the upper deltaic complex (north–north-east area), and is a high productivity confined aquifer. Silt and marl interspersed in sandy levels work as an aquitard, and lutites, sandstones and conglomerates give rise to local aquifer levels with low capacity and limited recharge. The regional flow direction is north–south for all the hydrogeological units of the Tertiary materials. The Lluçanès land uses distribution comprises forest (57%), crops (25%), fields (15%) and urban areas (3%). Since agricultural areas are mostly dry-farmed crops, water resources in the studied area are not as affected by agriculture water demand as they are by the application of manure onto fields as fertilizer. In the studied area the intensive livestock activity is predominantly pig raising: there are 366 farms with around 70 000 animals that produce more than 2500 t $year^{-1}$ of nitrogen as organic residues. On the other hand, the influence of sewage to nitrate contamination is not discarded, because some villages dump to surface waters. Hence, in the Lluçanès area, mainly there is a surplus application of nitrogen organic compounds from agricultural and livestock activities.

22.2.4 Empordà

In the nitrogen vulnerable zone of the Empordà the studied area is located in the south and covers 200 km^2. The geology of the Empordà area consists of Paleogene detritic and carbonate sedimentary rocks (in the east and south of the studied area), Neogene clay facies (in the west), and Holocene alluvial deposits of Ter river and its tributary. These Tertiary and Quaternary materials lay on Paleozoic discordant bedrock. Paleozoic outcrops are located in the western and southern parts of the watershed. This area presents a complex distribution of hydrogeological units due to the high lithological diversity (Puig *et al*. 2007). The main units are: (i) an unconfined aquifer with sand and gravel, and some clay in the matrix (mainly from Quaternary); and (ii) a confined and sometimes unconfined fractured aquifer with thickness discontinuity (mainly from Tertiary). This area has a notable agricultural activity (mainly maize, sunflower and fruit crops) which uses synthetic fertilizers, and the water demand for irrigation is remarkably increased in summer months. Organic fertilizers are also applied as a consequence of an intensive pig farming activity (462 pigs km^{-2}) which produces large amounts of organic residues. Thus, the Empordà area is considered a mixed area where both fertilizers and animal manure are used.

22.2.5 Selva

In the Selva vulnerable zone the studied area is 350 km^2. The area belongs to a tectonic basin surrounded by three ranges with 1000 m altitude above sea level. This basin was created during the distensive periods after the Alpine orogenesis, and it has a Neogene sedimentary poorly consolidated and volcanic filling. The surrounding ranges consist of Paleozoic igneous and metamorphic rocks, and pre-Alpine Paleogene sedimentary rocks (mainly limestone and sandstone). From a hydrogeological perspective in the Selva area we can differentiate a regional and a local flow system. Thus, four geological domains can be hydrogeologically distinguished: (i) the granitic materials of the surrounding ranges, which act as the main recharge area of the granitic basement of the depression; (ii) the Neogene materials of the sedimentary basin, whose local flows originate from the range areas as a lateral recharge, and from the uppermost parts of the basement; (iii) the main faults oriented north-west–south-east and north-east–south-west behaving as an independent hydrogeological unit connected with the rest of the units (fractures responsible for the thermal springs occurring within the basin); and (iv) the upper alluvial formations with two alluvial aquifers associated with two streams. This area is also considered a mixed area with regards to land use and nitrate pollution sources.

22.3 Analytical methods

All the sampling surveys were conducted on production wells. In the Maresme area, two sampling surveys in a small area (3 km^2) were performed: the first of 8 samples and the second of 23 samples. In the Osona area several sampling surveys were carried out: the first, in a reduced area of 36 km^2 with 38 samples, and three more surveys, in a larger area of 600 km^2, with 59, 58 and 32 samples, respectively. In the Lluçanès area one field sampling was done in an area of 400 km^2, with 30 samples. In the Empordà area two surveys were conducted in a 200 km^2 area: the first survey of 24 samples and the second of 40 samples. In the Selva area only one survey was executed, with 38 samples in a 350 km^2 area. Physicochemical

parameters (pH, temperature, electrical conductivity, dissolved O_2 and Eh) were measured *in situ*, using a flow cell to avoid contact with the atmosphere. Samples were stored at 4 °C and in a dark environment. Chemical parameters were determined by standard analytical techniques; the chemical characterization comprises major ions (Cl^-, SO_4^{2-}, HCO_3^-, Na^+, Ca^{2+}, Mg^{2+}, K^+), nitrogen compounds (NO_2^-, NO_3^-, NH_4^+), Fe and Mn. The δD and δ^{18}O of water were obtained by means of isotope ratio mass spectrometer (IRMS) with a Delta S Finnigan Mat, following the methodological approaches of Friedman (1953) and Epstein and Mayeda (1953), respectively. For $\delta^{15}N_{NO_3}$ and $\delta^{18}O_{NO_3}$ analysis, dissolved nitrate was concentrated using anion-exchange columns Bio Rad® AG 1-X8(Cl^-) 100–200 mesh resin, after extracting sulfates and phosphates by precipitation with $BaCl_2$ and filtration (Mayer *et al*. 2001). Afterwards dissolved nitrate was eluted with HCl and converted to $AgNO_3$ by the addition of silver oxide. The silver nitrate solution was then freeze-dried obtaining the pure $AgNO_3$ for analysis usign a method modified from Silva *et al*. (2000). Two surveys of the Osona area were analysed for nitrogen and oxygen isotopes of dissolved nitrate following the methods of Sigman *et al*. (2001) and Casciotti *et al*. (2002). For sulfur and oxygen isotopic analysis, the dissolved sulfate was precipitated as $BaSO_4$ by the addition of $BaCl_2 \cdot 2H_2O$, after acidifying the sample with HCl and boiling it. For δ^{13}C analysis unfiltered splits of samples were treated with NaOH−$BaCl_2$ solution to precipitate carbonates, and then filtered at 3 μm. The sulfur, nitrogen and carbon isotopic composition was determined with an Elemental Analyser (Carlo Erba 1108) coupled with an IRMS (Delta C Finnigan Mat). The oxygen isotopic composition of nitrate and sulfate was analysed in duplicate with a Thermo-Chemical Elemental Analyser (TC/EA Thermo-Quest Finnigan) coupled with an IRMS (Delta C Finnigan Mat). Results are expressed in terms of δ per mil relative to the following international standards: Vienna Standard Mean Ocean Water (V-SMOW) for δD and δ^{18}O, atmospheric N_2 (AIR) for N isotopes, Vienna Canyon Diablo Troilite (V-CDT) for S isotopes, and Vienna Peedee Belemnite (V-PDB) for C isotopes. The isotope ratios were checked using international and internal laboratory standards. Reproducibility precision ($=1\sigma$) of the samples calculated from standards systematically interspersed in the analytical batches is $\pm 1.5^{o}/_{oo}$ for δD, $\pm 0.2^{o}/_{oo}$ for $\delta^{18}O_{H_2O}$, $\pm 0.3^{o}/_{oo}$ for $\delta^{15}N_{NO_3}$, $\pm 0.2^{o}/_{oo}$ for δ^{34}S, $\pm 0.5^{o}/_{oo}$ for both $\delta^{18}O_{NO_3}$ and $\delta^{18}O_{SO_4}$, and $\pm 0.2^{o}/_{oo}$ for $\delta^{13}C_{HCO_3}$. Isotopic samples were prepared in the laboratory of the Applied Mineralogy and Environment Research Group and analysed at the Scientific-Technical Services of the University of Barcelona, except the isotopic composition of dissolved nitrates of two surveys in the Osona area, which were analysed at the Woods Hole Oceanographic Institution.

22.4 Statistical treatment

22.4.1 Data scaling

Before any statistical analysis can be done, we should scale the data set in an adequate way. This means transforming our variables in such a way that the variations in each variable (or set of variables) are comparable between them. For this particular study, this implies the following issues.

- **Removing the local mean water line from the isotopic composition.** As is well-known, the largest variation observed in δD and δ^{18}O in meteoric water is due to the altitude/continentality effects (Figure 22.2). As this has already a well-known

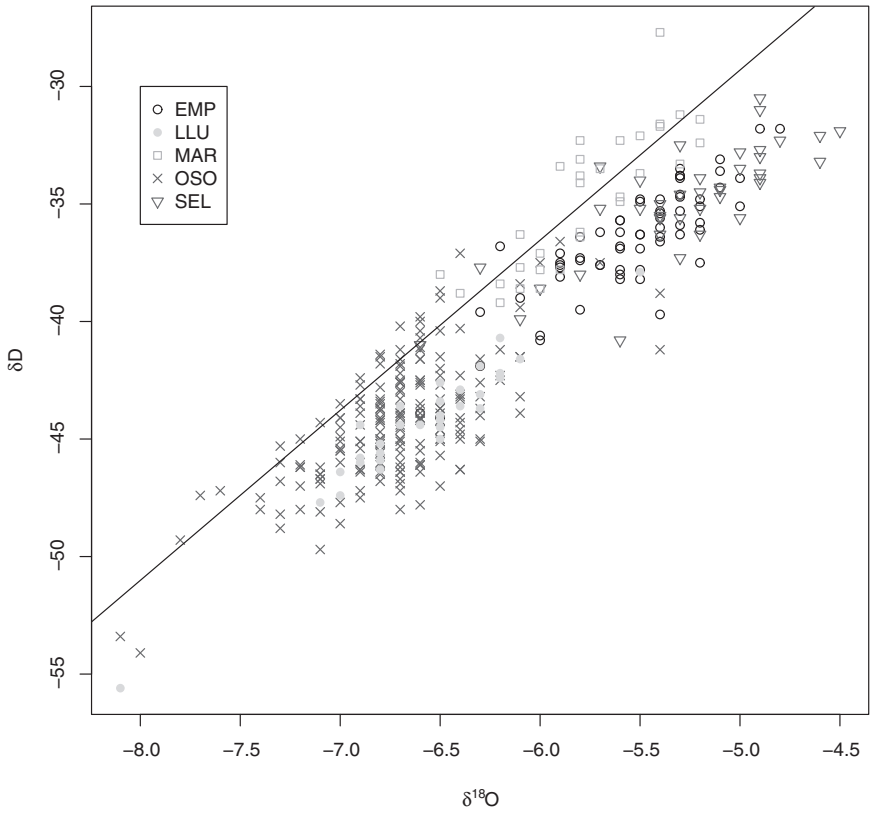

Figure 22.2 Scatterplot of hydrogen isotope (δD) versus oxygen istotope (δ^{18}O) compositions in water, with indication of the local meteoric water line (LMWL) calculated with data from the Global Network of Isotopes in Precipitation (GNIP) from stations 0818001 and 0818002 located in Barcelona (IAEA/WMO 2004).

explanation, this effect should be removed before any statistical analysis of isotopes can be aplied. Otherwise, it would mask any other effect. To do so, we can project the measured δD and $\delta^{18}O_{H_2O}$ onto the LMWL (IAEA/WMO 2004),

$$\delta D = 7.32 + 7.29\, \delta^{18}O - H_2O$$

and extract the orthogonal deviations of each data point with respect to this line. These deviations are going to enter the analysis of isotopes instead of δD and δ^{18}O.

- **Log-ratio transforming the compositional variables.** If we have $\mathbf{Z}$ a compositional data set, then we must apply our statistical analyses to the clr-transformed data set, $\mathbf{Y} = \text{clr}(\mathbf{Z})$, or to the ilr-transformed one, $\mathbf{X} = \text{ilr}(\mathbf{Z})$. Both are related through $\mathbf{X} = \mathbf{Y} \cdot \mathbf{V}$ and $\mathbf{Y} = \mathbf{X} \cdot \mathbf{V}^t$, where $\mathbf{V}$ is the $D \times (D-1)$-matrix of definition of the used ilr basis. In the following sections we will either use clr- or ilr- transformed compositions wherever a real-valued data set is needed.

- **Scaling both subsets to be comparable.** This contribution uses a combined data set, with a compositional $\mathbf{Z}$ and a real $\mathbf{X}^r$ subset of variables, actually an isotopic composition array. Tolosana-Delgado *et al*. (2005) showed that the isotopic delta ratios are an excellent first-order approximation to a full log-ratio treatment with isotopes differentiated as extra geochemical component. This is due to the extremely low variability that isotopes show in comparison with the common geochemical variation. In order to adequately combine these two sources of information, we will first construct a coordinate data set, joining the ilr-transformed composition with the isotopic deltas. However, the variability of each of the two parts is not going to be comparable. For instance, in the present data set the geochemical composition has a *metric variance* (a single-number measure of the total variability of a subset of samples) (Pawlowsky-Glahn and Egozcue 2001) of 4.93, whereas the metric variance of the isotopic delta variables (once the LMWL was removed) is almost 95. Thus, if we simply combine them, the delta variability is going to mask the compositional one, being around 19 times larger. One should therefore either *downweight* the isotopic delta set, or increase the importance of the geochemical part by multiplying each subset with a constant:

$$\mathbf{X} = \left[\alpha \mathrm{ilr}(\mathbf{Z}); \beta \mathbf{X}^r\right] . \tag{22.1}$$

  Lacking any way of deciding the values of α and β, it is reasonable to scale each of these two data sets by the inverse of the metric variance, i.e. to take

$$\alpha^{-1} = \sqrt{\mathrm{Tr}[\mathrm{Var}[\mathrm{ilr}(\mathbf{Z})]]}\,, \quad \beta^{-1} = \sqrt{\mathrm{Tr}[\mathrm{Var}[\mathbf{X}^r]]}\,.$$

  In this way, both isotopic and geochemical parts contribute equally to the total variability.

22.4.2 Linear discriminant analysis

Let $\mathbf{X}$ be a data set, of P real variables and N individuals (either previously ilr-transformed compositions, isotopic delta variables or a mix of both types). Assume that this set is split into K groups, each of N_k samples, and denote by $\mathbf{m}_k$ and $\mathbf{S}_k$ the empirical centre and variance matrix of each group. The goal of linear discriminant analysis (LDA) is to find $K-1$ directions of the P-dimensional real space, $\mathbb{R}^P$, where the separation between the groups is optimal (e.g. Mardia *et al*. 1979; Fahrmeir and Hamerle 1984; Krzanowski 1988; Krzanowski and Marriott 1994). Consider that each group has a prior likelihood of p_k^0, either chosen by the analyst or estimated as $\hat{p}_k^0 = N_k/N$. In a parametric framework, LDA hypotheses lead a sample $\mathbf{x}$ to have a posterior probability to belong to group k proportional to

$$p_k(\mathbf{x}) \propto p_k^0 \exp\left[-\frac{1}{2} d^2_{\mathrm{Mah}}(\mathbf{x}, \mathbf{m}_k|\mathbf{W})\right],$$

where $d^2_{\mathrm{Mah}}(\mathbf{x}, \mathbf{m}_k|\mathbf{W})$ is the squared Mahalanobis distance from the sample to the centre of the group, with regard to the pooled *within-groups variance* matrix

$$\mathbf{W} = \sum_{k=1}^{K} p_k^0 \mathbf{S}_k .$$

If we define the global centre as $\mathbf{m} = \sum_{k=1}^{K} p_k^0 \mathbf{m}_k$, and the *between-groups variance* as

$$\mathbf{B} = \sum_{k=1}^{K} p_k^0 \cdot (\mathbf{m}_k - \mathbf{m}) \cdot (\mathbf{m}_k - \mathbf{m})^t,$$

then the solution can be found as the eigen-decomposition of the matrix $\mathbf{Q} = (\mathbf{W}^{-1} \cdot \mathbf{B})$. Its first $K - 1$ eigenvectors are the sought directions of optimal separations between groups, whereas the corresponding eigenvalues represent the ratios of the between- and within-group variances projected onto these directions, i.e. the discriminating power of each eigenvector.

If we are dealing with a D-part compositional data set, then $P = D - 1$. The Mahalanobis distance can be taken as $d^2_{\text{Mah}}(\mathbf{x}, \mathbf{m}_k|\mathbf{W}) = \text{ilr}(\mathbf{x} \ominus \mathbf{m}_k) \cdot \mathbf{W}^{-1} \cdot \text{ilr}^t(\mathbf{x} \ominus \mathbf{m}_k)$, and the between-groups variance may be obtained with $\mathbf{B} = \sum_{k=1}^{K} p_k^0 \cdot \text{ilr}(\mathbf{m}_k - \mathbf{m}) \cdot \text{ilr}^t(\mathbf{m}_k - \mathbf{m})$, where $\text{ilr}(\mathbf{m}) = \sum_{k=1}^{K} p_k^0 \text{ilr}(\mathbf{m}_k)$ is the global centre. All these elements may also be computed with compositions and variance matrices expressed as alr coordinates or even with clr coefficients, if the within-groups variance matrix is inverted with the Moore–Penrose generalized inversion.

When dealing with a mixed data set, it is safer to keep all computations in ilr coordinates, previously normalized to have unit metric variance, as shown in Equation (22.1).

22.4.3 Discriminant biplots

Classical biplots are bad tools for displaying the discrimination between groups $\mathbf{Q}$, being optimized to display the global variance $\mathbf{S} = \mathbf{W} + \mathbf{B}$. However, we can construct a biplot (a joint graphical representation of variables and observations) devised to display differences between groups. Following Gabriel (1971), a biplot is constructed from the decomposition of a centred data matrix $\mathbf{X}^* = \mathbf{X} - \mathbf{1}_N^t \cdot \mathbf{m}$ in a couple of matrices

$$\mathbf{X}^* = \mathbf{F} \cdot \mathbf{H}^t,$$

where $\mathbf{F}$ has N rows and P columns and $\mathbf{H}$ is a square matrix in which P columns represent orthogonal directions of $\mathbb{R}^P$. The two-dimensional graphical representation is obtained plotting the first two columns of $\mathbf{F}$ as dots (one for each individual) and the first two columns of $\mathbf{H}$ as rays (one for each part). In a variance biplot, $\mathbf{H}$ is chosen as the matrix of eigenvectors of $\mathbf{S}$ scaled by the square roots of their eigenvalues, and $\mathbf{F}$ is estimated with generalized inversion (Gower and Hand 1996),

$$\hat{\mathbf{F}} = (\mathbf{X}^* \cdot \mathbf{H}) \cdot (\mathbf{H}^t \cdot \mathbf{H})^{-1}. \tag{22.2}$$

In the same way, we propose to obtain a discriminant biplot by defining

$$\mathbf{H} = \mathbf{E} \cdot \mathbf{D}, \tag{22.3}$$

where matrix $\mathbf{E}$ is the eigenvectors of $\mathbf{Q}$ stored in the columns, and the diagonal matrix $\mathbf{D}$ contains the square roots of their eigenvalues (in the right order), and estimating $\mathbf{F}$ with Equation (22.2).

In the case of having a compositional data set, the eigendecomposition of $\mathbf{Q}$ is actually done on the ilr scores, but we would like the biplot $\mathbf{H}$ matrix to have a row for each part in

the composition, so that we can draw its ray in the biplot. This is obtained simply as

$$\mathbf{H}_{\text{clr}} = \mathbf{V} \cdot \mathbf{E} \cdot \mathbf{D}. \tag{22.4}$$

The individual matrix **F** is estimated equally with Equation (22.2), using matrix **H** obtained from Equation (22.3). Remember that the link between two rays represents the log-ratio of the two involved parts, as in a classical compositional covariance biplot.

When using a combined data set, we compute the eigendecomposition of **Q** with the data set of Equation (22.1). The first $D - 1$ coordinates of each eigenvector can be applied to Equation (22.4) to obtain the positions of the clr-transformed parts in the joint biplot. The remaining coordinates of each eigenvector are associated with isotopic variables, and need only be scaled by Equation (22.3).

22.5 Results and discussion

The representation of the association between variables and sample groups is intended to (i) discriminate the five sampled zones, (ii) observe which variables or combination of variables condition this discrimination, and (iii) determine whether the associations showed by the plot are related either to the anthropogenic sources of pollution or to the geological background. In this sense the effect of altitude/continentality, that could mask a possible discrimination controlled by the origin of pollution, has been removed by using the deviations of δD and $\delta^{18}O_{H_2O}$ with regards to the local meteoric water line, instead of using the isotopic composition of water. In the following discriminant biplots, only geochemical data (Figure 22.3), only isotope data (Figure 22.4) and both data sets together (Figure 22.5) have been used.

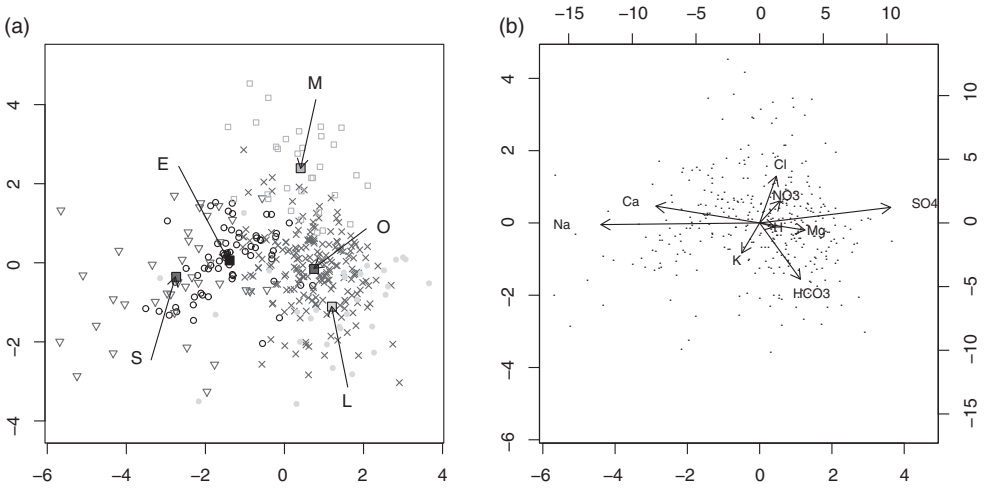

Figure 22.3 Discriminant plot (a) with indication of group means (plot centred using the global mean), and biplot (b), where arrows represent the explanatory variables using the geochemical data set. A clr transformation was used.

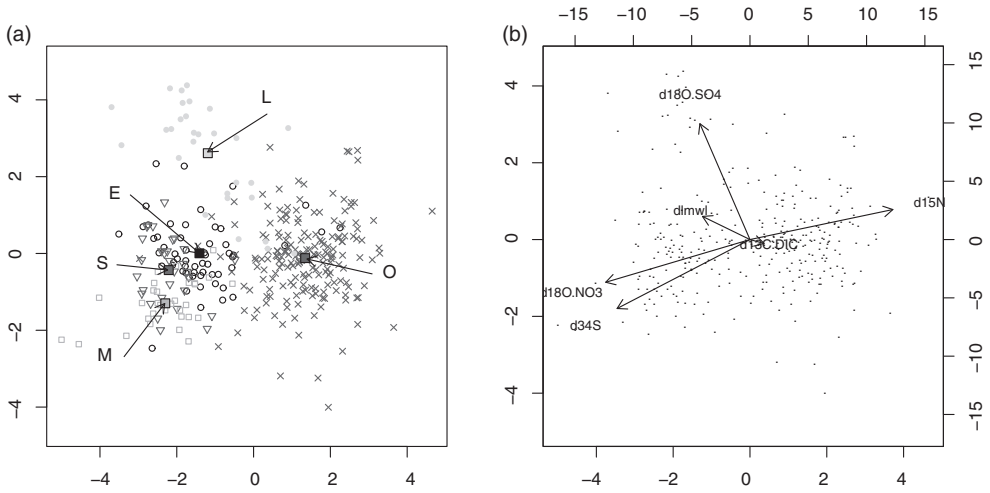

Figure 22.4 Discriminant plot (a) with indication of group means (plot centred using the global mean), and biplot (b), where arrows represent the explanatory variables using the isotopic data set.

In the discriminant plot using only geochemical data (Figure 22.3), we can discriminate Osona-Lluçanès, from Empordà-Selva, and from Maresme, but the sample groups are not perfectly split up. The explanatory variables are the couples of NO_3^--Cl^-, Ca^{2+}-Na^+ and Mg^{2+}-HCO_3^- contents. For instance, the Maresme area presents some of the highest NO_3^- concentrations due to the application of synthetic fertilizers, and is separated from the rest

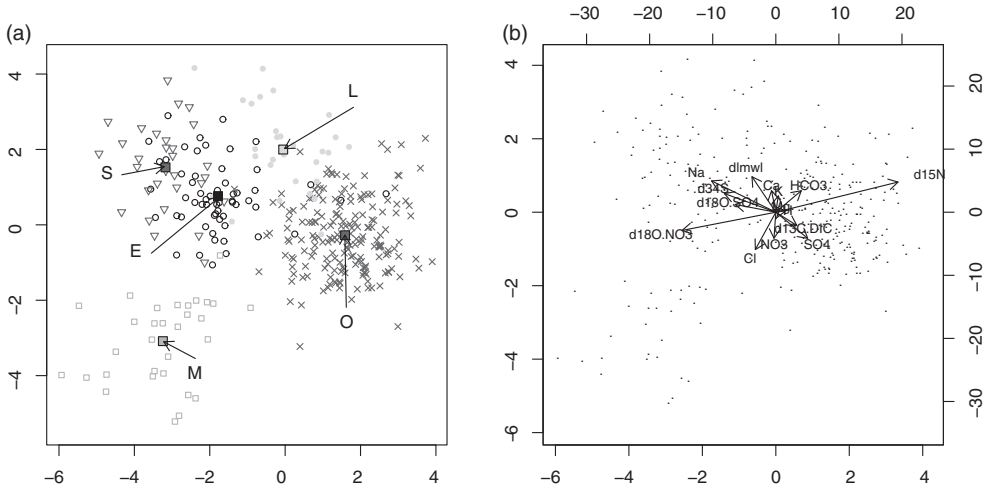

Figure 22.5 Discriminant plot (a) with indication of group means (plot centred using the global mean), and biplot (b), where arrows represent the explanatory variables, using both the geochemical (clr-transformed) and isotopic data sets.

of the zones in the direction of the NO_3^--Cl^- arrows, as mineral fertilizers have also high contents of chloride (Otero *et al*. 2005). On the other hand, Empordà and Osona-Lluçanès areas, which also present high NO_3^- contents (specially Osona), seem to be better explained by the Ca^{2+}-Na^+ and Mg^{2+}-HCO_3^- arrows, respectively. The Selva area appears to be discriminated in the direction of Ca^{2+}-Na^+ contents, which agrees with the hydrochemical facies of local (Ca^{2+}-HCO_3^-) and regional (Na^+-HCO_3^-) flow systems, and with the Ca^{2+}-Na^+ cation exchange process that is also occurring in this zone. SO_4^{2-} content cannot be considered an explanatory variable because it is not able to separate the Maresme and Osona-Lluçanès areas, which present high concentrations of this anion. With regard to SO_4^{2-}, it only can be concluded that the Na^+/SO_4^{2-} ratio in the Empordà-Selva areas is lower than the average for all zones. In this discriminant plot some of the studied areas are discriminated by NO_3^- contents, but the main nitrate sources that contribute to nitrate contamination, fertilizers and pig manure, represented by the Maresme and the Osona areas, respectively, are not in extreme positions. The separation of Osona-Lluççanès from Empordà-Selva is due to bedrock signature. Therefore, the discriminant plot entering only geochemical data does not allow an easy distinction of the five vulnerable zones according to the main nitrate source.

In the discriminant plot using only isotope data (Figure 22.4), Osona and Lluçanès samples are well separated from Maresme, Empordà and Selva samples. The explanatory variables are $\delta^{15}N$, $\delta^{18}O_{SO_4}$ and $\delta^{34}S$-$\delta^{18}O_{NO_3}$, indicating the combined influence of nitrate sources and the processes undergone by nitrate (mainly nitrate reduction favoured by sulfide and/or organic matter oxidation). In the link formed by $\delta^{15}N$ and $\delta^{34}S$-$\delta^{18}O_{NO_3}$ (which means using the difference between $\delta^{15}N$ and the sum of $\delta^{34}S$ and $\delta^{18}O_{NO_3}$), Osona and Maresme areas are in extreme positions, which agrees with their different nitrate contamination origin. Osona presents higher $\delta^{15}N$ values and lower $\delta^{34}S$ and $\delta^{18}O_{NO_3}$ values, because the main nitrate source in this area is pig manure and denitrification processes are occurring linked to sulfide oxidation. Maresme presents lower $\delta^{15}N$ and higher $\delta^{18}O_{NO_3}$ values because the main nitrate source is synthetic fertilizers and the reduction of nitrate is not detected. Anyhow, although Empordà and Selva samples plot next to the Maresme ones, they are not only affected by mineral fertilizers, but a nitrate contribution of pig manure is known in these areas. The Lluçanès sample group is remarkably well separated in the direction of the $\delta^{18}O_{SO_4}$, as the main contributions of SO_4^{2-} in this area are fertilizers and the presence of evaporites. If processes were not involved, from this discriminant plot we could relate pollution origin in the mixed areas mainly to fertilizers, with minor contribution of pig manure. However, we must take into account whether denitrification is occurring, and how it is occurring, because the $\delta^{34}S$ and $\delta^{18}O_{SO_4}$ variables can discriminate areas with the same nitrate source, depending on which is the main reaction that is controlling nitrate reduction. For instance, the $\delta^{34}S$ values in Osona, linked to the presence of pyrite and so to denitrification by pyrite oxidation, give rise to a clear separation of this sample group from the rest. The $\delta^{13}C_{DIC}$ and the deviation with respect to the local meteoric water line (dlmwl) do not exert an important role in discriminating the different areas. Thus, the use of only isotope data allows to distinguish the zones in a clearer way by the nitrate source influence, but some difficulties arise interpreting the mixed areas.

Using both data sets, in the discriminant plot obtained (Figure 22.5), the different sample groups are better separated. We have a clear discrimination of samples with the ratio ($\delta^{15}N$-$\delta^{18}O_{NO_3}$) + log (HCO_3^-/Cl^-): whereas the Maresme sample group is in one extreme and the Osona sample group in the opposite, which are considered as source end members, those samples from the mixed areas (Empordà and Selva) are in between. Taking in account the ratio

Table 22.1 LDA reclassification table obtained with each set of data, with percentage of correct reclassification.

		Geochemistry					Isotopes					Both				
Predicted group		E	L	M	O	S	E	L	M	O	S	E	L	M	O	S
True group	E	49	0	0	12	3	43	2	1	4	8	52	0	0	4	2
	L	1	14	0	13	2	4	21	0	4	0	2	21	0	6	0
	M	1	0	22	8	0	1	0	30	0	0	1	0	30	0	0
	O	6	8	6	176	0	6	1	2	180	0	3	1	0	185	0
	S	4	0	1	3	31	9	0	1	0	20	5	0	0	0	25
% good			81.111					87.24					92.88			

$\delta^{13}C_{DIC}$ - ($\delta^{34}S$-$\delta^{18}O_{SO_4}$), the sample group distribution can give us an idea of how denitrification processes are occurring: low $\delta^{13}C_{DIC}$ values (together with an increase of $\delta^{15}N$ and $\delta^{18}O_{NO_3}$) mean that organic matter oxidation is the reaction linked to denitrification processes; and low $\delta^{34}S$ and $\delta^{18}O_{SO_4}$ values imply that the reaction involved in natural attenuation of nitrate is sulfide oxidation. We must also bear in mind that the length of the arrows is related to the discriminant power of the variables that they represent, so the short length of the $\delta^{13}C_{DIC}$ arrow can be interpreted as if organic matter oxidation is taking place in all the areas where denitrification processes are occurring.

The discriminant biplots with only geochemical data, only isotope data and both data subsets separate the sample groups according to the following percentages of reclassification: 81, 87 and 93% (Table 22.1). As could be expected, the best discrimination is obtained when using both data subsets, but the discriminant biplot with only isotope data is useful enough to separate sample groups affected by different nitrate sources. Thus, the isotope data set is a powerful tool by itself, though some Empordà and Selva samples are missclassified.

22.6 Conclusions

A statistical methodology has been applied to the geochemical and isotope data set of five vulnerable zones. This procedure consists of a linear discriminant analysis of sample groups and the corresponding discriminant biplot, where the explanatory variables are plotted depending on their discriminant power. In order to implement this statistical methodology that integrates isotope with geochemical data together, both data subsets have been scaled so that their variations are comparable, and geochemical data have been transformed and treated as compositional data. A discriminant biplot has been generated by means of the eigendecomposition of $\mathbf{Q}$ matrix, that is defined as it follows: $\mathbf{Q} = (\mathbf{W}^{-1} \cdot \mathbf{B})$, where $\mathbf{W}$ and $\mathbf{B}$ are the *within-groups* and *between-groups variance matrices*, respectively. Note discrimination power when using only the isotope data set, although the optimum separation of sample groups is achieved using both geochemical and isotope data subsets. Moreover, in this case, in the direction defined by the variables $\delta^{13}C_{DIC}$, $\delta^{34}S$ and $\delta^{18}O_{SO_4}$, a separation of sample

groups depending on the reactions associated with denitrification processes is suggested. Further research is needed focusing on the assessment of natural attenuation of nitrate and the reactions involved, applying statistical methods to compositional data sets.

Acknowledgements

This study was funded by CICYT projects CGL-2008-06373-CO3-01/03-BTE from the Spanish Government, project 2009 SGR 103 from the Catalan Government, and the I3P Programme funded by the EU. Funding is also acknowledged from the Spanish Ministry of Science and Innovation through a *Juan de la Cierva* subprogramme, supported by the European Social Fund. The authors would like to thank the Serveis Cientifico-Tècnics of the University of Barcelona for their services.

References

ACA 2009 Data for groundwater quality in Catalunya http://aca-web.gencat.cat/aca/appmanager/aca/aca/. Accessed December 2009.

Aravena R , Robertson WD 1998 Use of multiple isotope tracers to evaluate denitrification in ground water: Study of nitrate from a large-flux septic system plume. *Ground Water* **36**(6), 975–981.

Bethke C 2008 *Geochemical and Biogeochemical Reaction Modelling*, 2nd edition Cambridge University Press, Cambridge (UK). 564 p.

Böttcher J, Strebel O, Voerkelius S and Schmidt HL 1990 Using isotope fractionation of nitrate-nitrogen and nitrate-oxygen for evaluation of microbial denitrification in sandy aquifer. *Journal of Hydrology* **114**, 413–424.

Casciotti KL, Sigman DM, Galanter M, Bölkhe JK and Hilkert A 2002 Measurement of the oxygen isotopic composition of nitrate in seawater and freshwater using the denitrifier method. *Analytical Chemistry* **74**, 4905–4912.

Cey E, Rudolph D, Aravena R and Parkin G 1999 Role of the riparian zone in controlling the distribution and fate of agricultural nitrogen near a small stream in southern Ontario. *Journal of Contaminant Hydrology* **37**, 45–67.

EC 1998 Council directive 98/83/EC, of 3 November 1998, on the quality of water intended for human consumption. Official Journal of the European Communities, L 330, of 5.12.1998, Brussels. http://eur-lex.europa.eu/LexUriServ/LexUriServ.do?uri=OJ:L:1998:330:0032:0054:EN:PDF. Accessed October 2004.

Epstein S and Mayeda T 1953 Variation of ^{18}O content of waters from natural sources. *Geochimica et Cosmochimica Acta* **4**, 213–224.

Fahrmeir L and Hamerle A 1984 *Multivariate Statistische Verfahren*. Walter de Gruyter, Berlin (Germany). 796 p.

Friedman I 1953 Deuterium content of natural waters and other substances. *Geochimica et Cosmochimica Acta* **4**, 89–103.

Gabriel KR 1971 The biplot – graphic display of matrices with application to principal component analysis. *Biometrika* **58** (3), 453–467.

Gower JC and Hand DJ 1996 *Biplots*. Chapman and Hall Ltd, London (UK). 277 p.

Grischek T , Hiscock KM , Metschies T 1998 Dennis PF W. N, Factors affecting denitrification during infiltration of river water into a sand and gravel aquifer in Saxony, Germany. *Water Research* **32** (2), 450–460.

Guimerà J, Marfà O, Candela L and Serrano L 1995 Nitrate leaching and strawberry production under drip irrigation management. *Agriculture, Ecosystems and Environment* **56**, 121–135.

IAEA/WMO 2004 Global network of isotopes in precipitation. The GNIP Database. http://www-naweb.iaea.org/napc/ih/IHS resources_gnip.html. Accessed October 2004.

IDESCAT 1999 Cens agrari del banc d'estadístiques de municipis i comarques http://www.idescat.cat/. Accessed October 2004.

Kendall C and McDonnell JJ 1998 *Isotope Tracers in Catchment Hydrology*. Elsevier Science BV, Amsterdam (The Netherlands). 839 p.

Krzanowski WJ 1988 *Principles of Multivariate Analysis: A User's Perspective*. Clarendon Press, Oxford (UK). 563 p.

Krzanowski WJ and Marriott FHC 1994 *Multivariate Analysis, Part 2 - Classification, Covariance Structures and Repeated Measurements*. Edward Arnold, London (UK). 280 p.

Letolle R 1980 Nitrogen-15 in the natural environment. In *Handbook of Environmental Isotope Geochemistry, Vol. 1. The Terrestrial Environment* (ed. Fritz P and Fontes JC). Elsevier, Amsterdam (The Netherlands). pp. 407–433.

Magee PN and Barnes JM 1956 The production of malignant primary hepatic tumors in the rat by feeding dimethylnitrosamine. *British Journal of Cancer* **10**, 114–122.

Mardia KV, Kent JT and Bibby JM 1979 *Multivariate Analysis*. Academic Press, London (UK). 518 p.

Mayer B, Bollwerk SM, Mansfeldt T, Hütter B, Vezier J 2001 The oxygen isotopic composition of nitrate generated by nitrification in acid forest floors. *Geochimica et Cosmochimica Acta* **65**(16), 2743–2756.

Mengis M, Schiff SL, Harris M, English MC, Aravena R, Elgood RJ and MacLean A 1999 Multiple geochemical and isotopic approaches for assessing ground water NO_3^- elimination in a riparian zone. *Ground Water* **37**(3), 448–457.

Otero N, Torrentó C, Soler A, Menció A and Mas-Pla J 2009 Monitoring groundwater nitrate attenuation in a regional system coupling hydrogeology with multi-isotopic methods: The case of Plana de Vic (Osona, Spain). *Agriculture, Ecosystems and Environment* **133**, 103–113.

Otero N, Vitòria L, Soler A and Canals A 2005 Fertilizer characterization: major, trace and rare earth elements. *Applied Geochemistry* **20**(8), 1473–1488.

Pauwels H, Foucher JC and Kloppmann W 2000 Denitrification and mixing in a schist aquifer: Influence on water chemistry isotopes. *Chemical Geology* **168**, 307–324.

Pawlowsky-Glahn V, Egozcue JJ 2001 Geometric approach to statistical analysis on the simplex. *Stochastic Environmental Research and Risk Assessment (SERRA)* **15**(5), 384–398.

Puig R, Soler A and Mas-Pla J 2007 Determination of the sources of nitrate pollution and evaluation of natural attenuation processes using multi-isotopic methods in the Baix Empordà basin (NE Spain). In *Water Pollution in Natural Porous Media at Different Scales. Assessment of Fate, Impact and Indicators* (ed. Candela L, Vadillo I, Aagaard P, Bedbur E, Trevisan M, Vanclooster M, Viotti P and López-Geta JA). Instituto Geológico y Minero de España, Madrid (Spain). pp. 239–245.

Sigman DM, Casciotti KL, Andreani M, Bradford C, Galanter M and Bölkhe JK 2001 A bacterial method for the nitrogen isotopic analysis of nitrate in seawater and freshwater. *Analytical Chemistry* **73**, 4145–4153.

Silva SR, Kendall C, Wilkison DH, Zieglerc AC, Chang CCY and Avanzino RJ 2000 A new method for collection of nitrate from fresh water and the analysis of nitrogen and oxygen isotope ratios. *Journal of Hydrology* **228**, 22–36.

Tolosana-Delgado R, Otero N and Soler A 2005 A compositional approach to stable isotope data analysis. In *Proceedings of CoDaWork'05, The 2nd Compositional Data Analysis Workshop* (ed. Mateu-Figueres G and Barceló-Vidal C). University of Girona, Girona (Spain).

Vitòria L, Soler A, Aravena R and Canals A 2005 Multi-isotopic approach (15N, 13C, 34S, 18O and D) for tracing agriculture contamination in groundwater. In *Environmental Chemistry: Green Chemistry and Pollutants in Ecosystems* (ed. Lichtfouse E, Schwartzbauer J and Robert D). Springer-Verlag, Berlin (Germany). pp. 43–56.

Vitòria L, Soler A, Canals A and Otero N 2008 Environmental isotopes (N, S, C, O, D) to determine natural attenuation processes in nitrate contaminated water: Example of Osona (NE Spain). *Applied Geochemistry* **23**, 3597–3611.

Volkmer BG, Ernst B, Simon J, Kuefer R, Bartsch GJ, Bach D and Gschwend JE 2005 Influence of nitrate levels in drinking water on urological malignancies: a community-based cohort study. *British Journal of Urology International* **95**(7), 972.

Ward MH, DeKok TM, Levallois P, Brender J, Gulis G, Nolan BT and VanDerslice J 2005 Workgroup report: Drinking-water nitrate and health-recent findings and research needs. *Environmental Health Perspectives* **113**(11), 1607–1614.

Wassenaar L 1995 Evaluation of the origin and fate of nitrate in Abbotsford Aquifer using the isotopes of ^{15}N and ^{18}O in NO_3^-. *Applied Geochemistry* **10**, 391–405.